Design, synthesis and single molecule force spectroscopy of biosynthetic polypeptides

Marie Asano

THÈSE EN COTUTELLE PRÉSENTÉE

POUR OBTENIR LE GRADE DE

DOCTEUR DE L'UNIVERSITÉ DE LIÈGE ET DE L'UNIVERSITÉ DE BORDEAUX

COLLÈGE DE DOCTORAT EN CHIMIE (Université de Liège)

ÉCOLE DOCTORALE DES SCIENCES CHIMIQUES (Université de Bordeaux)

SPÉCIALITÉ NANO-CHIMIE ET POLYMÈRES

Par Marie ASANO

Design, Synthesis and Single Molecule Force Spectroscopy of Biosynthetic Polypeptides

Sous la direction de
Prof. Dr. Anne-Sophie DUWEZ et de Prof. Dr. Sébastien LECOMMANDOUX

Soutenue à Liège le 14 Octobre 2016

Membres du jury :

M. MATAGNE, André	Professeur, Université de Liège	Président
M. ALSTEENS, David	Professeur, Université catholique de Louvain	Rapporteur
M. SURIN, Mathieu	Chercheur qualifié du FNRS, Université de Mons	Rapporteur
M. WILLET, Nicolas	Chef de projet R&D, PhysIOL s.a.	Examinateur
M. SANDRE, Olivier	Directeur de recherche, Université de Bordeaux	Examinateur

Design, synthèse et spectroscopie de force à l'échelle de la molécule unique de polypeptides biosynthétiques

Résumé: Le repliement des protéines est principalement gouverné par les interactions spécifiques des structures secondaires. [1, 2] Toutefois, il existe expérimentalement peu d'informations les propriétés mécaniques fondamentales des hélices α et des feuillets β isolées. Les recherches antérieures sur l'étude du déploiement des hélices sont peu concluantes [3-5] et à notre connaissance l'étude des propriétés mécaniques d'un feuillet β isolé, intramoléculaire est sans précédent.

Les copolymères PEG_{114}-*b*-poly(*L*-lysine)$_{134}$-(2-pyridyl disulfure), PEG_{114}-*b*-poly(*L*-lysine)-*b*-PEG_{114} et poly(*L*-acide glutamique)$_{85}$-*b*-(2-pyridyl disulfure) été synthétisés et utilisés comme systèmes modèles pour tester les propriétés mécaniques des motifs secondaires de type hélice α et feuillet β. Les résultats obtenus se sont révélés être en bon accord avec les résultats théoriques obtenus en utilisant un modèle statistique basé sur AGAGIR [6]. La différence de force de déroulement comparant les hélices de poly(*L*-Lysine) ≈ 30 pN et de poly(*L*-acide glutamique) ≈ 20 pN des copolymères diblocs a été attribuée à l'hydrophobicité différente des chaînes latérales. La plus grande hydrophobie du motif lysine conduit à de plus grandes interactions entre les chaînes latérales qui empêchent les fluctuations aléatoires au sein de l'hélice, et conduisent à une stabilité supérieure de l'hélice α. Lorsque les expériences ont été conduites dans des conditions favorisant la solubilité des chaînes latérales de lysine, les interactions ont diminué à une force de ≈ 20 pN, similaire à la force des interactions observées pour le poly(*L*-acide glutamique). Nous supposons qu'un minimum de ≈ 20 pN est nécessaire pour rompre la liaison hydrogène en maintenant l'hélice α, car cette force a été obtenue dans des conditions où les interactions de la chaîne latérale étaient minimisées.

La présence de plateaux de force constants et d'inflexions correspondantes démontre une force de dépliement indépendante de la longueur, qui supporte un mécanisme de déroulement tour-par-tour pour l'hélice.

De plus, la plus grande hydrophobie des chaînes latérales a été suggérée non seulement pour stabiliser la structure en hélice, mais également pour inhiber la formation d'une structure de type β–turn métastable intermédiaire lorsque les forces entropiques dominent.

Des études préliminaires ont été effectuées sur le système de PEG_{114}-*b*-poly(*L*-Lysine)$_{134}$-(2-pyridyl disulfure) après induction d'une transition α–β par

un traitement thermique dans des conditions basiques. Une inflexion à une force ≈ 70 pN a été obtenue, ce qui suggère la formation d'une interaction de type feuillet β.
Une stratégie bottom-up a ainsi été proposée avec succès, démontrant le potentiel d'utilisation de tels systèmes artificiels pour simplifier et modéliser des systèmes biologiques réels. La compréhension de ces modèles isolés plus simples aidera sans doute la compréhension de systèmes plus complexes.

Mots clés: spectroscopie de force sur molécule unique, copolymères à blocs, polypeptides stimulables, poly(*L*-acide glutamique), poly(*L*-lysine), biosynthétiques, hélice α, feuillet β

Références

1. V. Daggett and A. Fersht, *Nat Rev Mol Cell Biol*, 2003, **4**, 497-502.
2. A. R. Dinner, A. Sali, L. J. Smith, C. M. Dobson and M. Karplus, *Trends in Biochemical Sciences*, 2000, **25**, 331-339.
3. A. Idiris, M. T. Alam and A. Ikai, *Protein Engineering*, 2000, **13**, 763-770.
4. R. Afrin, I. Takahashi, K. Shiga and A. Ikai, *Biophysical Journal*, 2009, **96**, 1105-1114.
5. M. A. Lantz, S. P. Jarvis, H. Tokumoto, T. Martynski, T. Kusumi, C. Nakamura and J. Miyake, *Chemical Physics Letters*, 1999, **315**, 61-68.
6. K. Torabi and G. C. Schatz, *Macromolecules*, 2013, **46**, 7947-7956.

Design, Synthesis and Single Molecule Force Spectroscopy of Biosynthetic Polypeptides

Abstract: Proteins fold by the initial, preferential folding of secondary structures [1, 2], however surprisingly little is known about the basic mechanical properties of isolated α-helices and β-sheets from an experimental standpoint. Previous investigations into studying the generic unfolding behaviour of α-helices have proved inconclusive [3-5], and to our knowledge the study of an isolated, intramolecular β-sheet is unprecedented.

Bioinspired PEG_{114}-*b*-poly(*L*-glutamic acid)$_{85}$-(2-pyridyl disulphide), PEG_{114}-*b*-poly(*L*-lysine)$_{134}$-(2-pyridyl disulphide) and PEG_{114}-*b*-poly(*L*-lysine)$_{134}$–*b*-PEG_{114} were designed, synthesized and utilized as model systems to probe the mechanical properties of α-helix and β-sheet secondary motifs. The obtained results were shown to be in good agreement with theoretical results obtained by utilizing a AGAGIR-based statistical mechanical model [6]. The difference in unravelling force comparing the helices of poly(*L*-Lysine) ≈30 pN and poly(*L*-glutamic acid) ≈20 pN diblock copolymers was attributed to the differing hydrophobicity of the side chains. The greater hydrophobicity of the lysine allowed greater interactions between the side chains and sterically hindered random helix-coil fluctuations, which lead to a superior α-helix stability. When experiments were conducted in conditions promoting the solubility of the lysine side chains, the interactions decreased to a force of ≈20 pN, similar to the force of interactions observed for the poly(*L*-glutamic acid). We infer that a minimum of ≈20 pN is needed to rupture the hydrogen bonding maintaining the α-helix as this force was obtained in conditions where the side chain interactions were minimized.

The presence of constant force plateaus and corresponding inflections demonstrates a length independent unfolding force, which supports a turn-by-turn unfolding mechanism for the α–helix.

In addition, the greater hydrophobicity of the side chains was suggested to not only stabilize the α-helix structure, but also to inhibit the formation of an intermediate metastable β-hairpin-like structure when entropic forces dominate.

Preliminary studies were also conducted on the PEG_{114}-*b*-poly(*L*-Lysine)$_{134}$-(2-pyridyl disulphide) system after a α–β transition had been induced by heat in basic conditions, where an inflection at a much higher force of ≈ 70 pN was obtained suggesting the formation of a β-sheet interaction.

A bottom-up, investigative strategy has thus been successfully proposed demonstrating the potential of utilizing such artificial systems to simplify and exemplify real biological systems. The comprehension of these simpler isolated models will no doubt aid the understanding of more complex systems.

Keywords: single molecule force spectroscopy, stimuli-responsive, block copolymer polypeptides, poly(*L*-glutamic acid), poly(*L*-lysine), biosynthetic, α–helix, β–sheet

References

1. V. Daggett and A. Fersht, *Nat Rev Mol Cell Biol*, 2003, **4**, 497-502.
2. A. R. Dinner, A. Sali, L. J. Smith, C. M. Dobson and M. Karplus, *Trends in Biochemical Sciences*, 2000, **25**, 331-339.
3. A. Idiris, M. T. Alam and A. Ikai, *Protein Engineering*, 2000, **13**, 763-770.
4. R. Afrin, I. Takahashi, K. Shiga and A. Ikai, *Biophysical Journal*, 2009, **96**, 1105-1114.
5. M. A. Lantz, S. P. Jarvis, H. Tokumoto, T. Martynski, T. Kusumi, C. Nakamura and J. Miyake, *Chemical Physics Letters*, 1999, **315**, 61-68.
6. K. Torabi and G. C. Schatz, *Macromolecules*, 2013, **46**, 7947-7956.

Unités de recherche

Université de Liège
Faculté des Sciences, Département de Chimie
Nano-chimie et Systèmes Moléculaires

Allée du Six août (Bât. B6a)
4000 Sart Tilman (Liège)
Belgique

Université de Bordeaux
Laboratoire de Chimie des Polymères Organiques UMR 5629
INP-Bordeaux ENSCBP

16, Avenue Pey-Berland
33607 Pessac Cedex
France

Design, synthèse et spectroscopie de force à l'échelle de la molécule unique de polypeptides biosynthétiques

Dans cette étude, des copolymères biséquencés et triséquencés de PEG_{114}-*b*-poly(*L*-acide glutamique)$_{85}$-(2-pyridyl disulfure), PEG_{114}-*b*-poly (*L*- lysine)$_{134}$-(2-pyridyl disulfure), et PEG_{114}-*b*-poly(*L*-lysine)$_{134}$-*b*-PEG_{114} ont été conçus sur mesure, synthétisés et utilisés comme des systèmes artificiels modèles pour déterminer les propriétés mécaniques relatives aux structures secondaires naturelles par spectroscopie de force à l'échelle de la molécule unique.

Deux modèles moléculaires différents ont été étudiés dans le cadre de ce travail. Un design consistait en un système avec un groupe 2-pyridyl disulfure qui permettait à la macromolécule de se lier chimiquement sur une surface d'or, tandis que l'autre extrémité consistait en une attache de PEG (**Figure 1 g.**). Le PEG a permis la physisorption de molécule sur un levier AFM et par conséquent le segment polypeptidique entre les deux a pu être capturé et étiré.

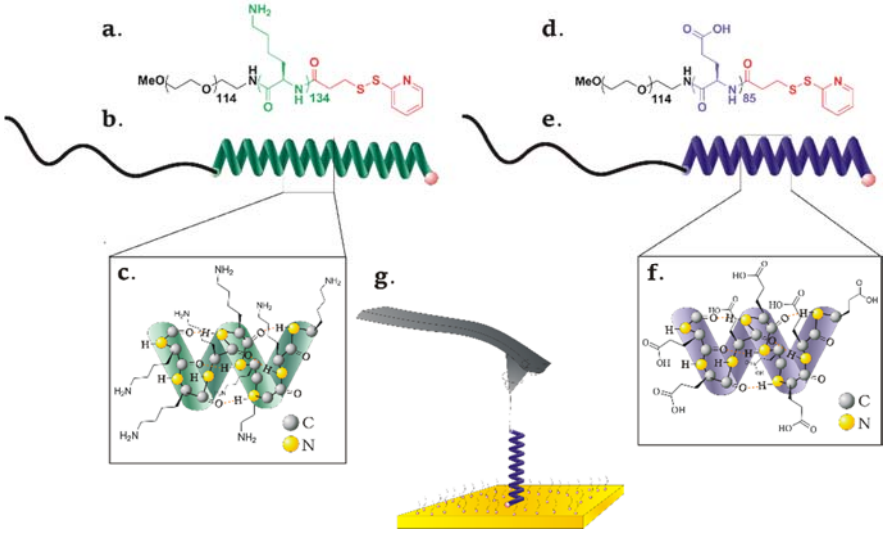

Figure 1. Les représentations schématiques des PEG_{114}-*b*-poly(*L*-lysine)$_{134}$-(2-pyridyl disulfure) et PEG_{114}-*b*-poly(*L*-acide-glutamique)$_{85}$-(2-pyridyl disulfure). a.) La structure chimique du poly(éthylène glycol)$_{114}$-*b*-poly(*L*-lysine)$_{134}$-(2-pyridyl disulfure). b.) Représentation schématique de PEG_{114}-*b*-poly(*L*-lysine)$_{134}$-(2-pyridyl disulfure) en une conformation hélice α. c.) Une représentation détaillée des chaînes latérales et des liaisons hydrogène de hélice α de poly-(*L*-lysine). d.) Structure chimique du poly(éthylène glycol) $_{114}$-*b*-poly(*L*-acide glutamique)$_{85}$-(2-pyridyl disulfure). e.) Représentation schématique de PEG_{114}-*b*-poly (*L*-acide glutamique)$_{85}$-(2-pyridyl disulfure) en une conformation en hélice α. f.) Une représentation détaillée des chaînes latérales et des liaisons hydrogène au sein de hélice α de poly(*L*-acide glutamique). g.) Représentation schématique d'une molécule greffée sur une surface d'or avec la chaîne de PEG physisorbé sur un levier AFM nu et le disulfure de 2-pyridyle (point rouge) à l'autre extrémité de la molécule comme

une fraction d'ancrage. La molécule est entourée par PEG_6-SH également greffée sur la surface, comme un agent de passivation.

Le second design impliquait l'addition d'un second espacer PEG entre le segment polypeptidique et la surface à la place de la groupe 2-pyridyl disulfure, qui devrait permettre au système de reposer uniquement sur l'adsorption directe du copolymère triséquencé sur une surface (**Figure 2 d.**).

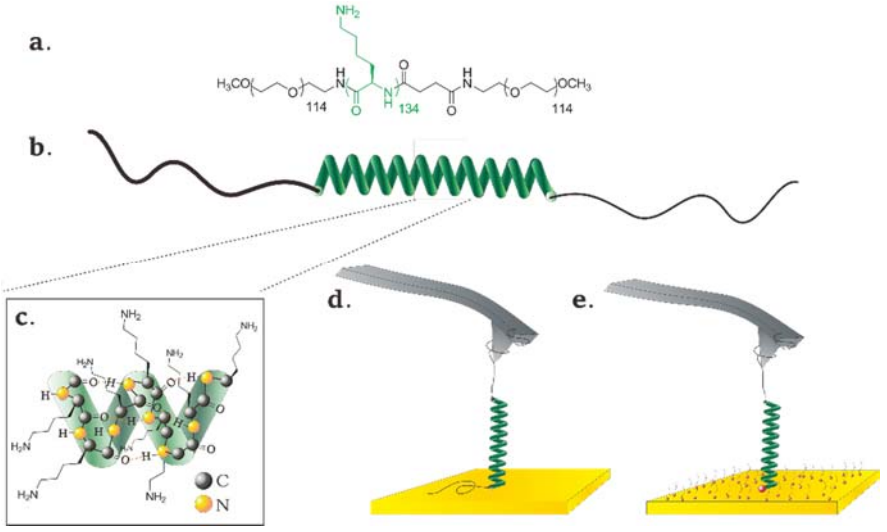

Figure 2. Représentations schématiques de PEG_{114}-*b*-poly(*L*-lysine)$_{134}$-*b*-PEG_{114}. a.) La structure chimique du poly(éthylène glycol)$_{114}$-*b*-poly(*L*-lysine)$_{134}$-*b*-poly(éthylène glycol)$_{114}$. b.) Représentation schématique de PEG_{114}-*b*-poly(*L*-lysine)$_{134}$-*b*- PEG_{114} dans une conformation hélice α. c.) Une représentation détaillée des chaînes latérales et des liaisons hydrogène de hélice α de poly-(*L*-lysine). d.) Représentation schématique du copolymère triséquencé avec un segment de PEG adsorbé sur la surface, et l'autre segment de PEG adsorbé sur un levier AFM nu. e.) Pour une comparaison, le polymère biséquencés poly(éthylène glycol)$_{114}$-*b*-poly(*L*-lysine)$_{134}$-(2-pyridyl disulfure) greffée sur une surface d'or avec la chaîne de PEG adsorbé sur une AFM levier nue et le 2-pyridyl disulfure (point rouge) à l'autre extrémité de la molécule comme une fraction d'ancrage. La molécule est entourée par PEG_6-SH également greffée sur la surface, comme un agent de passivation.

Le PEG_{114}-*b*-poly(*L*-lysine)$_{134}$-(2-pyridyl disulfure) et le PEG_{114}-*b*-poly(*L*-lysine)$_{134}$-*b*-PEG_{114}, copolymères bi et triséquencés, ont été synthétisés par ring opening polymerization de N^{ε}- trifluoroacetyl-*L*-lysine *N*-carboxyanhydride initié par PEG-NH_2. Le copolymère biséquencé résultant a ensuite été couplé avec une *N*-succinimidyl 3-(2-pyridyldithio) propionate (SPDP) ou le PEG_{114}-α-methoxy-ω-NHS et ensuite déprotégés. La dispersité mesurée avant la déprotection était $Đ \frac{Mw}{Mn}$ =1.16 (DMF: 1g·L^{-1} LiBr) pour PEG_{114}-*b*-poly(*L*-

lysine)$_{134}$-(2-pyridyl disulfure) et Đ$\frac{Mw}{Mn}$=1.14 (DMF: 1g·L^{-1} LiBr) pour PEG$_{114}$-*b*-poly(*L*- lysine)$_{134}$-*b* PEG$_{114}$.

Le PEG$_{114}$-*b*-poly(*L*-lysine)$_{134}$-(2-pyridyl disulfure) a été caractérisé par diffusion de lumière dynamique où il a été constaté qu'il ne subissait pas facilement d'auto-assemblage en réponse au changement de pH ou des concentrations ioniques différentes. En utilisant le dichroïsme circulaire, nous avons observé que le polymère subissait une transition conformationnelle entre hélice-random coil à un pH supérieur à 9. Le copolymère biséquencé est bien adapté pour des expériences de spectroscopie de force à l'échelle de la molécule unique, étant donné qu' il a été capable de subir une transition conformationnelle en réponse au pH mais restant bien dissous dans la solution. De la même façon, nous avons montré que le PEG$_{114}$-*b*-poly(*L*-lysine)$_{134}$-*b*-PEG$_{114}$ montrait une transition conformationnelle à pH supérieur à 8. La transition est plus progressive et à partir d'un pH plus bas en raison du segment PEG supplémentaire coopérant avantageusement avec le segment de la lysine, facilitant la nucléation et la stabilisation de la structure secondaire hélice.

La synthèse de PEG$_{114}$-*b*-poly(*L*-acide glutamique)$_{85}$-(2-pyridyl disulfure) a été effectuée avant cette étude par un auteur différent. La synthèse rapportée a été réalisée par la polymérisation par ouverture de cycle γ-benzyle *L*-glutamique *N*-carboxyanhydride qui a également été initiée par un initiateur PEG-NH$_2$. Le copolymère biséquencé résultant est couplé à *N*-succinimidyl 3-(2-pyridyldithio) propionate (SPDP) et ensuite déprotégés. La dispersité mesurée était Đ$\frac{Mw}{Mn}$=1.18 (DMF: 1g·L^{-1} LiBr) avant la déprotection. Du dichroïsme circulaire a également été réalisé pour confirmer que précédemment dans des conditions de faible pH du poly (*L*- acide glutamique), le segment adopte la structure secondaire en hélice et présente une transition entre hélice et random coil à un pH neutre à basique.

La spectroscopie de force à l'échelle de la molécule unique a été réalisée avec ces copolymères et les résultats expérimentaux ont été comparés, et montré en bon accord avec les résultats théoriques obtenus en utilisant un modèle mécanique statistique fondé sur le AGAGIR proposé par Torabi et Schatz [1].

Nous avons mis en évidence que l'hélice formée par PEG$_{114}$-*b*-poly(*L*-Lysine)$_{134}$-(2-pyridyl disulfure) subissait un dépliement tour-par-tour, indiqué par un plateau de force constante observé expérimentalement à 27 ± 4 pN et 34 ± 1 pN (**Figure 3**), et à 30 pN pour le modèle mécanique statistique. Une longueur de plateau de 27 ± 4 nm a été observée correspondant à la différence de longueur théorique (≈ 27 nm) entre l'hélice repliée et non décollée. Selon la littérature [2] une longue hélice de polypeptide telle que celle de la présente étude, serait repliée dans une structure d'ordre supérieur séparée par des résidus dénaturés entre les

segments hélicoïdaux. Lorsqu'une hélice complète ne pouvait pas se replier lors de l'application d'une petite force axiale, on a observé une longueur de plateau plus courte de 13 ± 3 nm, attribuée au déploiement de segments hélicoïdaux courts isolés. Si toutes les chaînes latérales ne sont pas positionnées dans une orientation géométrique optimale pour favoriser leurs interactions hydrophobes stabilisant l'hélice, la force de déploiement serait légèrement inférieure, expliquant pourquoi deux populations différentes pour la force du plateau ont été observées expérimentalement.

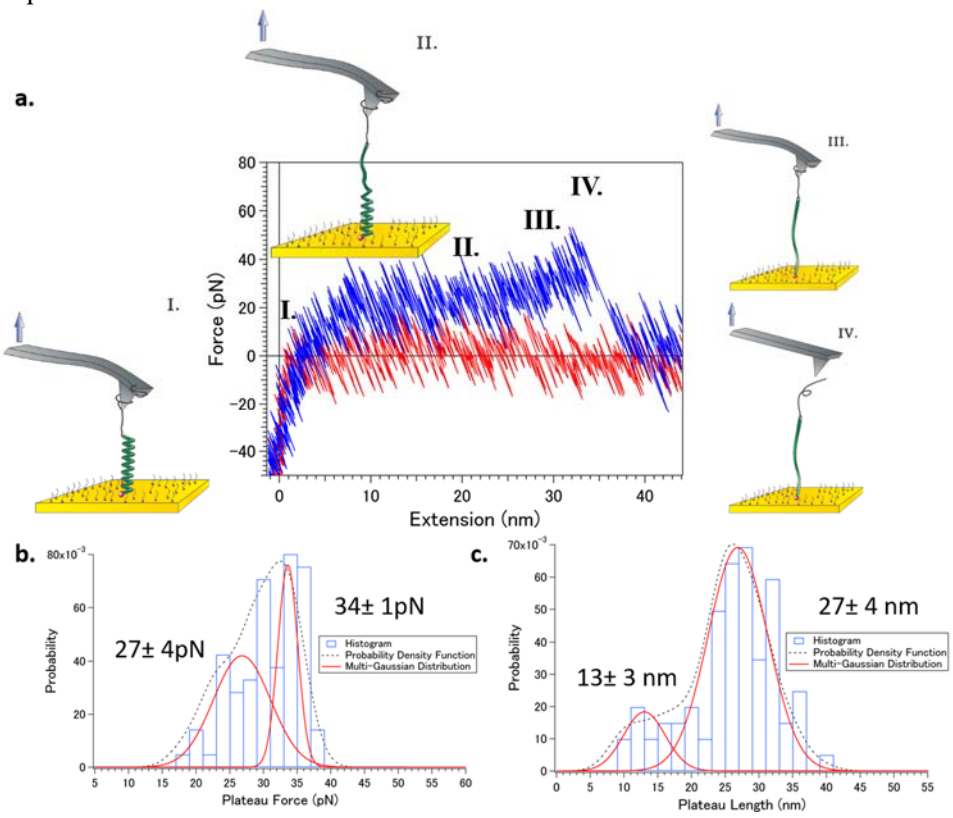

Figure 3 Une des deux courbes caractéristiques de force d'extension pour PEG$_{114}$-*b*-poly(*L*-lysine)$_{134}$-(2-pyridyl disulfure) en une conformation en hélice α et les histogrammes correspondants, des fonctions de densité de probabilité, et des distributions gaussiennes. a.) Un profil typique de force-extension montrant un vrai plateau. Les chiffres romains et les diagrammes correspondants représentent une interprétation des événements au cours du cycle force-extension. b.) Histogramme, fonction de densité de probabilité et distribution gaussienne de deux forces du plateau à 27 ± 4 pN (63%) et 34 ± 1 pN (37%) (± S.D, n = 86). c.) Histogramme, fonction de densité de probabilité et distribution gaussienne des longueurs de deux plateaux 13 ± 3 nm (16%) et 27 ± 4 nm (84%) (± S.D, n = 86).

Si les segments hélicoïdaux étaient moins aptes à s'aligner en raison du mauvais positionnement géométrique par le levier AFM, beaucoup d'autres

segments dénaturés resteraient dans l'hélice. Dans ce cas, un plateau incliné commençant à 13 ± 6 pN et se terminant à 36 ± 9 pN a été observé (**Figure 4**). La force finale du plateau incliné et la valeur du plateau vrai 34 ± 1 pN étaient en bon accord, ce qui témoigne du déroulement des petits segments hélicoïdaux restants.

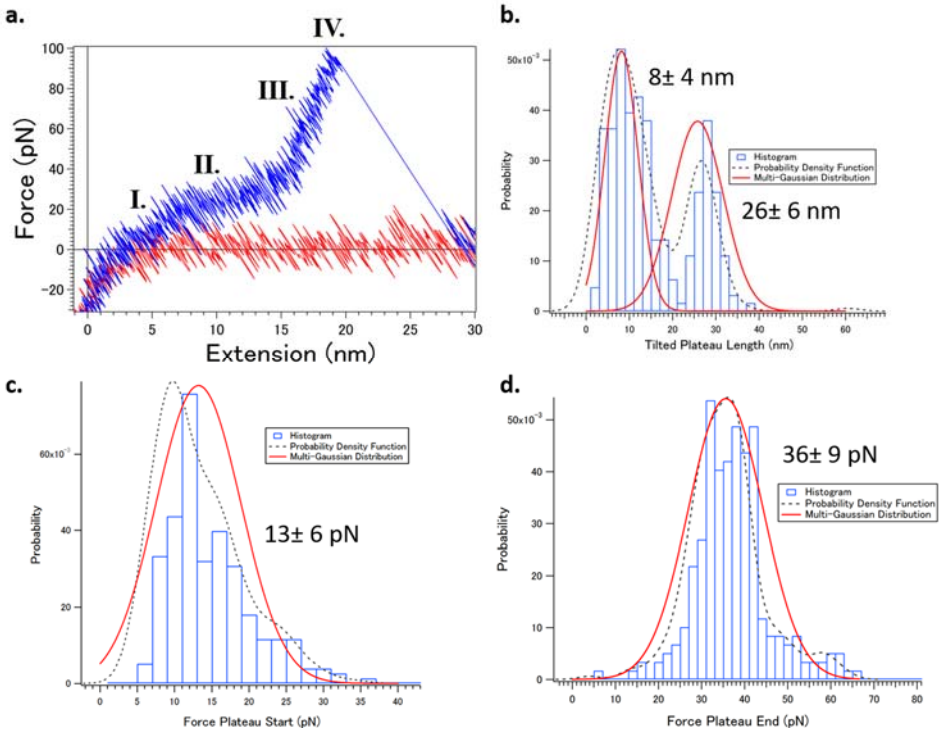

Figure 4. Une des deux courbes caractéristiques de force d'extension pour PEG_{114}-*b*-poly(*L*-lysine)$_{134}$-(2-pyridyl disulfure) en une conformation en hélice α et les histogrammes correspondants, des fonctions de densité de probabilité, et des distributions gaussiennes. a.) Un profil typique de force-extension montrant un plateau incliné. Les chiffres romains représentent une interprétation des événements au cours du cycle force-extension (voir Figure 3). b.) Histogramme, fonction de densité de probabilité et distribution gaussienne des longueurs de deux plateaux 8 ± 4 nm (66%) et 26 ± 6 (34%) (± S.D, n = 253). c.) Histogramme, fonction de densité de probabilité, et distribution gaussienne du plateau de départ force de 13 ± 6 pN (± S.D, n = 253). d.) Histogramme, fonction de densité de probabilité, et la distribution gaussienne du plateau vigueur se terminant 36 ± 9 pN (± S.D, n = 253).

Au contraire, le déroulement de hélice α de PEG_{114}-*b*-poly(*L*-acide glutamique)$_{85}$–*b*-(2-pyridyl disulfure) a été identifié par une inflexion observée à 18 ± 4 pN (**Figure 5**) et à 15 pN avec le modèle de mécanique statistique. Dans quelques cas, on peut observer un plateau à 19 ± 2 pN, où la longueur observée expérimentalement de 12 ± 5 pN correspond à la différence de longueur théorique (≈17 nm) entre l'hélice repliée et dépliée (**Figure 6**).

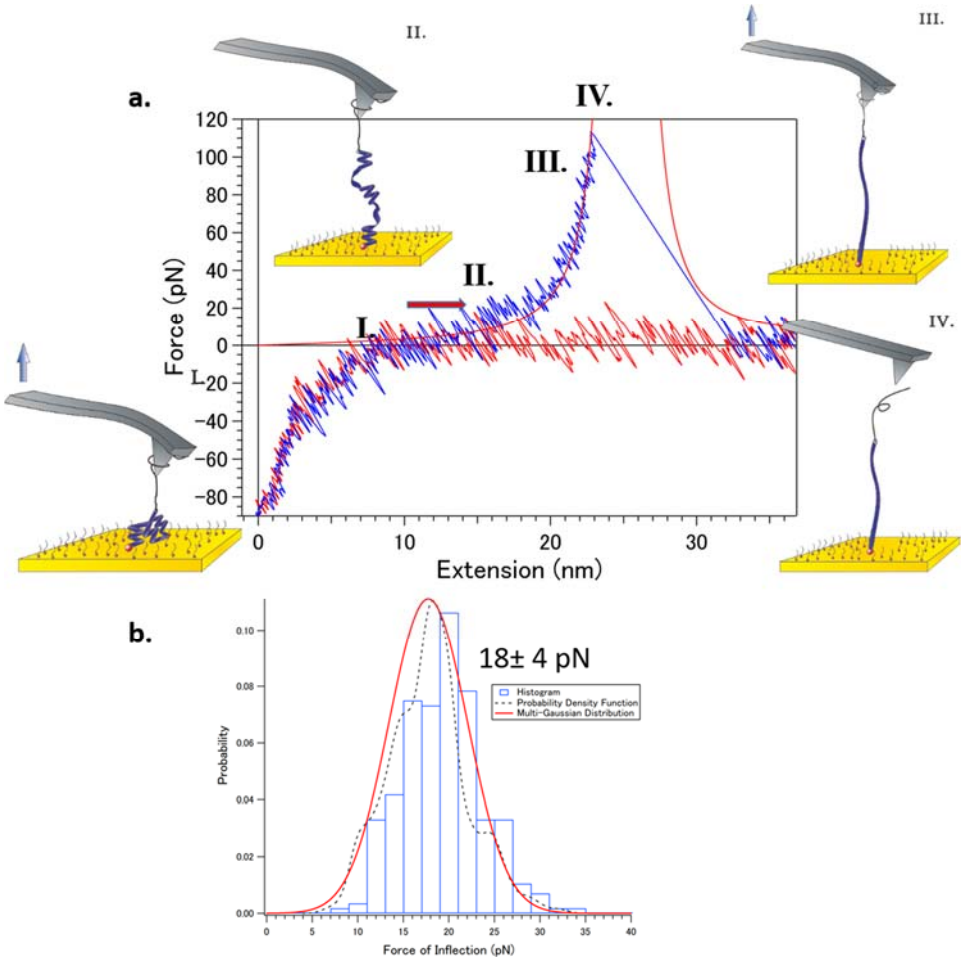

Figure 5. Courbe force-extension typique de la fonction de densité de probabilité PEG_{114}-*b*-poly(*L*-acide glutamique)$_{85}$-(2-pyridyl disulfure) en une conformation en hélice α et l'histogramme correspondant, et à la distribution gaussienne. a.) Un profil typique de force-extension montrant l'inflexion récurrent (flèche rouge). Les chiffres romains et les diagrammes correspondants représentent une interprétation des événements au cours du cycle force-extension. La ligne rouge indique un ajustement en utilisant le modèle WLC. b.) Histogramme, fonction de densité de probabilité et distribution gaussienne de la force de inflexion 18 ± 4 pN (± S.D, n = 232).

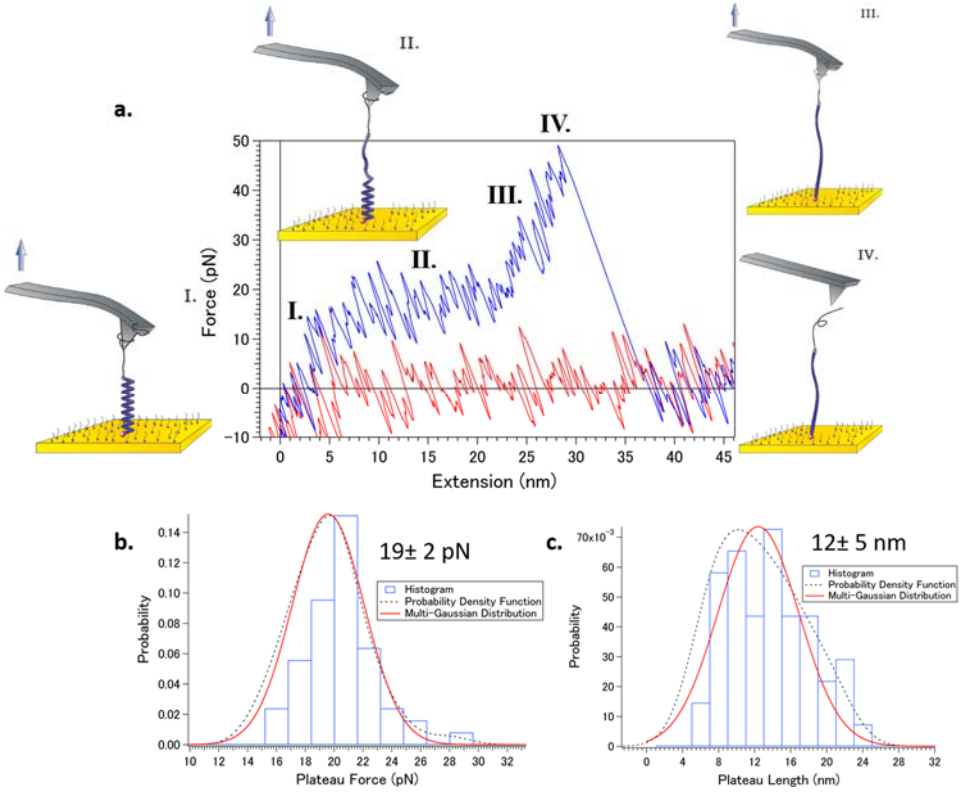

Figure 6. Une des deux courbes caractéristiques de force d'extension pour PEG_{114}-*b*-poly (*L*-acide glutamique)$_{85}$-(2-pyridyl disulfure) en une conformation en hélice α et les histogrammes correspondants, des fonctions de densité de probabilité, et des distributions gaussiennes. a.) Un profil typique de force-extension montrant un plateau. Les chiffres romains et les diagrammes correspondants représentent une interprétation des événements au cours du cycle force-extension. b.) Histogramme, fonction de densité de probabilité, et distribution gaussienne de la force du plateau 19 ± 2 pN (± S.D, n = 55). c.) Histogramme, fonction de densité de probabilité et distribution gaussienne de la longueur du plateau de 12 ± 5 nm (± S.D, n = 55).

Une deuxième inflexion à une force plus élevée de 60 ± 9 pN a été observée pour plus de la moitié des courbes qui présentaient la première inflexion, et a été attribuée à la formation d'une interaction métastable en épingle à cheveux β (**Figure 7**). Nous suggérons que la formation de cette structure intermédiaire se produit pendant le déroulement de la structure hélice alpha en raison de la structure en épingle à cheveux β possédant une entropie plus élevée [3], et occupant ainsi un minima d'énergie dans des conditions où la force entropique domine. La même inflexion n'a pas été observée pour le l'hélice de poly(*L*-lysine), à cause de

interactions hydrophobes entre des chaînes latérales que inhibent la formation d'une structure intermédiaire et par conséquent stabilisent l'hélice.

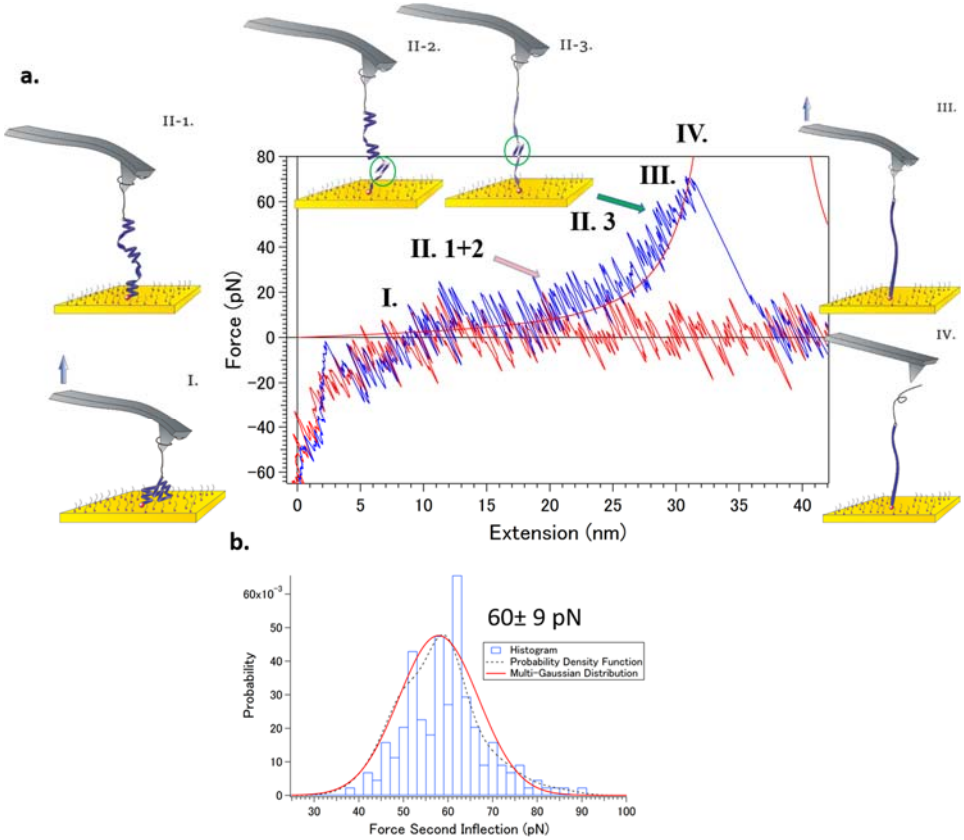

Figure 7. Courbes de force-extension pour le PEG_{114}-*b*-poly(*L*-acide glutamique)(2-pyridyl disulfure)$_{85}$ dans une conformation hélice où une seconde inflexion à une force plus élevée a été observée en plus de la première inflexion à ≈20pN, et l'histogramme correspondant, la fonction de densité de probabilité et la distribution gaussienne de la deuxième inflexion. a.) Un profil de force-extension typique montrant la première inflexion (flèche pourpre) et la deuxième inflexion (flèche verte) et les diagrammes correspondants représentent une interprétation des événements pendant le cycle force-extension. b.) Histogramme, fonction de densité de probabilité et distribution gaussienne de la seconde force d'inflexion 60 ± 9 pN (± d, n = 177).

La différence entre les forces de dépliement de ces deux hélices, et la probabilité de déploiement d'une hélice complète a été attribuée à l'hydrophobie différente des chaînes latérales. L'hélice de poly(*L*-lysine), a été stabilisée en raison de la plus grande hydrophobie des chaînes latérales, ce qui entraîne une augmentation des interactions entre les chaînes latérales et par allieurs l'encombrement stérique qui inhibe les fluctuations hélice-serpentin. Même quand on n'a pas observé de plateau parfait, le plateau incliné a mis en évidence les interactions de stabilisation même pour une structure partiellement hélicoïdale.

Dans une expérience de suivi de la solubilité des chaînes latérales du poly(*L*-lysine), l'hélice a été promu en augmentant légèrement la concentration de NaCl. À la place des plateaux, seulement de petites inflexions à 17 ± 4 pN ont été observées. La force d'inflexion a été remarquablement similaire à l'inflexion de l'hélice de poly(*L*-acide glutamique). Ainsi, nous concluons qu'une force minimale de ≈20 pN est nécessaire pour rompre la liaison hydrogène qui maintient l'hélice et que cette force a été obtenue dans des conditions où les interactions des chaînes latérales étaient minimes.

La présence de plateaux ou inflexions sur les forces correspondantes démontre qu'une force qui se déroule indépendamment de la longueur de l'hélice est nécessaire, ce qui supporte un mécanisme de dépliement tour-par-tour, qui avait été prédit théoriquement [4].

Pour les expériences utilisant PEG_{114}-*b*-poly(*L*- lysine)$_{134}$-*b*-PEG_{114}, seul un faible nombre de courbes force-extension de bonne qualité ont été obtenues en raison d'une forte possibilité d'interaction entre le polypeptide et les segments de PEG. Malgré l'incorporation d'une longueur de séparation supplémentaire, il est difficile d'obtenir des interactions favorables avec un système reposant sur une adsorption simultanée favorable de la molécule sur la pointe et la surface. Néanmoins les inflexions observées à 28 ± 9 pN et à ≈ 18 pN correspondaient à la force des plateaux et des inflexions obtenues aux mêmes deux concentrations de NaCl pour le copolymère biséquencé. Une inflexion au lieu d'un plateau a été observée à la même force, ce qui indique un système partiellement hélicoïdal.

Des études préliminaires ont été effectuées sur le système de PEG_{114}-*b*-poly(*L*-Lysine)$_{134}$-(2-pyridyl disulfure) en adoptant vraisemblablement une conformation β après une traitement thermique. La transition α–β a été suivie par dichroïsme circulaire et la transition a été trouvée pour des conditions de pH ≥ 11, et pour des températures supérieures à 50 °C. La majorité de la transition conformationnelle a été trouvée dans les première 10 minutes de chauffage de la molécule. Après refroidissement et au repos pendant 72 heures, la β -forme n'a pas été maintenue, à la place, il a été suggéré qu'une structure intermédiaire a été formée, qui avait des caractéristiques des deux structures alpha hélicoïdales et feuillet ß.

Au cours de simples expériences de spectroscopie de force, une force beaucoup plus élevée de ≈ 70 pN a été obtenue, ce qui suggère la formation d'une interaction similaire au feuillet β. Il n'est toutefois pas encore certain que la β-interaction a bien eu lieu sur toute la longueur du polypeptide ou plutôt une structure comme une épingle à cheveux β a été formée impliquant seulement quelques résidus.

Finalement, en comparant les deux modèles expérimentaux étudiés représentés par les systèmes de copolymères biséquencé et triséquencé, on a trouvé que le copolymère biséquencé contenant le 2-pyridyl disulfure offrait un système beaucoup plus contrôlé pour des expériences de spectroscopie de force à une seule molécule. Ceci est dû à une extrémité de la molécule étant fixée à la surface par liaison chimique et à l'absence d'un segment PEG supplémentaire qui pourrait former des interactions disruptives avec le segment polypeptidique.

Les perspectives en ce qui concerne les travaux présentés sont d'obtenir d'une part plus de données expérimentales afin de consolider notre hypothèse concernant la formation de feuillet β. Dans le futur, la possibilité de changer la température directement *in situ*, et la conduite des expériences de molécule unique directement à des températures élevées est recommandée. En plus, effectuer des expériences de pulling-relaxing sur les deux structures secondaires nous permettra de déterminer la réversibilité des interactions dans le temps de l'expérience de la molécule unique. Une prolongation intéressante de ce projet consisterait à maintenir les polypeptides entre la pointe et la surface alors qu'une transition dans la structure secondaire est induite, permettant la mesure directe du travail effectué par la molécule pendant la transition. Cependant, une nouvelle conception de l'expérience serait probablement nécessaire lorsque la molécule est chimiquement liée à la pointe ainsi que la surface. La réalisation de cette expérience par adsorption seule serait extrêmement difficile à juger par la faible force du détachement de la chaîne de PEG à partir de la pointe (≤ 80 pN) pour une grande majorité des courbes observées au cours de cette étude.

Il est également important de garder à l'esprit la limitation de l'approche actuelle. Bien que des expériences de force sur molécule unique en utilisant un microscope à force atomique est l'une des très rares techniques qui nous permettent de sonder les propriétés mécaniques d'une seule molécule à la fois en temps réel et in situ, cette approche est intrinsèquement différente de celle observée *in vivo*. L'extension mécanique avec un microscope à force atomique modifie le paysage énergétique ainsi que la distribution et la structure des intermédiaires, qui ne sont pas à l'équilibre. Même lors du dépliage des molécules qui sont impliquées mécaniquement dans des systèmes *in vivo*, de la géométrie et de la manière à laquelle la force est appliquée seront différentes dans un cadre expérimental artificiel.

L'avantage d'une expérience sur molécule unique est que le comportement d'une seule molécule isolée dans un environnement contrôlé peut être observé. Différentes sous-populations peuvent être mises en évidence, révélant des sous-structures, mais il est également possible de mettre en évidence différents comportements de la même molécule. Pour déterminer le comportement moyen

pertinent à un ensemble de molécules, de nombreuses expériences doivent être menées afin d'obtenir un comportement récurrent et reproductible qui décrit le comportement moyen de la molécule d'intérêt. Par conséquent, pour tirer une conclusion, il faut obtenir un nombre statistiquement pertinent de courbes force-extension et leur détermination est soumise au jugement du chercheur. Deuxièmement, bien que la spectroscopie de force de la molécule unique est une technique puissante qui nous permet de sonder et traiters des molécules simples, il est important de rappeler que les comportements qui se déroulent obtenus ne sont pas parfaitement comparables à la molécule dans un cadre *in vivo*, mais sert simplement à fournir une estimation probable de son comportement réel.

Enfin, les polymères-polypeptides stimuli-sensibles sont extrêmement polyvalents et ont été utilisés avec succès comme des systèmes modèles artificiels pour observer des structures secondaires isolées en hélice α et feuillet ß par spectroscopie de force à l'échelle de la molécule unique. L'importance des interactions entre les chaînes latérales dans la stabilisation de la structure en hélice a été démontrée à notre connaissance pour la première fois *in situ* à l'échelle de la molécule unique. Nous suggérons également que les mêmes interactions de chaînes latérales qui stabilisent l'une hélice inhibent également la formation d'une interaction en épingle à cheveux β intermédiaire lorsque le polypeptide est déformé mécaniquement, ce qui a été également été prédit dans la littérature [3].
Nous pensons qu'une telle stratégie d'investigation comme démontrée dans cette thèse par l'examen des propriétés mécaniques des structures secondaires simples facilitera sans doute la compréhension de systèmes protéiques plus complexes.

Références

1. K. Torabi and G. C. Schatz, *Macromolecules*, 2013, **46**, 7947-7956.
2. Z. Qin, A. Fabre and M. J. Buehler, *The European Physical Journal E*, 2013, **36**, 1-12.
3. F. Ding, J. M. Borreguero, S. V. Buldyrey, H. E. Stanley and N. V. Dokholyan, *Proteins: Structure, Function, and Bioinformatics*, 2003, **53**, 220-228.
4. R. Rohs, C. Etchebest and R. Lavery, *Biophysical Journal*, 1999, **76**, 2760-2768.

Acknowledgements

First and foremost I would like to thank my advisors Prof. Dr. Anne-Sophie Duwez and Prof. Dr. Sébastien Lecommandoux for allowing me to conduct this thesis under their joint supervision. Thank you for your guidance, support and words of encouragement. It was an honor and pleasure to have had the opportunity to learn from you.

I would also like to thank the members of my jury, Prof. Dr. André Matagne, Prof. Dr. David Alsteens, Dr. Mathieu Surin, Dr. Olivier Sandre and Dr. Nicolas Willet for your time, for evaluating my work and for travelling all the way to my defense.

Members of Nanochem: A special thank you to Nicolas for helping me the first days in Liège, and the valuable scientific input. Tiziana, I would have not managed without your moral support and scientific guidance. Perrine, Anastasia, Fouzia, Coralie, Arnaud, for all the good times in the lab although you left too soon! My newest officemates Sandrine, Damien, Floriane, thank you for listening to my complaints and worries, the French lessons and of course your scientific feedback. Andrea, thank you so much for the coffee breaks, cigarettes and discussions.

Members of LCPO: Anne-Laure, Paul, Manu, Loïc Petrault, Tuyen, Cony, Lucas, Maud, Ariane, An, Annie, Gauvin, Helene, Laura thank you for the great lab/office spirit. Camille, I appreciate very much that you let me stay at your place during all those months. Valérie, Elisabeth, Jeff, Christophe, Olivier, and Stéphane for the valuable scientific advice and additional guidance.

To all my friends who have a special place in my heart: Edgar for sticking through with me for all the good times and bad. Mathilde W.-M for the literary escapes, Maya for the words of encouragement. Thank you to my favourite accomplices Kévin, Romain, Colin, Nico (the SEC master), Silvia for teaching me, Anna für die gute Laune, Rosine and Yannick for the dinner parties, and the juicy gossip, Loïc Pichavant and William for the cocktail nights, and Floraine for the shoulder to lean on.

Réka for not letting me give up and being always there for me, James, Marie de Paris, Vincent, Marco, Cristian, Sara, Olivier. D for making my Liège life just brilliant, Zéila and Matthieu, my older and wiser friends who offered much needed advice in times of need. Chloi for always cheering me up, Mano and Dimitri for creative distractions.

Ira for letting me know there is a light at the end of the tunnel, Vilasini for the breath of fresh air, Nils for the laughs and reminding me that there is more to

life, István for the unwavering support, Katharina for the positive energy and love, Chrissie and Stefan for the much-needed catch-ups.

A special thank you to my brilliant high school science teachers, Mr. Zulauf for fostering a lifelong love for the sciences, and Mr. Gagner, for always encouraging me.

To Grandpa Bob, Liz, Claudia, Anette, Andrea, and Antonia. Thank you for being my loving Munich family and always reminding me that I have a second home to visit. Ich hab euch sehr lieb.

寒川先生、生化学部の宮里先生、森先生、美和先生、吉田先生、海谷先生、日野先生、細田先生、大山さん、皆様のおかげでここまでこれました。たいへん感謝してます。

Κυρία Oly, Κύριε Giorgo, my dear Zoi, Vangeli, little Maria and Giorgo thank you for welcoming me in to your family, I miss you and I will see you very soon.

Στο Νίκο μου. Σε ευχαριστώ για την υποστήριξη, την υπομονή και την αγάπη σου. Χωρίς εσένα δεν θα τα είχα καταφέρει. Σ' αγαπώ.

パピー、マミー、サユ、ここまで来れたのはみんなのサポートがあったからだよ。本当に感謝してるし、ありがたい気持ちでいっぱいだよ。パピー、マーの教育のためにいつも一生懸命頑張ってくれてありがとう。無理してても高い学費とか出してくれたことはちゃんと知ってるよ。心から本当にありがとう。

Thank you with love,

-Your Marie

実るほど頭を垂れる稲穂かな

Minoru hodo kobe wo tareru inaho kana

The boughs that bear the most hang the lowest[1]

[1] Japanese proverb: Literally translated as, the more fruit (or rice grains) that a bough bears, the heaver it will become and as a result will hang lower than the rest. The figurative meaning is that the greater the success and the greater the knowledge you attain, the more humble you become. The more you know, the more you know that there is so much you do not know. The more successful, the more you know that your success was not just a product of your own hard work, but was made possible due to the support of those around you.

General Table of Contents

Introduction and Objective of the Thesis

Contents

Protein Folding and the Importance of Studying Secondary Structure Formation. Why a Bottom-up Investigation Should be Considered.

Proteins govern the most essential and fundamental processes needed to maintain life including DNA replication, transcription, maintaining a basic metabolic pathway, and controlling cellular transport processes [1, 2]. If such essential biological processes are governed by proteins it is not surprising that a wide range of debilitating illnesses result from an error in its constitution. The misfolding of proteins and subsequent aggregation thereof, are thought to be the unifying cause and pathological mechanism behind a variety of neurodegenerative diseases including, but not limited to Alzheimer's disease, Parkinson's disease, Huntington's disease, and transmissible spongiform encephalopathies [3]. As there is a strong correlation between protein misfolding and disease, to uncover the mechanisms by which a protein can successfully fold and remain folded is crucial to the understanding and the prevention of these diseases.

The mechanism of protein folding is very complex, and cannot be simply justified by a simple random search where a polypeptide chain samples all possible conformations before arriving at one thermodynamically stable state. This is highlighted clearly by the Levinthal's paradox, which points out the glaring discrepancy between the actual time of protein folding (well within a second) compared with the estimated amount of time it would take if a protein with 100 residues were to fold by randomly accessing just two of the low energy regions in the Ramachandran plot (10^{30} main-chain conformations $\approx 10^{11}$ years) [4]. Instead, the protein is thought to fold by arriving at its lowest energy structure though following various pathways, where it undergoes a stochastic search of conformations [5] from those that are inherently the most accessible to the polypeptide chain based on favoured interactions between key residues. Therefore, these interactions are suggested to be relevant to the principles of statistical mechanics and polymer physics, as well as classical chemical dynamics [6]. The structural properties of intermediates suggest that proteins fold in modules largely independent of different domains and other segments [4, 6-8]. The interaction of a small number of key residues by non-covalent bonding forms a rudimentary scaffold similar to the native architecture allowing the rest of the molecule to condense around it [9]. The scaffold consists of the initial rapid formation of local secondary α-helix and β-sheet structures [4, 7].

As protein folding takes place by the initial preferential folding of local secondary structures, an in-depth investigation into the folding and unfolding of these secondary structures on the single molecule scale might further the understanding of the stability of these structures and the mechanisms behind the transitions. This is especially relevant if we consider that a combination of α-helices and β-sheets is found in nearly every native protein [6].

A mechanical investigation is suggested to be even more relevant due to the fact that *in vivo* polypeptides rarely fold without the aid of molecular chaperones. Molecular chaperones are crucial entities involved in maintaining proteostasis as not only do they mechanistically choreograph the folding of *de novo* proteins, but they are also involved in the maintenance of its active conformation by preventing the aggregation of misfolded proteins and mediating their refolding. When all else fails the chaperones also target and recognize misfolded proteins for degradation [10]. It can therefore be said that proteostasis is maintained on the basis of the mechanical interactions of chaperones with proteins, thus the study of how fundamental secondary motifs react to a mechanical force could provide further insight behind protein stability, folding and refolding. It is hoped that by deepening the understanding of the behaviour of isolated α-helices and β-sheets, the more complex protein systems which are composed of a combination these fundamental blocks can be further understood.

Biohybrid Materials

Despite the increase in complexity and variety of purely synthetic monomers, the resulting supramolecular assemblies still remain primitive in comparison to the multiple hierarchical levels accessible in biological systems [11]. This is especially true if we consider the enormous structural variety that is available in nature despite a limited number of available assembly blocks. For instance, all natural proteins are a combination of only 20 different amino acids, and DNA encodes all of the biological information crucial to the existence of an organism with just a combination of four different bases [11]. This argument has been summarized excellently by Lecommandoux [12] and Börner [11] **(Figure 1 a and b.)** who have depicted this disparity. New biohybrid materials are then anticipated to bridge this gap as it allows the development of materials that combine the enormous assortment and high synthetic control of synthetic systems with the functional complexity of biological systems.

The conjugation of synthetic and biological parts allows the synthesis of new materials with properties not available in any individual system. Most importantly it allows the precise selection, control and reproduction of specific attributes. Although biohybrids are still quite crude, especially when considering the still insufficient incorporation of biofunctionality, trends indicate that these materials are becoming increasingly sophisticated and it is a matter of time before new materials are synthetized which can fully benefit from the overlapping of both worlds.

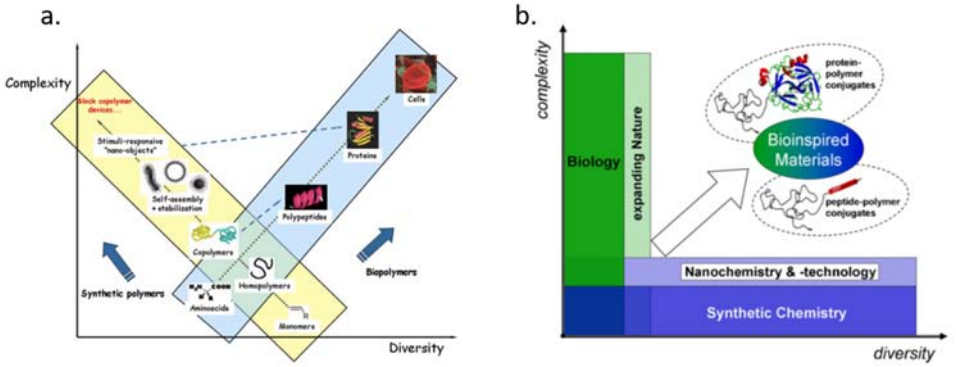

Figure 1.a and b. A comparison between the advantages of biological versus synthetic systems and how the development of bioinspired materials can combine the complexity afforded to biological systems with that of the diversity available for synthetic systems. These diagrams were adapted from **a.)** Lecommandoux [12].and **b.)** Börner [11] *Please note that polymer-oligosaccharides and polymer-oligonucleotides and other categories of bioinspired materials are not highlighted as emphasis will be on peptide-polymer hybrids).*

Biohybrid Polymersomes as Advanced Biofunctional Mimics for Natural Membranes

Biohybrid polymer vesicles or "polymersomes" are excellent examples demonstrating the overall aim of developing new materials by combining natural and synthetic components to create materials that are tailored to meet our specific demands. These systems are considered mimics for natural membranes [13], and in the following examples their increasing sophistication and incorporation of properties normally attributed to purely biological systems such as biotargeting and selective membrane permeability are shown.

Hybrid vesicles have been made from blending synthetic block copolymers with lipids to create hybrid lipid/polymer vesicles which have enhanced stability due to the incorporation of the synthetic polymer, yet retain many biologically relevant properties pertaining to natural lipid membranes [14]. Especially significant is the demonstration of molecular recognition between successfully imbedded GM1 membrane receptors in these hybrid membranes and a cholera toxin B protein [15].

In another strategy polymersomes have been assembled that were composed of amphiphilic systems made from synthetic polymers conjugated to a biologically relevant segment. The lack of permeability of these systems due to the hydrophobic nature of the membranes has been addressed through the synthesis of a semipermeable polymer vesicle formed by a polyion complex membrane (PICsomes) [16], which were shown to be permeable to small solutes while successfully segregating larger solutes.

Copolypeptides and polysaccharide-*b*-polypeptides containing synthetic polypeptides are not strictly biohybrid materials, however synthetic polypeptides, especially those that are chemically protected, are considered neither purely biological, nor synthetic and are thought to be an intermediate case [17]. Dextran-*b*-poly(γ-benzyl *L*-glutamate) vesicles [18] have been developed to mimic glycoproteins which are important integral membrane proteins allowing cell-cell recognition. In poly(γ-benzyl *L*-glutamate)$_{23}$-hyaluronan$_{10}$ the hyaluronan segment is a structurally relevant hydrophilic segment of the vesicle, but was also shown to function as a ligand that specifically targets a transmembrane glycoprotein CD44 found overexpressed in cancer cells [19]. Similarly, in poly(*L*-arginine)$_{60}$-*b*-poly(*L*-leucine)$_{20}$, the arginine is a structural component, but also mimics the arginine rich protein-transduction domains [20] which resulted in enhanced intracellular delivery of the formed vesicles.

Can Polymer-polypeptide Biohybrid Materials be Utilized as Model Artificial Systems?

Despite the fabrication of increasingly sophisticated new hybrid materials, to which extent can these systems be considered to behave analogous to the natural systems they are asserted to mimic? Can we utilize them as simplified models to isolate components from biological systems in order to study specific interactions in a controlled experimental setting? These questions are especially important to address as synthetic polymer-polypeptides will be utilized in later chapters as a

model system in a bottom-up investigative strategy to elucidate the mechanical properties of secondary structures.

Polypeptide-based copolymers have already been mentioned as a simplified model to study generic self-assemblies and interactions seen in natural proteins [21]. The parallel between synthetic polymers and natural systems is continuingly evident how individual monomers function as building blocks that determine the final supramolecular organization, analogous to amino acids and how they influence the formation of secondary conformations, which are then organized into tertiary and quaternary arrangements.

Synthetic polypeptide copolymers are indeed able to self-assemble into hierarchical structures which is the hallmark of natural protein organization.

α-helices and helix-coil transitions in response to pH have been observed in a numerous variety of poly(*L*-lysine) and poly(*L*-glutamic acid) containing block copolymers [22-30]. Furthermore in poly(butadiene)$_{107}$-*b*-poly(*L*-Lysine)$_{27}$ [31], the poly(*L*-lysine) chains in the corona were shown to undergo an additional transition from an α-helix to a β-sheet structure at high temperatures, and well-defined β-sheet structures were assembled with poly(acrylic acid)-*b*-poly(*L*-valine) [32].

Important tertiary motifs such as coiled-coils were observed for diblock copolymers containing PEG (polyethylene glycol) and a coiled-coil forming heptad repeating sequence $(abcdefg)_n$ [33-35]. The synthetically produced coiled-coils were utilized as a model in order to study the change in the self-assembly properties as a result of manipulating the sequence and pH [35].

The utilization of synthetic systems to study the aggregation mechanism of β-sheets into highly organized amyloid-like fibrils, might be even more compelling as these aggregates have been suggested to form by a generic mechanism [6, 36] and therefore more easily modelled by a synthetic system. Significantly a *de novo* α-helix-turn-α-helix peptide [37] and a poly(γ-methyl *L*-glutamate) grafted-polyallyamine system [38] were synthesized with the specific intent to utilize them as model systems to investigate the mechanistic features behind the intermolecular associations and conformational transitions [37] underlying the formation of amyloid-like fibrils.

Lastly, the similarity between synthetic polymers and natural polypeptides is further supported by an inverse example, where natural amyloid fibrils have been found to form spherulites [39], which is a property traditionally associated with linear, synthetic polymers such as polyethylene. This indicates that natural polypeptide chains can also behave analogous to synthetic polymers when partially denaturing [39, 40] .

A large range of biohybrid materials have been created which have conjugated properties traditionally separated into those pertaining to either synthetic or biological systems. However, synthetic polypeptides have been also shown to accurately mimic the secondary, tertiary and quaternary conformations observed in nature. The utilization of easily tailored biohybrid conjugates as model artificial systems has been done in the past, and no doubt as the complexity of synthetic systems will improve, this strategy will be increasingly adopted in the future. The use of hybrid systems as biological models allows the isolation of properties and the exact control of experimental conditions, which makes this strategy extremely beneficial.

Objective of the Thesis

Proteins fold by the initial preferential folding of local secondary structures [4, 5]. Then the understanding of the mechanistic properties of basic α-helix and β-sheet secondary structures could prove to be crucial to further the understanding of more complex protein systems. Despite previous investigations into the unfolding behaviour of single α-helices [41-43], no agreement concerning its force-extension behaviour has been obtained so far, and the study of the mechanistic properties of a single intramolecular β-interaction is to our knowledge unprecedented.

The aim of this investigation is to study the mechanochemical behaviour of basic α-helix and β-sheet secondary structures by utilizing poly-(*L*-glutamic acid) and poly-*(L*-lysine) containing block copolymers as model systems that are able to exhibit stimuli-responsive conformational transitions under differing pH and temperature conditions.

For the purpose of this investigation, diblock copolymers of poly(ethylene glycol)$_{114}$-*b*-poly(*L*-lysine)$_{134}$-(2-pyridyl disulphide) **(PEG$_{114}$-*b*-(PLys)$_{134}$-(2-pyridyl disulphide) (Figure 2 a.)** and poly(ethylene glycol)$_{114}$-*b*-poly(*L*-glutamic acid)$_{85}$-(2-pyridyl disulphide) (**PEG$_{114}$-*b*-(PGA)$_{85}$-(2-pyridyl disulphide**) **(Figure 2 b.)** were custom designed and synthesized to investigate and to compare the unfolding behaviour of their respective α-helical structures through single molecule force spectroscopy. In addition β-sheet-like interactions formed by poly(*L*-lysine) were investigated as α−β transitions occur at elevated temperatures. Such diblock systems have been synthesized in the past, however the utilization of these as a model system to observe their characteristic unfolding behaviours is entirely novel.

A novel triblock copolymer of poly(ethylene glycol)$_{114}$-*b*-poly(*L*-lysine)$_{134}$-*b*-poly(ethylene glycol)$_{114}$ **(PEG$_{114}$-*b*-(PLys)$_{134}$-PEG$_{114}$) (Figure 2 c.)** has also been synthesized to investigate the effect of adding another separation length, but also to study a different experimental design and immobilization strategy that depends solely on the adsorption of the molecule as opposed to chemically bonding the molecule onto the surface which is the strategy adopted for the diblock copolymers.

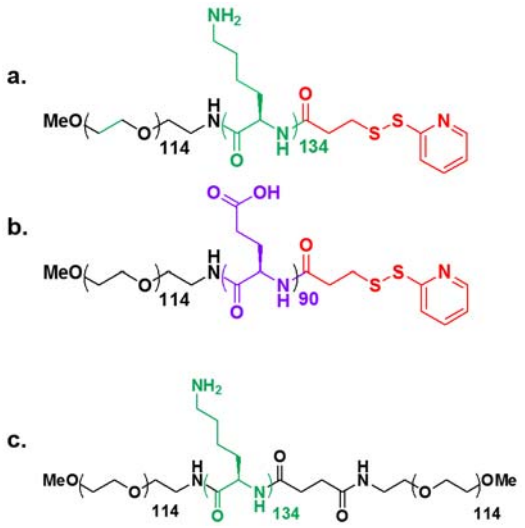

Figure 2. Chemical Structures of a.) poly(ethylene glycol)$_{114}$-*b*-poly(*L*-lysine)$_{134}$-(2-pyridyl disulphide), b.) poly(ethylene glycol)$_{114}$-*b*-poly(*L*-glutamic acid)$_{85}$-(2-pyridyl disulphide) and c.) poly(ethylene glycol)$_{114}$-*b*-poly(*L*-lysine)$_{134}$-*b*-poly(ethylene glycol)$_{114}$

References

1. X. Zhang, M. L. Acencio and N. Lemke, *Frontiers in Physiology*, 2016, **7**, 75.
2. C. Buddhapriya and L. Alex, *Physical Review E*, 2005, **71**.
3. C. Soto, *Nat Rev Neurosci*, 2003, **4**, 49-60.
4. A. R. Dinner, A. Sali, L. J. Smith, C. M. Dobson and M. Karplus, *Trends in Biochemical Sciences*, 2000, **25**, 331-339.
5. S. W. Englander and L. Mayne, *Proceedings of the National Academy of Sciences*, 2014, **111**, 15873-15880.
6. C. M. Dobson, *Nature*, 2003, **426**, 884-890.
7. V. Daggett and A. Fersht, *Nat Rev Mol Cell Biol*, 2003, **4**, 497-502.
8. M. Karplus and D. L. Weaver, *Nature*, 1976, **260**, 404-406.
9. A. R. Fersht, *Proceedings of the National Academy of Sciences*, 2000, **97**, 1525-1529.
10. E. K. Yujin, S. H. Mark, B. Andreas, H.-H. Manajit and F. U. Hartl, *Annual Review of Biochemistry*, 2013, **82**, 323-355.
11. H. G. Börner, *Progress in Polymer Science*, 2009, **34**, 811-851.
12. J. Rodriguez-Hernández, F. Chécot, Y. Gnanou and S. Lecommandoux, *Progress in Polymer Science*, 2005, **30**, 691-724.
13. B. M. Discher, Y.-Y. Won, D. S. Ege, J. C. M. Lee, F. S. Bates, D. E. Discher and D. A. Hammer, *Science*, 1999, **284**, 1143-1146.
14. M. Schulz and W. H. Binder, *Macromolecular Rapid Communications*, 2015, **36**, 2031-2041.

15. M. Schulz, S. Werner, K. Bacia and W. H. Binder, *Angewandte Chemie International Edition*, 2013, **52**, 1829-1833.
16. A. Koide, A. Kishimura, K. Osada, W.-D. Jang, Y. Yamasaki and K. Kataoka, *Journal of the American Chemical Society*, 2006, **128**, 5988-5989.
17. T. Borase and A. Heise, *Advanced Materials*, 2016, **28**, 5725-5731.
18. C. Schatz, S. Louguet, J.-F. Le Meins and S. Lecommandoux, *Angewandte Chemie International Edition*, 2009, **48**, 2572-2575.
19. K. K. Upadhyay, J. F. L. Meins, A. Misra, P. Voisin, V. Bouchaud, E. Ibarboure, C. Schatz and S. Lecommandoux, *Biomacromolecules*, 2009, **10**, 2802-2808.
20. E. P. Holowka, V. Z. Sun, D. T. Kamei and T. J. Deming, *Nat Mater*, 2007, **6**, 52-57.
21. H.-A. Klok and H. Schlaad, in *Peptide Hybrid Polymers*, Springer Berlin Heidelberg, Editon edn., 2006, vol. 202, pp. 53-73.
22. J. Babin, J. Rodriguez-Hernandez, S. Lecommandoux, H.-A. Klok and M.-F. Achard, *Faraday Discussions*, 2005, **128**, 179-192.
23. H. Kukula, H. Schlaad, M. Antonietti and S. Förster, *Journal of the American Chemical Society*, 2002, **124**, 1658-1663.
24. F. Chécot, A. Brûlet, J. Oberdisse, Y. Gnanou, O. Mondain-Monval and S. Lecommandoux, *Langmuir*, 2005, **21**, 4308-4315.
25. F. Chécot, S. Lecommandoux, Y. Gnanou and H.-A. Klok, *Angewandte Chemie International Edition*, 2002, **41**, 1339-1343.
26. H. Gao, G. Li, Z. Hu, Z. Xiao, G. Liang and Q. Wu, *Polymer*, 2014, **55**, 4593-4600.
27. R. Sigel, M. Losik and H. Schlaad, *Langmuir*, 2007, **23**, 7196-7199.
28. K. E. Gebhardt, S. Ahn, G. Venkatachalam and D. A. Savin, *Langmuir*, 2007, **23**, 2851-2856.
29. S. S. Naik, J. G. Ray and D. A. Savin, *Langmuir*, 2011, **27**, 7231-7240.
30. J. G. Ray, S. S. Naik, E. A. Hoff, A. J. Johnson, J. T. Ly, C. P. Easterling, D. L. Patton and D. A. Savin, *Macromolecular Rapid Communications*, 2012, **33**, 819-826.
31. K. E. Gebhardt, S. Ahn, G. Venkatachalam and D. A. Savin, *Journal of Colloid and Interface Science*, 2008, **317**, 70-76.
32. A. Sinaga, T. A. Hatton and K. C. Tam, *Biomacromolecules*, 2007, **8**, 2801-2808.
33. G. W. M. Vandermeulen, D. Hinderberger, H. Xu, S. S. Sheiko, G. Jeschke and H.-A. Klok, *ChemPhysChem*, 2004, **5**, 488-494.
34. M. Pechar, P. Kopečková, L. Joss and J. Kopeček, *Macromolecular Bioscience*, 2002, **2**, 199-206.
35. G. W. M. Vandermeulen, C. Tziatzios, R. Duncan and H.-A. Klok, *Macromolecules*, 2005, **38**, 761-769.
36. F. Ding, N. V. Dokholyan, S. V. Buldyrev, H. E. Stanley and E. I. Shakhnovich, *Journal of Molecular Biology*, 2002, **324**, 851-857.
37. Y. Fezoui, D. M. Hartley, D. M. Walsh, D. J. Selkoe, J. J. Osterhout and D. B. Teplow, *Nat Struct Mol Biol*, 2000, **7**, 1095-1099.
38. T. Koga, K. Taguchi, Y. Kobuke, T. Kinoshita and M. Higuchi, *Chemistry – A European Journal*, 2003, **9**, 1146-1156.
39. M. R. H. Krebs, E. H. C. Bromley, S. S. Rogers and A. M. Donald, *Biophysical Journal*, 2005, **88**, 2013-2021.
40. C. Fabrizio and M. D. Christopher, *Annual Review of Biochemistry*, 2006, **75**, 333-366.

41. R. Afrin, I. Takahashi, K. Shiga and A. Ikai, *Biophysical Journal*, 2009, **96**, 1105-1114.
42. A. Idiris, M. T. Alam and A. Ikai, *Protein Engineering*, 2000, **13**, 763-770.
43. M. A. Lantz, S. P. Jarvis, H. Tokumoto, T. Martynski, T. Kusumi, C. Nakamura and J. Miyake, *Chemical Physics Letters*, 1999, **315**, 61-68.

Chapter 1
Background and Related Work

Contents

Introduction

In this chapter selected works relevant to synthetic polymer-peptides from two perspectives are introduced as well as background information concerning the techniques and characterization methods utilized in later chapters.

In Part I relevant work concerning poly-*L*-glutamic acid and poly-*L*-lysine-based block copolymers are discussed from which the versatility of these systems can be appreciated from a polymer chemist's point of view.

This is followed by Part II where circular dichroism and dynamic light scattering techniques are introduced, which were utilized for the characterization of the block copolymers in the experimental sections in later chapters.

In Part III relevant work concerning single molecule force spectroscopy of α-helices are introduced, followed by a selection of theoretical works where the structure, and the behaviour of such structures under extension are investigated. In this section the helix-coil theory is also briefly introduced as a basic understanding thereof is vital to the prediction of the basic behaviour of α-helices.

Finally in Part IV the AFM equipment, the principles of single molecule force spectroscopy, and fundamental models that predict the elastic behaviour of ideal polymers, PEG and a generic polypeptide are introduced.

PART I:
Peptide-synthetic Hybrid Block Copolymers

Block copolymers have an incredible range of applications [1] including but not limited to, cosmetics [2], photovoltaics [3], thin films [4, 5], coatings [5], nanoporous membranes [6], nanomedicine, and targeted drug and gene delivery systems [7, 8]. Amphiphilic block copolymers have emerged as a particularly fascinating class of polymers as their hydrophilic and hydrophobic elements allow them to self-assemble into various morphologies such as micelles, rods, and vesicles. Polymer vesicles or "polymersomes" were first named in analogy to liposomes [8, 9], and are considered as new generation of nanomedicine and model systems for biological membranes [10].

The development of peptide-based block copolymers is especially significant in that it combines the properties pertaining to polypeptides with that of synthetic polymers. Purely synthetic stimuli responsive polymers are only able to undergo coil to globule transitions [11] whereas polypeptides are able to undergo

a secondary conformational transition depending on changes in pH temperature, and solvent conditions. They are also able to assemble into complex hierarchical structures when single peptides interact non-covalently through ionic, hydrophobic, hydrogen bonding and π stacking interactions [12]. By creating hybrid polymer-peptide structures it is hoped to harness the superior supramolecular assembly of peptides to diversify the self-assembly structures. The inclusion of a polypeptide segment also largely contributes to biocompatibility, and biofunctionality [13] making them especially suitable for biomedical applications such as drug and gene delivery systems.

1.1 Poly(*L*-glutamic acid) and Poly(*L*-Lysine)-based Polypeptide-block Copolymers

One of the first studies on synthetic polymer hybrid polypeptides was done as early as the mid to late 1970s by Gallot [14] who investigated the solid-state structure of polybutadiene-*b*-poly(γ-benzyl-*L*-glutamate) and polybutadiene-*b*-poly(N^5-hydroxypropyl-*L*-glutamine) as well as polybutadiene-*b*-poly(ε-benzyloxycarbonyl-*L*-lysine) and polybutadiene-*b*-(poly-*L*-Lysine) [15]. Nakajima et al. [16, 17] studied synthetic ABA poly(γ-benzyl-*L*-glutamate)-*b*-polybutadiene-*b*-poly(γ-benzyl-*L*-glutamate) systems where they first reported the formation of polymer micelles in organic solvents [18].

Since then field has expanded to studies in aqueous solutions, where the polypeptide is the ionisable entity. Therefore their property to undergo conformational transitions can be harnessed permitting structures that are sensitive to external factors such as pH and temperature.

1.1.1 Solution Properties of Poly(*L*-glutamic acid)

The well-studied poly(*L*-glutamic acid) is considered a model system to study helix-coil transitions. The conformational transition occurs due to the ionization or deionization of the side chains governed by the pH conditions of the solution. The polypeptide backbone is able to fold into a α-helix when the carboxylic acid moiety is fully protonated at low pH conditions. Therefore the $pK_a \approx 4.5$ value of the carboxylic acid moiety[19] on the glutamic acid side chain gives a good estimation for the pH range of the conformational transition, where typically half of the groups are dissociated. Above this pH the side chains are fully deprotonated, and the random coil structure will be exhibited. Below this pH the polypeptide would adopt the α-helix conformation.

1.1.2 Poly-*L*-glutamic Acid-based Block Copolymers

Pioneering work by Kukula et al. [20] on polybutadiene$_{27\text{-}119}$-*b*-poly(*L*-glutamate)$_{64\text{-}24}$ and Chécot et al. [21, 22] on polybutadiene$_{48}$-*b*-poly(*L*-glutamic acid)$_{20\text{-}145}$ demonstrated that by varying the ratio of hydrophilic to hydrophobic segments of the block copolymer, it is possible to control the morphology of the resulting aggregates which varied from micelles to vesicles.

Typically the helix-coil transition was evidenced by the variation of the hydrodynamic radius in response to pH. The hydrodynamic radius decreased at lower pH due to lower electrostatic repulsion, and the denser packing resulting from the coil to helix conformation change. The block copolymers were shown to be pH responsive even at high salt concentrations of 1 M NaCl [21, 22]. This was significant as electrostatic repulsions are fully screened at 1 M NaCl, thus it could be proven that the change in size originated from the conformational transition and not simply the change in electrostatic repulsion as a consequence of the side chain ionization state. It also demonstrated that the reversible coil-helix transition is able to occur even at high salt conditions.

In a triblock poly(*L*-glutamic acid)-*b*-poly(propylene oxide)-*b*-poly(*L*-glutamic acid) [23] block copolymer, a change in morphology was observed by changing the pH to induce the coil-helix transition of the poly(*L*-glutamic acid) as well as by varying the ratio of hydrophilic to hydrophobic segments. The morphological transition from a micelle at high pH to a vesicle structure at low pH was justified as follows. The folding of the poly(*L*-glutamic acid) into a more compact α-helix structure at low pH effectively decreased the relative area of the hydrophilic segment, thus the free energy penalty was compensated by reducing the interfacial area between the hydrophobic and hydrophilic areas thereby inducing the change in morphology. Therefore, the conformational transition had energetically the same effect as reducing the length of the hydrophilic segment. The block copolymer was also thermosensitive as the poly(propylene oxide) underwent dehydration at higher temperatures and thus the aggregates were shown to decrease in size with increasing temperature [23].

Dual temperature and pH responsive schizophrenic block copolymers epitomize the high level of control that can be attained by taking advantage of opposing solubility properties assigned to the peptide and the synthetic polymer. Notably, poly(*N*-isopropylacrylamide)-*b*-poly(*L*-glutamic acid) [24] was doubly hydrophilic at alkaline pH and room temperature, but assembled into structures with the thermoresponsive poly(*N*-isopropylacrylamide) as the insoluble core and the poly(*L*-glutamic acid) as the corona at elevated temperatures and alkaline

conditions. At acidic pH and at room temperature, the α-helical poly(*L*-glutamic acid) became the hydrophobic core with the poly(*N*-isopropylacrylamide) as the hydrophilic shell.

1.1.3 Solution Properties of Poly-*L*-lysine

Poly-*L*-lysine is capable of exhibiting random coil, α-helix and β-sheet structures [25, 26] depending on differing pH and temperature conditions and is therefore considered an ideal model polypeptide to study conformational transitions. The transition is dependent on the ionization of the amine group of the side chains, which is governed by the pH conditions of the solution. The helix is able to form when the amine group is deprotonated and thus uncharged at alkaline pH conditions. The pK_a ≈10 gives a good indication of the pH of the conformational transition [19]. In self-assembled structures however, local pK_a effects must also be taken into consideration as the close proximity of ionisable groups as well as the core hydrophobicity [1] have been suggested to affect the pK_a value [27]. Nevertheless, typically above pH≈10 the lysine polypeptide adopts the helix conformation, and below this value the random coil conformation would be normally observed.

At alkaline conditions and temperatures of ≥50 °C the β-sheet secondary conformation of poly-*L*-lysine was observed to form. [28-30]

1.1.4 Poly-*L*-lysine-based Block Copolymers

The helix-coil transition of poly-(*L*-lysine) has been investigated in various works and different morphologies ranging from spherical micelles [31, 32], rod-like micelles[27], vesicles[31, 33] and disk micelles [31] were obtained depending on the fraction of the hydrophilic to the hydrophobic block and the secondary conformation of the lysine in response to pH.

The aggregates at higher pH were smaller due to the denser packing of the α-helical structure. In comparison, at low pH the structures were larger due to 1) electrostatic repulsion of the charged lysine side chains, 2) the rigid nature of the peptide bond forcing the chains to extend outwards and 3) the charges created along the chain also drawing in counter-ions creating an osmotic pressure [32]. This was also observed for a polyisoprene$_{49}$-*b*-poly(*L*-lysine)$_{123}$ [34] system where the size of the observed micelles decreased to almost half its size in alkaline conditions where the lysine segment adopted the α-helix conformation. Significantly, although the change in size was not as dramatic, this transition was also observed

at 1 M NaCl demonstrating that the conformational transition was able to take place in response to pH even at high salt conditions.

When the change of the hydrodynamic radius did not obey this trend it suggested that changes in morphology took place in response to pH as a result of the secondary structure of the lysine segment. For instance for poly(*L*-lysine)-*b*-poly(propylene oxide)-*b*-poly(*L*-lysine) [31] the hydrodynamic radius of the aggregates appeared to either remain relatively constant or increase at higher pH conditions, which is the inverse of what is typically expected. Depending on the relative hydrophilic to hydrophobic segment ratio, which varied with the helix-coil transition of the lysine, the triblock underwent a transition from a spherical micelle at low pH to a vesicle or a disk micelle morphology at high pH. In another example, polybutadiene$_{107}$-*b*-poly(*L*-lysine)$_{100}$, and polybutadiene$_{60}$-*b*-poly(*L*-lysine)$_{50}$ [32] copolymers displayed a rod-like micelle morphology at high pH which transitioned into a spherical micelle at low pH.

The temperature-responsive properties of poly(*L*-Lysine) was also exploited in poly(butadiene)$_{107}$-*b*-poly(*L*-Lysine)$_{27}$ [27] where the hydrodynamic radius of the vesicles could be controlled as a function of pH and temperature. The increase in size of the vesicles at high pH and temperature was attributed to interfacial relief as a result of the formation of parallel β-sheet interactions between adjacent lysine corona chains.

Poly(propylene oxide)-*b*-poly(*L*-lysine) [1] was shown to assemble into micelles with the poly(*L*-lysine) as the soluble corona at acidic pH and temperatures above 8 °C. However when temperatures were decreased below 8 °C in alkaline conditions, the poly(*L*-lysine) became increasingly helical and as a result formed the hydrophobic core.

1.1.5 Copolypeptide of Poly-*L*-lysine and Poly-*L*-glutamic acid

Schizophrenic, water-soluble vesicles from poly(*L*-glutamic acid)$_{15}$-*b*-poly(*L*-lysine)$_{15}$ have been studied by Rodriguez-Hernandez and Lecommandoux [35]. At low pH <4 the poly(*L*-glutamic acid) is folded into a α-helix and thus formed the hydrophobic core, while the poly(*L*-lysine) formed the hydrophilic shell. The opposite occurred at basic pH >10 when poly(*L*-lysine) became insoluble due to adopting the α-helical conformation and poly(*L*-glutamic acid) adopted the soluble random coil conformation.

1.2 PEGylation of Poly(*L*-lysine) and Poly(*L*-glutamic acid)

The attachment of poly(ethylene glycol) or the "PEGylation" of polypeptides improves their solubility and stability [36] as well as preventing flocculation, and unspecific interaction with blood components [37]. PEG has low toxicity and longer chains have been shown to prolong the circulation time inside the body [37]. The "stealth effect" of polymeric assemblies can be promoted by the incorporation of PEG as an outer biocompatible shell which makes this strategy very beneficial for drug delivery systems and gene vectors [37]. Some selected works concerning PEG-poly(*L*-glutamic acid) and PEG-poly(*L*-lysine) systems are briefly presented so as to observe how these two systems have been utilized in the context of delivery systems in the past.

1.2.1 PEG-poly(*L*-glutamic acid) Systems

PEG-*b*-poly(*L*-glutamic acid-*co*-*L*-pheylalanine) was developed as a drug delivery system for cisplatin (cis-diaminodichloroplatinum, CDDP) nanoparticles (**Figure 1**), which have exhibited high anti-tumour behaviour, yet also causes a wide range of side-effects due to its toxicity. The cisplatin can be loaded on the carrier through metal conjugation to the carboxyl groups of the glutamic acid unit, while the incorporation of the phenylalanine prevents rapid release, and affords a degree of hydrophobicity which allows the self-assembly of the micelles to take place. The PEG outer layer prevents recognition from the immune system and unspecific protein adsorption. By utilizing this system the side effect of the nanoparticles can be minimized while a sustained and controlled release of the nanoparticles was observed due to an inverse ligand change in an environment with a high concentration of chloride ions [38]

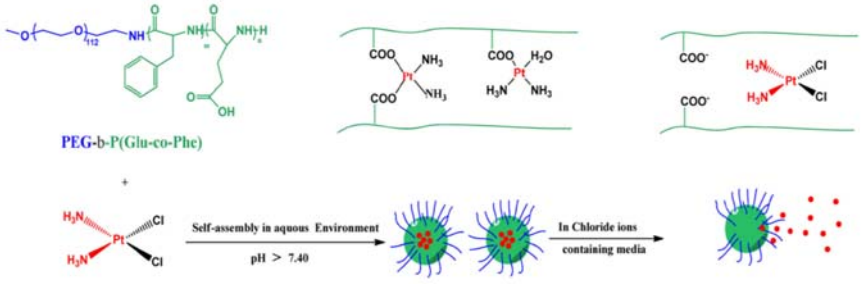

Figure 1. Schematic representation of the preparation of cisplatin loaded PEG-*b*-poly(*L*-glutamic acid-co-*L*-pheylalanine) and mechanism of release. Adapted from a publication by Ahmad et al. [38].

Nanocapsules have been developed in which a hydrophobic anti-cancer drug docetaxel was loaded within an oily core, shielded by a protective layer of PEG-*g*-poly(*L*-glutamic acid) with 57% PEG which was deposited through electrostatic interactions (**Figure 2**)[39]. Nanocapusles have also been prepared where the core is encapsulated by the sequential adsorption of poly(*L*-lysine) and poly(*L*-glutamic acid) polyelectrolytes to from polyelectrolyte multilayer shells. PEG-*g*-poly(*L*-glutamic acid) was utilized in the external layer in order to improve biocompatibility and nonspecific adhesion to cells [40, 41].

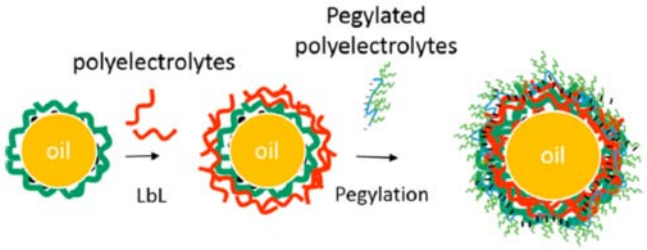

Figure 2. Schematic representation of the formation of polyelectrolyte multilayer nanocapsules where the dark green line indicates the adsorbed positively charged poly(*L*-lysine) and the red line indicates the negatively charged poly(*L*-glutamic acid). Finally the external PEG-*g*-poly(*L*-glutamic acid) is represented by the blue/green line. Adapted from a publication by Lukasiewicz et al. [40]

1.2.2 PEG-poly(*L*-Lysine) Systems

When the lysine segment is in a helical conformation at alkaline pH, PEG_{98}-poly(*L*-Lysine)$_{19}$ was found to assemble into a spherical micelle-like dimer with PEG forming a protective shell around two lysine helices associating with each other in an anti-parallel manner [42]. The incorporation of PEG was found to stabilize the lysine helix though segregation of the folded polypeptide from the aqueous media [42].

Polycations such as poly(*L*-lysine) can associate with DNA through electrostatic interactions and as a result have been investigated as possible gene vectors. PEG-poly(*L*-lysine) was shown to form a spontaneous polyion complex micelles with antisense oligonucleotides [43] and later also with plasmid DNA [44].

A PEG-*b*-poly(*L*-lysine-DOTA) [45] (DOTA= 1,4,7,10-tetra-azacyclododecane-1,4,7,10-tetraacetic acid) was prepared and utilized as a polymeric carrier for a MRI contrast agent (**Figure 3**). The conjugation of DOTA allowed the chelation of gadolinium (III) which is a clinically known contrast agent. The conjugated block copolymer was able to successfully assemble into a micellar structure, however it was not able to form even if a small amount lysine

residues were left unmodified, emphasizing the importance of the strong interaction among conjugated DOTA, which aids the self-assembly [45].

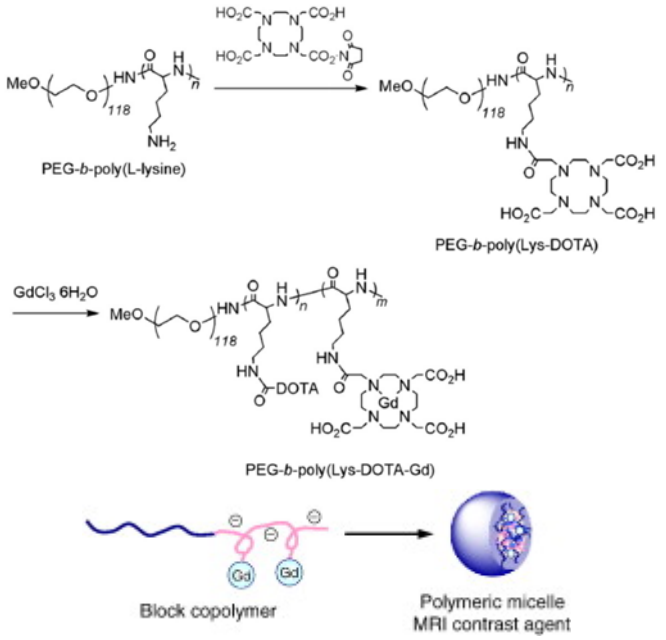

Figure 3. Synthesis of PEG-*b*-poly(*L*-lysine-DOTA-Gd) (Top). Schematic representation of the formation of the micellar structure of PEG-*b*-poly(*L*-lysine-DOTA-Gd) (bottom). Adapted from a publication by Shiraishi et al. [45].

Section Summary: The suitability and novelty of a PEG-poly(*L*-lysine) and PEG-poly(*L*-glutamic acid) as a Model System for Single Molecule Force Spectroscopy Experiments.

In the precedent section, the versatility of poly(*L*-lysine) and poly(*L*-glutamic acid) containing polymeric systems could be appreciated. The morphology of the self-assemblies was mostly regulated by the relative composition of the block copolymers. Most importantly the incorporation of the polypeptide segments allowed the acquisition of stimuli-responsive control based on harnessing the intrinsic property of the polypeptides which underwent secondary conformational transitions from α-helix-coil and α-helix-β-sheet depending on differing pH and temperature conditions.

When these polypeptides were conjugated to PEG, they offered highly biocompatible systems which could be incorporated in functional delivery systems for a variety of materials such as nanoparticles, hydrophobic drugs, oligonucleotides and metal ions.

Finally, we would like to mention that although PEG-*b*-poly(*L*-glutamic acid) and PEG-*b*-poly(*L*-Lysine) systems are not novel, the use of these systems as models to observe secondary structures on the single molecule scale is unprecedented.

Lastly, the synthesis of PEG-*b*-poly(*L*-Lysine)-*b*-PEG is to our knowledge novel. This is despite other triblock copolymers with the same components but differing composition such as poly(*L*-lysine)-*b*-PEG-*b*-poly(*L*-lysine) and poly(*L*-glutamic acid)-*b*-PEG-*b*-poly(*L*-glutamic acid) [46], having been synthesized in the past.

PART II:
Molecular Characterization

2.1 Circular Dichroism Spectroscopy

Optical rotatory dispersion experiments conducted by Urnes and Doty [47], showed a distinct difference between the dispersion of a synthetic poly(γ-benzyl-*L*-glutamate) peptide at random coil and α-helical conformation between 300-600 nm wavelengths. Based on this significant study, circular dichroism (CD) experiments of polypeptides were performed in the ultraviolet range (185-250 nm wavelength) and compared to the adsorption spectra of these molecules to assign the electronic transitions that occur within and between the peptide groups that account for its optical activity [48].

CD spectrometry is possible due to chiral molecules having a difference in the absorption of left and right circularly polarized light. When the molecule is excited by this circularly polarized light, electronic transitions are able to take place where the electrons in the non-bonding and bonding orbitals are excited to the antibonding orbitals. Depending on the secondary conformation that the peptides adopt, their electronic transitions interact with each other by shifting and splitting into different multiple transitions [49]. As a result, different secondary conformations have characteristic spectra and to this day CD is used as a powerful tool to estimate the secondary structure of proteins and polypeptides.

When the synthetic peptide is in α-helix conformation, a characteristic positive peak at 190 nm and two characteristic negative peaks at 206 and 222 nm can be observed. The peaks were assigned to π^0-π^* transitions that occur at 190 and 206 nm and n-π^* transitions that occur at 222 nm between the non-bonding molecular orbitals of the carbonyl electron lone pairs and the antibonding π^* orbital [48]. When the backbone of the polypeptide is folded into a α-helix, the carbonyl group comes into close proximity to the N-H group (i+4) residues away. Thus the value of the ellipticity [θ] at 222 nm is often used as an estimate to predict the percent helicity of a peptide by comparing it to the theoretical ellipticity of an infinite α-helix and a random coil.

The raw data obtained from a CD experiment is reported in degrees of ellipticity [θ][deg]. The linear dependence of the molar concentration and cuvette path length can be accounted for by calculating the molar ellipticity $[\theta_{molar}]$ [deg·cm^2·dmol^{-1}].

$$[\theta_{molar}] = \frac{100 \cdot \theta_{ellip}\ [deg]}{C \cdot l}$$

Where θ_{ellip} [deg] is the measured ellipticity, C is the molar concentration [mol·L^{-1}], and l is the path length [cm].

The molar ellipticity can be converted into a normalized value by dividing it by the number of chromophores within the polypeptide. The number of peptide bonds was calculated as the number of residues estimated by ^{1}HNMR minus one. Thus,

$$[\theta_{mean\ molar}] = \frac{[\theta_{molar}]}{(Number\ of\ Residues - 1)}$$

2.1.1 Estimating Helix Content with Mean Molar Ellipticity Values at 222 nm

The helix content or percent helicity of a polypeptide can be estimated by making an assumption that the helical content f_H of a peptide is proportional to the value of the mean molar ellipticity at 222 nm [deg·cm^2·dmol^{-1}].

$$f_H = \frac{(\theta_{222} - \theta_C)}{(\theta_H - \theta_C)}$$

θ_H is the theoretical mean molar ellipticity of an infinite α-helix and θ_C is the baseline mean molar ellipticity of a random coil.

$$\theta_C = 2220 - 53T$$

$$\theta_H = (-44000 + 250T) \cdot (1 - \frac{3}{N_r})$$

Where T is the temperature in °C and N_r is the number of residues.

The expression and values above were adapted from a paper by Luo and Baldwin [50] where the mean ellipticities of Ac-(AAKAA)$_n$GY-NH$_2$ (n=1-4) were measured in different concentrations of 2,2,2 trifluroethanol (TFE) for a range of different temperatures. The values were then extrapolated back to water.

The limitation of this method is that the ellipticity, θ_H of a completely folded helix remains dependent on its chain length due to contributions of unsatisfied amide backbone hydrogen bonds at the peptide termini [50], and side chain contributions to the spectra [51]. In addition, it is also strictly incorrect to assume a fixed fractional helix percentage as in reality helices have differing

segment lengths that constantly fluctuate between random coil and α-helix conformations.

Consequently, the fractional helicity of the peptides were calculated purely as an estimate in the following sections, however it is a useful method to quantify the change in helicity of the molecule in respect to pH, and also to compare the value between di and triblock copolymers.

2.2 Dynamic Light Scattering [52, 53]

The use of light scattering techniques allows us to access the size, shape and other essential structural parameters of materials. In the domain of light scattering there are notably static and dynamic light scattering techniques, however for the scope of the thesis only dynamic light scattering will be discussed.

The scattering of an incident monochromatic light $\vec{l}_0$ when it is shone on a particle, can be explained if we consider light as an electromagnetic wave that interacts with the oscillating dipole of a given molecule which is dependent on its charge distribution. The dipole emits an electromagnetic wave of the same wavelength as the incident light in all directions perpendicular to itself. The difference in angle between the incident $\vec{l}_0$ and scattered light $\vec{l}_s$ is defined as the scattering angle θ (**Figure 4**). For light scattering of molecules larger than 20 nm, there are multiple scattering centres (oscillating dipoles) within a molecule leading to interference patterns of the scattered light. The interference of the scattered light leads to an angular dependence of the scattering intensity, which is characteristic for the size and shape of the particles[1]. Particles suspended in a solution undergo random thermal displacement (Brownian motion), and therefore the resulting interference and corresponding change in scattered intensity at a given angle undergoes a fluctuation with respect to time. (For static light experiments the average scattering intensity for each angle is measured, for dynamic light scattering the evolution and fluctuation of the scattering intensity with respect to time is followed).

A photomultiplier at a known angle compares the evolution of intensity, I of the scattered light at a given spot with time, t.

[1] The following relations can be observed from scattering of dilute solutions of particles larger than λ/20. For smaller particles the scattered intensity will be independent of the scattering angle and will not be discussed here.

Within a specific time scale between t and $t + \tau$ the fluctuation in scattering intensity I can be measured leading to an normalized time autocorrelation function $g_{(2)}(\mathrm{q}, \tau)$, where $\mathrm{I(t)}$ is the intensity of the scattering light at a specific time, and $\mathrm{I(t + \tau)}$ is the intensity of the scattered light at a later time $(\mathrm{t + \tau})$.

$$g_{(2)}(\mathrm{q}, \tau) = \frac{< I(\mathrm{q}, \mathrm{t})\mathrm{I}(\mathrm{q}, \mathrm{t} + \tau) >}{< I(\mathrm{q}, \mathrm{t}) >^2}$$

As more time passes the correlation between the initial intensity and the measured intensity changes. The measurement of the decay in the intensity signal over a known period of time forms the basis for dynamic light scattering.

Using the Siegert relation,

$$g_{(2)}(q, \tau) = B + \beta g_{(1)}(q, \tau)^2$$

Where B denotes the baseline which is theoretically 1, and β is a factor which depends on experimental geometry.
When the sample is assumed to be perfectly monodisperse the amplitude correlation function $g_{(1)}$ can be approximated as a monoexponential decay, from which further information can be derived.

$$g_{(1)}(\mathrm{q}, \tau) = \exp^{-\Gamma\tau}$$

$$\Gamma = \mathrm{Dq}^2$$

The decay constant Γ is dependent on D, the diffusion coefficient and on q^2, the square of the scattering vector.

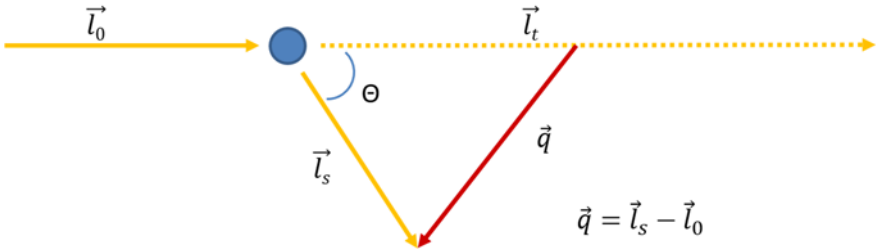

Figure 4. Schematic representation of the scattering wave vector $\vec{q}$ which is the difference between the wave vectors of the incident light $\vec{l}_0$ and the scattered light $\vec{l}_s$. $\vec{l}_t$ represents the transmitted light and θ the angle of scattering.

The scattering wave vector $\vec{q}$ is the difference between the scattered light vector l_s and the incident light vector l_0. For an elastic process $l_0 = \frac{2\pi}{\lambda}$. Thus $\vec{q}$ is defined as,

$$\vec{q} = q = \frac{4\pi n}{\lambda_0} \sin\left(\frac{\theta}{2}\right)$$

n denotes the refractive index of the solvent, λ_0 is the wavelength of the laser in vacuum.

The hydrodynamic radius (R_h) can thus be calculated by using the diffusion coefficient D and the Stokes-Einstein equation.

$$D \approx \frac{k_B T}{6\pi\eta R_h}$$

Where T denotes the temperature in K, k_B the Boltzmann constant, and η, the viscosity of the solvent.

However, for polydisperse solutions $g_{(1)}$ can no longer be represented by a monoexponential decay, but rather must be generalized as a superposition, or distribution of several single decay rates $G(\Gamma)$.

$$g_{(1)}(q,\tau) = \int_0^\infty G(\Gamma)\exp(-\Gamma\tau)\, d\Gamma$$

With,

$$\int_0^\infty G(\Gamma)d\Gamma = 1$$

The characterization and analysis of $G(\Gamma)$ is most often done by utilizing the cumulant analysis method introduced by Koppel [54], or by the constrained regularization method (CONTIN) proposed by Provencher [55]. The detailed explanation of both is beyond the scope of this thesis, however it suffices to say that the cumulant method is used for resolving narrow distributions, whereas the CONTIN method is used for more polydisperse systems, keeping in mind both methods have its advantages and but also limitations.

PART III:
Atomic Force Microscopy and Single Molecule Force Spectroscopy

Atomic Force Microscopy (AFM) was introduced in 1986 by Binnig, Quate and Gerber [56] and since then has become an indispensable tool in the field of nanobiosciences. The most significant attribute that sets AFM apart from most other high resolution techniques is that it allows the visualization and manipulation of single molecules under physiological conditions in real time. Accordingly, it was the development of the fluid cell and the first images of human blood protein fibrinogen clotting in water [57] that ushered a completely new field of study: the study of biological systems on the nanoscale under near-native conditions [58]. Within a decade of its discovery, AFM developed from just an imaging-based application to a technique able to quantify interactions between single molecules. It was shown to be applicable to a large variety of biological systems, such as the investigation of interaction forces between individual ligand-receptor pairs [59], binding of drug-transporter complexes in living cells [60], forces between complementary DNA strands [61], structure and conformational transitions of polysaccharides [62, 63] and the unfolding of individual titin protein domains [64], to name but a few, all studies that demonstrate the immense breadth and potential of this technique.

3.1 The α-Helix and Investigations into the Mechanical Behaviour by Single Molecule Force Spectroscopy Experiments

The α-helix is the most commonly observed secondary structure, reflecting up to 30 % of the entire Protein Data Bank of proteins [65]. The structure was first prosed by Pauling, Corey and Brandson in 1951 [66], who by predicting partial double bond nature of peptide bonds by resonance, postulated a helical structure composed of 3.69 residues per turn and a translation of 0.15 nm along the helical axis . It was however only in 1960 that a detailed atomic arrangement and a preference for the right-handed α–helix in nature was established by the x-ray analysis of a natural myoglobin protein [67, 68].

Although peptide secondary structure can be characterized by a variety of different ensemble techniques such as x-ray analysis, NMR, circular dichroism and FTIR, single molecule force spectroscopy by AFM and optical tweezers experiments are unique in that they allow the study of the molecular structure and mechanical properties of a single molecule. Probing single molecules allows us to evidence different sub-populations in an ensemble of molecules (not all the molecules have exactly the same structure or show the same behaviour), as well as different behaviours for a single molecule (a single molecule can behave differently from time to time).

3.1.1 Poly-(*L*-alanine)-based Homopolypeptide

The tensile mechanics of an alanine based α-helical polypeptide was probed by Afrin, Takahashi, Shiga, and Ikai [69] to investigate the basic stability and mechanical properties of a α-helical polypeptide with minimal side chain interactions. They synthesized a $[C(KAAAA)_{10}KC]_n$ polyalanine-based polypeptide with residues substituted by lysine to promote the solubility of the molecule in buffer, and cysteine residues on both ends so that the molecule can be covalently immobilized onto the AFM tip and surface. The obtained force extension profile of the polyalanine-based polypeptide was almost identical to that of a polypeptide without the α-helix motif, except for the appearance of a small peak or an inflection at the end of the extension at 0.5-1 nN **(Figure 5 A and B)**. However, in a helix promoting agent TFE, a tilted plateau was observed **(Figure 5 C)**, which was a feature lost when a helix denaturing agent 6M guanidium chloride was added **(Figure 5 D)**. It was suggested that force-extension behaviour was dominated by the preferred stretching of the locally denatured segments within the polypeptide chain. The denatured segments within the helix were

thought to spontaneously occur due to fluctuations in the helix-coil transition equilibrium along the helix, which were more accessible as a consequence of alanine possessing non-bulky side chains [69].

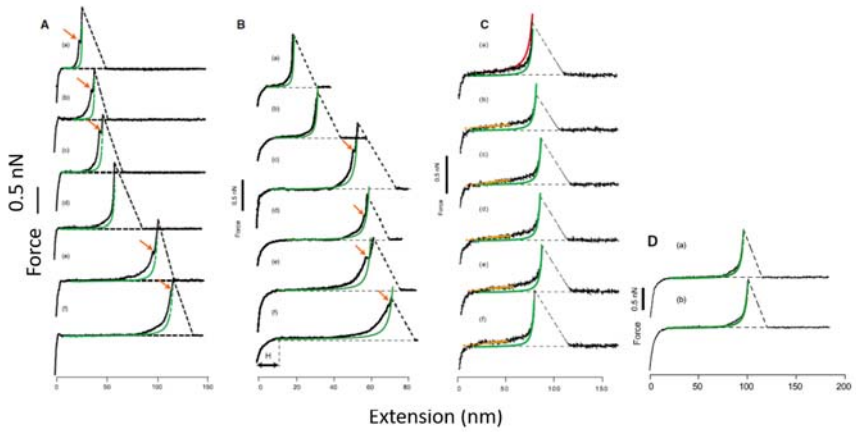

Figure 5. Four typical force-extension profiles observed in four different experimental conditions. A.) 50 mM Tris buffer at pH 7.4. B.) 400 mM NaCl and 50 mM Tris buffer. C.) 50% TFE and 50 mM Tris buffer at pH 7.4. D.) 50 mM Tris buffer at pH 7.4 and 6 M GdmCl. The green and red curves indicate a fitting utilizing the WLC model, the orange arrows mark the inflections observed at 0.5-1 nN and the yellow lines represents the linear fitting of the tilted plateau. Adapted from a publication by Afrin, Takahashi, Shiga, and Ikai [69].

3.1.2 Poly-(*L*-glutamic acid) Homopeptide

In a study by Idris, Alam, and Ikai [70] a poly(*L*-glutamic acid) α-helix was extended which was covalently sandwiched between the AFM tip and the surface with a PEG spacer in between both. The obtained force-extension profile was very smooth without any characteristic peaks or plateaus indicating the breaking of the hydrogen bonding maintaining the helical structure. Instead by integrating the normalized force-extension curves obtained in different pH conditions, they reported that the work required for unfolding increased at low pH conditions coinciding with the formation of the helical structure (**Figure 6**). As a result they hypothesized that the helical chain stretches uniformly along its length, making a gradual transition from helix to coil form as opposed to a turn-by-turn unravelling [70].

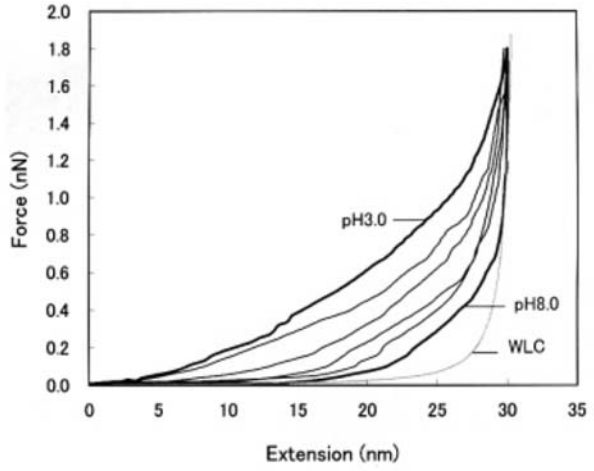

Figure 6. Comparison of the normalized force-extension profiles of the poly(*L*-glutamic acid) with the contribution of the PEG tether subtracted. The thick curves indicate the pH at both extremities pH 3.0 and pH 8.0. Intermediate pH conditions indicated by the thin lines are pH 4.0, 5.0, 6.0, and 7.0. The WLC indicates a fit utilizing the worm-like chain model. Adapted from a publication by Idiris, Alam and Ikai, reference [70].

3.1.3 Poly-(*L*-Lysine) Homopeptide

The elastic behaviour of a self-assembled monolayer of cysteine$_3$-poly(*L*-lysine)$_{30}$-cysteine α-helices on a gold surface was investigated by Lantz et al.[71]. To obtain single molecule extension of the lysine α-helices, monolayers were synthesized with 0.5% reactive polypeptides with cysteine on both ends, allowing chemical Au-S bonding of the molecule to both the gold tip and the gold surface. The rest of the molecules had only one cysteine group attached to the polypeptide thereby remaining only chemically bonded to the surface, and could not form strong interactions with the tip. Therefore in this experiment it was assumed that upon tip retraction, only the doubly cysteine functionalized polypeptides could be fully extended. As an indication of the rupture of the intermolecular interactions maintaining the lysine helix, a collection of peaks was observed (**Figure 7**).

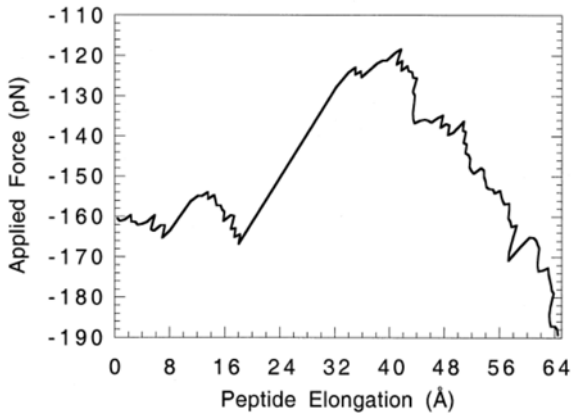

Figure 7. Typical Force-Elongation curves obtained for a self-assembled monolayer of poly(*L*-lysine) end-functionalized with cysteine on gold. In this particular sample only 0.5% of the poly(*L*-lysine) was doubly functionalized thereby allowing it to chemically bond with the gold tip. Adapted from a publication by Lantz et al. [71].

3.1.4 The Unfolding of Free-standing α-Helical Linkers Within a Myomesin Protein

Typically, the unfolding behaviour of proteins and those of isolated synthetic helices like those mentioned above should be compared with caution as proteins can display complex interactions due to the presence of domains that consist of a combination of different secondary motifs. On the other hand the unfolding behaviour of myomesin, which has a long free-standing α-helix linker connecting domains may provide insight into the unfolding of natural isolated α-helices. The unfolding of such a protein was investigated by Rief et al.[72] who observed a plateaus at 24.0± 0.5 pN (n=72), which was attributed to the unravelling of individual α-helical linkers between My12 domains in a homooctameric $(My12)_8$ construct (**Figure 8**). The plateau length per domain was found to be 6.1±0.2 nm which was in excellent agreement with the calculated increase in contour length of a My12 helix ≈6.3 nm [72].

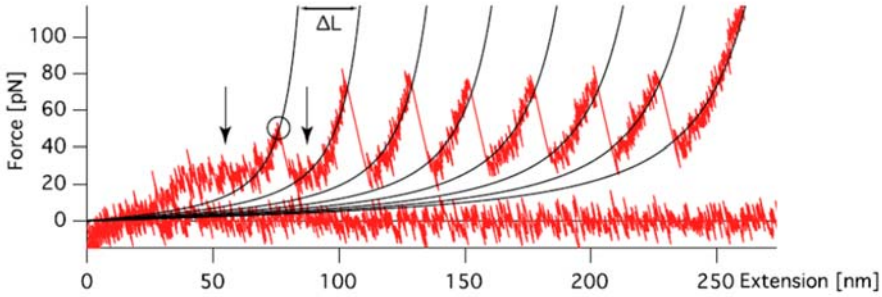

Figure 8. Typical force-extension profile of a homooctameric construct $(M12)_8$ of myomesin. The black lines indicate a fitting using the WLC model, and the black arrows indicate the force plateaus attributed to the extension of the individual α-helical linkers. Adapted from a publication by Rief et al. [72].

3.1.5 A Remark Concerning Earlier Experimental Investigations

It is important to note that single molecule force spectroscopy is still a relatively new technique where major developments in bioconjugation techniques, surface chemistry, and data analysis have been done within the two most recent decades [58]. The resolution of the instrument which we have at our disposal today, and our comprehension of single molecule interactions is understandably far beyond what was available when the first studies on the unravelling of α-helices were conducted. Therefore, it is only with the knowledge available today that we can cautiously point out some weaknesses in the early works.

For instance in the study conducted on the poly(*L*-glutamic acid) α-helix [70], the force-extension curves were normalized to the same length for comparison. However, if plateau features were apparent as suggested by the study on the α-helical linker of myomesin [72], the normalization of curves would make the identification of such a plateau feature extremely difficult.

When observing the elastic behaviour of poly(*L*-lysine) helices, self-assembled monolayers were utilized where only 0.5 % of the polypeptides were chemically reactive to the tip. This experimental design was not optimal for single molecule experiments because even if the polypeptides are not doubly functionalized with cysteine, they are still capable of interacting with the tip through unspecific adsorption. This unspecific adsorption gives rise to very broad rupture peaks, eclipsing the signals from single interactions. The signal they observed **(Figure 7)** is clearly not a force curve from single molecules, but an indefinable signal from a big mass of molecules. Such a force curve would have been discarded today.

Finally in the earlier works much emphasis was made on the overall shape of the curves, however small features at lower forces may have gone unnoticed. Keeping in mind the speed dependence on the unfolding forces, some key works below can provide an estimation at which range of forces the unfolding interactions of isolated α-helices should be expected.

Rief et al.[72] observed a plateau at 24.0± 0.5 pN which was attributed to the unravelling of the helical linker obtained at pulling speeds of 5 nm·sec^{-1}. Although coiled-coils are helices displaying a tertiary assembly and thus expected to display additional contributions from hydrophobic associations, the unfolding of such structures might still offer a rough approximation at which range of forces the unravelling of individual helices might occur. In a two α-helix coiled-coil myosin[73] a shallow plateau was observed between forces of 20-25 pN at a pulling speed of 40-130 nm·sec^{-1}. In a triple α-helix coiled-coil spectrin[74] the forces needed to unfold these structures were within the range of 25-35 pN at pulling speeds of 300 nm·sec^{-1} .

3.2 Theoretical Works that Predict the Properties of the α-Helix and their Behaviour under Mechanical Extension

Although the number of experimental studies conducted on the extension of single α-helices is very few, there are many more theoretical works that predict the structural properties of α-helices as well as their behaviour when extended mechanically. Some selected relevant works are presented below.

3.2.1 The Critical Length of a α-Helix Strand is Between 9-17 Amino Acids

Using a combination of thermodynamic analysis, well-tempered metadynamics molecular simulation and statistical analysis, Qin, Fabre and Buehler [65] investigated the thermal equilibrium between helix folding, random coil, and the formation of a tertiary structure. They demonstrated that for very short peptides $N< 5$ the random coil conformation dominates (**Figure 9**). As the peptide length N increases so does the probability of the formation of an intact helix. However, beyond a tripoint at $N=13$ this probability starts to decrease as transitions into a tertiary structure becomes more energetically favourable. The tripoint is interesting as it indicates the most stable length of a α-helix, and that at this length all three conformations also may exist.

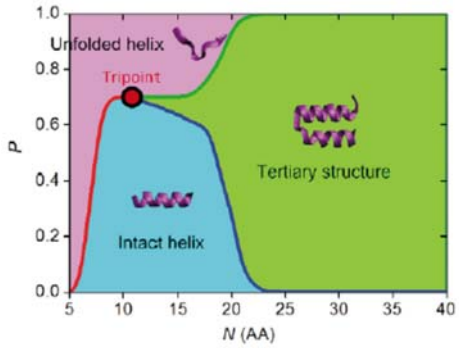

Figure 9. Schematic conformation diagram depicting the probability of formation *P*, of a random coil, helix or tertiary conformation, as a function of the length of the peptide *N*. The tripoint indicates the most stable length of a single α-helix strand. Adapted from a publication by Qin, Fabre and Buehler [65].

3.2.2 Energetically it is More Favourable That a α-Helix Unravels Turn-by-turn

An internal coordinate mechanics study was conducted by Rohs, Etchebest and Lavery [75], who modelled the unfolding of a α-helix by mechanical extension. In this work two different pathways of unfolding the helix were investigated, comparing scenarios where the helix unwinds turn-by-turn or is uniformly stretched like a spring until all interactions rupture simultaneously (**Figure 10**).

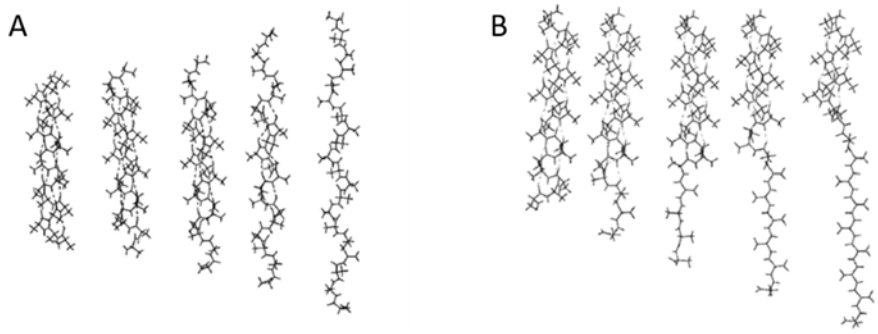

Figure 10. Snapshots of two different pathways a (Ala)$_{20}$ α-helix can unfold under extension. A.) A uniform extension until eventual rupture of hydrogen bonding interactions. B.) A turn-by-turn unfolding. Adapted from a publication by Rohs, Etchebest and Lavery [75].

A right-handed α-helix was modelled composed of 20 alanine residues, where it was found that the uniform extension of the α-helix results in a rapid

increase in conformational energy **(Figure 11 A.)**. In comparison a turn-by-turn unwinding of the helix was found much more energetically preferable. In addition they predicted that the force observed for a turn-by-turn unravelling of the helical structure would be length independent, and thus for the force-extension profile a plateau-like interaction **(Figure 11 B.)** would be observed.

Although interactions were observed at much higher forces of (≈ 500 pN) and cannot be used as a reference, the shape of the resulting force-extension curve and the predicted pathway of the unfolding of the α-helix were still considered experimentally relevant.

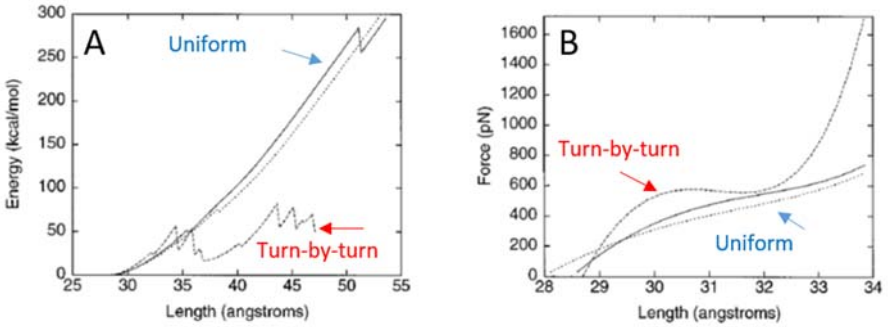

Figure 11. Theoretical α-helix extensions obtained by internal coordinate mechanics. A.) Conformational energy as a function of length comparing two $(Ala)_{20}$ and $(Ala)_9$-Pro-$(Ala)_{10}$ helices unfolding uniformly and a $(Ala)_{20}$ helix unfolding turn-by-turn. B.) Resulting force-extension curves comparing two $(Ala)_{20}$ and $(Ala)_9$-Pro-$(Ala)_{10}$ helices unfolding uniformly and a $(Ala)_{20}$ helix unfolding turn-by-turn. Adapted from a publication by Rohs, Etchebest and Lavery [75].

3.2.3 A Pseudoplateau Feature is Apparent in the Intermediate Force Regime, and the Extension of Weak Helix Formers Resembles the WLC

The non-linear elastic response of α-helical polypeptides was investigated by Chakrabarti and Levine [76] with Monte Carlo studies and compared to results already obtained using mean field studies for the same phenomenon. Using Monte-Carlo studies random fluctuations between helix and coil form in response to an intermediate applied force can be taken to consideration which allowed a better determination of the pseudoplateau feature that was apparent in the intermediate force regime before the unfolding of the α-helical domains.

This work is particularly interesting as the mechanical property of weak helix formers was investigated where the limit of the pseudoplateau formation was defined. Firstly they determined that at an intermediate force a pseudoplateau feature is apparent due to the applied force enhancing random fluctuation between random coil and helix state along the helix before denaturation. Secondly, it was

also shown that the behaviour of a weak helix former resembles a worm-like chain (WLC) extension of an ideal, featureless, polymer, due to the increasing number of denatured segments within the helix.

Firstly, the extension of a α-helical polypeptide molecule was divided into four force regimes. The first commences at the lowest force, where the helix orients towards the direction of the applied force. In the second regime the applied force will increase the mean length of the helix as the molecule "straightens out", restricting the random movement of the molecule due to thermal energy. In the third regime, (F_-) to (F_+) **(Figure 12 B.)** the increasing force enhances fluctuations between helical and random coil states within the α-helix. These fluctuations result in a pseudoplateau in the force-extension curve, where the spontaneous appearance of random coil segments in the helix provides additional length, thus increasing compliance towards extension. In the final force regime above (F_+) the α–helix domains will denature leading to an additional increase in length over a short range of forces.

It was found that the pseudoplateau feature was a finite effect and the onset depended on various factors. The force of the beginning of the pseudoplateau (F_-) increases with the length of the helix chain. This makes sense as longer chains need larger forces to orient the molecule and restrict its random movement due to thermal energy. Therefore the onset is dependent on the degree of polymerization (N), the thermal persistence length of the helix ($\kappa_>$), and the segment length of the helix ($\gamma_<$).

$$F_- \sim N^{2/3} {\kappa_>}^{-1/3} {\gamma_<}^{-1}$$

At an applied force of $F > F_-$ the pseudoplateau commences. The end of the pseudoplateau and the beginning of the force needed unravel the helix, F_+ is defined as,

$$F_+ \approx \frac{\varepsilon_w + h}{\Delta\gamma}$$

Where, ε_w is the free energy cost of a domain wall in the helix, h is the free energy cost of the monomer to be a random coil configuration and $\Delta\gamma = \gamma_> - \gamma_<$ which is the difference in length between the segment length of the coil $\gamma_>$ and the helix $\gamma_<$.

The existence of a pseudoplateau requires the conditions $F_- < F_+$ to be fulfilled. If related to chain length,

$$N \leq \left(\frac{h + \varepsilon_w}{\gamma_< \Delta\gamma}\right)^{3/2} \kappa^2_>$$

Therefore usually as typical α-helices are short and stiff (large κ and small N) this condition is fulfilled and a pseudoplateau should be apparent. However, it is important to note that as the value of (ε_w), the free energy cost of a domain wall in the helix, becomes smaller and smaller (progressively weaker helix former) the chain becomes a mix of random coil and helix segments and the force extension curves begins to resemble those of a parabolic WLC extension instead.

The comparison of the two force-extension curves **(Figure 12 A and B)** indicates that the pseudoplateau feature disappears for helices that have a longer polymerization degree, and where the free energy cost of a domain wall in the helix is low **(Figure 12 A)**. If only the free energy cost of the domain wall of the helix (ε_w) is lowered a similar trend is observed **(Figure 12 C.-E)**.

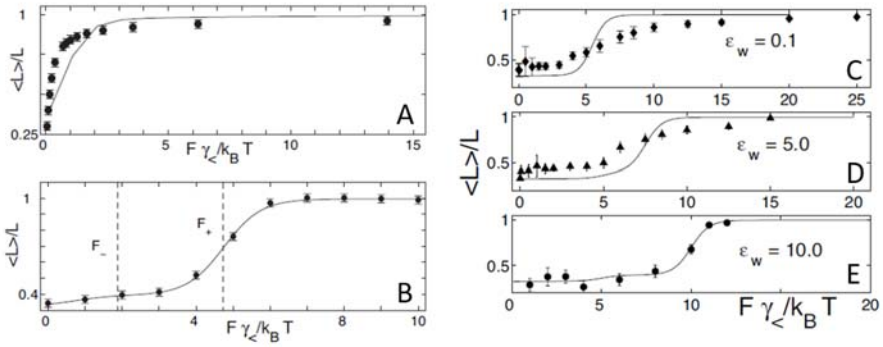

Figure 12. Theoretical force-extension profile obtained by Monte Carlo (points) and mean field (solid line) . A.) An example where the $F_- < F_+$ inequality is violated resulting a disappearance of the pseudoplateau. $\varepsilon_w = 0.5$, h=1.0, $\kappa_> = 4.0$, $\kappa_< = 2.0$, N=20. **B.)** An example where the $F_- < F_+$ holds true and the pseudoplateau can be observed. $\varepsilon_w = 8$, h=1.5, $\kappa_> = 100$, $\kappa_< = 1.0$, N=10. F_- and F_+ denotes the beginning and the end of the pseudoplateau force regime. C.)-E.) Keeping all other parameters constant, h=10.0, $\kappa_> = 100.0$, $\kappa_< = 1.0$, N=20, only the ε_w is varied from 0.1 to 10. (In each graph the mean length of the chain was normalized by the maximum chain length, and the applied force was normalized by the length of the helix). Adapted from a publication by Chakrabarti and Levine [76].

3.2.4 The α-Helix Content Initially Increases Before the Unfolding Event

Although this counter intuitive property of α-helices has been reported mathematically [77], Torabi and Schatz [78] modelled the behaviour of α-helical polypeptides under extension where the applied force as a function of helical content was plotted. They utilized a statistical mechanical model that coupled an inhomogeneous partially freely rotating chain model (iPFRC) with a helix-coil algorithm AGADIR.

They reported that when a force of 10 pN was applied, the formation of the helical content increased initially due to the formation of a helix being energetically more favourable (**Figure 13**). At small extensions, the helix can extend a greater distance in the direction of the applied force, compared to the random coil conformation and therefore has a smaller entropic penalty [78]. This makes the formation of the α-helix energetically more favourable at small extensions.

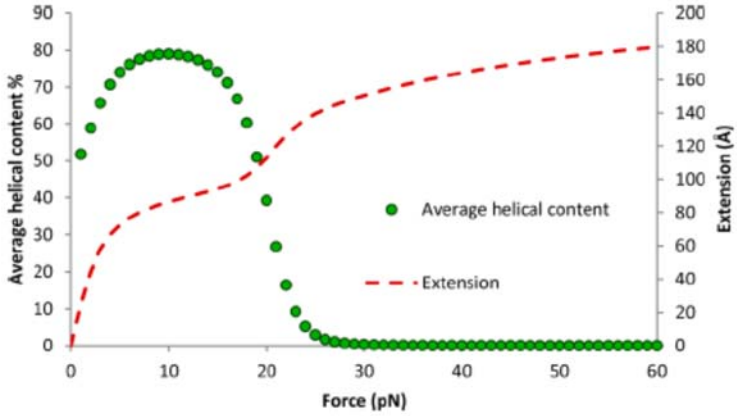

Figure 13. The average helical content as a function of force of poly(*L*-glutamic acid)$_{60}$ obtained utilizing a AGADIR coupled with iPFRC. Adapted from a publication by Torabi and Schatz [78].

3.3 The Helix-Coil Theory

It is important to keep in mind that a α–helix-coil transition cannot be described by a simple two state equilibrium where all populations are either helical or denatured. Instead a helical polypeptide is a dynamic, statistical ensemble of interconverting conformations with helical segments of varying degrees [79]. Usually in solution this frequently involves central helices of varying lengths with denatured ends [80]. Therefore to predict the average theoretical behaviour of a α–helix it is necessary to utilize a statistical mechanical approach that considers

every possible location of a helical segment within a sequence [80]. By assigning statistical weights for all possible sequence of conformations, the helix-coil equilibrium within a polypeptide sequence can be mathematically represented and written as a partition function [79]. (The population of a conformation is given by its statistical weight divided by the sum of the statistical weight of all other populations [80]). The method of assigning statistical weights for conformations can differ based on which models utilized. There are two basic helix-coil models: Zimm-Bragg, and Lifson-Roig. More complex helix-coil transition models are based largely on one of the two, or utilize a combination of these two models.

3.3.1 Zimm-Bragg Model

In the Zimm-Bragg model, the basic unit is the peptide bond and each unit is evaluated on its ability to participate in hydrogen bonding with another peptide unit. The polypeptide is spit into its basic units which are the individual peptide bonds CONH. Unlike the Lifson-Roig model the basic unit in the model is not an amino acid residue, but rather one peptide bond that effectively straddles two amino acid residues (**Figure 14**).

If a unit is non-bonded (random coil) it is given a statistical weight of 1. The first hydrogen bonded unit pair from the N-terminus has a statistical weight of σs, where σ is the nucleation parameter and s is the propagation parameter. Each subsequent hydrogen bonding after the first hydrogen bonding unit pair however has a statistical weight of s. This is because the Zimm-Bragg model takes into consideration the difficulty of nucleation versus just propagation. The nucleation penalty needs to be paid only once, where three residues need to be fixed for a hydrogen bond to form. Each subsequent turn of the helix requires only residue fixed on top of the existing helix. Thus if a second hydrogen bonded pair would be represented it would have a statistical weight of σs^2. The statistical weight of a helix containing *N* hydrogen bonds is then σs^{N-1} [80].

3.3.2 Lifson-Roig Model

In contrast to the Zimm-Bragg model, the basic unit is an amino acid residue centred on the α-carbon, and each residue is assigned a conformation of helix or coil depending on whether the backbone ϕ and φ angles are favourable for helix formation (**Figure 14**) [80]. The statistical weight of each residue thus depends on its conformation and that of its two neighbours. If a residue adopts a coil conformation it is assigned a statistical weight of 1. If a residue adopts a

helical conformation it is assigned a statistical weight of *v*, and if the helical residue is between two helical residues it is assigned a weight of *w*. The *v* value compares to the nucleation parameter in the Zimm-Bragg model where distinction is made between the residues at the ends of a helical segment that nucleate the helix and the residues in the middle of the helix. Thus, a helical segment with M residues has a weight of v^2w^{M-2} where *M-2* denotes possible number of hydrogen bonds that can form if we consider that in order to form a hydrogen bond with a residue at *(i, i+4)*, three consecutive residues need to be fixed.

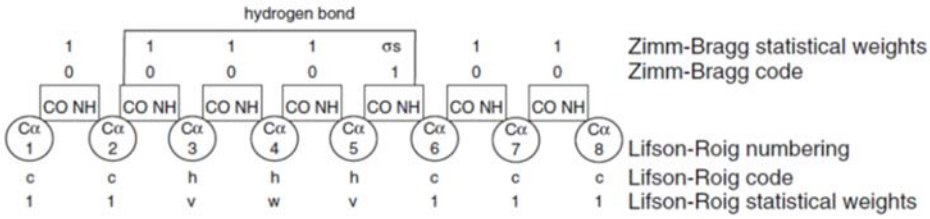

Figure 14. Zimm-Bragg and Lifson-Roig coding and weighting for an 8 residue polypeptide with a helical turn in between. Adapted from a publication by Doig [80].

Both models make a distinction between helix nucleation from helix propagation. The nucleation parameter is often regarded as purely entropic therefore it is considered independent of temperature and often also of the type of amino acids involved [81]. The propagation parameter is however dependent on the nature of the side chain within the residues, as it is affected by side chain-helix interactions [81]. It is to be mentioned that the Lifson-Roig model is conceptually easier to handle and is utilized for polypeptides containing different amino acid residues as its propagation and nucleation parameters *w* and *v* can be assigned to individual residues [80]. In addition the propagation parameter relates directly to the helix propensity of an amino acid residue, which can be helix forming, helix breaking or indifferent [79].

3.3.3 Brief remark Concerning AGADIR

The AGADIR algorithm by Munoz and Serrano has similarities in respect to both models, yet also a number of crucial differences [82] . It is a highly complex model which is to the present day the only model that can yield accurate predictions of helix propensity for any sequence of amino acids [78, 80]. It includes updated knowledge of α-helix stability which takes factors such as capping effects, pH dependence, minimal helix length, and temperature into consideration in addition to incorporating large amounts of experimental data. The difference in the AGADIR algorithm versus Zimm-Bragg and Lifson-Roig will not be

discussed as it is not within the scope of this thesis. However the reader is advised to refer to publications by Munoz and Serrano [82, 83] for further information.

3.4 The β-Sheet and Single Molecule Force Spectroscopy of Polypeptides that Exclusively Exhibit only β-Sheet Secondary Structures

In the β-sheet structure the polypeptides interact with adjacent chains through hydrogen bonding between the C=O and N-H groups. The chains can lie adjacent to each other in an anti-parallel arrangement where the N-terminus and C-terminus of each strand are oppositely oriented, or in a parallel arrangement where the termini are oriented in the same direction (**Figure 15**) [84]. Both parallel and antiparallel motifs can be exhibited within the same polypeptide chain with loop, turns and twists occurring in between [85]. The result is that polypeptides and proteins containing β-sheet motifs have far greater structural diversity [85, 86] than α-helices making their characterization and study far more challenging.

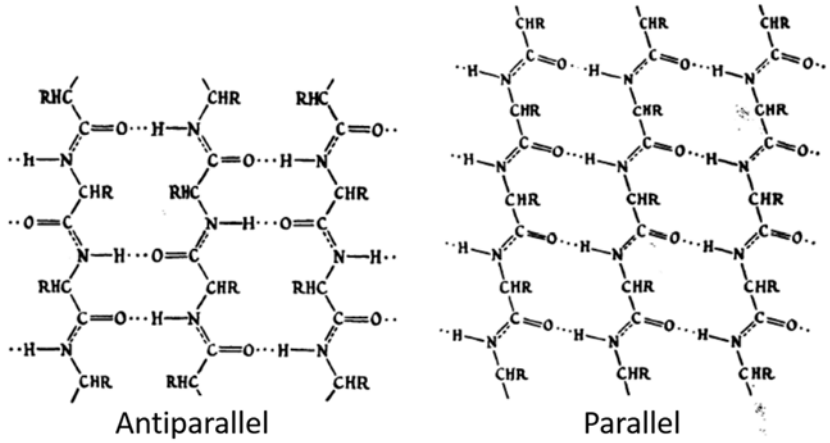

Figure 15. The antiparallel and parallel arrangement of the β-sheet structure. Adapted from a publication by Pauling and Corey [84].

3.4.1 Single Molecule Force Spectroscopy of β-Sheet Polypeptides

To our knowledge single molecule force spectroscopy experiments on a single β-strand has not been conducted so far. The mechanical behaviour of proteins are far more complex due to the presence of domains and additional interactions that establish the tertiary structure. Therefore, their behaviour is

certainly not analogous to the extension behaviour of single secondary structures. Despite this, some selected works on polypeptides that exclusively display the β-sheet structure are introduced that also had similar lengths as the polypeptides synthesized in later chapters, in the hope that a rough estimate on the force needed to unravel β-sheet interactions can still be gleaned.

The domains of Fibronectin III which are composed of 94 residues arranged into seven antiparallel β-strands were found to unfold at ≈80 pN for the weakest domains and ≈200 pN for the most mechanically robust domains at pulling speeds of 600 nm·sec^{-1} [87]. The C2 domain of synaptotagim I (C2A) which is composed of 127 residues, arranged into eight antiparallel β-strand was found to unfold at forces of ≈60 pN at pulling speeds of 600 nm·sec^{-1} [88, 89].

However, it is important to mention that the unfolding of β-sheet structures and the determination of a characteristic force generic to all such structures might not be as straightforward as the mechanical resistance of a β-sheet structure has been shown to vary greatly depending on pulling geometry [75, 90] which influences the orientation of the β-strands relative to the applied force. It has been shown that the mechanical resistance depending on longitudinal or lateral shearing (**Figure 16**) of the strands can also differ greatly in force [75].

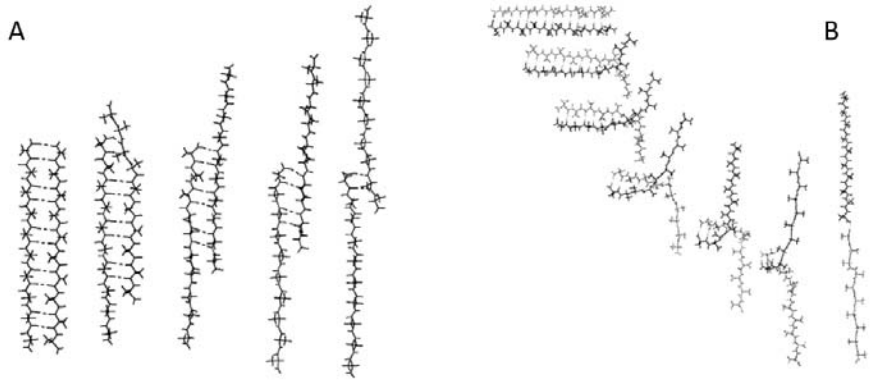

Figure 16. Longitudinal versus lateral shearing for two $(Ala)_{10}$ polypeptides β-strands. A.) Longitudinal shearing. B.) Lateral shearing. Adapted from a publication by Rohs, Etchebest and Lavery, reference [75].

3.4.2 Comparison of the Unfolding Forces Between Proteins Containing Predominantly α-Helix or β-Sheet Secondary Structures

The average unfolding force of predominantly β-sheet or all β-sheet containing polypeptides, has been found to occur at higher forces than predominantly or all α-helical polypeptides indicating the superior mechanical stability of the β-sheet secondary structure. This trend has been depicted by Hoffmann and Dougan [89] where the unfolding force of various proteins at similar pulling velocities (500 ±200 nm) have been summarized in an informative diagram (**Figure 17**).

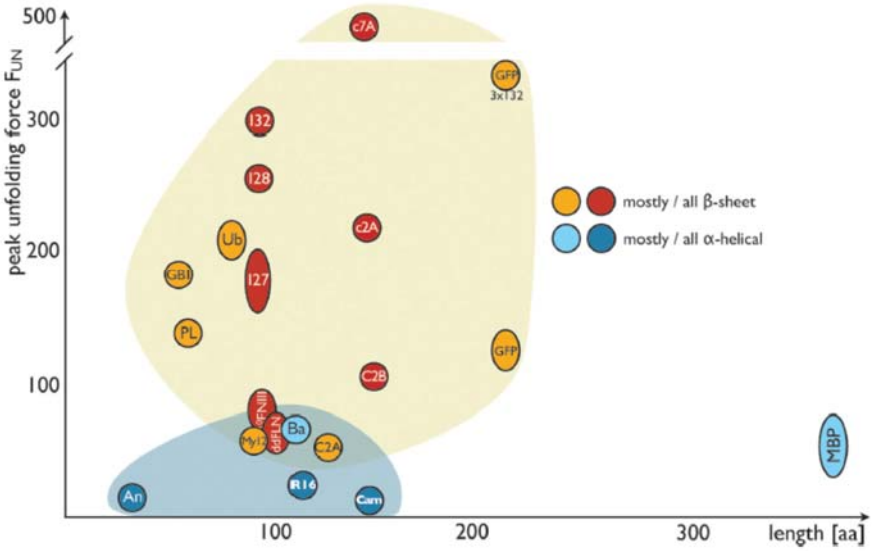

Figure 17. A diagram summarizing the unfolding forces of a selection of proteins comparing their mechanical stability and length depending on their predominant secondary structure. Predominantly or all α-helical proteins are depicted with an orange or red marker, and predominantly or all β-sheet proteins are depicted with a light blue or dark blue marker. Elongated markers indicate the range of forces where the unfolding event was observed. The abbreviation of the proteins are as follows: An= Ankyrin, Ba= barnase, Cam= calmodulin, C2A and C2B= synaptotagmin I domain, c7A and c2A= cohesion I domain of scaffoldin, ddFLN= D. *discoideum* filamin, ^{10}FNIII= 10th domain of fibronectin III, GB1= B1 domain of protein G, GFP= green fluorescent protein, I27, I28, I32= immunoglobulin-like domain of titin, MBP= maltose binding protein, My12= myomesin, PL= B1 domain of protein L, R16= α-spectrin, UB= ubiquitin. **Adapted from a publication by Hoffmann and Dougan [89].**

3.5 The α–β transition

The α–β transition is a deformation mechanism by which the α-helical secondary structure transitions into the β-sheet structure in response to pH, temperature, solvent and also mechanical deformation [91].

This transition was shown to have a chain dependence as demonstrated by Dzwolak et al.[25] who studied the heat induced α–β transition of poly(*L*-Lysine) by FTIR. The thermodynamic propensity of a poly(*L*-lysine) to transition from a α-helix to an antiparallel β-sheet structure was found to increase with increasing length. This was attributed the presence of more turns and distortions within a longer helix, which lead to a greater number of interacting helical segments. The interaction between these segments created a hydrophobic environment within the inter-helical space promoting the formation of the β-sheet structure [25].

The interconversion between the α-helix to β-hairpin states was also found to take place via a random coil state by Ding et al.[92] who utilized discrete molecular dynamics on a model polyalanine. It was found that the metastable β-form becomes less stable with increasing hydrophobic interactions between the side chains and that the although the β-hairpin has a greater potential energy than the α-helix, it has greater entropy due to less constraints imposed by hydrogen bonding [92].

Section Summary: The Necessity of an Experimental Reinvestigation into the Unfolding Behaviour of Single α-Helices and the Novelty of Investigating Intramolecular β-Sheets on the Single Molecule Level

There is a surprising lack of consensus on the unfolding behaviour of the α-helix structure despite three separate experimental studies on α-helical homopolypeptides [69-71], and one study on a natural free-standing α-helical linker [72]. The hydrogen bonding between the N-H and C=O between (*i*, *i*+4) amino acid residues of the helix backbone is identical for all polypeptides. Thus, it is inconceivable that such vastly different force-extension behaviour should be observed for the same secondary conformation, even if differing side chain interactions are considered.

Much work has been done on the theoretical behaviour of α-helices and not all could be introduced here. However by referring to selected works

predictions on their structure [65], properties at equilibrium [79, 80], unfolding pathway[75], and behaviour under mechanical extension [76-78] can be made.

The unfolding behaviour of single α-helices should be then re-examined with the instrumentation and knowledge available today. By referring to various theoretical studies their potential behaviour under experimental conditions can be predicted.

Lastly an in-depth investigation of a β-sheet interaction formed within a single polypeptide is unprecedented. Previous studies have been conducted on the unfolding of polypeptides that exclusively displayed the β-sheet structure that had similar lengths as the polypeptides synthesized in this study. It is hoped that by referring to them, some theoretical work on α–β transitions and the unfolding of β-sheets, the interpretation of results concerning the extension behaviour of a single β-strand can be facilitated.

PART IV: The Atomic Force Microscope, Single Molecule Force Spectroscopy and Models that Predict the Elastic Behaviour of Ideal Polymers and Polypeptides

4.1 The AFM Instrument

The basic principle (**Figure 18**) of an atomic force microscope (AFM) is that the change in interaction between the tip and the sample can be determined by measuring the variation of the laser deflection off the back of a highly, reflective cantilever. The laser deflection from the cantilever is detected by a photodiode. The tip sample distance is controlled by a piezoscanner with which the vertical and lateral position of the sample can be adjusted. When the tip interacts with the sample the cantilever is bent changing the position of the deflection compared to the deflection in the absence of the interactions.

It is important to mention that many different interactions can be observed in a force-extension curve, ranging from van der Waals interactions, electrostatic forces, capillary forces and adhesion forces. For an approach between two hard surfaces van der Waals forces will be dominant, if the surface is covered in a polymer brush repulsive forces will be observed, and in fluids adhesive forces will depend on interfacial energies between the tip and the surrounding solution [93]. When probing a specific interaction like the extension of a single molecule, all

other interactions must be kept to a minimum by favourable experimental conditions so that they do not eclipse the interactions we wish to observe.

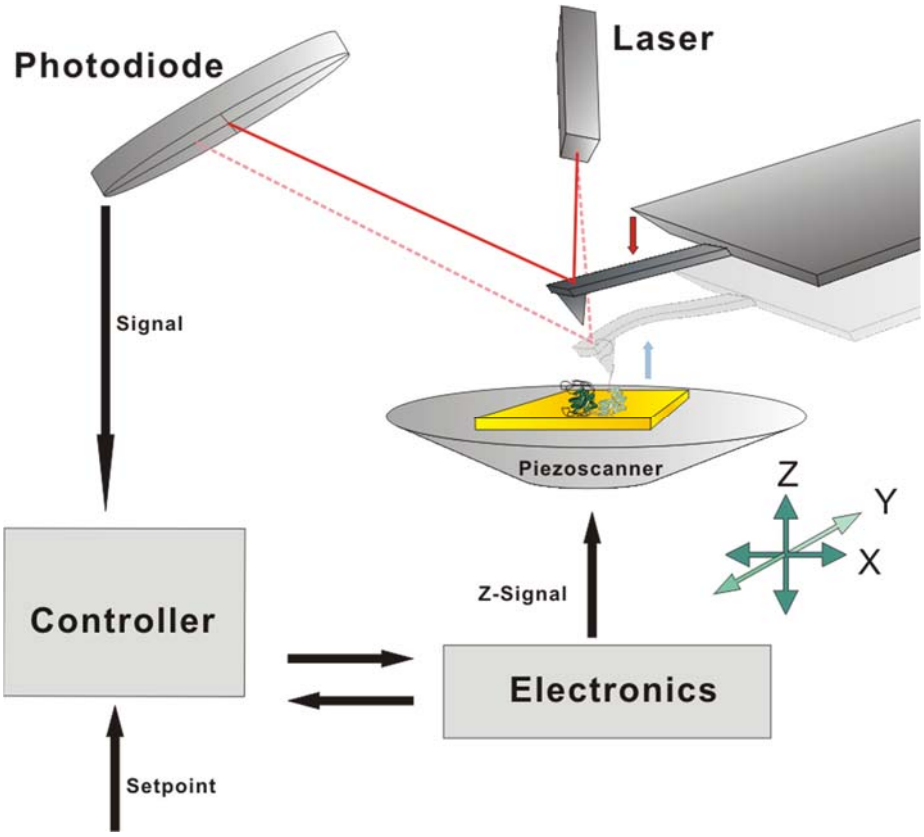

Figure 18. Principle components of an atomic force microscope showing the detection of the laser deflection from the cantilever by a photodiode. An approach (red arrow) is shown where the laser deflection remains constant throughout the approach. A retraction (blue arrow) is shown where upon catching the molecule the cantilever is bent, changing the laser deflection path. (Although the arrows indicating the direction of displacement during the approach and retraction are drawn next to the corresponding cantilever drawings, in reality, the vertical and lateral directions are controlled by the piezoscanner beneath the sample stage).

The raw data obtained from an AFM experiment is the cantilever deflection [V| versus the piezo displacement [nm]. This must be converted into a force-extension profile by utilizing Hooke's law:

$$F = k_c \cdot d$$
$$z = z_p - d$$

F denotes the force, k_c the cantilever spring constant, d the cantilever deflection, z the extension [nm] and z_p the piezo displacement [nm].

The photodiode signal must be converted into a cantilever deflection d in [nm] by obtaining the gradient of the linear portion of the cantilever deflection [V| versus the piezo displacement [nm] graph when the tip is in contact with the surface (**Figure 19**). The obtained gradient is called the deflection sensitivity$\left[\frac{v}{nm}\right]$. The deflection sensitivity serves as a conversion factor between the cantilever deflection in [V] to cantilever deflection in [nm]. The difference between the piezo displacement and the cantilever deflection [nm] yields the extension [nm]. The product of the cantilever deflection [nm] and the spring constant $\left[\frac{pN}{nm}\right]$ k_c yields the force [pN] [94, 95].

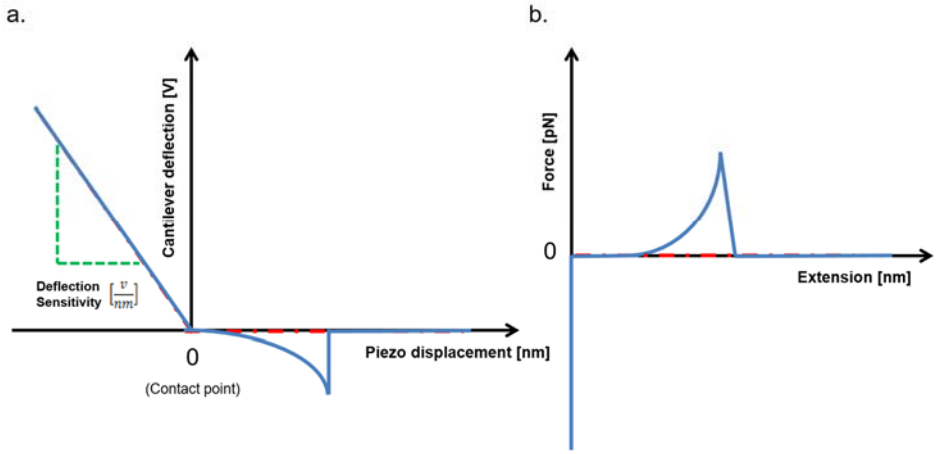

Figure 19. Simplified scheme of conversion of the raw data obtained on the AFM machine to a force [pN] versus extension [nm] graph. a.) Cantilever deflection [V] versus piezo displacement [nm]. The red line indicates the approach and the blue line indicates the retraction curve. The deflection sensitivity is the gradient of the linear position of the graph, when the tip is in contact with the surface (indicated by the green dotted line). b.) Force [pN] versus extension [nm].

Although the nominal spring constant k_c of a cantilever is always given as a range by the manufacturer, it is important to calibrate and obtain the real spring constant for k_c for each of the cantilevers used in the following experiments. The real spring constant can vary greatly between different cantilevers, due to variations in tip geometry and therefore can affect the

calculated force greatly. The spring constants were obtained by utilizing the thermal oscillation spectra for each cantilever.

4.1.1 Obtaining the Spring Constant by Thermal Oscillation [94]

The spring constant of a tip can be obtained by a non-destructive thermal oscillation method, where the tip oscillates due to thermal fluctuations away from the sample surface.

Where,

$$\frac{1}{2}\mathrm{k}_c\Delta x^2 = \frac{1}{2}k_B T$$

Where k_c is the cantilever spring constant, Δx^2 is the time averaged square of the thermal fluctuations (determined experimentally), k_B is the Boltzman constant and T is the absolute temperature.

A small correction for laser geometry has to be made effectively resulting in,

$$k_c = \frac{0.8\ k_B T}{\Delta x^2}$$

4.2 Single Molecule Force Spectroscopy

In single molecule force spectroscopy (SMFS) experiments it is crucial to ensure the interaction of single molecules with the AFM tip. Each cycle of a SMFS experiment can be divided into an approach and a retraction curve, and the events that take place during each phase can be generalized into six events.
During the approach, the tip is brought in contact with the molecule on the surface **(Figure 20 a.-b.).** The molecule can be grafted or also simply deposited on the surface. (There are also various strategies to chemically link the molecule directly on to the AFM tip, but these strategies will not be discussed here). As the approach phase continues the cantilever is pushed against the surface with increasing force beyond its contact point **(Figure 20 c.)**. During the retraction cycle the tip is moved away from the surface **(Figure 20 d.)** decreasing the force applied on the cantilever. If the molecule is successfully caught by the tip, the captured molecule

is then stretched by the cantilever displacement away from the substrate **(Figure 20 f.)**. Eventually the molecule detaches from the tip as the force applied by the cantilever displacement exceeds the force of interaction between the tip and the molecule **(Figure 20 g.)**. The detachment of the molecule causes the cantilever to jump back to its original shape, and the laser deflection resumes to the initial value of the baseline.

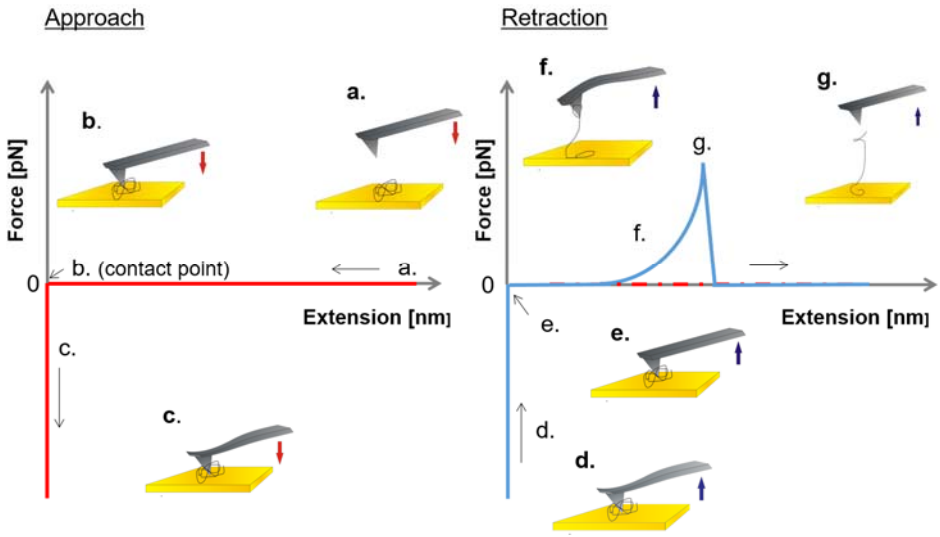

Figure 20. Schematic representation of an approach and retraction cycle and the corresponding events of a single molecule force spectroscopy experiment of a single linear macromolecule.

4.3 The Elastic Response of an Ideal Polymer Approximated by Polymer Statistical Mechanics

Many strategies can be adopted, such as favourable immobilization of the molecule on the surface,that permit single molecule interactions to be isolated from multiple molecule interactions. Among them, the usage of a polymer tether that functions as a separation length to isolate specific interactions from surface adhesion and multiple molecule interactions, is well known [70, 96, 97]. A flexible polymer tether also increases the conformational freedom between the interacting species. When identifying single molecule interactions the profile of the polymer can also function as a reference if the signature elastic profile has been previously determined. The elastic response of the stretched polymer + molecule of interest

can then be compared to known theoretical statistical models from polymer mechanics. The elastic behaviour of a random coil polymer can be described by the non-linear entropic restoring force against the extension of the polymer. As an extending force is applied to the polymer the number of conformations that it can adopt decreases with increasing extension. The entropic restoring force thus increases with extension in a parabolic manner. There are two well-known theoretical models, the freely jointed chain, and the worm-like chain model, which traditionally model the elastic behaviour of a random coil linear polymer independent of molecular composition. The models described below are valid until ≈ 50-100 pN [98] when only entropic contributions are considered. Beyond an extension force of 100 pN where dihedral distortions and stretching of covalent bonds beyond the contour length of the polymer become significant [95], enthalpic contributions must be taken into consideration by an additional Hookean term.

4.3.1 Freely Jointed Chain (FJC) Model

The conformation of a random polymer is described as a random walk, where starting from a single point in space, the chain can be described as being made up of N equal rigid segments of length l_k, which is referred to as the Kuhn length (**Figure 21**). The joints between each segment are flexible, and each subsequent segment can point in any spatial direction with equal probability. l_k is the only experimental fitting parameter for this model where only entropic contributions are considered. l_c denotes the contour length of the molecule, which is equal to $l_c = l_k \cdot N_{segments}$. The FJC model when only entropic contributions are considered can be written as,

$$x(F) = l_c \left[\coth\left(\frac{F l_k}{k_B T} - \frac{k_B T}{F l_k}\right)\right]$$

When enthalpic contributions are included another experimental fitting parameter κ is introduced which denotes the segment elasticity.

$$x(F) = l_c \left[\coth\left(\frac{F l_k}{k_B T} - \frac{k_B T}{F l_k}\right)\right] \left(1 + \frac{F}{\kappa l_c}\right)$$

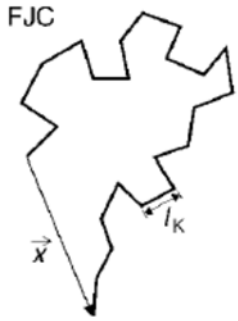

Figure 21. Schematic representation of the Freely Jointed Chain (FJC) model . l_k refers to the Kuhn length, which is the length of each rigid segment. $\vec{x}$ is the point-to-point distance vector connecting the starting and ending of the polymer chain. Adapted from a publication by Fuchs et al [95].

4.3.4 Worm-like Chain (WLC) Model

The worm-like chain model of Kratky and Porod [99] and Marko and Siggia [100] describes a semi-flexible polymer, where there is no discrete structure along the entirety of its length, but it rather describes an irregular, curvaceous string (**Figure 22**). The persistence length is a measure of flexibility of the polymer chain and describes a certain length where the direction of propagation of the chain remains linear, thus higher the persistence l_p the stiffer the polymer. The extension of the molecule is limited by its contour length l_c [101].

$$F(x) = \frac{k_B T}{l_p}\left[\frac{1}{4}\left(1 - \frac{x}{l_c}\right)^{-2} + \frac{x}{l_c} - \frac{1}{4}\right]$$

The WLC model takes into account correlations of orientations at small scales and is thus more correct than the FJC model to describe the extension of a semi-flexible polymer under an external force.
At higher forces when contributions from enthalpic stretching are accounted, another term $\frac{F}{\Phi}$ is introduced which denotes the extension of the chain due beyond its contour length as a result of the stretching force, F.

$$F(x) = \frac{k_B T}{l_p}\left[\frac{1}{4}\left(1 - \frac{x}{l_c} + \frac{F}{\Phi}\right)^{-2} + \frac{x}{l_c} - \frac{F}{\Phi} - \frac{1}{4}\right]$$

Figure 22. Schematic representation of the Worm-like chain (WLC) model. l_p refers to the persistence length, which is indicative of the flexibility of the polymer chain. $\vec{x}$ is the point-to-point distance vector connecting the starting and ending of the polymer chain. Adapted from a publication by Fuchs et al [95].

4.4 The Elastic Behaviour of a PEG-Polypeptide System Approximated by Polymer Statistical Mechanics

The WLC model provides an excellent basis for the estimation of the force-extension profiles for a generic, structure-less polymer-polypeptide as it takes correlations of orientations at small scales into account. This model is more than satisfactory for a quick analysis of force-extension curves to determine a characteristic deviation from the behaviour of an ideal, featureless polymer, which would indicate the unfolding event of the secondary structure. When both the polypeptide and the PEG are in a random coil conformation a fit utilizing the WLC model should be superimposable to the obtained force-extension profile. However it is important to note that small-scale structural parameters of PEG and polypeptides are neglected in such a generic model which may influence numerical parameters such as persistence length and contour length if such values are to be derived from the fit.

It is also to be mentioned that due to the architecture of the molecule and design of the experiment utilized in this thesis, the persistence and contour length derived from such a fit would not be accurate. (The design of the system utilized in this thesis consisted of a PEG tether by which one end of the molecule can adsorb onto the AFM cantilever, and the other end of the molecule was chemically bonded to a gold surface. (**Please refer to Chapter 2. Figure 1**) Therefore, both persistence and contour lengths will vary depending on the length of the PEG

tether caught by the AFM cantilever for each cycle. The overall persistence of such a system would be the sum of contributions from both the PEG and the polypeptide, thus if the extended length of the PEG segment varies for each cycle the persistence will also differ. In addition the length of the α-helix for all extended molecules should remain approximately the same in order to obtain the same value for the persistence length. This is difficult as the α-helices are known exist as a statistical ensemble of varying lengths.

Therefore for the purpose of this thesis only a WLC model was utilized for a qualitative analysis of force-extension curves. Nevertheless two models are briefly described below which were optimized to describe the extension of PEG and of a generic polypeptide to acknowledge that for each separated system there are more optimal models than the WLC.

4.4.1 The Elastic Behaviour of PEG

Oesterhelt, Rief and Gaub [102] showed that in apolar conditions, the elastic properties of PEG follows the extended freely jointed chain model, (FJC model + enthalpic contributions) very closely. However, an IR spectroscopy study by Begum and Matsuura showed [103] that PEG retains its helical structure in water that was originally also observed in its crystalline state. Keeping in mind that the deformation of PEG is fully reversible, Oesterhelt et al. hypothesized that the deviations of the force-extension of PEG in aqueous conditions from the extended FJC model is due to the PEG undergoing a rapid conformational transition between an elongated planer and helical structure. Thus, they derived a force-extension relation that is built upon the extended FJC model, but with additional terms. Their model takes into account the difference in contour lengths between the PEG in its shorter helical state and the elongated planer state, the Boltzmann distributed population between the two states and how the applied force alters the difference in free energy, ΔG.

For a PEG polymer comprised of, $N_{segments}$, the force extension relation is defined as [102],

$$l_c(F) = N_{segments} \cdot \left(\frac{l_{c\ planar}}{e^{\frac{-\Delta G}{k_B T}} + 1} + \frac{l_{c\ helical}}{e^{\frac{\Delta G}{k_B T}} + 1} \right) \cdot \left[\coth\left(\frac{F l_k}{k_B T} - \frac{k_B T}{F l_k} \right) \right] \left(N_{segments} + \frac{F}{K_s} \right)$$

Where l_k denotes the Kuhn length, $l_{c\ planar}$ and $l_{c\ helical}$ are the contour lengths of the planar and helical states and K_s is the segment elasticity measured in hexadecane for the same study.

The total contour length $l_{c\ total}$ is a sum of the contour lengths of the planar and helical states,

$$l_{c\ total} = N_{planar} \cdot l_{c\ planar} + N_{helical} \cdot l_{c\ helical}$$

The Boltzmann distributed ratio of the two populations is defined as,

$$\frac{N_{helical}}{N_{planar}} = e^{\frac{\Delta G}{k_B T}}$$

and ΔG is the energy difference between the two states when a force is applied.

$$\Delta G(F) = \left(G_{planar} - G_{helical} \right) - F \cdot (l_{c\ planar} - l_{c\ helical})$$

4.4.2 The Elastic Behaviour of Polypeptides

The WLC model has been utilized as a standard to fit the unfolding events of various proteins and polypeptides in single molecule force spectroscopy experiments [64, 72, 74, 104, 105] for decades, and still remains a valid model to use today. The inhomogeneous partially freely rotating chain model (iPFRC) reported by Hanke et al. [106], has been utilized by Torabi and Schatz [78] for the development of a statistical mechanical model of the force-extension of α-helical polypeptides. In their paper it is discussed that the WLC model has been shown to reproduce the results of the iPFRC model, however the fitted contour length has about a 10% overestimation. Therefore, if only a fitting of the unfolding event is done without

taking the numerical value of the contour length, the WLC model is more than sufficient for the fitting of a random coil polypeptide.

The inhomogeneous partially freely rotating chain model (iPFRC), is a modified freely rotating chain model (FRC), and in continuum, the FRC model originates from the FJC model. In the FJC model, arbitrary angles are assigned between segments of fixed length. The FRC mimics chemical bonding more closely in that there are fixed bond angles between successive segments, which are still able to rotate freely around the fixed angles. In a real peptide bond, the amide bond forms resonance hybrids, which results in the C=O and N-H residing in a single plane with no rotation around the hybridized C=N (ω) bond. The other two bonds (ψ and φ) within a peptide repeat are able to rotate more freely. Thus, in the inhomogeneous partially freely rotating chain model (iPFRC), one of the three bonds are fixed at 180 ° mimicking the C=N (ω) bond, and a multi-bond unit is defined with three different bond lengths and bond angles.
Using this model the following force-extension curve of a random coil polypeptide was obtained as a function of the extension ξ [78, 106],

$$f = \frac{k_B T \xi}{l_{c\ molecule}} \left(\frac{3}{l_k} + \frac{1}{c \cdot l_{c\ residue}} \cdot \frac{\xi / l_{c\ molecule}}{1 - \xi / l_{c\ molecule}} \right)$$

Where $l_{c\ molecule}$ is the contour length of the entire molecule, and $l_{c\ residue} = 3.65$ Å is the calculated length of an amino residue. $l_k = 7.45$ Å is the Kuhn length and c= 0.807 is a constant describing the peptide near full extension [106].

References

1. S. S. Naik, J. G. Ray and D. A. Savin, *Langmuir*, 2011, **27**, 7231-7240.
2. R. Y. Lochhead, in *Cosmetic Nanotechnology*, American Chemical Society, Editon edn., 2007, vol. 961, pp. 3-56.
3. R. A. Segalman, B. McCulloch, S. Kirmayer and J. J. Urban, *Macromolecules*, 2009, **42**, 9205-9216.
4. R. A. Segalman, *Materials Science and Engineering: R: Reports*, 2005, **48**, 191-226.
5. J. N. L. Albert and T. H. Epps Iii, *Materials Today*, 2010, **13**, 24-33.
6. E. A. Jackson and M. A. Hillmyer, *ACS Nano*, 2010, **4**, 3548-3553.
7. Y. Bae, H. Cabral and K. Kataoka, in *Block Copolymers in Nanoscience*, Wiley-VCH Verlag GmbH & Co. KGaA, Editon edn., 2008, pp. 73-89.

8. H. De Oliveira, J. Thevenot and S. Lecommandoux, *Wiley Interdisciplinary Reviews: Nanomedicine and Nanobiotechnology*, 2012, **4**, 525-546.
9. B. M. Discher, Y.-Y. Won, D. S. Ege, J. C. M. Lee, F. S. Bates, D. E. Discher and D. A. Hammer, *Science*, 1999, **284**, 1143-1146.
10. K. Kita-Tokarczyk, J. Grumelard, T. Haefele and W. Meier, *Polymer*, 2005, **46**, 3540-3563.
11. G. Fuks, R. Mayap Talom and F. Gauffre, *Chemical Society Reviews*, 2011, **40**, 2475-2493.
12. R. V. Ulijn and A. M. Smith, *Chemical Society Reviews*, 2008, **37**, 664-675.
13. J.-P. G. Senet, *Chemistry Today chimica oggi*, 2004, 24-26.
14. B. Perly, A. Douy and B. Gallot, *Die Makromolekulare Chemie*, 1976, **177**, 2569-2589.
15. H.-A. Klok, H. Schlaad and S. Lecommandoux, in *Peptide Hybrid Polymers*, Springer Berlin Heidelberg, Editon edn., 2006, vol. 202, pp. 75-111.
16. A. Nakajima, K. Kugo and T. Hayashi, *Macromolecules*, 1979, **12**, 844-848.
17. A. Nakajima, T. Hayashi, K. Kugo and K. Shinoda, *Macromolecules*, 1979, **12**, 840-843.
18. A. Carlsen and S. Lecommandoux, *Current Opinion in Colloid & Interface Science*, 2009, **14**, 329-339.
19. J. Clayden, N. Greeves, S. Warren, P. Wothers, *Organic Chemistry*, Oxford University Press, 2001.
20. H. Kukula, H. Schlaad, M. Antonietti and S. Förster, *Journal of the American Chemical Society*, 2002, **124**, 1658-1663.
21. F. Chécot, A. Brûlet, J. Oberdisse, Y. Gnanou, O. Mondain-Monval and S. Lecommandoux, *Langmuir*, 2005, **21**, 4308-4315.
22. F. Chécot, S. Lecommandoux, Y. Gnanou and H.-A. Klok, *Angewandte Chemie International Edition*, 2002, **41**, 1339-1343.
23. C. Cai, L. Zhang, J. Lin and L. Wang, *The Journal of Physical Chemistry B*, 2008, **112**, 12666-12673.
24. J. Rao, Z. Luo, Z. Ge, H. Liu and S. Liu, *Biomacromolecules*, 2007, **8**, 3871-3878.
25. W. Dzwolak, T. Muraki, M. Kato and Y. Taniguchi, *Biopolymers*, 2004, **73**, 463-469.
26. J. J. Grigsby, H. W. Blanch and J. M. Prausnitz, *Biophysical Chemistry*, 2002, **99**, 107-116.
27. K. E. Gebhardt, S. Ahn, G. Venkatachalam and D. A. Savin, *Journal of Colloid and Interface Science*, 2008, **317**, 70-76.
28. L.-K. Li and A. Spector, *Journal of the American Chemical Society*, 1969, **91**, 220-222.
29. B. Davidson and G. D. Fasman, *Biochemistry*, 1967, **6**, 1616-1629.
30. P. K. Sarkar and P. Doty, *Proceedings of the National Academy of Sciences of the United States of America*, 1966, **55**, 981-989.
31. J. G. Ray, S. S. Naik, E. A. Hoff, A. J. Johnson, J. T. Ly, C. P. Easterling, D. L. Patton and D. A. Savin, *Macromolecular Rapid Communications*, 2012, **33**, 819-826.
32. K. E. Gebhardt, S. Ahn, G. Venkatachalam and D. A. Savin, *Langmuir*, 2007, **23**, 2851-2856.
33. R. Sigel, M. Losik and H. Schlaad, *Langmuir*, 2007, **23**, 7196-7199.
34. J. Babin, J. Rodriguez-Hernandez, S. Lecommandoux, H.-A. Klok and M.-F. Achard, *Faraday Discussions*, 2005, **128**, 179-192.

35. J. Rodriguez-Hernandez and S. Lecommandoux, *Journal of the American Chemical Society*, 2005, **127**, 2026-2027.
36. I. W. Hamley, *Biomacromolecules*, 2014, **15**, 1543-1559.
37. K. Osada and K. Kataoka, in *Peptide Hybrid Polymers*, eds. H.-A. Klok and H. Schlaad, Springer Berlin Heidelberg, Berlin, Heidelberg, Editon edn., 2006, pp. 113-153.
38. Z. Ahmad, Z. Tang, A. Shah, S. Lv, D. Zhang, Y. Zhang and X. Chen, *Macromolecular Bioscience*, 2014, **14**, 1337-1345.
39. G. Lollo, G. R. Rivera-Rodriguez, J. Bejaud, T. Montier, C. Passirani, J.-P. Benoit, M. Garcia-Fuentes, M. J. Alonso and D. Torres, *European Journal of Pharmaceutics and Biopharmaceutics*, 2014, **87**, 47-54.
40. S. Lukasiewicz, K. Szczepanowicz, E. Blasiak and M. Dziedzicka-Wasylewska, *Langmuir*, 2015, **31**, 6415-6425.
41. S. Lukasiewicz and K. Szczepanowicz, *Langmuir*, 2014, **30**, 1100-1107.
42. A. Harada, S. Cammas and K. Kataoka, *Macromolecules*, 1996, **29**, 6183-6188.
43. K. Kataoka, H. Togawa, A. Harada, K. Yasugi, T. Matsumoto and S. Katayose, *Macromolecules*, 1996, **29**, 8556-8557.
44. K. Itaka, K. Yamauchi, A. Harada, K. Nakamura, H. Kawaguchi and K. Kataoka, *Biomaterials*, 2003, **24**, 4495-4506.
45. K. Shiraishi, K. Kawano, T. Minowa, Y. Maitani and M. Yokoyama, *Journal of Controlled Release*, 2009, **136**, 14-20.
46. H. Cui, X. Zhuang, C. He, Y. Wei and X. Chen, *Acta Biomaterialia*, 2015, **11**, 183-190.
47. P. Urnes, P. Doty, M. L. A. K. B. C.B. Anfinsen and T. E. John, in *Advances in Protein Chemistry*, Academic Press, Editon edn., 1962, vol. Volume 16, pp. 401-544.
48. G. Holzwarth and P. Doty, *Journal of the American Chemical Society*, 1965, **87**, 218-228.
49. N. J. Greenfield, *Nat. Protocols*, 2007, **1**, 2876-2890.
50. P. Luo and R. L. Baldwin, *Biochemistry*, 1997, **36**, 8413-8421.
51. N. R. Kallenbach, P. Lyu and H. Zhou, in *Circular Dichroism and the Conformational Analysis of Biomolecules*, ed. G. D. Fasman, Springer US, Boston, MA, Editon edn., 1996, pp. 201-259.
52. W. Schaertl, in *Light Scattering from Polymer Solutions and Nanoparticle Dispersions*, Springer Berlin Heidelberg, Berlin, Heidelberg, Editon edn., 2007, pp. 1-24.
53. B. J. Frisken, *Applied Optics*, 2001, **40**, 4087-4091.
54. D. E. Koppel, *The Journal of Chemical Physics*, 1972, **57**, 4814-4820.
55. S. W. Provencher, *Computer Physics Communications*, 1982, **27**, 213-227.
56. G. Binnig, C. F. Quate and C. Gerber, *Physical Review Letters*, 1986, **56**, 930-933.
57. B. Drake, C. B. Prater, A. L. Weisenhorn, S. A. Gould, T. R. Albrecht, C. F. Quate, D. S. Cannell, H. G. Hansma and P. K. Hansma, *Science*, 1989, **243**, 1586-1589.
58. W. Ott, M. A. Jobst, C. Schoeler, H. E. Gaub and M. A. Nash, *Journal of Structural Biology*, 2016.
59. E. L. Florin, V. T. Moy and H. E. Gaub, *Science*, 1994, **264**, 415-417.
60. L. Wildling, C. Rankl, T. Haselgrübler, H. J. Gruber, M. Holy, A. H. Newman, M.-F. Zou, R. Zhu, M. Freissmuth, H. H. Sitte and P. Hinterdorfer, *Journal of Biological Chemistry*, 2012, **287**, 105-113.

61. G. U. Lee, L. A. Chrisey and R. J. Colton, *Science*, 1994, **266**, 771-773.
62. M. Rief, F. Oesterhelt, B. Heymann and H. E. Gaub, *Science*, 1997, **275**, 1295-1297.
63. P. E. Marszalek, A. F. Oberhauser, Y.-P. Pang and J. M. Fernandez, *Nature*, 1998, **396**, 661-664.
64. M. Rief, M. Gautel, F. Oesterhelt, J. M. Fernandez and H. E. Gaub, *Science*, 1997, **276**, 1109-1112.
65. Z. Qin, A. Fabre and M. J. Buehler, *The European Physical Journal E*, 2013, **36**, 1-12.
66. L. Pauling, R. B. Corey and H. R. Branson, *Proceedings of the National Academy of Sciences of the United States of America*, 1951, **37**, 205-211.
67. J. C. Kendrew, R. E. Dickerson, B. E. Strandberg, R. G. Hart, D. R. Davies, D. C. Phillips and V. C. Shore, *Nature*, 1960, **185**, 422-427.
68. A. Ikai, in *Biopolymers: Lignin, Proteins, Bioactive Nanocomposites*, eds. A. Abe, K. Dusek and S. Kobayashi, Springer Berlin Heidelberg, Berlin, Heidelberg, Editon edn., 2010, pp. 65-96.
69. R. Afrin, I. Takahashi, K. Shiga and A. Ikai, *Biophysical Journal*, 2009, **96**, 1105-1114.
70. A. Idiris, M. T. Alam and A. Ikai, *Protein Engineering*, 2000, **13**, 763-770.
71. M. A. Lantz, S. P. Jarvis, H. Tokumoto, T. Martynski, T. Kusumi, C. Nakamura and J. Miyake, *Chemical Physics Letters*, 1999, **315**, 61-68.
72. F. Berkemeier, M. Bertz, S. Xiao, N. Pinotsis, M. Wilmanns, F. Gräter and M. Rief, *Proceedings of the National Academy of Sciences*, 2011, **108**, 14139-14144.
73. I. Schwaiger, C. Sattler, D. R. Hostetter and M. Rief, *Nat Mater*, 2002, **1**, 232-235.
74. M. Rief, J. Pascual, M. Saraste and H. E. Gaub, *Journal of Molecular Biology*, 1999, **286**, 553-561.
75. R. Rohs, C. Etchebest and R. Lavery, *Biophysical Journal*, 1999, **76**, 2760-2768.
76. B. Chakrabarti and A. J. Levine, *Physical Review E*, 2006, **74**, 031903.
77. A. Buhot and A. Halperin, *Macromolecules*, 2002, **35**, 3238-3252.
78. K. Torabi and G. C. Schatz, *Macromolecules*, 2013, **46**, 7947-7956.
79. A. Chakrabartty, R. L. Baldwin, F. M. R. J. T. E. C.B. Anfinsen and S. E. David, in *Advances in Protein Chemistry*, Academic Press, Editon edn., 1995, vol. Volume 46, pp. 141-176.
80. A. J. Doig and P. M. Conn, in *Progress in Molecular Biology and Translational Science*, Academic Press, Editon edn., 2008, vol. Volume 83, pp. 1-52.
81. H. Qian and J. A. Schellman, *The Journal of Physical Chemistry*, 1992, **96**, 3987-3994.
82. V. Muñoz and L. Serrano, *Biopolymers*, 1997, **41**, 495-509.
83. V. Muñoz and L. Serrano, *Nat Struct Mol Biol*, 1994, **1**, 399-409.
84. L. Pauling and R. B. Corey, *PNAS*, 1951, **37**, 251-256.
85. I. H. McColl, E. W. Blanch, A. C. Gill, A. G. O. Rhie, M. A. Ritchie, L. Hecht, K. Nielsen and L. D. Barron, *Journal of the American Chemical Society*, 2003, **125**, 10019-10026.
86. A. Micsonai, F. Wien, L. Kernya, Y.-H. Lee, Y. Goto, M. Refregiers and J. Kardos, *Proceedings of the National Academy of Sciences*, 2015, **112**, E3095-E3103.
87. A. F. Oberhauser, C. Badilla-Fernandez, M. Carrion-Vazquez and J. M. Fernandez, *Journal of Molecular Biology*, 2002, **319**, 433-447.

88. M. Carrion-Vazquez, A. F. Oberhauser, T. E. Fisher, P. E. Marszalek, H. Li and J. M. Fernandez, *Progress in Biophysics and Molecular Biology*, 2000, **74**, 63-91.
89. T. Hoffmann and L. Dougan, *Chemical Society Reviews*, 2012, **41**, 4781-4796.
90. D. J. Brockwell, E. Paci, R. C. Zinober, G. S. Beddard, P. D. Olmsted, D. A. Smith, R. N. Perham and S. E. Radford, *Nat Struct Mol Biol*, 2003, **10**, 731-737.
91. Z. Qin and M. J. Buehler, *Physical Review Letters*, 2010, **104**, 198304.
92. F. Ding, J. M. Borreguero, S. V. Buldyrey, H. E. Stanley and N. V. Dokholyan, *Proteins: Structure, Function, and Bioinformatics*, 2003, **53**, 220-228.
93. W. F. Heinz and J. H. Hoh, *Trends in Biotechnology*, 1999, **17**, 143-150.
94. T. Hugel and M. Seitz, *Macromolecular Rapid Communications*, 2001, **22**, 989-1016.
95. A. Janshoff, M. Neitzert, Y. Oberdörfer and H. Fuchs, *Angewandte Chemie International Edition*, 2000, **39**, 3212-3237.
96. A. Ikai, A. Idiris, H. Sekiguchi, H. Arakawa and S. Nishida, *Applied Surface Science*, 2002, **188**, 506-512.
97. T. Sulchek, R. W. Friddle and A. Noy, *Biophysical Journal*, 2006, **90**, 4686-4691.
98. A.-S. Duwez and N. Willet, *Molecular manipulation with atomic force microscopy*, CRC Press, 2011.
99. O. Kratky and G. Porod, *Recueil des Travaux Chimiques des Pays-Bas*, 1949, **68**, 1106-1122.
100. J. F. Marko and E. D. Siggia, *Macromolecules*, 1995, **28**, 8759-8770.
101. C. G. Baumann, S. B. Smith, V. A. Bloomfield and C. Bustamante, *Proceedings of the National Academy of Sciences*, 1997, **94**, 6185-6190.
102. F. Oesterhelt, M. Rief and H. E. Gaub, *New Journal of Physics*, 1999, **1**, 6.
103. R. Begum and H. Matsuura, *Journal of the Chemical Society, Faraday Transactions*, 1997, **93**, 3839-3848.
104. A. F. Oberhauser, P. E. Marszalek, H. P. Erickson and J. M. Fernandez, *Nature*, 1998, **393**, 181-185.
105. C. He, C. Hu, X. Hu, X. Hu, A. Xiao, T. T. Perkins and H. Li, *Angewandte Chemie International Edition*, 2015, **54**, 9921-9925.
106. F. Hanke, A. Serr, H. J. Kreuzer and R. R. Netz, *EPL (Europhysics Letters)*, 2010, **92**, 53001.

Chapter 2

Synthesis of PEG_{114}-*b*-$(PGA)_{85}$-(2-pyridyl disulphide) and PEG_{114}-*b*-$(PLys)_{134}$-(2-pyridyl disulphide) and Investigation of the Unfolding of Homopeptide α-Helices by Single Molecule Force Spectroscopy

Abbreviations:

AFM- Atomic Force Microscopy

CD- Circular Dichroism

DLS- Dynamic Light Scattering

FJC Model- Freely Jointed Chain Model

iPFRC Model- Inhomogeneous Partially Freely Rotating Chain Model

NCA- *N*-carboxyanhydride

Bn-Glu NCA –γ-Benzyl-*L*-glutamate *N*-carboxyanhydride

N^{ε}-TFA-*L*-Lys-NCA- N^{ε}-Trifluoroacetyl-*L*-lysine *N*-carboxyanhydride

PEG_{114}-*b*-$(PGA)_{85}$-(2-dipyridyl disulphide)- Poly(ethylene glycol)$_{114}$-*b*-poly(*L*-glumatic acid)$_{85}$- (2-pyridyl disulphide)

PEG_{114}-*b*-$(PLys)_{134}$-(2-dipyridyl disulphide)- Poly(ethylene glycol)$_{114}$-*b*-poly(*L*-lysine)$_{134}$-(2-pyridyl disulphide)

ROP-Ring Opening Polymerization

SEC- Size Exclusion Chromatography

SMFS- Single Molecule Force Spectroscopy

WLC Model- Worm-like Chain Model

Contents

Introduction

The study of the underlying mechanisms of protein folding and misfolding is crucial to further our understanding into the cause and prevention of many human diseases. In recent years, the study of intermediates have suggested that the folding of proteins occurs by the rapid folding of local secondary structures stabilized through interactions with key amino-acid residues, which forms a scaffold around which the rest of the residues condenses [1, 2]. The initial formation of the local secondary structures during protein folding indicates that the successful folding of the secondary structures is a crucial component in determining that the protein adopts its correct native structure. Acknowledging the high prevalence and importance of the α-helix structure in natural proteins, it merits an in-depth study on the single molecule scale, where an investigation under controlled conditions will allow us to better understand the factors that influence its mechanical properties and stability. Although it is not claimed that a model polypeptide system is perfectly comparable to a natural protein, the use of synthetic polymer-peptides allows us to tune and isolate desirable properties and, as a result gain an insight into more complex biological systems by observing the isolated property in a carefully controlled environment. Indeed, polymer-peptides have been used as a model system to study generic self-assemblies and interactions seen in natural proteins [3].

Thus, for the further study into the unfolding of α-helical motifs, two stimuli-responsive, bioinspired, poly(ethylene glycol)$_{114}$-*b*-poly(*L*-glutamic acid)$_{85}$-(2-pyridyl disulphide) (**PEG_{114}-*b*-$(PGA)_{85}$-(2-pyridyl disulphide**) and poly(ethylene glycol)$_{114}$-*b*-poly(*L*-lysine)$_{134}$-(2-pyridyl disulphide) **(PEG_{114}-*b*-$(PLys)_{134}$-(2-pyridyl disulphide)** were designed and synthesized for use in single-molecule force experiments (SMFS) with an atomic force microscope (AFM) **(Figure 1)** In this chapter the synthesis of the diblock copolymers and their characterization in bulk are introduced, followed by single molecule force spectroscopy experiments (SMFS) in differing pH and salt conditions. Although previous SMFS studies have been done in unfolding synthetic peptide α-helices [4-6] in the present work the unfolding of polypeptides that undergo helix coil transitions at opposing pH conditions were compared *in situ* in order to further understand the factors that affect helix mechanical stability.

The Design of Poly-*L*-glutamic acid and Poly-*L*-Lysine Containing Polymer-polypeptide Hybrids for use in Single Molecule Force Spectroscopy Experiments

Poly(ethylene glycol)$_{114}$-*b*-poly(*L*-glutamic acid)$_{85}$- (2-pyridyl disulphide) (**PEG_{114}-*b*-$(PGA)_{85}$-(2-pyridyl disulphide)** and poly(ethylene glycol)$_{114}$-*b*-poly(*L*-lysine)$_{134}$-(2-pyridyl disulphide) **(PEG_{114}-*b*-$(PLys)_{134}$-(2-pyridyl disulphide)** were custom-designed with the intent of optimizing single molecule force spectroscopy (SMFS) experiments. SMFS is an extraordinarily precise and powerful technique that when successful can elucidate the mechanochemical behaviour of molecules *in situ* on the single molecular level. However despite it being a well-developed technique, experimental throughput has always been hampered by low event probability. In a typical experiment many thousand force-extension curves are recorded, but the majority (≈80%-99%) of the curves contain either no interactions, multiple interactions resulting from pulling multiple molecules, or unspecific adhesion [7]. Yet, even from the small percentage of usable single-molecule interaction curves, only a very small fraction of them will be an exemplary force-extension curve. This is why the design process of a SMFS experiment is so crucial to its success, as reliable immobilization techniques that leads to the isolation of single molecules will increase the probability that for each experiment successful force-extension profiles are obtained.

The design of the molecules used in this study consisted of a PEG tether by which one end of the molecule could physisorb on to a bare AFM cantilever, and a 2-dipyridyl disulphide moiety grafting the other end onto a gold surface through Au-S bonding (**Figure 1**). Direct physisorption of the molecule of interest on to a cleaned surface have been successfully utilized [8-10], and as well the use of PEG as the physisorbing entity [11]. Physisorption alone was shown to withstand forces up to ≈200 pN well within the range we hope to observe our interactions. The use of PEG as a heterobifunctional linker for peptide and DNA samples has been reported in literature [5, 12], and has been used as a separation length [13, 14] to separate the specific interactions from the non-specific. We chose to graft the molecules on to a gold surface through Au-S bonding, and not covalently link our molecule to the AFM cantilever, as this allows us to sample multiple molecules per experiment. The Au-S bond between the disulphide group of the 2-pyridyl disulphide and the gold surface is stronger than the force of detachment [15] of the physisorbed PEG from the bare AFM cantilever. Thus for every cycle that a

molecule is caught, it can be stretched until eventual detachment from the cantilever, and the bare cantilever is free to pull on another molecule at another location on the surface for subsequent cycles. A similar design of the molecule has already been successfully utilized by Lussis et al. for SMFS experiments of a rotaxane molecule [16].

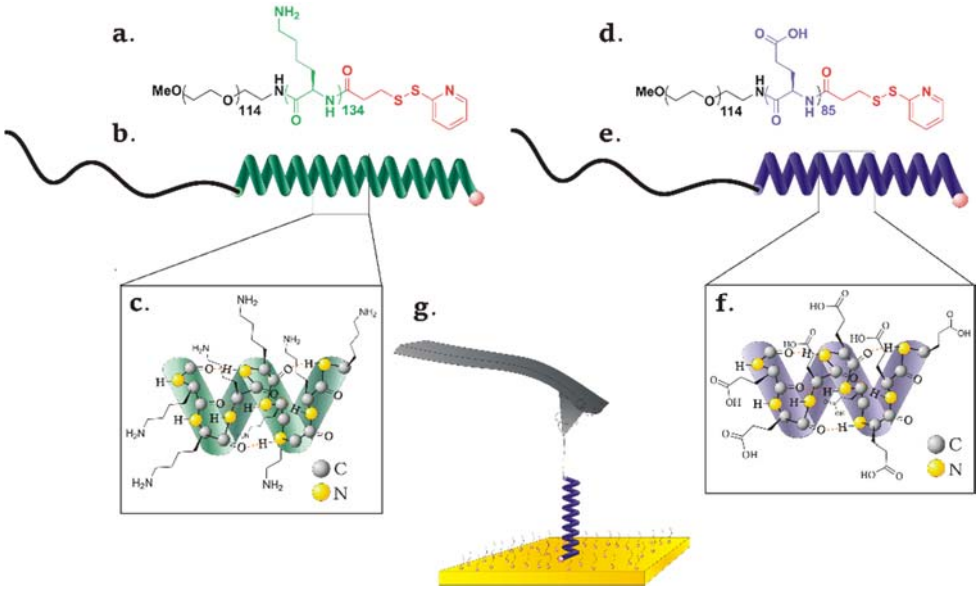

Figure 1. Schematic Representations of PEG_{114}-*b*-poly(*L*-lysine)$_{134}$-(2-pyridyl disulphide) and PEG_{114}-*b*-poly(*L*-glutamic acid)$_{85}$-(2-pyridyl disulphide). a.) Chemical structure of poly(ethylene glycol)$_{114}$-*b*-poly(*L*-lysine)$_{134}$-(2-pyridyl disulphide). b.) Schematic representation of PEG_{114}-*b*-poly(*L*-lysine)$_{134}$-(2-pyridyl disulphide) in a α-helix conformation. c.) Detailed representation of side chains and hydrogen bonding within the poly-*L*-lysine α-helix. d.) Chemical structure of poly(ethylene glycol)$_{114}$-*b*-poly(*L*-glutamic acid)$_{85}$- (2-pyridyl disulphide). e.) Schematic representation of PEG_{114}-*b*-poly(*L*-glutamic acid)$_{85}$-(2-pyridyl disulphide) in an α-helix conformation. f.) Detailed representation of side chains and H-bonding within the polyglutamic acid α-helix. g.) Schematic representation of a molecule grafted onto a gold surface with the PEG chain physisorbed onto a bare AFM cantilever and the 2-pyridyl disulphide (red dot) on the other end of the molecule as an anchoring moiety. The molecule is surrounded by PEG_6-SH also grafted on to the surface as a passivating agent.

PART I
Synthesis and Characterization of PEG_{114}-*b*-poly(*L*-glutamic acid)$_{85}$-(2-pyridyl disulphide) and PEG_{114}-*b*-poly(*L*-lysine)$_{134}$-(2-pyridyl disulphide) for use in Single Molecular Force Spectroscopy Experiments.

1.1 Synthesis of PEG-polypeptide Block Copolymers by Ring Opening Polymerization of Amino acid *N*-carboxyanhydrides.

PEG_{114}-*b*-poly(*L*-glutamic acid)$_{85}$-(2-pyridyl disulphide) and PEG_{114}-*b*-poly(*L*-lysine)$_{134}$-(2-pyridyl disulphide) were synthesized by ring-opening polymerization (ROP) of *N*- Trifluoroacetyl-*L*-lysine *N*-carboxyanhydride (N^{ε}-TFA-*L*-nLys-NCA) and γ-Benzyl-*L*-glutamate *N*-carboxyanhydride (Bn-Glu NCA) initiated by a PEG_{114}-NH_2 initiator (M_n= 5000 $\frac{g}{mol}$). The protected molecules were then coupled with *N*-Succinimidyl-3(2-pyridyldithio) propionate (SPDP).

Precision synthesis of polypeptides can be achieved through solid-phase peptide synthesis, however it is tedious, and not practical for the synthesis of large polypeptides. The most economical and facile synthesis route of polypeptides is through the ring-opening polymerization of amino acid *N*-carboxyanhydrides (NCA) [17, 18]. However, NCA polymerization is often affected by unwanted side-reactions, which is why the purity of the reagents used, and working under strictly anhydrous conditions is paramount. The great advantage of NCA polymerization is the facile control of the degree of polymerization of the resulting polypeptide by controlling the monomer to initiator ratio. Nonetheless, when side-reactions occur it inevitably leads to polypeptides that have a different structure from those predicted from the initial monomer feed. The desired amine-initiated polymerization is oft accompanied by an activated monomer initiated polymerization, which unavoidably leads to high dispersities and the presence of unwanted homopolymers that are extremely difficult to separate from the desired polypeptide. The activated monomer mechanism is initiated by the deprotonation of the nitrogen of the NCA. The deprotonated NCA functions as the nucleophile which then attacks another NCA monomer in lieu of the amine initiator [17]. To further complicate matters spontaneous solvent-induced reactions have also been shown to occur when monomers were left in nucleophilic solvents such as dimethylformamide (DMF), and dimethyl sulfoxide (DMSO) [19]. It is often the case

that the use of these solvents, especially DMF, is unavoidable as they often are the only solvents that solubilize both the NCA monomers and the resulting polypeptides successfully. Thankfully in the past decades much research has been done to eliminate these side reactions, notable examples include the use of N-protected NCAs where a protecting group is attached to the nitrogen of the NCA, and the use of organometallic initiators [20, 21]. The use of N-protected NCAs, and organometallic initiators in preventing side reactions has been largely successful, notable examples are the urethane protected NCAs [22] and organonickel initiators [20]. However, the disadvantage that these strategies share is that after the polymerization, these protecting species must be separated from the final product. As the polymer-polypeptides synthesized in this study were destined for use in SMFS experiments, potential contaminants must be kept to a minimum. A much simpler and cleaner way of controlling side reactions and obtaining better defined polymers has been reported by decreasing the reaction temperature to 0 °C [18, 23]. Naturally the time of polymerization increases with decreasing the temperature, but the benefit of this strategy far outweighs this disadvantage. Low temperature synthesis is particularly necessary and important to minimize cyclization reactions for ring-opening polymerization reactions of γ-Benzyl-*L*-glutamate *N*-carboxyanhydride. A low temperature strategy was also adopted for the ring opening polymerization reactions of N^{ε}-Trifluoroacetyl-*L*-lysine *N*-carboxyanhydride (N^{ε}-TFA-*L*-Lys-NCA) utilized in this work.

In the following sections the synthesis and characterization of PEG_{114}-*b*-(poly-*L*-lysine)$_{134}$-(2-pyridyl disulphide) is discussed in detail. The synthesis of PEG_{114}-*b*-(poly-*L*-glutamic acid)$_{85}$-(2-pyridyl disulphide) was not done by the author of this thesis as it had been already previously synthesized by Dr. Nicolas Willet. Nonetheless the synthesis and characterization of this molecule are discussed briefly at the end of the section.

1.1.1 Synthesis of PEG_{114}-*b*-poly(N^{ε}-trifluoroacetyl-*L*-lysine)$_{134}$-NH_2 by ROP of N^{ε}-TFA-*L*-Lys-NCA.

The synthesis of polypeptides with ring-opening polymerization of NCA proceeds by a well-documented amine mechanism, where a nucleophilic primary amine initiates the polymerization [21]. The primary amine used to initiate the polymerization of N^{ε}-TFA-*L*-Lys-NCA was PEG_{114}-NH_2 **(2)** which was synthesized from PEG_{114}-OH with PEG_{114}-SO_3CH_3 **(1)** as an intermediate

compound (**Figure 2**).

.

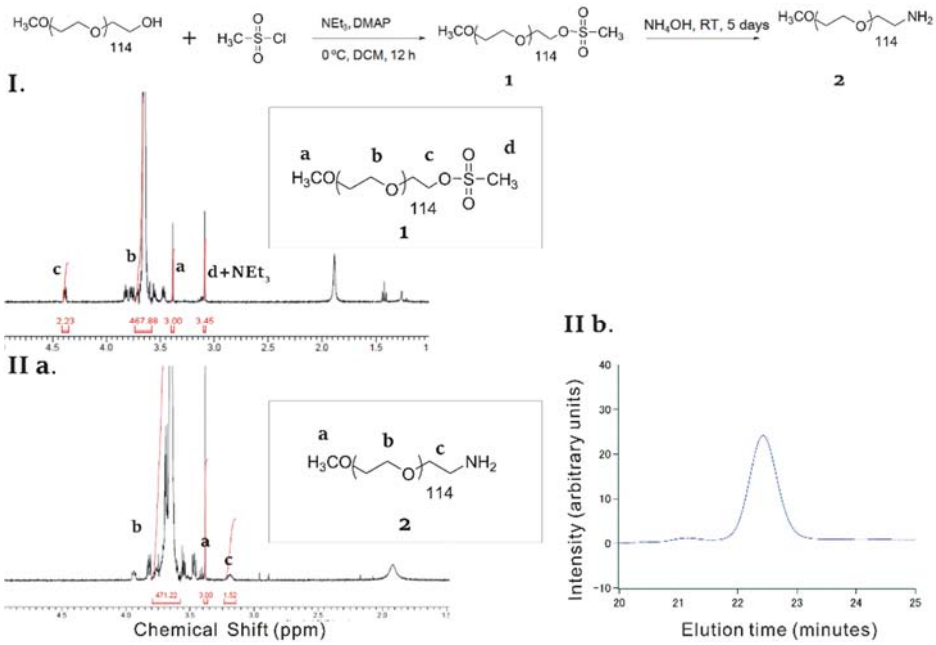

Figure 2. Synthesis of PEG_{114}-NH_2 from PEG-OH with PEG-SO_3CH_3 as an intermediate compound. I.) ^{1}H NMR of PEG-SO_3CH_3 in $CDCl_3$ (Bruker 400MHz). The degree of functionalization was confirmed by comparing the integration of the protons on the methyl group labelled as **a** in (CH_3O, σ= 3.38) with that of the ethyl protons beside the mesylate **c**, ($CH_2OS(O_2)CH_3$, σ= 4.38). II a.) ^{1}H NMR of PEG-NH_2 in $CDCl_3$ (Bruker 400MHz). The degree of functionalization was confirmed by ^{1}H NMR by comparing the integration of the protons on the methyl end-group labelled as **a** (CH_3O, σ= 3.38) with that of the ethyl protons beside the amine end-function **c**, (CH_2NH_2, σ= 3.19) II b.) SEC of PEG-NH_2 in DMF: 1g·L^{-1} LiBr, $Đ\frac{Mw}{Mn}$=1.02.

After PEG_{114}-NH_2 **(2)** was successfully obtained, it was used for subsequent ROP polymerization of N$^{\varepsilon}$-TFA-*L*-Lys-NCA (**Figure 3**). The temperature of the reaction was lowered to 5 °C, but not lower so as to not compromise solubility. The combined reactants formed a highly viscous solution as the targeted degree of polymerization was relatively high and the PEG initiator was also relatively long. By raising the temperature slightly good solubility was maintained without adding extra DMF to the reaction vessel, as it has to be partially removed prior to precipitation. The degree of polymerization was controlled by adjusting the monomer/initiator ratio.

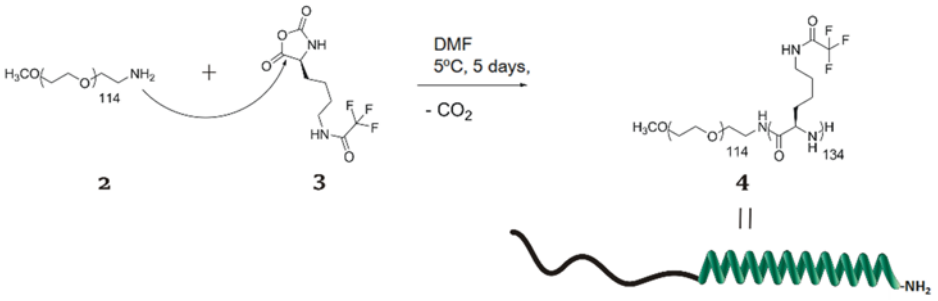

Figure 3. Initiation and growth of PEG-NH_2 initiated ROP of N^{ε}-TFA-*L*-Lys-NCA

The resulting degree of polymerization (D.P≈ 134) was determined by comparing the integration of the peak corresponding to the CH_2 signal nearest to the trifluoroacetyl group labelled as **(d)** ($C\mathbf{H_2}NHCOCF_3$, σ=3.13 ppm) with that of the integration of the peak corresponding to the PEG_{114} ($C\mathbf{H_2}C\mathbf{H_2}O$, σ=3.51) labelled as **(a)** (**Figure 4**). A small secondary peak can be seen in the SEC trace, which was thought to be the unreacted PEG and other small contaminants. The SEC trace of the triblock copolymer (Please refer to Chapter 3 Figure 3) does not show this secondary peak as additional purification steps such as ultrafiltration and dialysis were utilized. Thus, when only precipitation used as a purification step, some small contaminants remained in the sample.

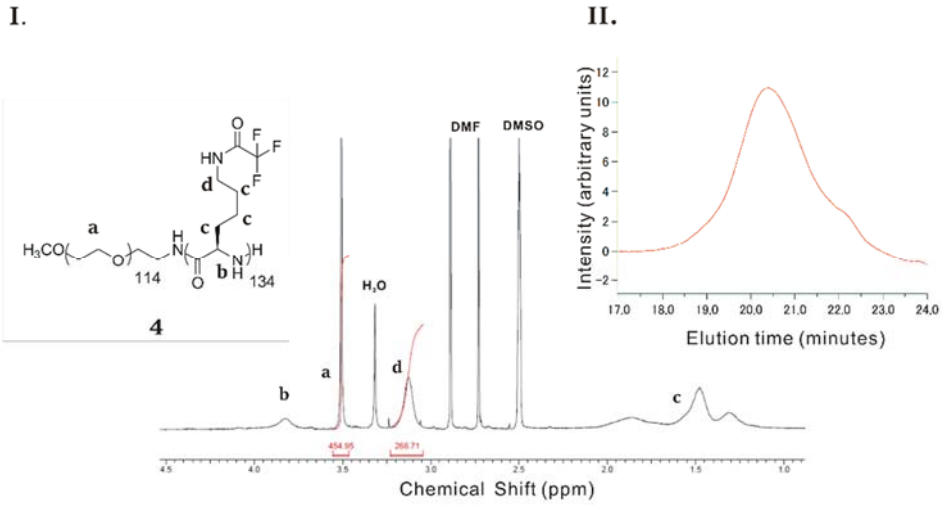

Figure 4. ^{1}H NMR spectrum and SEC trace of the resulting PEG_{114}-*b*- poly (N^{ε}- trifluoroacetyl -*L*-lysine) $_{134}$-NH_2. II a.) ^{1}H NMR of PEG_{114}-*b*- poly (N^{ε}- trifluoroacetyl-*L*-lysine) $_{134}$-NH_2 in DMSO-d_6 (Bruker 400MHz). II b.) SEC of PEG_{114}-*b*- poly (N^{ε}- trifluoroacetyl -*L*-lysine) $_{134}$-NH_2 in

DMF: 1g·L^{-1} LiBr , $Đ\frac{Mw}{Mn}$=1.16; 80 °C.

1.1.2 Synthesis of PEG_{114}-*b*-poly(N^{ε}-trifluoroacetyl-*L*-lysine)$_{134}$-(2-pyridyl disulphide) by Coupling Reaction of *N*-succinimidyl 3-(2-pyridyldithio)propionate (SPDP) to the N-terminal Amino Group.

Amine-coupling reaction by an *N*-hydroxysuccinimide (NHS) ester, *N*-succinimidyl 3-(2-pyridyldithio)propionate (SPDP) was used to couple a 2-pyridyl disulphide group to the terminal amine of PEG_{114}-*b*-poly(N^{ε}-trifluoroacetyl-*L*-lysine)$_{134}$-NH_2 **(4)**. A homobifunctional NHS ester, dithiobis (succinimidyl propionate) was introduced in the mid 1970's [24, 25] as a protein crosslinking agent. Since then NHS esters have been widely used as an amine modification reagent for bioconjugation techniques as their reaction with a primary or secondary amines results in a stable amide or imide linkage [26]. A heterobifunctional reagent *N*-succinimidyl 3-(2-pyridyldithio)propionate (SPDP) was introduced in 1978 [27], which could be further reduced to a thiol group by dithiothreitol.

After coupling the SPDP group to the PEG_{114}-*b*-poly (N^{ε}-trifluoroacetyl-*L*-lysine)$_{134}$-NH_2 **(4)**, the disulphide moiety was not reduced to a thiol as disulphides tend to be more stable and they are similarly capable forming Au-S bonds with a gold surface. The PEG_{114}-*b*-poly(N^{ε}- trifluoroacetyl-*L*-lysine)$_{134}$-(2-pyridyl disulphide) **(5)** was deprotected by the addition of KOH which cleaved the trifluoroacetyl group, resulting in the final product PEG_{114}-*b*-(poly-*L*-lysine)$_{134}$-(2-pyridyl disulphide) **(6)**.

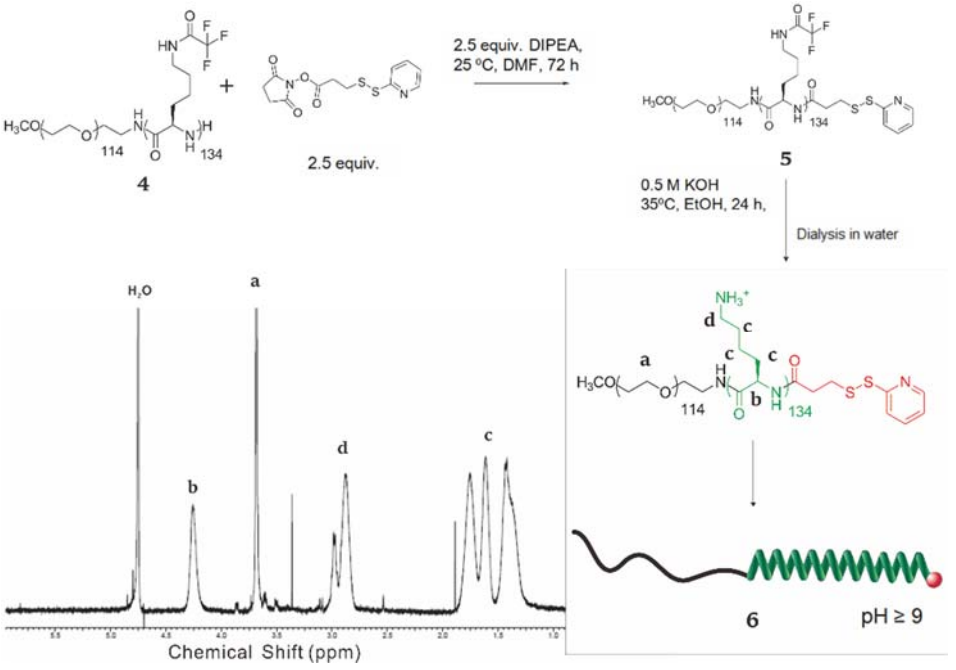

Figure 5. Coupling reaction of *N*-succinimidyl 3-(2-pyridyldithio)propionate (SPDP) with PEG_{114}-*b*-poly(N^{ε}- trifluoroacetyl-*L*-lysine)$_{134}$-NH_2, and subsequent deprotection. ^1H NMR of PEG_{114}-*b*-(poly-*L*-lysine)$_{134}$-(2-pyridyl disulphide) in D_2O (Bruker 400MHz). The schematic representation depicts the deprotonated lysine side chain at high pH allowing the polypeptide segment to fold into a α-helix. In the conditions utilized for the synthesis, and purification the molecule would adopt a random coil conformation as also indicated by the position of the ε–CH_2 peak **(d)** ≈ 3.0 ppm

The ^1H NMR spectrum of PEG_{114}-*b*-poly (N^{ε}-trifluoroacetyl-*L*-lysine)$_{134}$-(2-pyridyl disulphide) **(5)** is not shown as the signal of the 2-pyridyl disulphide molecule is comparatively small to the rest of the molecule and cannot be seen in the ^1H NMR spectrum. We acknowledge this significant weakness in the characterization, however the same coupling conditions were used for the coupling of PEG_{114}-α-methoxy-ω-NHS ester to the same PEG_{114}-*b*-poly(N^{ε}-trifluoroacetyl-*L*-lysine)$_{134}$-NH_2 molecule for the synthesis of the triblock molecule, which resulted in 100% conversion. In addition both syntheses used an excess of the NHS ester (2.5 molar equivalent) to ensure full conversion. The excess was removed in the subsequent purification steps. In this regard, as we were able to synthesize the triblock copolymer by the same NHS coupling conditions we assume that the NHS coupling of the smaller SPDP to the PEG-polypeptide was successful.

The SEC trace comparing the diblock copolymer PEG_{114}-*b*-poly(*L*-lysine)$_{134}$-(2-pyridyl disulphide) and the triblock copolymer PEG_{114}-*b*-poly(*L*-lysine)$_{134}$-PEG_{114} can be found in Chapter 3 Figure 3.

1.2 The pH responsiveness of PEG_{114}-*b*-poly(*L*-lysine)$_{134}$-NH_2 determined by Circular Dichroism.

The pH of the coil-helix transition for a poly-*L*-lysine has been previously determined by CD [28, 29] and can be estimated to be at the range of the pK_a value of the lysine side chain ≈10. The pH range where the transition occurs for a PEG_{98}-*b*-poly(*L*-lysine)$_{19}$ copolymer was determined to be between pH 9.0 - 11.0 [30]. Beyond the pK_a value of the lysine side-chain, the backbone of the polypeptide is able to fold into a helix as the amine groups of the side-chains become progressively deprotonated, and the electrostatic repulsions are inhibited.

The behaviour of PEG_{114}-*b*-poly(*L*-lysine)$_{134}$-NH_2 under different pH conditions was determined with circular dichroism spectrometry prior to coupling with SPDP. The molecule after coupling was not directly used as the 2-pyridyl disulphide is very small in comparison to the rest of the molecule and assumed to not influence the pH responsive conformational transition of the molecule.

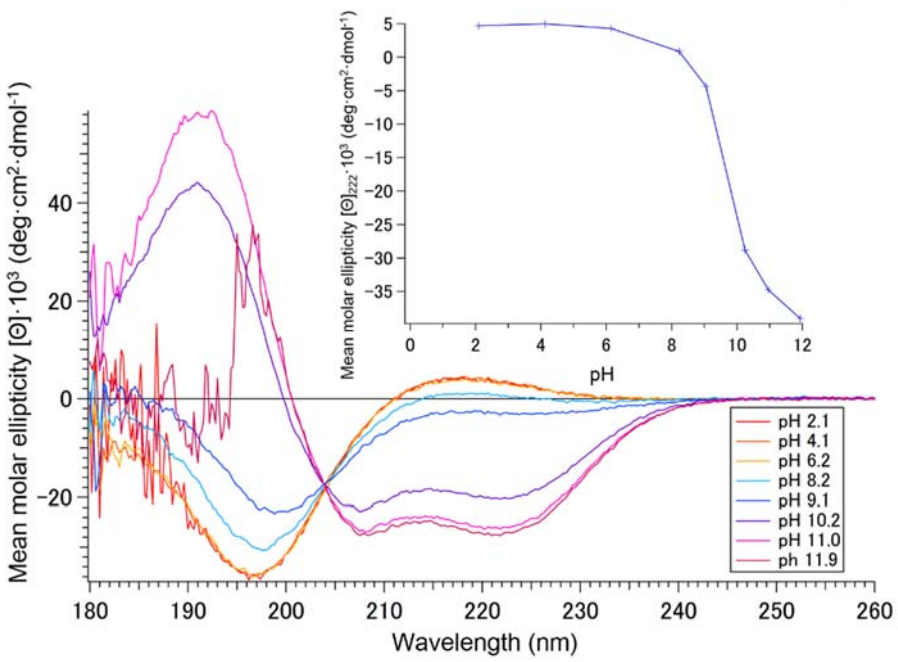

Figure 6. Circular dichroism spectra between 180 nm-260 nm of PEG_{114}-*b*-poly(*L*-lysine)$_{134}$-NH_2 in different pH conditions from pH 2-12. Concentration=0.25 mg/ml; cell length=0.1cm; 20 °C. The inset shows the variation of the mean molar ellipticity $|\theta_{mean\ molar}|$ at 222 nm with pH.

The obtained CD spectrum (**Figure 6**) shows that PEG_{114}-*b*-poly(*L*-lysine)$_{134}$-NH_2 is able to undergo a coil-helix transition in response to pH. At pH 9 and below the molecule adopts a random coil structure, indicated by a characteristic strong negative mean molar ellipticity $[\theta_{mean\ molar}]$ between 195-197 nm and a weakly positive $[\theta_{mean\ molar}]$at around 215 nm. From pH 10 and above the block copolymer adopts a α-helix conformation, indicated by a characteristic positive $[\theta_{mean\ molar}]$ at 190 nm and two negative peaks at 208 nm and 222 nm respectively. A clear transition from a predominantly random coil to that of a helix conformation occurs rapidly between pH 9 and 10. The transition from coil to a helix is almost completed at pH 11 and is completed at pH 12. The inset shows a graph following the evolution of the $[\theta_{mean\ molar}]$ at 222 nm with change in pH.

Using the expressions and values proposed by Luo and Baldwin [31], the estimated helix content was 53.2% at pH 10, 67.5% at pH 11 and 70.9% at pH 12 (Please see explanatory section in Chapter 1) . The helix content is considered only as an estimate, because it is strictly incorrect to assume a fixed fractional helical percentage. The peptides in bulk are rather an ensemble of helices of

varying, fluctuating lengths. In addition it is important to keep in mind that the properties obtained for molecules in bulk solution do not necessarily correspond to the behaviour of the molecule at the single molecule scale. Nonetheless, the CD spectra demonstrates that the molecule is able to undergo a conformational transition in response to pH and that most of the available polypeptide segment can fold into the helix.

1.3 Dynamic Light Scattering of PEG_{114}-*b*-poly(*L*-lysine)$_{134}$-NH_2.

The samples were prepared at a concentration of 1 $mg \cdot ml^{-1}$ of copolymer dissolved in 10 mM, 50 mM and 0.1 M NaCl. All of the solutions used to dissolve the copolymer were filtered, however the solution was not filtered after the copolymer was dissolved inside. The solutions were well mixed and put in an ultrasonic bath for 5-10 min prior to measurement. The pH of the solution was adjusted immediately before the measurement with either NaOH or HCl (0.1 M and 1 M), which was freshly prepared on the day of the experiment.

Intensity, volume and number distributions can be shown on the DLS. The intensity distribution (**Figure 7**) showed two peaks. When the most prominent peak was plotted against pH it showed that the detected hydrodynamic radius varied haphazardly and there was no apparent trend when the pH or the ionic concentration was changed. When the number distribution was shown there was only one apparent peak below 10 nm. The detected hydrodynamic radius varied little for all pH conditions and ionic concentrations. The difference between the distributions can be explained when we consider that for the intensity distribution the scattering of a particle is proportional to 10^6 of its radius, whereas the number distribution shows the relative number of scattering particles for each size. From looking at both the intensity weighted and number weighted distributions, we can hypothesize that the diblock forms few aggregates in the solutions that originate most of the scattering. However, the vast majority of the diblock copolymers are well dissolved in the solution and in the form of unimers, despite variation of the pH to induce a conformational transition from a random coil to α-helix.

The inability of block copolymers to self-assemble is not commonly reported, however as the intended use for our molecule is single molecule force spectroscopy these results are encouraging. It indicates that the PEG_{114}-*b*-poly(*L*-lysine)$_{134}$ diblock does not readily form aggregates or self-assemble in the conditions used to graft the molecules onto the surface prior to single molecule experiments. It also shows that even if a conformational transition is induced during the experiment, the molecule remains well dissolved in the solution. In order to enforce the formation of self-assemblies for a doubly hydrophilic PEG_{114}-

b-poly(*L*-lysine)$_{134}$, vastly greater concentrations must be used than that of which is relevant for single molecule force spectroscopy experiments (≈0.1 mg·ml^{-1}).

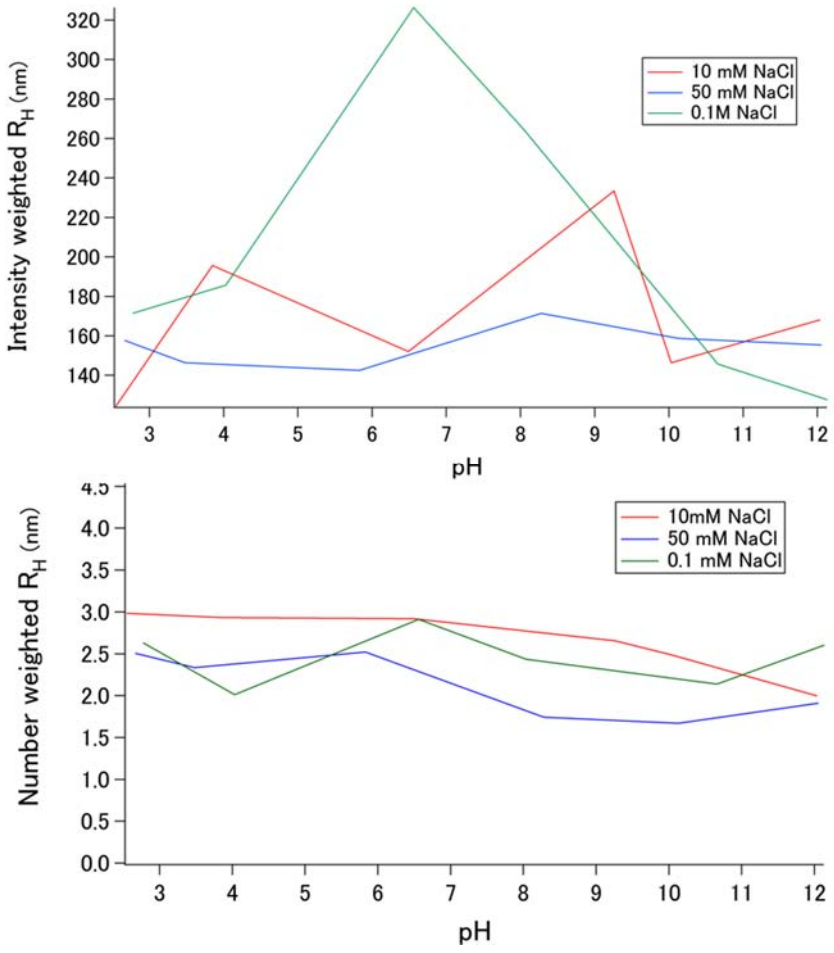

Figure 7. Intensity weighted and number weighted distributions for the hydrodynamic radius (R_H) of PEG_{114}-*b*-poly(*L*-lysine)$_{134}$-NH_2 for pH 2-12 and 10 mM, 50 mM and 0.1 M NaCl concentrations. All measurements were done at a detector angle of 90 °.

1.4 Section Summary: Synthesis and Characterization of PEG_{114}-*b*-poly(*L*-lysine)$_{134}$-(2-pyridyl disulphide).

PEG_{114}-*b*-poly(*L*-lysine)$_{134}$-(2-pyridyl disulphide) was successfully synthesized with a measured $Đ\frac{Mw}{Mn}$=1.16 determined by SEC in DMF: 1g·L^{-1} LiBr. The ring opening polymerization of N^{ε}- trifluoroacetyl-*L*-lysine *N*-carboxyanhydride (N^{ε}-TFA-*L*-Lys-NCA) was initiated by PEG_{114}-NH_2 conducted under low temperature conditions, followed by the coupling reaction of *N*-succinimidyl 3-(2-pyridyldithio)propionate (SPDP) to the terminal amine. The resulting PEG_{114}-*b*-poly(N^{ε}-trifluoroacetyl-*L*-lysine)$_{134}$-(2-pyridyl disulphide) was subsequently deprotected with KOH yielding the final product. For each step, products were characterized by ^{1}H NMR and SEC.

Molecular characterization in solution by circular dichroism spectroscopy and dynamic light spectroscopy revealed that the molecule transitions rapidly from a random coil to a α-helix structure above between pH 9 and 10. The estimated helix content was 70.9 % at pH 12. Despite the conformational transition, the molecule does not self-assemble neither in response to pH or ionic concentration. Although the properties of the molecule in bulk does not necessarily correspond to how it will behave on the single molecule scale, the results suggest that it is well suited for single molecule force experiments.

1.5 Brief Summary of the Synthesis and Characterization of PEG_{114}-*b*-poly(*L*-glutamic acid)$_{85}$-(2-pyridyl disulphide).

The synthesis of PEG_{114}-*b*-(poly-*L*-glutamic acid)$_{85}$-(2-pyridyl disulphide) was not done by the author of this thesis as it had been already previously synthesized by Dr. Nicolas Willet. A brief summary of the synthesis can be seen below.

PEG_{114}-*b*-poly(*L*-glutamic acid)$_{85}$-(2-pyridyl disulphide) was synthesized by the ring-opening polymerization (ROP) of γ-Benzyl-*L*-glutamate *N*-carboxyanhydride (Bn-Glu NCA) initiated by a PEG-NH_2 initiator (**Figure 8**). The resulting PEG_{114}-*b*-poly(γ-benzyl-*L*-glutamate) was then coupled with *N*-Succinimidyl-3(2-pyridyldithio) propionate (SPDP) and subsequently deprotected by H_2+ Pd/C yielding our final product (**Figure 9**).

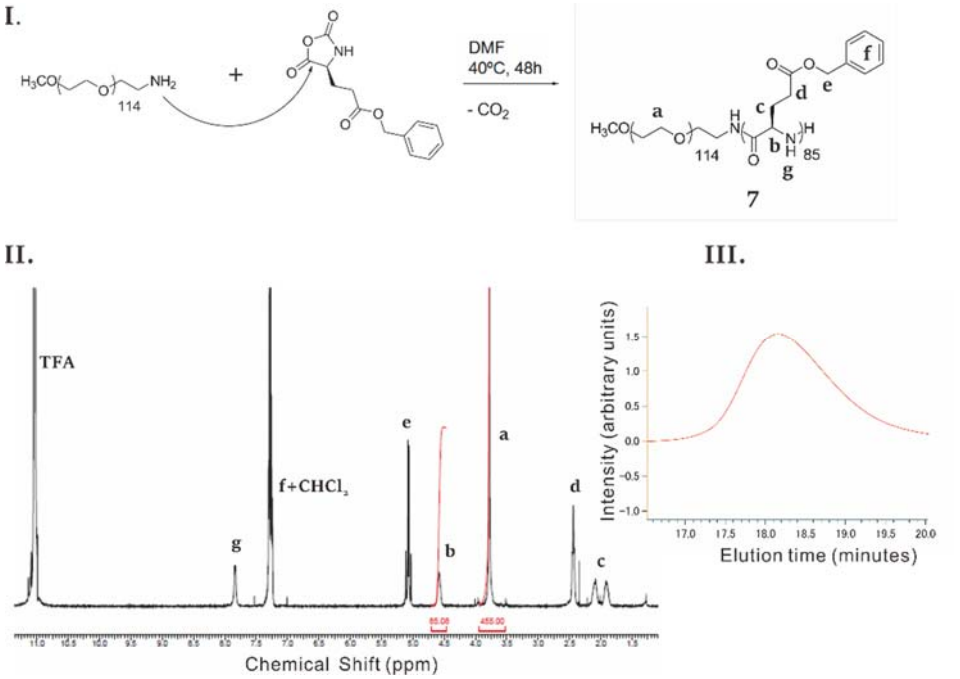

Figure 8. Initiation and growth of PEG-NH_2 initiated ROP of γ-Benzyl-L-glutamate N-carboxyanhydride. I.) ^{1}HNMR of PEG_{114}-*b*- poly(γ-benzyl-*L*-glutamate)$_{85}$-NH_2 in $CDCl_3$ + TFA (Bruker 400MHz). II.) SEC of PEG_{114}-*b*- poly(γ-benzyl-*L*-glutamate)$_{85}$-NH_2 in DMF: 1g·L^{-1} LiBr , $Đ\frac{Mw}{Mn}$=1.18; 60 °C.

The resulting degree of polymerization (D.P≈ 85) was determined by comparing the integration of peak **b**, corresponding to the proton of the α-carbon the peptide backbone (COC**H**RNH, σ=4.57 ppm) with that of the integration corresponding to the PEG_{114} (C**H$_2$**C**H$_2$**O, σ=3.78) labelled as **a** (**Figure 8**).

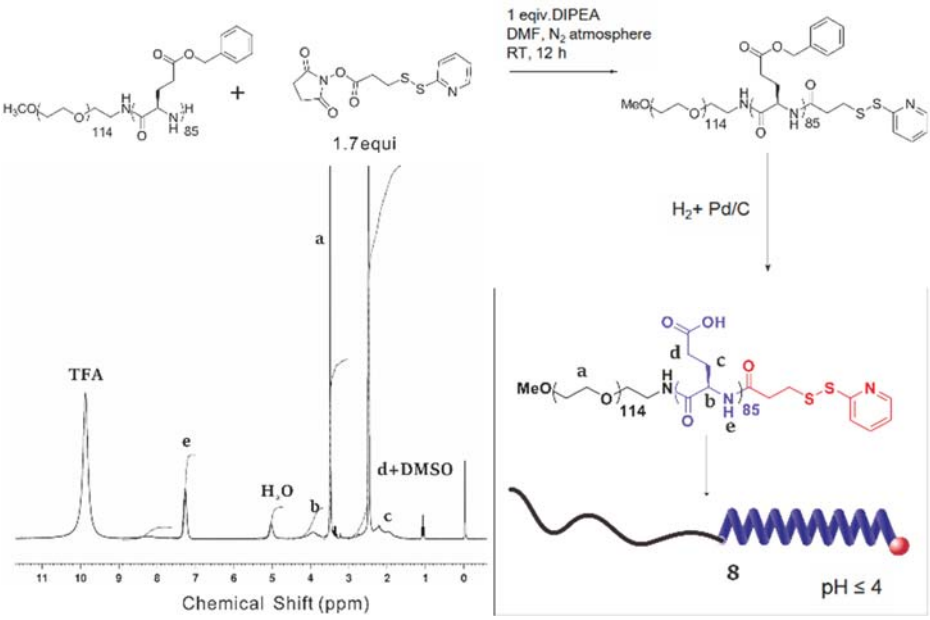

Figure 9. Deprotection of PEG_{114}-*b*-poly(γ-benzyl-*L*-glutamate)$_{85}$-(2-pyridyl disulphide). ^{1}HNMR of PEG_{114}-*b*-poly(*L*-glutamic acid)$_{85}$-(2-pyridyl disulphide) in DMSO-d_6 + TFA (Bruker 400MHz).

The pH responsiveness of PEG_{114}-poly(*L*-glutamic acid)$_{85}$-(2-pyridyl disulphide) Determined by Circular Dichroism.

The CD spectrum **(Figure 10)** shows that the molecule is able to undergo a coil-helix transition in response to pH. At pH 6.3 the molecule adopts a random coil structure, indicated by a characteristic strong negative mean molar ellipticity $[\theta_{mean\ molar}]$ between 195-197 nm and a weakly positive $[\theta_{mean\ molar}]$ at around 215 nm. At pH 2.3 the block copolymer adopts a α-helix conformation, indicated by a characteristic positive $[\theta_{mean\ molar}]$ at 190 nm and two negative peaks at 208 nm and 222 nm respectively. The pH of transition should be at pH ≈4.5 as previously determined [5].

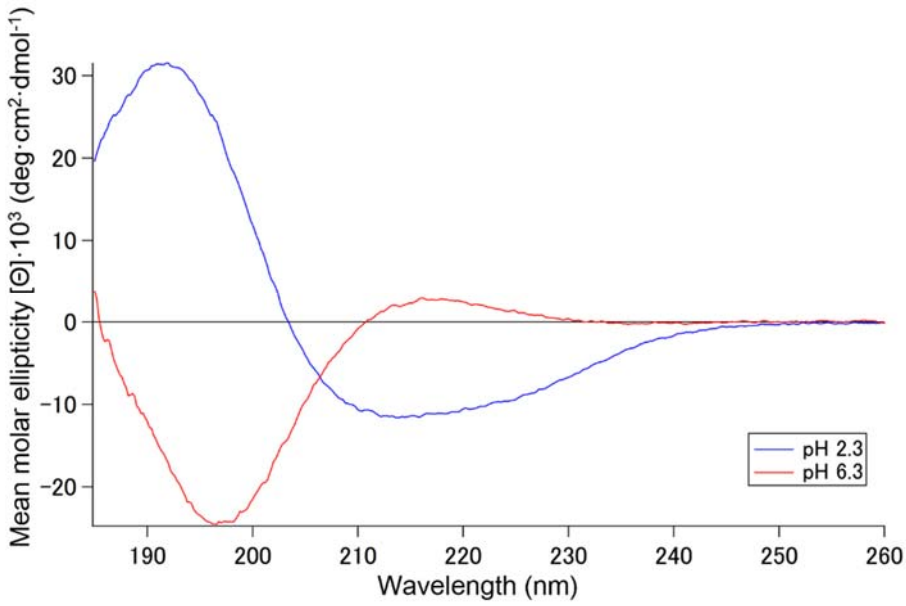

Figure 10. Circular dichroism spectrum between 180 nm-260 nm of PEG_{114}-*b*-poly(*L*-glutamic acid)$_{134}$-(2-pyridyl disulphide) in pH 2.3 and 6.3 Concentration=0.1 mg/ml; cell length=0.1cm; 25 °C.

Using the expressions and values proposed by Luo and Baldwin [31], the estimated helix content was 28%. The percent helicity was dramatically lower in comparison with the PEG_{114}-poly(*L*-Lysine) system (≈70%). A study done by Harada, Cammas and Kataoka [30] on a PEG_{98}-poly(*L*-Lysine)$_{19}$ molecule offered an explanation of a helix stabilizing effect observed for a poly(*L*-lysine) copolymerized with PEG. The stabilization effect is due to the increasing hydrophobicity of the lysine side chain with deprotection that causes the PEG segment to form a protective shell around the lysine, facilitating its segregation from the aqueous medium. The association with PEG was shown to protect the lysine helix in the presence of urea, by isolating and maintaining the helical structure. Despite copolymerization with PEG, there is a limited stabilization effect for the PEG-*b*-poly(*L*-glutamic acid) as the side chains are negatively charged when not protonated. The negatively charged side chains would rather repel the PEG, which has long-pair electrons on the oxygen atoms along the chain. In comparison the lysine side chains are positively charged at lower pH and forms an attractive interaction with the lone-pair electrons on the oxygen atoms along the PEG chain. In addition due to a shorter aliphatic chain and a carboxyl moiety, the poly(*L*-glutamic acid) is highly hydrophilic. The polypeptide is also coupled

to long PEG, which in the absence of the stabilization effect is thought to further solubilize the diblock and disrupt the helix formation.

As previously mentioned, the bulk solution properties do not necessarily correspond to the properties of the molecule at the single molecule scale. In addition the helicity of an unprotected molecule is always much lower as a result of frayed ends in solution. The two extremities of the helix are well dissolved in the solution, decreasing the overall helical content [32]. In the SMFS experiment the end of the molecule will be grafted on a gold surface, and the other extremity pulled by an AFM tip, thus the helical content is expected be much higher for each molecule.

PART II
Single Molecule Force Spectroscopy Experiments of PEG_{114}-*b*-poly(*L*-glutamic acid)$_{85}$-(2-pyridyl disulphide) and PEG_{114}-*b*-poly(*L*-lysine)$_{134}$-(2-pyridyl disulphide).

2.1 Grafting Strategy of PEG_{114}-*b*-poly(*L*-glutamic acid)$_{85}$-(2-pyridyl disulphide) and PEG_{114}-*b*-poly(*L*-lysine)$_{134}$-(2-pyridyl disulphide) on a gold surface.

Immediately prior to performing single molecule force spectroscopy experiments, the gold substrates were dipped in a diluted solution of the diblock molecules ($0.1 mg \cdot ml^{-1}$) and PEG_6-SH, a passivating agent, to enable single molecules to be individually distributed and immobilized onto the cleaned surface (see the detailed protocol in the **Materials and Methods, pg 114**).

Intermittent contact imaging in air was done to determine whether the grafting strategy was successful. During intermittent contact imaging the cantilever is oscillated close to its resonance frequency. The amplitude of oscillation decreases upon tip-surface contact due to interactions allowing the topography of the surface to be mapped.

PEG_{114}-*b*-poly(*L*-glutamic acid)$_{85}$-(2-pyridyl disulphide) was grafted onto a Au-mica surface for imaging with the same conditions used for SMFS experiments. Intermittent contact images of PEG_{114}-*b*-poly(*L*-lysine)$_{134}$-(2-pyridyl disulphide) is not shown below as the grafting conditions were identical.

The resulting images (**Figure 11**) were obtained in air at a resolution of

1.0 µm by 1.0 µm and 0.5 µm by 0.5 µm. We observed the presence of larger isolated white spots of similar sizes that we attribute to the isolated immobilized diblock molecules. A population of smaller white spots are thought to be the smaller PEG-SH also grafted on the surface. The white lines around the gold terraces were thought to originate from the remaining salt from the buffer that accumulated at the edges of the terraces. The single molecule force spectroscopy experiments will be done directly in solution so the issue of salt crystallization and accumulation is not applicable.

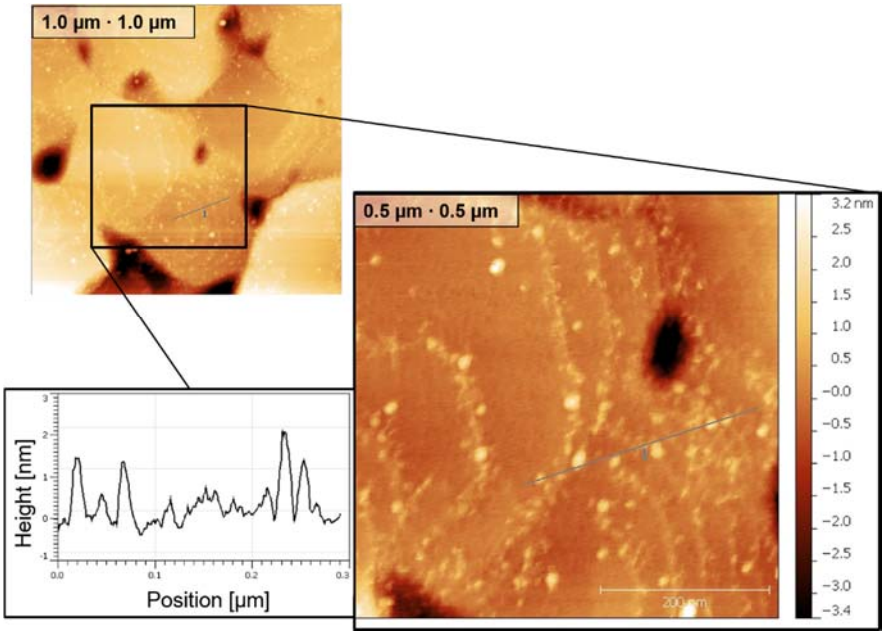

Figure 11. Intermittent contact images in air of a Au-mica surface grafted with PEG_{114}-*b*-poly(*L*-glutamic acid)$_{85}$-(2-pyridyl disulphide). Two images are shown, one done at a resolution of 1.0 µm·1.0 µm and second image was done at 0.5 µm·0.5µm which is a close-up of the section indicated by the black square. The blue line indicates the line where the profile of the surface was measured. The corresponding profilograph can be seen next to the images.

2.2 The Method of Identification of the Relevant Force-Extension Curves, and the Use of the Worm-like Chain Model as a Guide.

As previously mentioned, in a typical SMFS experiment many thousands of force-extension curves are recorded and of those only a very small fraction contain force-extension profiles of single molecules. If the percentage of observed

interactions is higher than ≈10% it is doubtful that single molecules are successfully isolated on the surface and that the interactions observed are truly the result of single molecule interactions. Nonetheless, as the volume of obtained force-extension curves is so large, it is admittedly still a tedious and time-consuming task to separate and identify true single-molecule interactions from multiple-molecule interactions. This is especially true when SMFS experiments are performed on a new molecule where the typical profile is still unknown. There are however some strategies that can be adopted to facilitate the identification of curves.

Firstly only profiles with minimal unspecific adhesion and consistent features are selected as it is considered statistically unlikely that multiple chains will stretch and detach in same reoccurring manner.

Secondly, the force-extension profile of a known polymer such as PEG is often used as a reference. When both the polypeptide and PEG are in a random coil conformation, the profile of the force-extension curve should be that of a simple parabola, indicative of a polymer where the degrees of freedom are reduced with increasing force, and as a result, an increasing counter entropic restoring force is observed. This behaviour can be correlated with the elastic response approximated by statistical models of polymer mechanics. When the polypeptide is folded into a secondary conformation, a characteristic deviation from the predicted parabolic elastic response should be apparent in the range of forces were the secondary conformation is unravelling. Immediately after the unravelling of the secondary structure, and before the detachment of the molecule from the tip, the mechanical behaviour of the fully extended PEG-polypeptide should again display the parabolic extension profile of a random coil system.

For the identification of the α-helical structure of the poly-*L*-Lysine at 10 mM NaCl the characteristic feature was very apparent, and thus for quick identification of the force-extension curves it was sufficient to simply observe a simple deviation from the predicted parabolic extension by eye.

For the identification of the α-helical structure of the poly-*L*-glutamic acid at 10 mM NaCl and poly-*L*-Lysine at 50 mM NaCl the characteristic feature was more difficult to identify, and thus a theoretical fit using the worm-like chain (WLC) model [33, 34] is utilized as a guide. In addition, a fit using the WLC model is superimposed with curves obtained when both polypeptides were in a random coil conformation, and for the extension of the PEG alone as a negative control. It should be mentioned that a model predicting the extension of a PEG chain has been proposed by Oesterhelt, Rief and Gaub [11] which utilized a modified extended freely jointed chain (FJC) model. The elastic behaviour of PEG in water was

predominantly that of a simple parabolic extension profile, even though a very slight tilted plateau could be discerned. Nevertheless, for a combined polymer-polypeptide system the theoretical behaviour can be better approximated by assuming that the polymer is an irregular semi-flexible string (WLC model) rather than consisting of rigid segments connected by joints (FJC model). Indeed, the WLC model is more correct to describe the extension of a semi-flexible polymer under an external force at small extension as it takes into account correlations of orientations at small scales. It has been used for decades as a fit for a variety of proteins and polypeptides [8-10, 35]. More recently, a newly introduced inhomogeneous partially freely rotating (iPFRC) model [32, 36] has been suggested as a better alternative if the fit is to be used to obtain a more accurate numerical value for the contour length of the molecule. However as the fit is to be utilized as a guide without deriving any numerical fit values such as persistence length and contour length, the well-studied WLC model is more than sufficient for this use.

In summary, the obtained force-extension curves of PEG_{114}-*b*-poly(*L*-glutamic acid)$_{85}$-(2-pyridyl disulphide) and PEG_{114}-*b*-poly(*L*-lysine)$_{134}$-(2-pyridyl disulphide) could be interpreted by four general events. **1.)** Due to the axial force that is applied by the cantilever displacement, the molecule aligns towards the direction of the displacement **(I.) (Figure 13, 14, 17, 18, 19, 21). 2.)** A characteristic profile is observed attributed to the unravelling of the α-helix due to the hydrogen bonds of the main-chain and the interactions between the side-chains breaking. **(II.) (Figure 13, 14, 17, 18, 19, 21**. **3.)** As the cantilever displacement continues, the main peak is observed which resembles that of a random coil extension as the PEG tether and peptide void of any remaining structure, is extended **(III.) (Figure 13, 14, 17, 18, 19, 21)**. **4.)** Finally, the molecule detaches from the AFM tip as the applied force exceeds the force of interaction between the molecule and tip **(IV.) (Figure 13, 14, 17, 18, 19, 21)**. Due to the stronger Au-S bond, the molecule remains anchored on the surface and the tip is free to interact with another molecule for subsequent cycles.

2.3 SMFS experiments of PEG_{114}-*b*-poly(*L*-lysine)$_{134}$-(2-pyridyl disulphide)

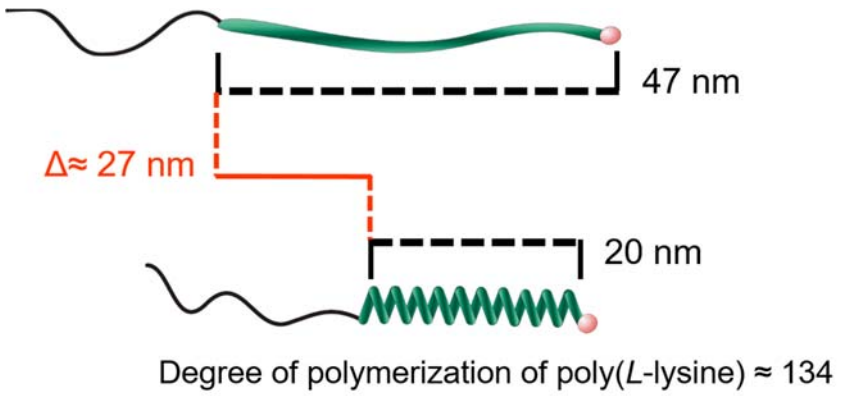

Figure 12. Theoretical difference in length between the folded and unfolded poly(*L*-Lysine) α-helix segment within the synthesized PEG_{114}-*b*-poly(*L*-lysine)$_{134}$-(2-pyridyl disulphide) block copolymer calculated from the degree of polymerization obtained by ^{1}HNMR.

A dataset of 13000 curves were recorded and analysed, and the probability of event was 3.9% (**Table 1**). Only single peaks with consistent features were analysed. Profiles with multiple peaks were considered as multiple molecule interactions and disregarded. There were two reoccurring force-extension profiles of PEG_{114}-*b*-poly(*L*-lysine)$_{134}$-(2-pyridyl disulphide) in α-helix conformation at pH 12. In 0.66% of the cases a true plateau profile shown (**Figure 13**) was observed and in 1.9% of the cases a tilted plateau profile (**Figure 14**) was obtained.

In comparison, the force-extension profiles for PEG-*b*-poly(*L*-lysine) at pH 7 when it is a random coil conformation does not show the noted features **(Figure 20 a.)** Force-extension curves for just PEG **(Figure 20 c.)** were also obtained for comparison. In both cases the typical parabolic force-extension of a random coil was observed, analogous to that of a simple polymer, where with increased extension of the coil there is an increasing entropic restoring force as the internal degrees of freedom are decreased.

Table 1. Typical force-extension profiles and their percentage of occurrence observed for PEG_{114}-*b*-poly(*L*-lysine)$_{134}$-(2-pyridyl disulphide) at pH 12. Event probability indicates the total

number of interactions (single molecule and multiple) observed out of 13000 force-extension cycles.

Tilted Plateau	True Plateau	Multiple Peaks	Event Probability	Number of Recorded Curves
253 (1.9%)	86 (0.66%)	182 (1.4%)	3.90%	13000

Literature data report that the PEG-*b*-poly(*L*-lysine)-(2-pyridyl disulphide) is folded on the surface into a higher order structure with the α-helix segments separated by denatured residues in between. It has been reported [37] that the resulting length and stability of a α-helix strand is driven by an interplay between different thermal equilibria. The equilibria being between the unfolding of the helix into a random coil, maintaining the α-helix, and the formation of higher order assemblies. The most stable and thermodynamically favoured length of a single α-helix was shown to be between 9 - 17 amino acids. Helices that are longer, which is the case with our molecule (D.P≈ 134 obtained by ^{1}H NMR), form higher-order structures that lower the total energy by the appearance of helix-helix adhesion [38, 39].

The appearance of the true plateau force-extension profile **(Figure 13)** can be explained as follows. As the cantilever displacement begins to apply a slight perpendicular force to the surface, it aligns the grafted molecule in the direction of the displacement. The higher order structure is lost as the separated α-helix segments align on top of each other. As a small axial force is continuingly applied, it allows the denatured residues between the helical segments to refold, resulting in a single, uniform α-helix strand. **(Figure 15 1. b.-f).** Although counter-intuitive, it has been determined theoretically [40, 41] and experimentally [42, 43] that when a low force ≈ 10 pN [32] is applied, the α-helix content initially increases before upon stronger extension, the interactions maintaining the secondary conformation breaks. The length of the obtained plateau 27 ±4 nm was in good agreement with the theoretical length difference between the folded and the stretched α-helix of the molecule calculated from the degree of polymerization obtained through ^{1}HNMR≈27 nm (**Figure 12**). The appearance of a constant force plateau supports the turn-by-turn unravelling of the helix predicted theoretically [44, 45].

The presence of a second population of plateau length at 13 ±3 nm is explained by the fact that the separated α-helical segments do not always fold back perfectly resulting in a single uniform helix. Consequently, sometimes only a shorter, isolated helical segment was extended resulting in a shorter plateau length.

The presence of two slightly different populations for the plateau force observed at 27 ±4 pN and 34 ±1 pN is justified as follows. We propose that the α-helix was stabilized by hydrophobic interactions between the lysine side chains at

positions (*i, i+ 4)* and (*i, i- 4*), however some discrepancy in the force could be observed depending on whether the geometric positioning of the side chains was favourable for the interactions. If a uniform, straight α-helix was able to form due to favourable alignment of the helical segments, it would allow the most favourable interactions between the side chains. If there were small denatured segments (kinks) remaining within the helix, the not all side chains would be positioned in an optimal orientation to promote these interactions and consequently the average force of unfolding would be slightly lower.

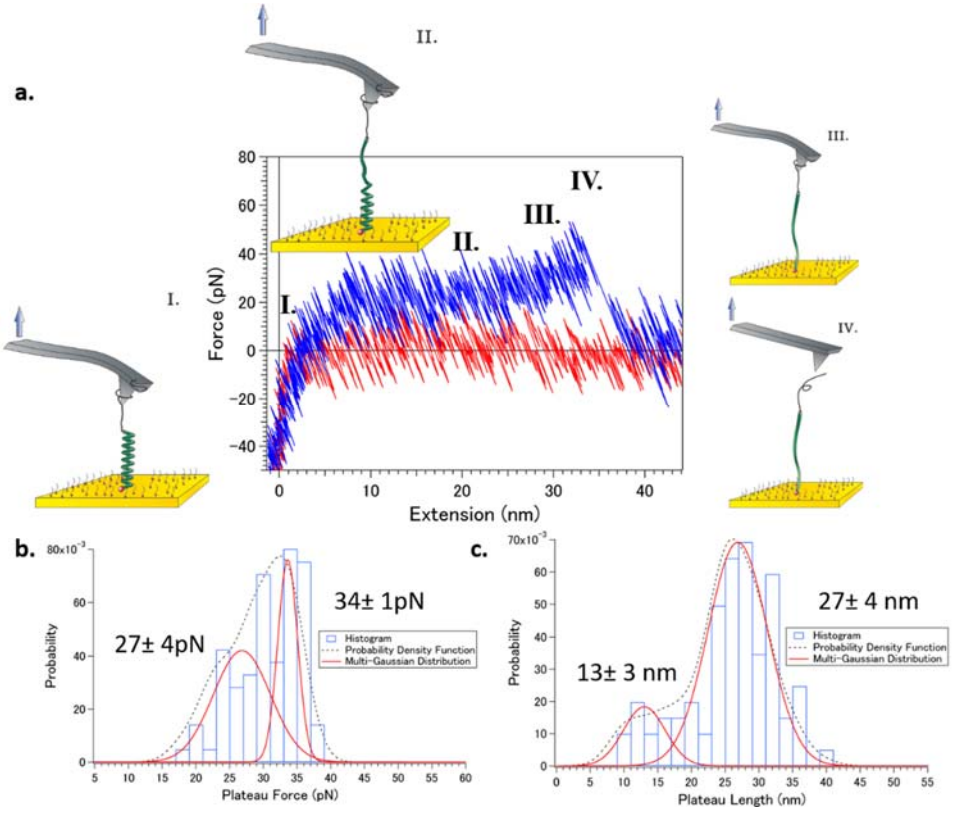

Figure 13. One of two typical force-extension curves for PEG_{114}-*b*-poly(*L*-lysine)$_{134}$-(2-pyridyl disulphide) in a α-helix conformation and the corresponding histograms, probability density functions, and Gaussian distributions. a.) A typical force-extension profile showing a true plateau. Roman numerals and the corresponding diagrams represent an interpretation of the events during the force-extension cycle. b.) Histogram, probability density function, and Gaussian distribution of two plateau forces 27±4 pN (63 %) and 34±1 pN (37 %) (± s.d, n=86). c.) Histogram, probability density function, and Gaussian distribution of two plateau lengths 13±3 nm (16 %) and 27±4 nm (84 %) (± s.d, n=86).

However, more often it is the case that the cantilever does not catch the molecule so that a perfect perpendicular force can be applied, making it even less likely that the separated helical segments align. In this scenario the formation of a single uninterrupted helix is hindered, and a helix retaining many additional denatured segments is extended (**Figure 15 2. b.-e.)**, resulting in a tilted plateau **(Figure 14).** The occurrence of a tilted plateau has been theoretically predicated by Chakrabarti and Levine [44]. In this paper the pseudo-plateau was predicted to be an intermediate between zero extension and the onset of a true plateau. The pseudo-plateau was explained by a higher preference of the locally denatured parts of the chain to extend, leading the chain to incrementally increase in length with extension before the onset of the unravelling of the helical domains. In our case however, as the helix did not reform completely the tilted plateau contained contributions of the locally denatured segments followed by a small contribution of the few helical segments unravelling. This offers an explanation as to why the ending force of the tilted plateau 36 ± 9pN and the force of the true plateau 34 ±1 pN are in good agreement.

This explains also why 66% of the tilted plateaus has a much smaller observed length of 8±4 nm **(Figure 14 b.)** as a second population. Many more denatured segments remained within the helix, therefore the average length of the helical portion that was unfolded was as a consequence much shorter in length.

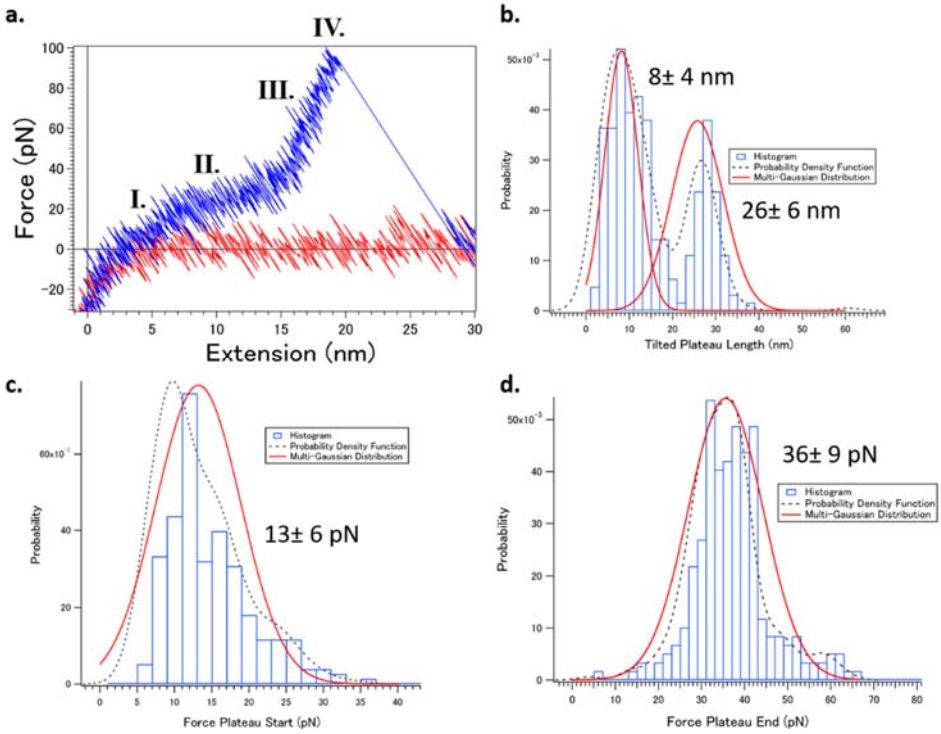

Figure 14. One of two typical force-extension curves for PEG_{114}-*b*-poly(*L*-lysine)$_{134}$-(2-pyridyl disulphide) in a α-helix conformation and the corresponding histograms, probability density functions, and Gaussian distributions. a.) A typical force-extension profile showing a tilted plateau. Roman numerals represent an interpretation of the events during the force-extension cycle (see Figure 13). b.) Histogram, probability density function, and Gaussian distribution of two plateau lengths 8±4nm (66%) and 26±6 (34%) (± s.d, n=253). c.) Histogram, probability density function, and Gaussian distribution of the plateau starting force 13±6 pN (± s.d, n=253). d.) Histogram, probability density function, and Gaussian distribution of the plateau ending force 36±9 pN (± s.d, n=253).

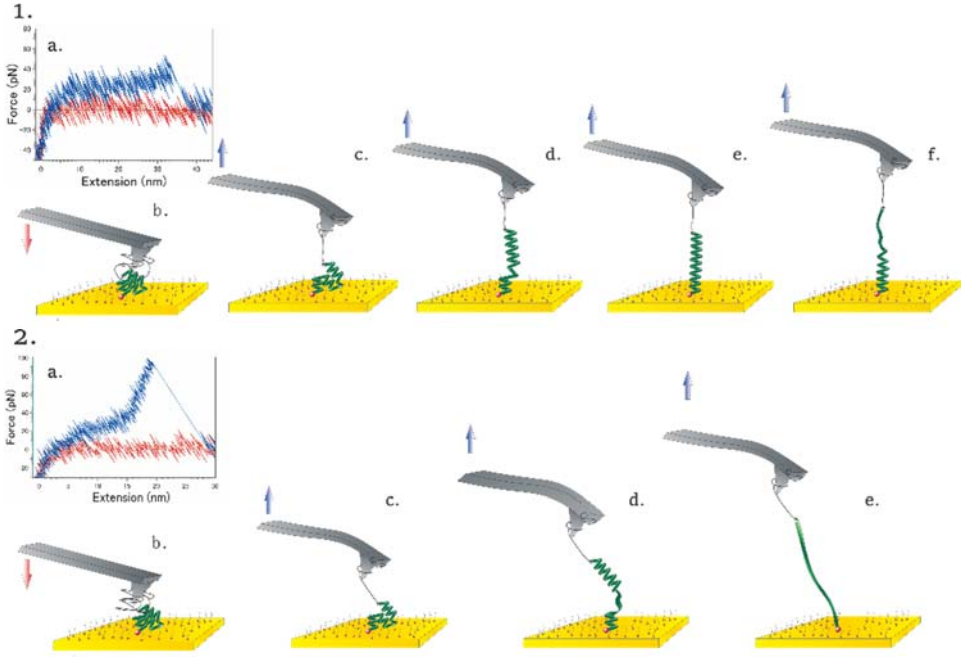

Figure 15. Schematic representations showing how the two force-extension profiles for PEG_{114}-*b*-poly(*L*-lysine)$_{134}$-(2-pyridyl disulphide) could be conceived. 1.a.) The inlet shows a miniature of the typical true plateau force-extension profile. b.)-f.) Schematic representation of events where the separated helical segments align, and a complete, single-strand α-helix is able to reform. 2.a.) The inlet shows a miniature of a typical tilted plateau force-extension profile. b.)-f.) Schematic representation of events where the separated helical segments do not reform into a single α-helix due to unfavourable pulling geometry and thus, a preferring extension from the denatured segments is observed.

2.4 SMFS experiments of PEG_{114}-*b*-poly(*L*-glutamic acid)$_{85}$-(2-pyridyl disulphide)

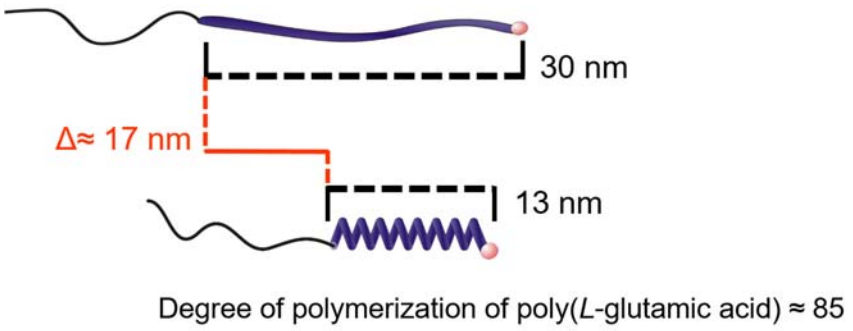

Figure 16. Theoretical difference in length between the folded and unfolded poly(*L*-glutamic acid) α-helix segment within the synthesized PEG_{114}-*b*-poly(*L*-glutamic acid)$_{85}$-(2-pyridyl disulphide) block copolymer calculated from the degree of polymerization obtained by ^{1}HNMR.

For PEG_{114}-*b*-poly(*L*-glutamic acid)$_{85}$-(2-pyridyl disulphide) in a α-helical conformation at pH 3, a dataset of 30000 curves were recorded and analysed, and the probability of event was 1.47% (**Table 2**). Only single peaks with consistent features were analysed. Profiles with multiple peaks were considered as multiple molecule interactions and disregarded. There are two typical force-extension profiles. The most commonly observed profile (0.8% of the total curves) could be differentiated by the appearance of a characteristic inflection at 18±4 pN (indicated on **Figure 17.a.** by a red arrow. See b. and c. for histograms). In over half of the force-extension curves that displayed the first inflection, a second inflection at a higher force could be identified (**Figure 19**). In 0.18% of the curves a plateau **(Figure 18)** could be observed.

In comparison, the force-extension profiles for PEG-*b*-poly(*L*-glutamic acid)-(2-pyridyl disulphide) when it is in a random coil conformation at pH 7 does not show the characteristic inflection or the plateau **(Figure 20. b.)** and instead the parabolic force-extension profile of a random coil was observed.

Table 2. Typical force-extension profiles and their percentage of occurrence observed for PEG_{114}-*b*-poly(*L*-glutamic acid)$_{85}$-(2-pyridyl disulphide) at pH 3. Event probability indicates the total number of interactions (single molecule and multiple) observed out of 30000 force-extension cycles

Inflection	True Plateau	Multiple Peaks/ Unspecific Adhesion	Event Probability	Number of Recorded Curves
232 (0.8%)	55 (0.18%)	148 (0.49%)	1.47%	30000

Similar to the PEG-*b*-poly(*L*-lysine)-(2-pyridyl disulphide), the helix of the PEG-*b*-(poly-*L*-glutamic acid)-(2-pyridyl disulphide) (D.P≈85) is most probably folded into a higher-order structure on the surface, displaying helical segments of various lengths. The residues between the separated α-helix segments are denatured, allowing the structure to fold, promoting helix-helix adhesion.

In the majority of the cases (0.8%) when a single molecule was caught, it did not prompt the formation of one single α-helix strand. Instead, during the cycle only a partially helical molecule was extended. The extension of a partially helical poly-*L*-glutamic acid was highly biased towards the extension of the denatured segments more than that of the helical domains [44] resulting in a force-extension profile resembling that of a random coil very strongly (**Figure 17**). The small inflection at 18±4 pN indicates the unravelling of the isolated helical segments.

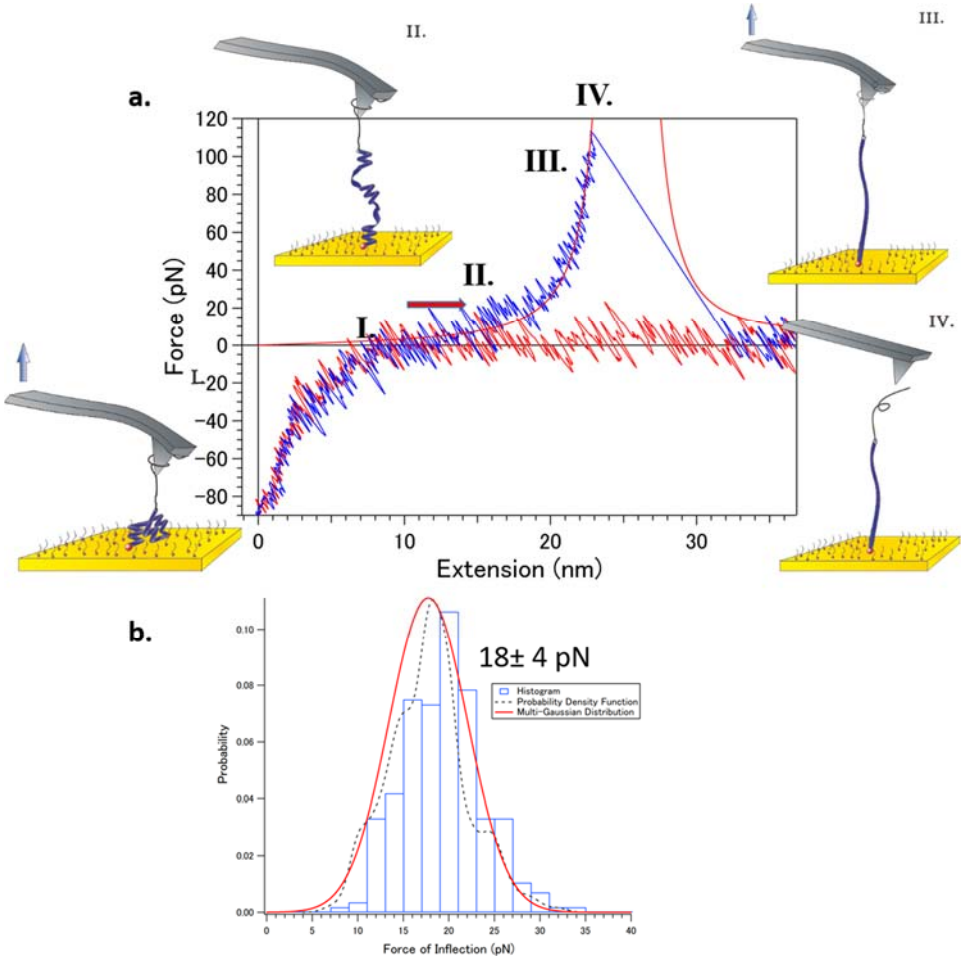

Figure 17. A typical force-extension curve for PEG_{114}-*b*-poly(*L*-glutamic acid)$_{85}$-(2-pyridyl disulphide) in a α-helix conformation and the corresponding histogram, probability density function, and Gaussian distribution. a.) A typical force-extension profile showing the reoccurring inflection (red arrow). Roman numerals and the corresponding diagrams represent an interpretation of the events during the force-extension cycle. The red line indicates a fit using the WLC model. b.) Histogram, probability density function, and Gaussian distribution of the force of the inflection 18±4 pN (± s.d, n=232).

In 0.18% of the cases the separated helical segments were able to align in the direction of the cantilever displacement favourably, and the denatured segments between the helical segments were able to refold into a complete glutamic acid α-helix. Upon further extension the complete helix could be unfolded, resulting in a plateau at 19±2 pN **(Figure 18)**.The length of the plateau, if a little short, 12±5 nm corresponds to the theoretical length difference between the folded and the stretched α-helix of the molecule calculated from the degree of polymerization obtained through ^{1}HNMR≈17 nm (**Figure 16**).
The force of the inflection at 18±4 pN, and the force of the plateau at 19±2 pN, are at the same force providing further evidence that the unravelling of the helix begins at this force. As the helical domains undergo a turn-by-turn unravelling [44, 45], the force at which the domains unravel should be constant and independent of the helix length. If only a few helical segments were unravelling, an inflection could be observed. In this scenario the force-extension profile was largely influenced by the extension of remaining denatured segments between the helical segments. If the helix was able to refold completely with no denatured segments remaining, a plateau at the same force could be observed.

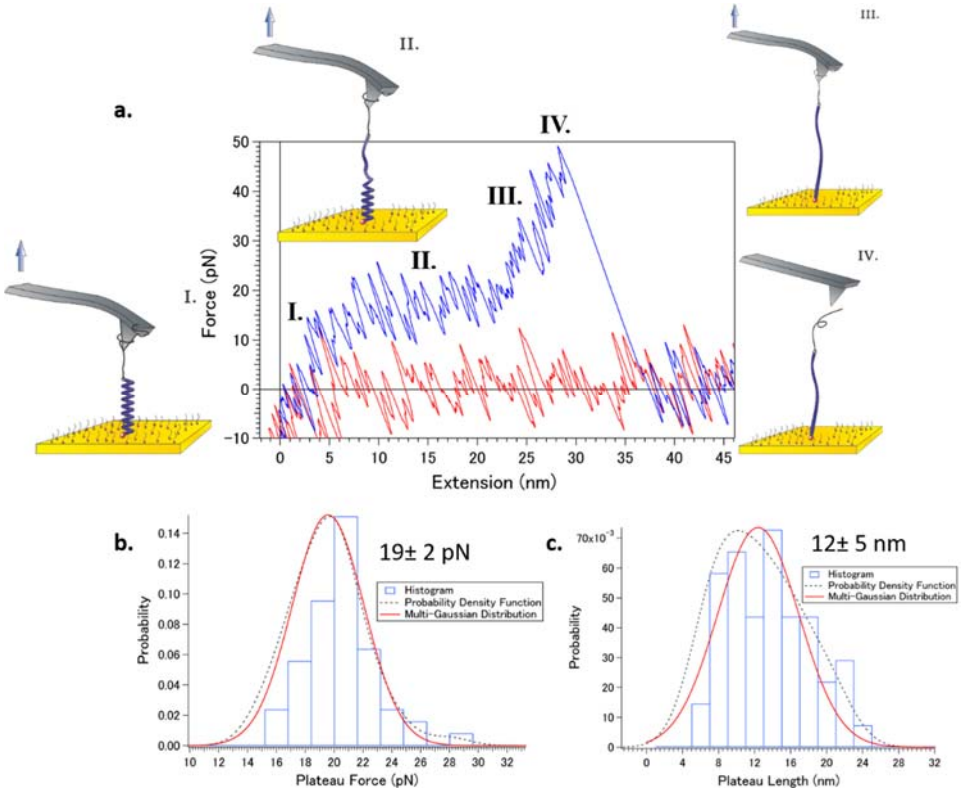

Figure 18. One of two typical force-extension curves for PEG_{114}-*b*-poly(*L*-glutamic acid)$_{85}$-(2-pyridyl disulphide) in a α-helix conformation and the corresponding histograms, probability density functions, and Gaussian distributions. a.) A typical force-extension profile showing a plateau. Roman numerals and the corresponding diagrams represent an interpretation of the events during the force-extension cycle. b.) Histogram, probability density function, and Gaussian distribution of the plateau force 19 ± 2 pN (± s.d, n=55). c.) Histogram, probability density function, and Gaussian distribution of the plateau length 12 ±5 nm (± s.d, n=55).

2.4.1 A Second Inflection Observed for PEG_{114}-*b*-poly(*L*-glutamic acid)$_{85}$-(2-pyridyl disulphide) Suggests the Presence of a Metastable β-hairpin Interaction

In total 287 curves were observed that displayed an inflection at 18 ±4 pN attributed to the unravelling of the helical domains of PEG-*b*-(poly-*L*-glutamic acid). Out of those observed with the first inflection, 177 curves (62 %) displayed a second inflection at a much higher force of 60 ±9 pN (Indicated on **Figure 19.a** by a green arrow). The second inflection was observed only in force-extension

profiles where the first inflection was observed, indicating that the presence of the second inflection was dependent on the formation of the α-helix secondary structure.

We offer an explanation for the second inflection as follows. It is well known that the α−β deformation mechanism from a α-helix to a β-sheet structure can occur in response to pH, temperature, solvent composition and also mechanical deformation [46]. However, α−β transitions by mechanical deformation have only been traditionally reported for protein coiled-coil structures both experimentally [47, 48], and theoretically [46].

Nevertheless, a theoretical study utilizing discrete molecular dynamics by Ding et al.[49] has suggested firstly, the presence of a metastable β-hairpin intermediate state, and most importantly they indicated that although the potential energy of the β-hairpin state is indeed higher than the α-helix state, the entropy of the β-hairpin intermediate is significantly higher due to less constraints imposed by the hydrogen bonding. At higher temperatures the free energy of the β-hairpin can even be smaller than that of the α-helix.

We postulate that the formation of a metastable β-hairpin-like interaction occurs during the unfolding of the α-helix structure as a result of the β-hairpin structure possessing a higher entropy, and thus occupying an energy minima in conditions where the entropic forces dominate. As the force applied to the partially helical poly(*L*-glutamic acid) becomes increasingly larger, the helix structure starts to destabilize further as the residues within undergo increasing spontaneous fluctuations between their random coil and helix states **(Figure 19.a. II-1)**. As enough force is applied to break the hydrogen bonding of the helix, the β-hairpin structure is expected to form starting from the available denatured segments **(Figure 19.a. II-2+3 green circle)**. In literature [49], the α-helix to β-hairpin transition was found to proceed via a random coil structure, so it would make sense if such a structure were to form in a transitional state when enough mechanical force has been applied to pull the helix out of its energy minima, yet not enough force has been applied to pull the molecule completely taunt, allowing backbone entropic forces to dominate. When such an intermediate force is applied it allows enough conformational freedom for a few hydrogen bonding sites to come into close enough contact to form the β-hairpin interaction.

A similar inflection at high forces was observed in a study by Afrin et al.[4] on a poly(*L*-alanine)-based polypeptide. They could not however offer an explanation as to why the inflection at higher forces was a property that disappeared when experiments were conducted in 50% trifluoroethanol, a helix

stabilizing agent. We would like to propose an explanation that explains the results reported by Afrin et al.[4] and also explains why this second inflection at high forces could not be obtained for the poly(*L*-lysine) helix. (Although it should be mentioned that for many of the force extension curves obtained for the poly(*L*-lysine), the force at which the molecule detached from the AFM was below the forces observed for the second inflection, and therefore could not be compared).

Again in the study conducted by Ding et al,[49] simulations were performed on a peptide with increasingly hydrophobic side chains. The increasing hydrophobicity of the side chains was found to stabilize the helix structure, and prevented the formation of the metastable β-hairpin. In the same way we propose that the formation of a metastable β-hairpin-like interaction is a property unique to poor helix formers that do not possess sterically hindered side chains that can effectively form helix-stabilizing hydrophobic interactions such as poly(*L*-alanine) and poly(*L*-glutamic acid).

Finally, the value of the second inflection observed for poly(*L*-glutamic acid) 60 ±9 pN was observed at approximately the same range as the force attributed to a β-hairpin-like interaction ≈ 70 pN observed for poly(*L*-Lysine) after exposing it to elevated temperatures to induce the α−β transition (Please refer to Chapter 4 Figure 6). This suggests that in both cases the same type of β-interactions are involved, which result in inflections observed at higher forces.

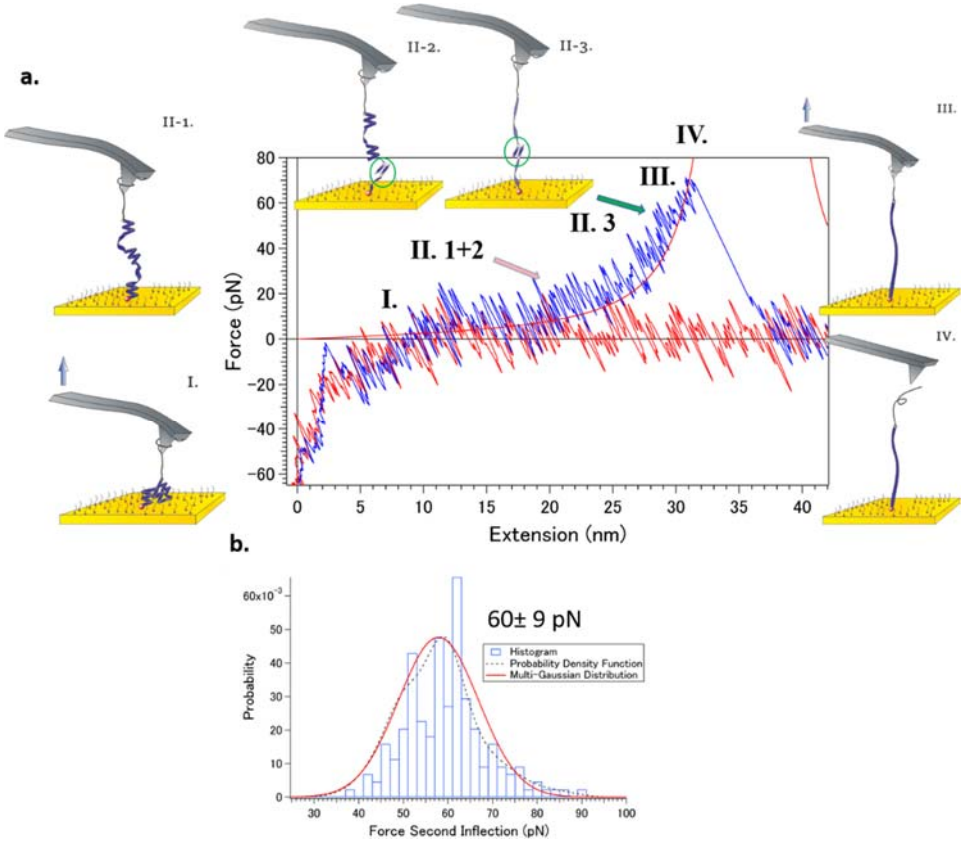

Figure 19. A force-extension curves for PEG_{114}-*b*-poly(*L*-glutamic acid)$_{85}$-(2-pyridyl disulphide) in a α-helix conformation where a second inflection at a higher force was observed in addition to the first inflection at ≈20pN, and the corresponding histogram, probability density function, and Gaussian distribution of the second inflection. a.) A typical force-extension profile showing the first inflection (transparent red arrow) and second inflection (green arrow) Roman numerals and the corresponding diagrams represent an interpretation of the events during the force-extension cycle. b.) Histogram, probability density function, and Gaussian distribution of the second inflection force 60 ± 9 pN (± s.d, n=177).

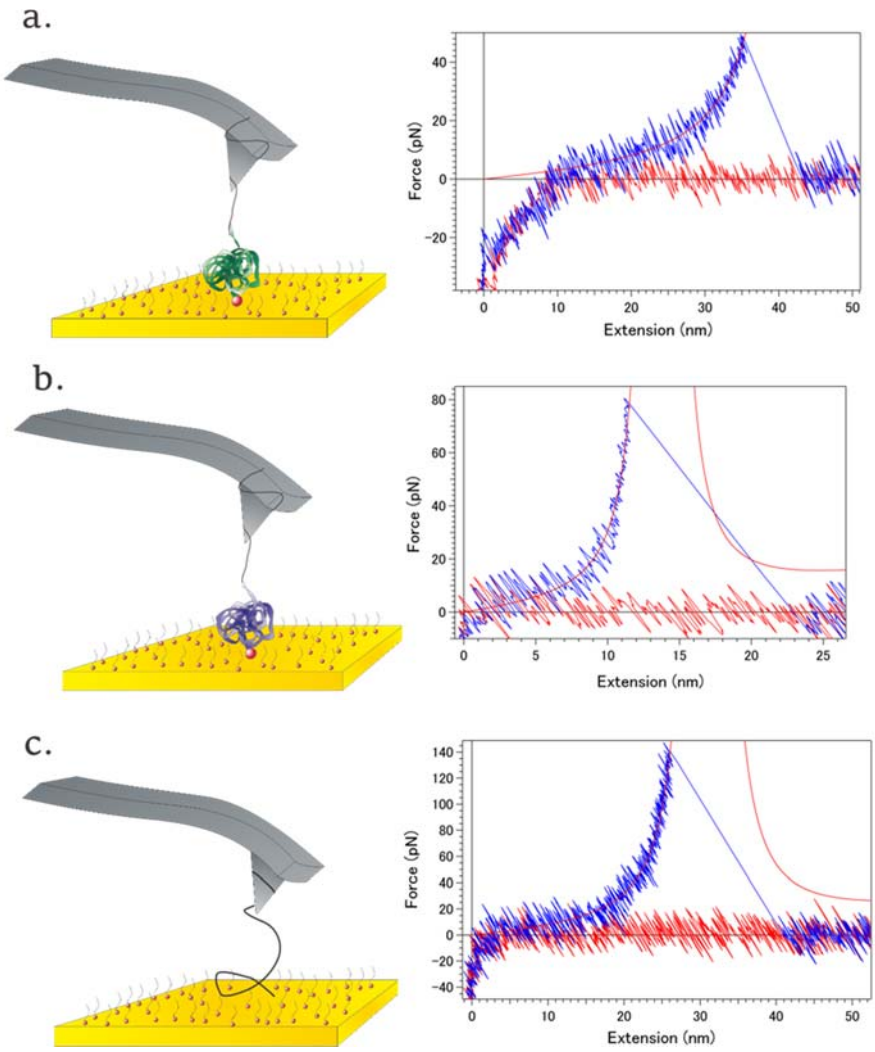

Figure 20. Force-extension profiles and schematic representations for PEG_{114}-*b*-poly(*L*-glutamic acid)$_{85}$-(2-pyridyl disulphide), PEG_{114}-*b*-poly(*L*-lysine)$_{134}$-(2-pyridyl disulphide), and PEG_{114}-OH, when each is in a random coil conformation. a.) PEG_{114}-*b*-poly(*L*-lysine)$_{134}$-(2-pyridyl disulphide) at pH 7. b.) PEG_{114}-*b*-poly(*L*-glutamic acid)$_{85}$-(2-pyridyl disulphide) at pH 7. c.) PEG_{114}-OH at pH 7. The red line indicates a fit using the WLC model, which predicts the behaviour of an ideal, random coil polymer.

Our results indicate that the behaviour of a α-helix under tension is strongly governed by the interactions of the side chains, and much less by the actual hydrogen bonding within the main chain backbone. The higher hydrophobicity of the lysine side chains helps to stabilize the helix. The lysine is

more hydrophobic due its longer aliphatic chain, and the presence of just an amine group as compared to a shorter aliphatic chain and a carboxyl moiety for the glutamic acid side chain. A stronger hydrophobicity of the side chains has been shown to theoretically support a longer α-helix with greater stability [37]. A α-helix behaves as a multistate system consisting of numerous likely helical, and random coil segments that form at different locations along the chain. There is an equilibrium probability associated with each segment, and a typical helix fluctuates between these interchanging states at different locations along the entirety its length [32, 50]. The hydrophobicity of the lysine residue increases the free energy barrier between these two states, and therefore inhibits somewhat these fluctuations. Thus, when the molecule is caught by the AFM cantilever, the higher stability allows the denatured segments between the separated helical segments to reform more easily when a small axial force was applied. Even when the lysine helix was not able to refold completely the stabilizing interactions of the side-chains were still evident in the tilted-plateau.

On the contrary, the glutamic acid side chains which are not as hydrophobic or sterically hindered cannot inhibit the spontaneous helix-coil fluctuations as successfully, leading to a lower free energy barrier between these two states. Therefore, it was more difficult for the glutamic acid helix to refold into a complete α-helix when a small force was applied. When only a partially helical system was extended the force-extension curve looked very similar to a random coil extension due to the stronger influence of the remaining denatured segments. For chains exhibiting a mix of helix and coil states, a force-extension curve similar to those of the WLC has been predicted theoretically [44]. Even when a plateau was evident it occurred less frequently and at a lower force than that of the lysine helix. It should be mentioned that a similar explanation has been offered by Afrin et.al [4] for the extension of a poly-(*L*-alanine)-based polypeptide. The obtained force-extension profiles of poly-(*L*-alanine) looked very similar to that of a random coil due to the non-bulky nature of the alanine side chains. The smaller side chains did not prevent the spontaneous fluctuation between the helix and coil states, and as a result the tensile mechanics are dominated by the preferred stretching of these randomly occurring denatured segments within the helix.

In addition, as a result of poly(*L*-glutamic acid) possessing smaller side chains that did not stabilize the helix as well, it was also able to form metastable β-hairpin-like interactions during the unfolding event of the helix. This was attributed to the β-hairpin possessing a higher entropy than the α-helix structure, and therefore some residues were suggested to occupy this energy minima after the initial denaturing of some helical domains.

2.5 SMFS experiments of PEG-*b*-poly(*L*-lysine)-(2-pyridyl disulphide) at 50 mM NaCl.

To test our hypothesis on the stabilizing hydrophobic interactions between the side chains, single molecule force spectroscopy experiments for PEG-*b*-poly(*L*-lysine)-(2-pyridyl disulphide), at pH 12 were conducted in 50 mM NaCl. A total of 5341 curves were obtained and the event probability was 1.44% (**Table 3**).

Even a small increase in the salt concentration from 10 mM to 50 mM screens the weak van der Waals interactions [51] between the hydrophobic lysine side chains. In addition, the increased concentration of sodium ions increases the solubility of the side chains by interacting with the end amine group. Therefore the overall effect of increasing the salt concentration is that the stabilizing hydrophobic interactions between the side chains are weakened.
At 50 mM NaCl one can hypothesise that the helix forming ability is not affected. Indeed it has been demonstrated qualitatively that micelles and vesicles of synthetic polypeptides were shown to be pH responsive up to 1 M NaCl [52, 53]. From this we infer that at 50 mM NaCl only the hydrophobic interactions between the lysine side chains were affected and not the main hydrogen bonding of the α- helix.

Table 3. Typical force-extension profiles and their percentage of occurrence observed for PEG_{114}-*b*-poly(*L*-lysine)$_{134}$-(2-pyridyl disulphide) at pH 12 with 50mM NaCl. Event probability indicates the total number of interactions (single molecule and multiple) observed out of 5341 force-extension cycles.

Inflection	Multiple Peaks	Event Probability	Number of Recorded Curves
67 (1.25%)	10 (0.19%)	77 (1.44%)	5341

At 50 mM NaCl none of the obtained force-extension curves had the plateau feature observed previously. Instead, the curves had a very strong random coil characteristic **(Figure 21)** which resembled the force extension profiles obtained for PEG-*b*-poly(*L*-glutamic acid)-(2-pyridyl disulphide. The profiles were characterized by a reoccurring inflection at 17±4 pN, which is almost identical to the inflection observed for the helix of glutamic acid at 18±4 pN. This gives further weight to the following arguments. Firstly, that the hydrophobic interactions of the side chains are vital to maintain the stability of the α-helix. Secondly, that the force extension profile of a truly helical system has a constant

force plateau and that when a system is only partially helical it quickly acquires random coil characteristics except for inflections close to 20 pN. The inflection around the 20 pN range indicates the unravelling of the isolated helical segments, and perhaps reflects the force required to unravel the hydrogen bonding maintaining the helix motif more faithfully as side chain interactions are smaller.

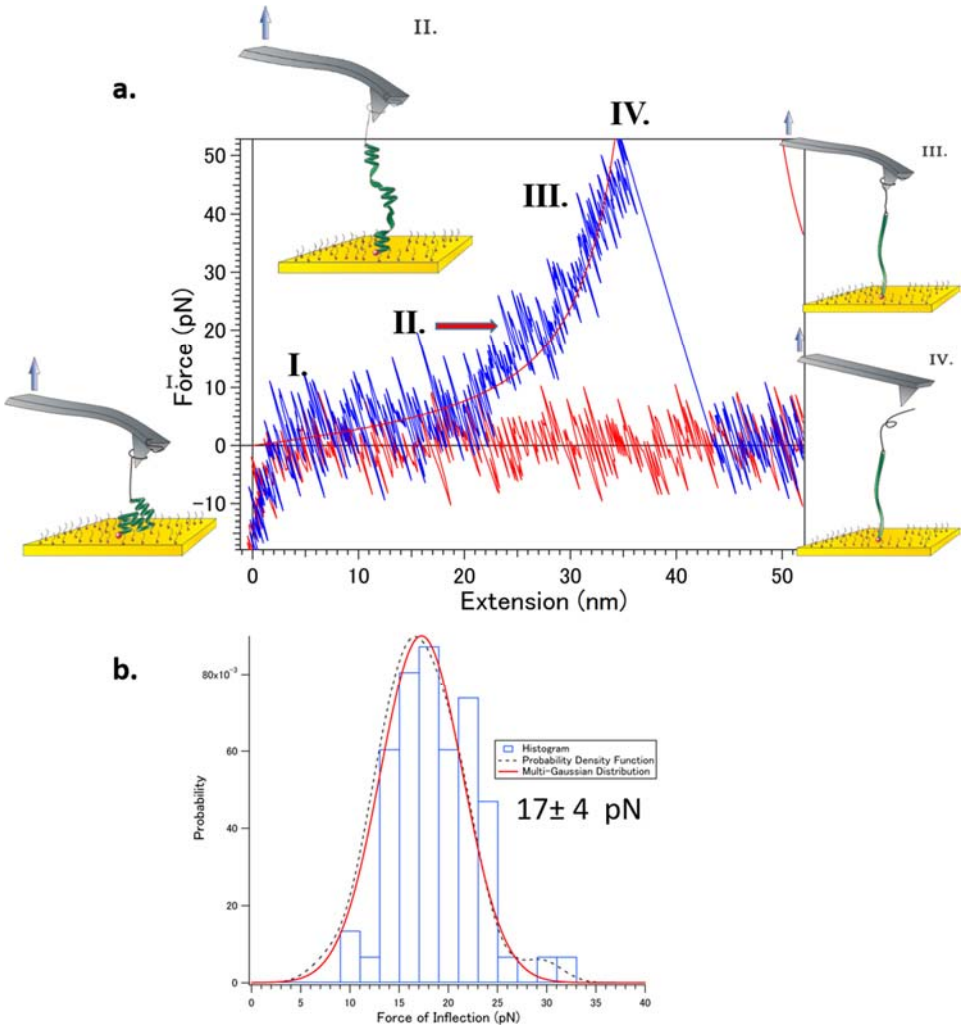

Figure 21. A typical force-extension curve for PEG_{114}-*b*-poly(*L*-lysine)$_{134}$-(2-pyridyl disulphide) in a α-helix conformation at 50 mM NaCl and the corresponding histogram, probability density function, and Gaussian distribution. a.) A typical force-extension profile showing the reoccurring inflection (red arrow). Roman numerals and the corresponding diagrams represent an interpretation of the events during the force-extension cycle. The red line indicates a fit using the

WLC model. b.) Histogram, probability density function, and Gaussian distribution of the force of the inflection 17± 4 pN (± s.d, n=67).

2.6 Force-Extension Behaviour of Poly(*L*-lysine)$_{134}$ and Poly(*L*-glutamic acid)$_{85}$ using a Statistical Mechanical Model of Helix-Coil Transitions.

In addition to the experimental studies, we took the liberty of utilizing a helix-coil transition model AGADIR [54] coupled with a random-coil polypeptide elastic model proposed by Torabi and Schatz [32]. The authors kindly left a link to a web application of their model on their publication. It was promising that the simulated force-extension curves were in good agreement with our experimental data **(Figure 22)**.

On the application it was possible to insert the type and the number of amino acids, as well as the ionic concentration and the pH of the solution. It was also possible to insert an N-terminal and/or C-terminal protection as this influences the number of resides that are denatured on both sides of the calculated helix. For the simulations the N-terminal was left protected as our molecule is grafted on to a gold surface by a 2-pyridyl disulphide group. The C-terminal was left unprotected approximating the high solubility of the PEG tether in water. A model AFM setup was used where one end of the molecule is fixed on a surface and the other trapped in a parabolic potential well. The force exerted on the molecule is equal to $f = k(L - \xi)$ [32] where L is the displacement of the cantilever, ξ is the extension of the molecule and k is the cantilever spring constant. An average value of the cantilever spring constant (9.5 $\frac{pN}{nm}$) was inserted, which was obtained by the thermal noise method prior to each SMFS experiment.

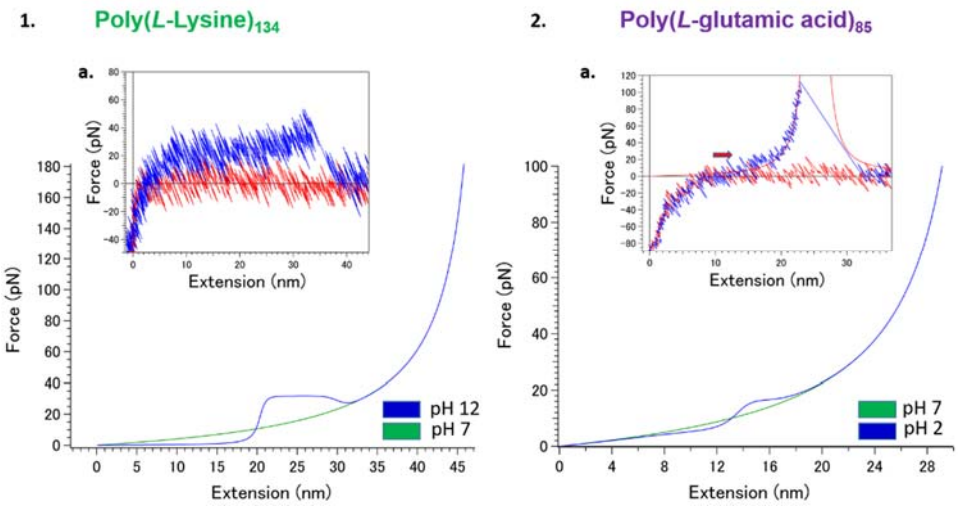

Figure 22. Force extension profiles obtained using a modified helix-coil transition model AGADIR proposed by Torabi and Schatz [32] for poly(*L*-lysine)$_{134}$ and poly(*L*-glutamic acid)$_{85}$ in both random coil and α-helix conformations. 1.) Force extension profiles for poly(*L*-lysine)$_{134}$ at pH 12 (blue line, α-helix) and pH 7 (green line, random coil) a.) The inset shows a miniature of the typical force-extension profile obtained experimentally at pH 12. 2.) Force extension profiles for poly(*L*-glutamic acid)$_{85}$ at pH 2 (blue line, α-helix) and pH 7 (green line, random coil) a.) The inset shows a miniature of the typical force-extension profile obtained experimentally at pH 3.

The model accurately predicted the shape of the force-extension curves obtained for the two different helices. For the poly-(*L*-lysine) helix it predicted the occurrence of a constant force plateau. The force of the plateau obtained in the simulation was in the 30 pN range, which is in agreement with the force plateau we were able to experimentally show at 27 ±4 pN (63%) and 34 ±1 pN (37%). The length of the plateau in the simulated force-extension profile is shorter.

The difference in the plateau length observed in model and experimentally can be justified as follows. In the paper the authors predicted the extremities of the helix to be frayed, and with the application of a small force the helical content increased. However as mentioned by the authors, the simulations were developed for polypeptides void of a tertiary structure. We predict that our molecule adopts a higher order assembly, and that the denatured segments occur between the separated helical segments of a folded structure. Therefore perhaps for our system it was easier for denatured segments sandwiched between two helical segments to refold versus denatured segments at just both extremities of the molecule. If the random coil segment is between two helical segments it should be easier for the random coil segment to snap back into a helix as the propagation can occur from both sides. If the random coil segments only exists at the extremity

of the molecule the helix can only propagate from one side.

For the poly-*L*-glutamic acid the model predicted the high random coil nature evident in the force-extension profiles. The inflection observed experimentally at 18±4 pN was also evident in the simulated profile at approximately 15 pN, which is again in good agreement. The simulation did not predict the occurrence of a plateau of poly-*L*-glutamic acid. This is understandable as the plateau occurs infrequently. We believe that again the difference can be attributed to the peptide adopting a tertiary structure (**Chapter 1, Figure 9**) and that this arrangement makes it possible for the helix to successfully refold along its complete length.

Conclusion

In this study two stimuli responsive peptides, PEG_{114}-*b*-poly(*L*-glutamic acid)$_{85}$-(2-pyridyl disulphide) and PEG_{114}-*b*-poly(*L*-lysine)$_{134}$-(2-pyridyl disulphide) were designed, synthesized and used as a bioinspired model to conduct an in-depth study to observe the mechanics within the unravelling of two different α-helices that fold under opposite pH conditions.

PEG_{114}-*b*-poly(*L*-lysine)$_{134}$-(2-pyridyl disulphide) was successfully synthesized by the ring opening polymerization of trifluoroacetyl-*L*-lysine *N*-carboxyanhydride (N^{ε}-TFA-*L*-Lys-NCA) initiated by a PEG-NH_2 initiator. The protected molecule was then coupled with *N*-succinimidyl-3(2-pyridyldithio) propionate (SPDP), and subsequently deprotected. The measured dispersity was $Đ \frac{Mw}{Mn}$=1.16 before deprotection. The synthesis of PEG_{114}-*b*-poly(*L*-glutamic acid)$_{85}$-(2-pyridyl disulphide) was performed previously and not by the author of this thesis, however the synthesis is briefly summarized in this chapter.

Molecular characterization of both molecules by circular dichroism spectroscopy revealed that the molecules were able to undergo a helix-random coil transition in response to pH. Dynamic light scattering studies of PEG_{114}-*b*-poly(*L*-lysine)$_{134}$-(2-pyridyl disulphide) revealed that despite the conformational transition, the molecule does not self-assemble neither in response to pH or changes in the ionic concentration in the range of concentrations relevant for single molecule force experiments.

The diblock copolymers, designed and synthesized for single molecule force spectroscopy applications, offered stable systems with which clean force-extension curves could be obtained. In this system one end of the molecule was

chemically bond to a gold surface and the other end was conjugated with a PEG segment, which functioned as a tether allowing the molecule to be caught and extended by the AFM cantilever. The addition of the PEG tether was found to not negatively impact helix formation as a complete α-helix structure for both the poly(*L*-glutamic acid) and poly(*L*-lysine) was found to refold and unfold successfully during the experiments.

Single molecule force spectroscopy was performed where the conformation of the peptides could be changed *in situ* during the AFM experiment. In addition, a AGADIR based statistical mechanical model proposed by Torabi and Schatz [32] was utilized to compare our experimental data with a theoretical study of the tensile mechanics of poly-*L*-lysine and poly-*L*-glutamic acid.

The unravelling of the helix formed by PEG-*b*-poly(*L*-Lysine)-(2-pyridyl disulphide) was observed in the force-extension profiles as a constant force plateau. The experimentally obtained plateau force was 34 ±1 pN (37%), and 30 pN was obtained by the AGADIR based model. It can be inferred that the helices formed by poly-*L*-lysine are more stable due to the higher hydrophobicity of the side chains. A plateau length of 27 ±4 nm (84%) corresponding to the theoretical difference in length (≈27 nm) between the folded and unravelled helix could also be observed. Although the peptide adopts a higher order structure on the surface, the denatured segments in between the separated helical segments are able to refold when a slight axial force was applied, allowing a single long α-helix to be unfolded. The presence of a second population of plateau length 13 ±3 nm (16%) was attributed to instances where the helix was not able to refold perfectly and as a result only an isolated, shorter helical segment was unfolded. The second plateau force of 27 ±4 pN (63%) was justified by instances where the stabilizing hydrophobic interactions between the side chains were not completely optimal due not all side chains being positioned in a perfect geometric position to interact with neighbouring side chains and thus the average force of unfolding was slightly lower.

When many more denatured segment remained within the helix due to the helical segments not aligning favourably, a tilted plateau for the force-extension profile was observed instead. The ending force of the tilted plateau 36 ±9 pN was in good agreement with the plateau force 34 ±1 pN obtained for the true plateau indicating the contribution of the unfolding of small remaining helical segments.

On the contrary, the unravelling of the helix formed by PEG-*b*-poly(*L*-glutamic acid)- (2-pyridyl disulphide) yielded a force-extension profile very similar to that of a random coil, apart from a characteristic reoccurring inflection

accounted for in both experimental (18± 4 pN) and theoretical studies (15 pN). The profile of the poly-*L*-glutamic acid helix was more stochastic due the lack of the stabilizing hydrophobic interactions. This is further supported by the CD measurement of the molecule in bulk, which showed an estimated fractional helicity of 28%. This offers an explanation as to why it is more difficult for a complete α-helix to reform under a small axial force. When a partially helical molecule was extended it conferred a greater WLC character to the force-extension profile as the random coil segments have a natural compliance towards extension [44]. Even when a complete helix was able to refold, it occurred less frequently and the plateau occurred at a lower force (19±2 pN) than that of the lysine helix ≈ 30pN.

A second inflection at 60± 9pN was also observed for 62 % of curves which exhibited the first inflection. This second inflection at a higher force was suggested to result from the formation of a metastable β-hairpin structure. It was suggested that some residues may occupy a second energy minima during the unfolding of the α-helix in conditions where entropic forces dominate, due to the β-hairpin structure possessing a higher entropy than the α-helix structure [49]. A similar inflection at higher forces was observed in a study conducted by Afrin et al.[4] which was a feature that also disappeared when experiments were conducted with a helix stabilizing agent. The authors did not report an explanation for the disappearance of this peak. We would therefore like to offer an explanation for the helices formed by the reported poly(*L*-alanine)-based polypeptide and our poly(*L*-glutamic acid). We believe that the appearance of the second peak at higher forces depended on both polypeptides possessing non-bulky side chains which did not stabilize the α-helix structure very well. A theoretical study has reported [49] that increasing stabilization of the α-helix structure due to hydrophobic side chain interactions inhibits the formation of the metastable β-hairpin structure.

Force-extension profiles for PEG-*b*-poly(*L*-Lysine)-(2-pyridyl disulphide) were also obtained at 50 mM NaCl where the hydrophobic interactions between the side chains were weakened. The obtained profiles looked remarkably similar to that of PEG-*b*-poly(*L*-glutamic acid)-(2-pyridyl disulphide) with a characteristic inflection at 17± 4 pN. None of the profiles retained the plateaus observed at 10 mM NaCl. We concluded that the force extension profile of a helical system has a constant force plateau and that when a system is only partially helical it pertains more to a random coil force-extension profile. We observed a plateau at ≈ 30 pN when the side-chain interactions were stabilizing through higher hydrophobicity, thus promoting the denatured segments between separated

helices to refold. In addition, the higher steric hindrance inhibits the helix-coil fluctuations that occur randomly along the chain due to a higher free energy barrier.

When helix stabilizing interactions were not as apparent, force interactions were observed around the 20 pN range. We thus infer that a minimum force of 20 pN is needed to unfold helical segments and that this reflects the required force to rupture the hydrogen bonds maintaining the α-helix more accurately as this force was observed in conditions where the side chain interactions were minimized.

Finally, the pivotal role that the side chain interactions play in stabilizing the α-helix has been appreciated for some time [55-57]. However, it is to our knowledge the first time that this was shown *in situ* on the single molecular level. In addition we believe we have also shown that a single, isolated α-helix is able to refold when a small axial force is applied, which had only been predicted theoretically [32, 40, 41] or shown experimentally in bulk [42, 43]. We also suggest that this study also indicates the importance of helix-stabilizing side chain interactions in preventing the formation of a metastable β-sheet-like interaction when the polypeptide is exposed to mechanical deformations.

Our study was in agreement with a previous experimental study done on a synthetic poly-*L*-alanine system [4] and most importantly, it could also be correlated with studies done on natural molecules, [35, 43] demonstrating the promising potential for using biomimicry in order to simplify and exemplify real biological systems. In addition, we were able to correlate our study to various theoretical studies done on helix-coil transitions [32, 37, 40, 41, 44, 45].

Material and Methods

Material and Methods for the Polymerization and Characterization of PEG_{114}-*b*-poly(*L*-lysine)$_{134}$-(2-pyridyl disulphide) :

The chemicals and reagents used for the synthesis of PEG-NH_2 and polymerization and coupling reactions to obtain PEG_{114}-*b*-poly(*L*-lysine)$_{134}$-(2-pyridyl disulphide) are listed below. Unless otherwise stated, the chemicals were used as received.

Chemicals	Manufactuer	Prior processing
1,4 dioxane	Sigma Aldrich	
4-Dimethylaminopyridine (DMAP)	Sigma Aldrich	
CaH_2	Sigma Aldrich	
Dichloromethane (anhydrous)	Sigma Adrich	Kept in solvent purification system
Diethylether	Sigma Aldrich	
ε-TFA-L-Lysine NCA	IsoChem	Stored in a glove box and used as supplied
HCl 37%	Sigma Aldrich	
KOH 85%	Merck	
Magnesium Sulphate (anhydrous)	Alfa Aesar	
Methanesulfonyl chloride (MsCl)	Sigma Aldrich	
Methoxy poly(ethylene glycol) , average M_n= 5000 g mol^{-1}	Fluka	Dissolved in anhydrous toluene and the moisture was azeotropically distilled
NaOH 97%	Alfa Aesar	
NH_4OH 28%	Prolabo	
N,N-Diisopropylethylamine (DIPEA)	Alfa Aesar	
N,N-Dimethylformamide (DMF 99.8% anhydrous)	Sigma Adrich	Dried over CaH2 (Sigma Aldrich) and cryodistilled.
N,N,N-Triethyl amine	Fischer	Dried over CaH_2 (Sigma Aldrich) and cryodistilled
N-Succinimidyl 3-(2-pyridyldithio)-propionate (SPDP)	Thermo Fischer	
Tetrahydrofuran (THF)	Sigma Aldrich	
Toluene (anhydrous)	Sigma Aldrich	Kept in solvent purification system

Synthesis of PEG_{114}-SO_3CH_3 from PEG-OH (Mn= 5000 g mol^{-1}):
10.0 g (2.0 mmol) of dry PEG-OH was dissolved in 15 ml of anhydrous dichloromethane under argon atmosphere. 840 µL (5.99 mmol) of dry triethylamine was added dropwise to the solution followed by 48.9 mg (0.40 mmol) of DMAP. After all the reactants were completely solubilized the solution was cooled to 0 ºC over an ice bath. Finally, 387 µL (5.0 mmol) of MsCl was added dropwise to the cooled solution and the reaction was left for 18 h on ice.
After the reaction the resulting solution was washed twice with 4 ml of 2M HCl. The phase containing the PEG-Mesylate intermediate was then concentrated to approximately one fourth of its initial volume and precipitated in 10 times the volume of ice-cold diethyl ether. The resulting cream-white solid was then

recovered by filtration and dried under vacuum overnight to remove traces of solvent before proceeding to the next step. The intermediate was confirmed by ^{1}H NMR, yield= 91.2%, (9.12 g), and the degree of functionalization was confirmed by comparing the integration of the protons on the methyl group labelled as **a** in ($C\mathbf{H_3}O$, σ= 3.38) with that of the ethyl protons beside the mesylate **c**, ($C\mathbf{H_2}OS(O_2)CH_3$, σ= 4.38) (
Figure 2).

Synthesis of PEG_{114}-NH_2 (Mn= 5000 g mol^{-1}):
5.00 g (1 mmol) of PEG-SO_3CH_3 was added to 100 ml of 28
% aqueous ammonia solution and the reaction was left to stir at 25 ºC in a tightly sealed round-bottom flask for 5 days. Subsequently, the lid was left ajar and the ammonia was left to evaporate in air over the course of 2 days. The pH of the solution was adjusted to 13 by the dropwise addition of freshly prepared 5 M NaOH, and the polymer was extracted three times in 40 ml of dichloromethane. The combined dichloromethane phase was then washed with 10 ml of brine and dried with the addition of dry magnesium sulphate. Thereafter, the dichloromethane phase containing the polymer was concentrated to less than one fourth of its volume, and precipitated in ice-cold diethylether. The product was dried under vacuum, and recovered as a pure-white powder, yield= 72%, (3.6 g). The degree of functionalization was confirmed by ^{1}H NMR by comparing the integration of the protons on the methyl end-group labelled as **a** ($C\mathbf{H_3}O$, σ= 3.38) with that of the ethyl protons beside the amine end-function **c**, ($OC\mathbf{H_2}NH_2$, σ= 3.19) (
Figure 2).

Synthesis of PEG_{114}-*b*-poly(N^{ε}-trifluoroacetyl-*L*-lysine)$_{134}$-NH_2 by ring-opening polymerization of *N*-trifluoroacetyl-*L*-lysine *N*-carboxyanhydride
The synthesis of the copolymer was performed by NCA polymerization under low temperature conditions. Immediately prior to the reaction, 0.2 g (0.04 mmol) of PEG-NH_2 (Mn= 5000 g mol^{-1}) from the previous synthesis was dissolved in 1,4 dioxane and any remaining moisture was azeotropically distilled out. After the PEG-NH_2 was completely dry it was redissolved in 2ml of freshly distilled DMF. 1.18 g (4.4 mmol) of N^{ε}-TFA-*L*-Lys-NCA was recovered in a flame-dried schlenk under inert atmosphere, and dissolved in 13 ml of freshly distilled DMF. Immediately after all of the monomer had dissolved in DMF (10 min<), the monomer solution was added to the schlenk containing the PEG-NH_2 initiator. The

mixture was left under dynamic vacuum for 10 minutes to allow the generated CO_2 to escape. Subsequently, the schlenk was sealed off and the polymerization was left to run for 5 days at 5 ºC under constant stirring and monitored by ^{1}H NMR. After 5 days half of the volume of the DMF was extracted through cryo-distillation, after which the polymer was precipitated in 10 times the volume excess of ice-cold diethyl ether. The precipitated PEG_{114}-*b*-poly(N^{ε}-trifluoroacetyl-*L*-lysine)$_{134}$-NH_2 was recovered by centrifugation and finally dried under vacuum.
The resulting degree of polymerization (D.P≈ 134) was determined by comparing the integration of the peak corresponding to the CH_2 signal nearest to the trifluoroacetyl group labelled as **d** ($CH_2NHCOCF_3$,σ=3.13 ppm) with that of the integration corresponding to the PEG_{114} (CH_2CH_2O, σ=3.51) labelled as **a** (**Figure 4**).

Coupling of PEG_{114}-*b*-poly(N^{ε}-trifluoroacetyl-*L*-lysine)$_{134}$-NH_2 with *N*-Succinimidyl 3-(2-pyridyldithio)-propionate (SPDP)

0.05 g (0.0014 mmol) of PEG_{114}-*b*-poly(N^{ε}-trifluoroacetyl-*L*-lysine)$_{134}$-NH_2 (was dissolved in 400 µl of DMF. In a separate vial 0.89 mg (0.0029 mmol) of *N*-Succinimidyl 3-(2-pyridyldithio)-propionate (SPDP) was dissolved in 100 µl of DMF. To the vial containing the copolymer 0.49 ml (0.0029 mmol) of DIPEA (Sigma Aldrich) was added and was left to stir for no more than 15 minutes. Finally the SPDP was carefully added to the vial containing the copolymer and the DIPEA. The reaction was left to stir for 3 days, after which reaction was diluted with water and dialyzed with 3500 Dalton membranes Spectra/Por® for a minimum of 4 days. Subsequently the samples were collected and lyophilized.

Deprotection of PEG_{114}-*b*- poly (N^{ε}-trifluoroacetyl-*L*-lysine) $_{134}$-(2-dipyridyl disulphide)

0.025 g (0.00071 mmol) of PEG_{114}-*b*-poly(N^{ε}-trifluoroacetyl-*L*-lysine)$_{134}$-(2-dipyridyl disulphide) was dissolved in 1.08 ml of ethanol containing 120 µl of 5M KOH. The turbid mixture as left to stir overnight in a water bath set to 35 ºC. The mixture was dialyzed with 3500 Dalton membranes from Spectra/Por®. Subsequently the samples were collected and lyophilized.

Molecular Characterization:

^{1}HNMR. All ^{1}HNMR experiments were performed on a Bruker Avance 400MHz spectrometer using TMS as a zero-point standard. The machine was equipped with a Bruker multinuclear z-gradient direct probe head producing gradients in the z-

direction with a strength of 53.5 $G \cdot cm^{-1}$. The spectra was acquired with a DI of 9 seconds and 32 scans. ^{1}HNMR samples were dissolved at 5$mg \cdot ml^{-1}$ in $CDCl_3$, $(CD_3)_2SO$ and D_2O.

Size-Exclusion Chromatography. Size-exclusion chromatographs were performed using DMF LiBr 1$g \cdot L^{-1}$ at 80 °C as the eluent, at a flow rate of 0.80 $ml \cdot min^{-1}$. A SHODEX KD-804 column was used and calibrated with PEG standards. Dilute samples of 5.0 $mg \cdot ml^{-1}$ were prepared and injected.

Circular Dichroism Spectroscopy.
The CD experiments were performed using a JASCO J-815 spectrometer equipped with a JASCO CDF-426S Peltier temperature control system. The scans were recorded between wavelengths of 180 to 260 nm and are a result of three accumulations. Block copolymer solutions were prepared at a concentration of 0.25 $mg \cdot ml^{-1}$ and 0.1 cm quartz cuvettes were used. The pH 2-12 was adjusted by the addition NaOH or HCl (0.1M and 1M). The base or acid was added by using a micropipette and the exact amount of added liquid was recorded so that the difference in dilution could be taken into consideration. All solutions were filtered with a 0.22 μm syringe filter before use.

Dynamic Light Scattering
Light scattering experiments were done at 90 ° on a CGS5000 multi-angle light scattering spectrometer equipped with a 22 mW He-Ne laser (λ=632.8 nm). The software used for analysis was ALV-5000/EPP. Three measurements were done per sample and the scattering was recorded for 30 seconds. Block co-polymer samples were prepared at a concentration of 1$mg \cdot ml^{-1}$ dissolved in 10 mM, 50 mM or 0.1 mM NaCl solutions. The pH 2-12 was adjusted by the addition of NaOH or HCl (0.1 M and 1 M). All solutions were filtered with a 0.22 μm syringe filter before use.

Materials and Methods for AFM Experiments.
Immobilization of the polymer-polypeptides on to an Au-Si surface.
2 cm by 2 cm Au/Si surfaces (Sigma-Aldrich) were cleaned by using a TL1 cleaning solution (H_2O: NH_3: H_2O_2, 5:1:1, v/v/v) at 70 °C for 15 minutes. The cleaned surfaces were carefully rinsed with ultra-pure water (milliQ) before drying under nitrogen flow. The functionalization solution was prepared by either dissolving 0.1$mg \cdot ml^{-1}$ of PEG_{114}-*b*-PGA_{85}-(2-pyridyl disulphide) or 0.1$mg \cdot ml^{-1}$ of PEG_{114}-*b*-$PLys_{134}$-(2-pyridyl disulphide), with a short PEG_6-SH oligomer

(Polypure) with a $mol \cdot mol^{-1}$ ratio of (80:20, PEG-SH: copolymer) in 100mM KH_2PO_4 (Sigma Aldrich) at pH 7.0 adjusted with NaOH or HCl (both Sigma Aldrich) respectively. After functionalization the surfaces were used rinsed repeatedly with ultra-pure water (milliQ) and used immediately for single molecule force spectroscopy experiments.

Intermittent Contact Imaging

Intermittent contact imaging was done on AC mode using PPP-NCH silicon tips (Nanosensors) with a nominal spring constant between 10-130 $N \cdot m^{-1}$. The nominal resonance frequency is between 204-497 kHz. The images were obtained in air and the processing was done using the software, Gwyddion version 2.41. The diblock copolymers were immobilized on the surface using the same procedure as the one used for SMFS experiments. After immobilization the surface was left to dry before imaging.

Single Molecule Force Spectroscopy Experiments

SMFS was performed on a PicoPlus 5500 from Agilent Technologies with a closed loop scanner. A conventional fluid cell was used during experimentation. Force-distance curves were obtained by using gold coated silicon-nitride cantilevers (OBL series, Brucker) with a nominal spring constant at 0.06 $N \cdot m^{-1}$. The real spring constant of the cantilevers were determined by the thermal noise method after every experiment. Two different types of salt solutions were used depending on the copolymer. All salt solutions, base and acids were prepared with ultra-pure water, filtered and prepared fresh prior to every experiment.

For measurements done with PEG_{114}-*b*-PGA_{85}-(2-pyridyl disulphide), 10 mM NaCl with 5 mM KH_2PO_4 was used. The pH of the solution was adjusted to either pH 7 (random coil) or pH 3 (helix) with the addition of NaOH or HCl. The pH was monitored throughout the experiment.

For measurements done with PEG_{114}-*b*-$P(Lys)_{134}$-(2-pyridyl disulphide) 10 mM and 50 mM NaCl was used. The pH of the solution was adjusted to either pH 7 (random coil) or pH 12 (helix) with the addition of NaOH or HCl. The pH was monitored throughout the experiment.

Statistical Mechanical Model developed by Schatz and Torabi.

Access to the model was obtained by registering an account at www.nanoHUB.org. For all of the simulations an ionic concentration of 10 mM was used. To mimic the architecture of our molecules as close as possible, the N terminal was assumed to be protected and the C terminal was left unprotected. A spring constant of 9.5

$pN \cdot nm^{-1}$ was used, which is the average value of spring constant of the OBL tips (n= 23) obtained during the SMFS experiments by the thermal noise method. Simulations were done at pH 7 and 12 for $poly(lysine)_{134}$, and at pH 2 and 7 for $poly(glutamic\ acid)_{85}$.

References

1. A. R. Dinner, A. Sali, L. J. Smith, C. M. Dobson and M. Karplus, *Trends in Biochemical Sciences*, 2000, **25**, 331-339.
2. V. Daggett and A. Fersht, *Nat Rev Mol Cell Biol*, 2003, **4**, 497-502.
3. H.-A. Klok and H. Schlaad, in *Peptide Hybrid Polymers*, Springer Berlin Heidelberg, Editon edn., 2006, vol. 202, pp. 53-73.
4. R. Afrin, I. Takahashi, K. Shiga and A. Ikai, *Biophysical Journal*, 2009, **96**, 1105-1114.
5. A. Idiris, M. T. Alam and A. Ikai, *Protein Engineering*, 2000, **13**, 763-770.
6. M. A. Lantz, S. P. Jarvis, H. Tokumoto, T. Martynski, T. Kusumi, C. Nakamura and J. Miyake, *Chemical Physics Letters*, 1999, **315**, 61-68.
7. W. Ott, M. A. Jobst, C. Schoeler, H. E. Gaub and M. A. Nash, *Journal of Structural Biology*, 2016.
8. A. F. Oberhauser, P. E. Marszalek, H. P. Erickson and J. M. Fernandez, *Nature*, 1998, **393**, 181-185.
9. M. Rief, J. Pascual, M. Saraste and H. E. Gaub, *Journal of Molecular Biology*, 1999, **286**, 553-561.
10. M. Rief, M. Gautel, F. Oesterhelt, J. M. Fernandez and H. E. Gaub, *Science*, 1997, **276**, 1109-1112.
11. F. Oesterhelt, M. Rief and H. E. Gaub, *New Journal of Physics*, 1999, **1**, 6.
12. G. Wei, Q. Li, S. Steckbeck and L. C. Ciacchi, *Physical Chemistry Chemical Physics*, 2014, **16**, 3995-4001.
13. A. Ikai, A. Idiris, H. Sekiguchi, H. Arakawa and S. Nishida, *Applied Surface Science*, 2002, **188**, 506-512.
14. T. Sulchek, R. W. Friddle and A. Noy, *Biophysical Journal*, 2006, **90**, 4686-4691.
15. M. Grandbois, M. Beyer, M. Rief, H. Clausen-Schaumann and H. E. Gaub, *Science*, 1999, **283**, 1727-1730.
16. P. Lussis, T. Svaldo-Lanero, A. Bertocco, C.-A. Fustin, D. A. Leigh and A.-S. Duwez, *Nat Nano*, 2011, **6**, 553-557.
17. J. Cheng and T. J. Deming, in *Peptide-Based Materials*, ed. T. Deming, Springer Berlin Heidelberg, Berlin, Heidelberg, Editon edn., 2011, pp. 1-26.
18. G. J. M. Habraken, M. Peeters, C. H. J. T. Dietz, C. E. Koning and A. Heise, *Polymer Chemistry*, 2010, **1**, 514-524.
19. H. R. Kricheldorf, C. von Lossow and G. Schwarz, *Macromolecules*, 2005, **38**, 5513-5518.
20. T. J. Deming, *Nature*, 1997, **390**, 386-389.
21. H. R. Kricheldorf, *Angewandte Chemie International Edition*, 2006, **45**, 5752-5784.
22. W. D. Fuller, M. P. Cohen, M. Shabankareh, R. K. Blair, M. Goodman and F. R. Naider, *Journal of the American Chemical Society*, 1990, **112**, 7414-7416.

23. W. Vayaboury, O. Giani, H. Cottet, A. Deratani and F. Schué, *Macromolecular Rapid Communications*, 2004, **25**, 1221-1224.
24. P. D. Bragg and C. Hou, *Archives of Biochemistry and Biophysics*, 1975, **167**, 311-321.
25. A. J. Lomant and G. Fairbanks, *Journal of Molecular Biology*, 1976, **104**, 243-261.
26. G. T. Hermanson, in *Bioconjugate Techniques (Second Edition)*, Academic Press, New York, Editon edn., 2008, pp. 169-212.
27. J. Carlsson, H. Drevin and R. Axen, *Biochemical Journal*, 1978, **173**, 723-737.
28. G. Holzwarth and P. Doty, *Journal of the American Chemical Society*, 1965, **87**, 218-228.
29. E. M. Bradbury, C. Crane-Robinson, H. Goldman and H. W. E. Rattle, *Biopolymers*, 1968, **6**, 851-862.
30. A. Harada, S. Cammas and K. Kataoka, *Macromolecules*, 1996, **29**, 6183-6188.
31. P. Luo and R. L. Baldwin, *Biochemistry*, 1997, **36**, 8413-8421.
32. K. Torabi and G. C. Schatz, *Macromolecules*, 2013, **46**, 7947-7956.
33. O. Kratky and G. Porod, *Recueil des Travaux Chimiques des Pays-Bas*, 1949, **68**, 1106-1122.
34. J. F. Marko and E. D. Siggia, *Macromolecules*, 1995, **28**, 8759-8770.
35. F. Berkemeier, M. Bertz, S. Xiao, N. Pinotsis, M. Wilmanns, F. Gräter and M. Rief, *Proceedings of the National Academy of Sciences*, 2011, **108**, 14139-14144.
36. F. Hanke, A. Serr, H. J. Kreuzer and R. R. Netz, *EPL (Europhysics Letters)*, 2010, **92**, 53001.
37. Z. Qin, A. Fabre and M. J. Buehler, *The European Physical Journal E*, 2013, **36**, 1-12.
38. Z. Qin, S. Cranford, T. Ackbarow and M. J. Buehler, *International Journal of Applied Mechanics*, 2009, **01**, 85-112.
39. P. Palenčár and T. Bleha, *Macromolecular Theory and Simulations*, 2010, **19**, 488-495.
40. M. N. Tamashiro and P. Pincus, *Physical Review E*, 2001, **63**, 021909.
41. A. Buhot and A. Halperin, *Macromolecules*, 2002, **35**, 3238-3252.
42. S. Zahouani, A. Chaumont, B. Senger, F. Boulmedais, P. Schaaf, L. Jierry and P. Lavalle, *ACS Applied Materials & Interfaces*, 2016, **8**, 14958-14965.
43. S. Courty, J. L. Gornall and E. M. Terentjev, *Proceedings of the National Academy of Sciences of the United States of America*, 2005, **102**, 13457-13460.
44. B. Chakrabarti and A. J. Levine, *Physical Review E*, 2006, **74**, 031903.
45. R. Rohs, C. Etchebest and R. Lavery, *Biophysical Journal*, 1999, **76**, 2760-2768.
46. Z. Qin and M. J. Buehler, *Physical Review Letters*, 2010, **104**, 198304.
47. L. Kreplak, J. Doucet, P. Dumas and F. Briki, *Biophysical Journal*, 2004, **87**, 640-647.
48. L. Kreplak, H. Herrmann and U. Aebi, *Biophysical Journal*, 2008, **94**, 2790-2799.
49. F. Ding, J. M. Borreguero, S. V. Buldyrey, H. E. Stanley and N. V. Dokholyan, *Proteins: Structure, Function, and Bioinformatics*, 2003, **53**, 220-228.
50. A. Chakrabartty, R. L. Baldwin, F. M. R. J. T. E. C.B. Anfinsen and S. E. David, in *Advances in Protein Chemistry*, Academic Press, Editon edn., 1995, vol. Volume 46, pp. 141-176.
51. H. B. Lodish, Arnold, L. Zipursky, P. Matsudaira, D. Baltimore and J. Darnell, in *Molecular Cell Biology. 4th edition.*, W. H. Freeman, New York, Editon edn.,

2000.
52. F. Chécot, A. Brûlet, J. Oberdisse, Y. Gnanou, O. Mondain-Monval and S. Lecommandoux, *Langmuir*, 2005, **21**, 4308-4315.
53. F. Chécot, S. Lecommandoux, Y. Gnanou and H.-A. Klok, *Angewandte Chemie International Edition*, 2002, **41**, 1339-1343.
54. E. Lacroix, A. R. Viguera and L. Serrano, *Journal of Molecular Biology*, 1998, **284**, 173-191.
55. S. Marqusee and R. L. Baldwin, *Proceedings of the National Academy of Sciences*, 1987, **84**, 8898-8902.
56. J. M. Scholtz and L. B. Robert, *Annual Review of Biophysics and Biomolecular Structure*, 1992, **21**, 95-118.
57. J. M. Scholtz, H. Qian, V. H. Robbins and R. L. Baldwin, *Biochemistry*, 1993, **32**, 9668-9676.

Chapter 3

Synthesis of PEG_{114}-*b*-$(PLys)_{134}$-*b*-PEG_{114} and Investigation of an Alternative Experimental Design for the Unfolding of Homopeptide α-Helices by Single Molecule Force Spectroscopy

Abbreviations:

AFM- Atomic Force Microscopy

CD- Circular Dichroism

FJC-Model- Freely Jointed Chain Model

iPFRC Model- Inhomogeneous Partially Freely Rotating Chain Model

PEG- Poly(ethylene glycol)

PEG_{114}-*b*-$(PLys)_{134}$-b-$(PEG)_{114}$- Poly(ethylene glycol)$_{114}$-*b*-poly(*L*-lysine)$_{134}$-*b*-poly(ethylene glycol)$_{114}$

ROP-Ring Opening Polymerization

SEC- Size Exclusion Chromatography

SMFS- Single Molecule Force Spectroscopy

WLC Model- Worm-like Chain

Contents

Introduction

A stimuli-responsive polymer-peptide poly(ethylene glycol)$_{114}$-*b*-poly(*L*-lysine)$_{134}$-*b*-poly(ethylene glycol)$_{114}$ **(PEG_{114}-*b*-$(PLys)_{134}$-*b*-PEG_{114})** triblock was synthesized for used in single-molecule force experiments (SMFS) **(Figure 1)**.The secondary conformation of the lysine was changed *in situ* from a random coil to a α-helix, and the transition was investigated at two different ionic concentrations which allow or weaken hydrophobic side chain interactions.

The addition of a PEG separation length has been shown to minimize the adhesion of investigated molecules to the surface [1] and to separate the interaction of interest from unspecific tip-surface adhesion [2-5]. In comparison to the previously synthesized poly(ethylene glycol)$_{114}$-*b*-poly(*L*-lysine)$_{134}$-(2-pyridyl disulphide) **(PEG_{114}-*b*-$(PLys)_{134}$-(2-pyridyl disulphide)**, it was hoped that the addition of the second separation length would position the polypeptide section further away from the surface, as the majority of interactions observed for the diblock started within an extension of 10 nm. Displacing the polypeptide segment further away from the surface would reduce the number of force-extension curves where the presence of unspecific adhesion conceals parts of the interaction **(Figure 2)**, thereby improving the acquisition percentage of good curves.

By utilizing the triblock copolymer it is possible to rely on just the direct adsorption of the molecule onto a cleaned surface. The passivating layer of small PEG oligomers is no longer necessary, and by reducing the number of species that come in contact with the surface, possible contamination can be minimized. Adsorption alone was shown to withstand forces up to several hundred piconewtons [6, 7], and shown to be suitable for SMFS experiments on various polymers and proteins [8-11]. Finally in addition to studying a different architecture and immobilization strategy, it is also particularly interesting to compare the results obtained with this triblock copolymer with SMFS results obtained for the diblock. Using the diblock copolymer, it was shown that the α-helix of the poly-(*L*-lysine) was stabilized through hydrophobic side chain interactions. By coupling a highly soluble PEG to both ends of the poly-(*L*-lysine) polypeptide, the solubility of the molecule can be increased, and it would be interesting to see how this would affect the helix stability and formation.

Additionally from a polymer chemistry perspective, the attachment of PEG to polypeptides offer many attractive properties such as improved solubility in water and stability [12]. PEG has FDA approval as a biocompatible material [13], and long chains thereof promote longer circulation time in the body making PEG-

polypeptide hybrids very attractive for drug and gene delivery systems [14]. Although not investigated here, an additional PEG might further decrease *in vivo* toxicity of PEG-poly(*L*-lysine) systems which been introduced by Kataoka et al. [15] as a possible gene delivery vector

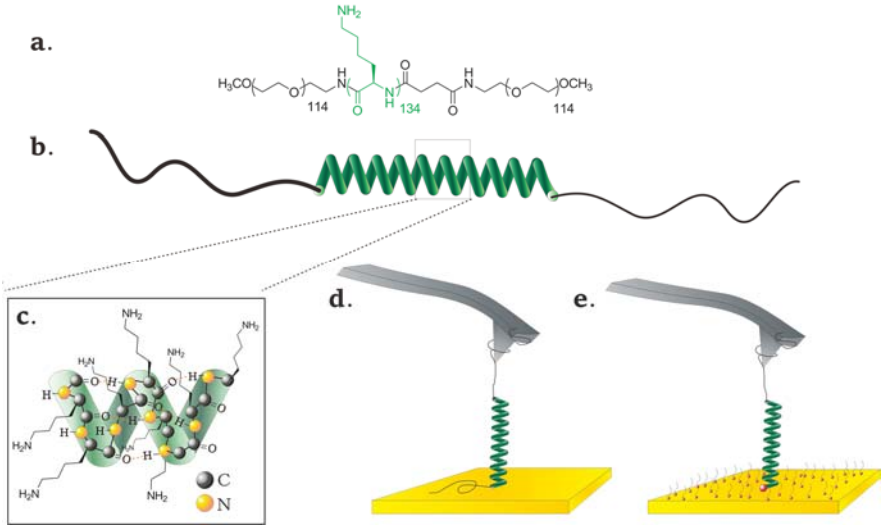

Figure 1. Schematic Representations of $(PEG)_{114}$-*b*-poly(*L*-lysine)$_{134}$-*b*-$(PEG)_{114}$. a.) Chemical structure of poly(ethylene glycol)$_{114}$-*b*-poly(*L*-lysine)$_{134}$-*b*-poly(ethylene glycol)$_{114}$. b.) Schematic representation of $(PEG)_{114}$-*b*-poly(*L*-lysine)$_{134}$-*b*-$(PEG)_{114}$ in a α-helix conformation. c.) Detailed representation of the side chains and hydrogen bonding within the poly-*L*-lysine α-helix. d.) Schematic representation of the triblock copolymer with one PEG segment adsorbed onto the surface, and the other PEG segment adsorbed onto a bare AFM cantilever. e.) In comparison, a schematic representation of the diblock copolymer poly(ethylene glycol)$_{114}$-*b*-poly(*L*-lysine)$_{134}$-(2-pyridyl disulphide) molecule grafted onto a gold surface with the PEG chain adsorbed onto a bare AFM cantilever and the 2-pyridyl disulphide (red dot) on the other end of the molecule as an anchoring moiety. The molecule is surrounded by PEG_6-SH also grafted on to the surface as a passivating agent.

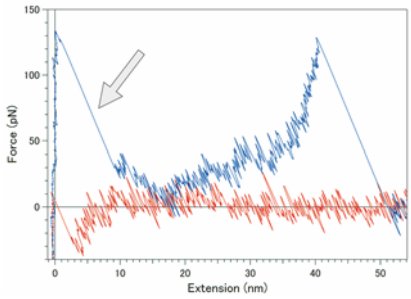

Figure 2. An example force-extension curve displaying the presence of unspecific adhesion (grey arrow) concealing the beginning of the interaction.

PART I
Synthesis and Characterization of PEG_{114}-*b*-$(PLys)_{134}$-*b*-PEG_{114}

1.1 Synthesis of Poly(ethylene glycol)$_{114}$-*b*-poly(*L*-lysine)$_{134}$-*b*-poly(ethylene glycol)$_{114}$ (PEG_{114}-*b*-$(PLys)_{134}$-*b*-PEG_{114}) by Amine-coupling reaction

PEG_{114}-*b*-$(PLys)_{134}$-*b*-PEG_{114} **(10)** was synthesized through an amine coupling reaction of an intermediate PEG_{114}-*b*-poly(N^{ε}-trifluoroacetyl-*L*-lysine)$_{134}$-NH_2 **(4),** with a PEG_{114}-α-methoxy-ω-NHS ester (**Figure 3**). The resulting protected triblock, PEG_{114}-*b*-poly(N^{ε}-trifluoroacetyl-*L*-lysine)$_{134}$-*b*-PEG_{114} **(9)** was subsequently deprotected yielding the final product (**Figure 4**).

The intermediate **(4)** was synthesized through a PEG-NH_2 initiated ring opening polymerization of N^{ε}- Trifluoroacetyl-*L*-lysine *N*-carboxyanhydride and the degree of polymerization (DP≈ 134) was determined by ^{1}H NMR. (Please refer to **Chapter 2, Figure 4**)

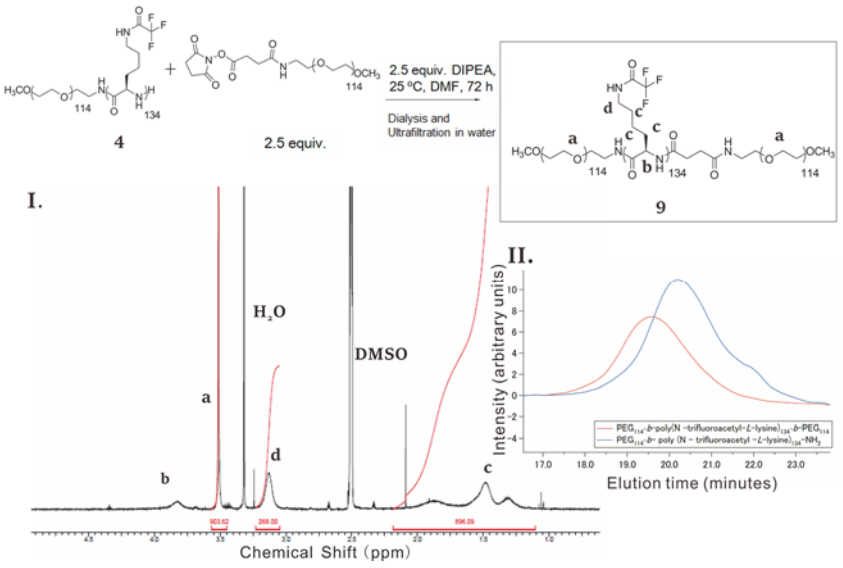

Figure 3. General scheme of reaction, ^{1}H NMR and SEC trace of PEG_{114}-*b*-poly(N^{ε}-trifluoroacetyl-*L*-lysine)$_{134}$-*b*-PEG_{114}. I.) ^{1}H NMR of PEG_{114}-*b*-poly(N^{ε}-trifluoroacetyl-*L*-lysine)$_{134}$-*b*-PEG_{114} in DMSO-d_6 (Bruker 400MHz). II.) SEC of PEG_{114}-*b*- poly (N^{ε}- trifluoroacetyl

-*L*-lysine) $_{134}$-NH_2 (blue) and PEG_{114}-*b*-poly(N^{ε}-trifluoroacetyl-*L*-lysine)$_{134}$-*b*-PEG_{114} (red) in DMF: 1g·L^{-1} LiBr , $Đ\frac{Mw}{Mn}$=1.14; 80 °C.

After purification, the integration of the peak corresponding to the CH_2 signal nearest to the trifluoroacetyl group labelled as **d** ($C\mathbf{H_2}NHCOCF_3$,σ=3.13 ppm) was compared with that of the integration of the peak corresponding to the PEG_{114} ($C\mathbf{H_2}C\mathbf{H_2}O$, σ=3.51) labelled as **a (Figure 3)**. The integration corresponding to the PEG_{114} had doubled, confirming the success of the coupling reaction.

A comparison of the SEC traces between the diblock and triblock copolymers **(Figure 3.II)** shows that the completion of the reaction with a good conversion. The trace of the triblock does not show the small secondary peak as additional purification steps were utilized to separate the excess unreacted PEG_{114}-α-methoxy-ω-NHS ester and other contaminants from the final product. In the synthesis of the diblock only precipitation in diethylether was used, which was probably not sufficient to eliminate all the contaminants.

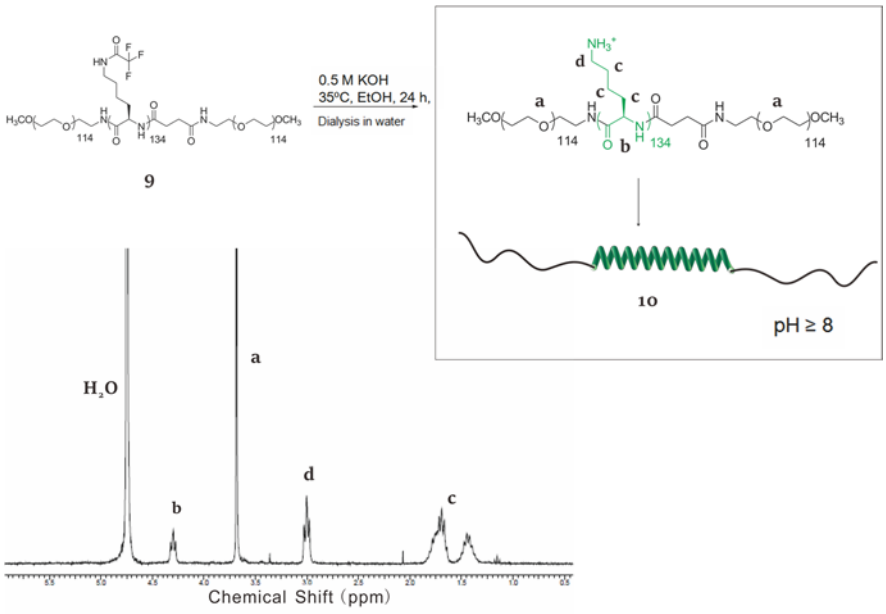

Figure 4. Deprotection of PEG_{114}-*b*-poly(N^{ε}-trifluoroacetyl-*L*-lysine)$_{134}$-*b*-PEG_{114}. ^1H NMR of PEG_{114}-*b*-(poly-*L*-lysine)$_{134}$-PEG_{114} in D_2O (Bruker 400MHz). The schematic representation depicts the deprotonated lysine side chain at high pH allowing the polypeptide segment to fold in to a α-helix. In the conditions utilized for the synthesis, and subsequent purification the molecule adopted a random coil conformation as also indicated by the position of the ε–CH_2 peak **(d)** at 3.0 ppm.

1.2 The pH responsiveness of PEG_{114}-*b*-poly(*L*-Lysine)$_{134}$-*b*-PEG_{114} determined by Circular Dichroism

The pH of the coil-helix transition for the diblock copolymer PEG_{114}-*b*-poly(*L*-lysine)$_{134}$-NH_2 was determined to occur between pH 9-11, thus for the triblock copolymer PEG_{114}-poly(*L*-Lysine)-PEG_{114} it was predicted to occur at approximately the same range. Beyond the $pK_a \approx 10$ value of the lysine side chains, the side chain amine groups are deprotonated allowing the main chain backbone to fold into a helix conformation.

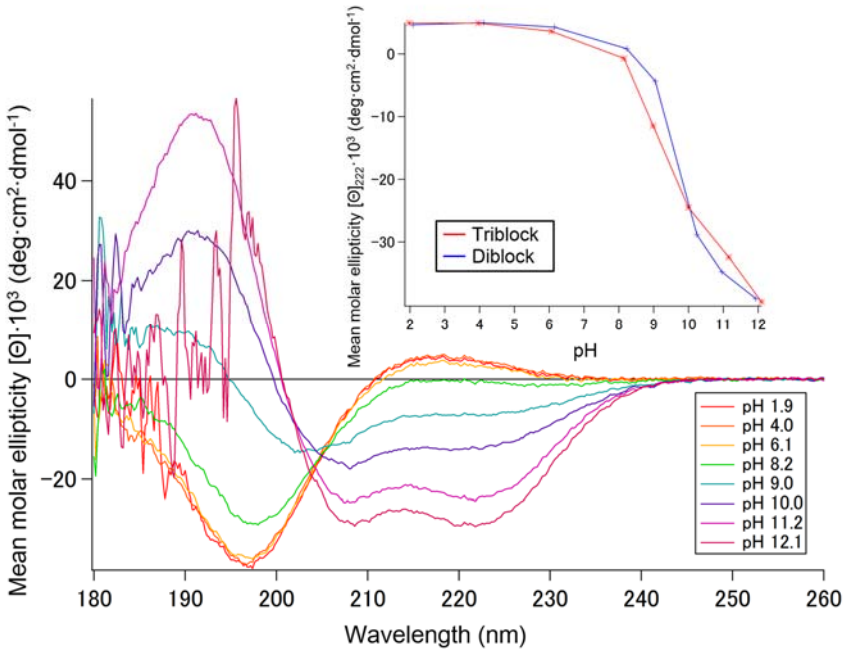

Figure 5. Circular dichroism spectra between 180 nm-260 nm of PEG_{114}-poly(*L*-lysine)$_{134}$-PEG_{114} in different pH conditions from pH 2-12. Concentration=0.25 mg/ml; cell length=0.1cm; 20 °C. The inset shows the evolution of the mean molar ellipticity at 222 nm with pH for the triblock PEG_{114}-poly(*L*-lysine)$_{134}$-PEG_{114} (red) and the diblock, PEG_{114}-*b*-poly(*L*-lysine)$_{134}$-NH_2 (blue).

The CD spectrum (**Figure 5**) indicates that PEG_{114}-*b*-poly(*L*-Lysine)$_{134}$-*b*-PEG_{114} is able to undergo a coil-helix transition in response to pH. At pH 8 and below, a strong negative molar ellipticity between 195-197 nm and a weakly positive molar ellipticity at 215 nm can be observed, indicative of a molecule in a random coil conformation. Gradually from pH 8 and up, the molecule transitions into a helical conformation. The helical conformation of the molecule is indicated by a characteristic positive molar ellipticity at 190 nm and two negative peaks at

208 nm and 222 nm respectively. The inset in (**Figure 5**) shows the evolution of the peak at 222 nm with pH comparing the transition between the diblock and the triblock systems.

Compared to the diblock the triblock undergoes the helix-coil transition more gradually, and the onset of the transition happened at lower pH conditions. A similar stabilization effect by block copolymerization of poly(*L*-Lysine) with PEG had been observed by Harada, Cammas and Kataoka [16] for a PEG_{98}-poly(*L*-Lysine)$_{19}$ system. Their reasoning was that the increasing hydrophobicity of the lysine segment caused by deprotonation causes the lysine segment to surround itself with the PEG segment as an outer shell. The correlation between the two segments was determined by 2D-NOSEY and they predicted the formation of a dimer with a spherical micelle-like structure, with the lysine segments associating side-by-side in an antiparallel manner to compensate for the helix dipole moment (**Figure 6**).

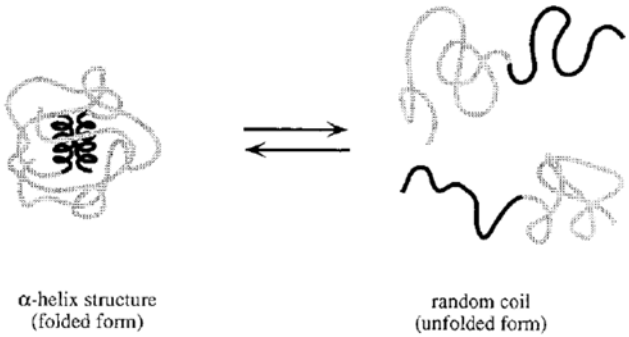

Figure 6. Schematic representation of the helix-coil equilibrium for a PEG_{98}-b-poly(L-Lysine)$_{19}$ showing the formation of a spherical micelle-like dimer with PEG forming a shell around two lysine helices associating in an anti-parallel manner. This diagram is reproduced directly from a work published by Harada, Cammas and Kataoka from reference [16].

A similar explanation can be offered to interpret the difference in behaviour between the diblock and the triblock systems. The additional PEG segment allowed further stabilization of the lysine segment through increased segregation of the lysine from the aqueous media. The onset of the transition was at a lower pH for the triblock as the association of the additional PEG segment with the lysine, most likely further aided the nucleation of the helix. The increased segregation of the lysine segment is further supported by the slower transition of the triblock into the α-helical conformation after pH 10. The association of the

lysine segment with PEG aided the nucleation but also isolated the lysine from the surrounding solution, preventing the full transition into a helix from taking place rapidly. The estimated helix content using the expression and values proposed by Luo and Baldwin [17] was 75.5 % at pH 12. The value was slightly higher than the percent helicity obtained for the diblock at pH 12 (70.9 %), and further supports the stabilizing effect of the additional PEG segment.

The results obtained from CD are interesting as it demonstrates that when characterized in solution the PEG segment of the molecule interactions with the lysine segment. For the SMFS experiments conducted with the diblock architecture this would not be a largely problematic issue as the diblock molecules were bound by Au-S bonding directly on the gold surface, with the PEG segments collapsed above. If the diblock molecule was caught by the AFM tip as long as the strength of the adsorption of the PEG tether to the AFM tip was strongest interaction next to the Au-S bond, the molecule including the helix would be extended completely. With the triblock architecture both PEG segments must be favourably adsorbed to the tip and the surface so any competing interaction between the PEG and lysine segments is problematic.

PART II
Single Molecule Force Spectroscopy Experiments of PEG_{114}-*b*-poly(*L*-Lysine)$_{134}$-*b*-PEG_{114} in different pH and Salt Conditions

2.1 Immobilization of PEG_{114}-*b*-poly(*L*-Lysine)$_{134}$-*b*-PEG_{114}

Immediately prior to performing single molecule force spectroscopy experiments, the triblock molecules were diluted (0.1 mg·ml^{-1}), and 50 µL of the solution was pipetted onto a freshly cleaved mica surface or a TL1 (H_2O: NH_3: H_2O_2, 5:1:1, v/v/v) treated gold surface (Please refer to **Materials and Methods, pg. 144**). The surface was left to functionalize for an hour, and then rinsed thoroughly before use.

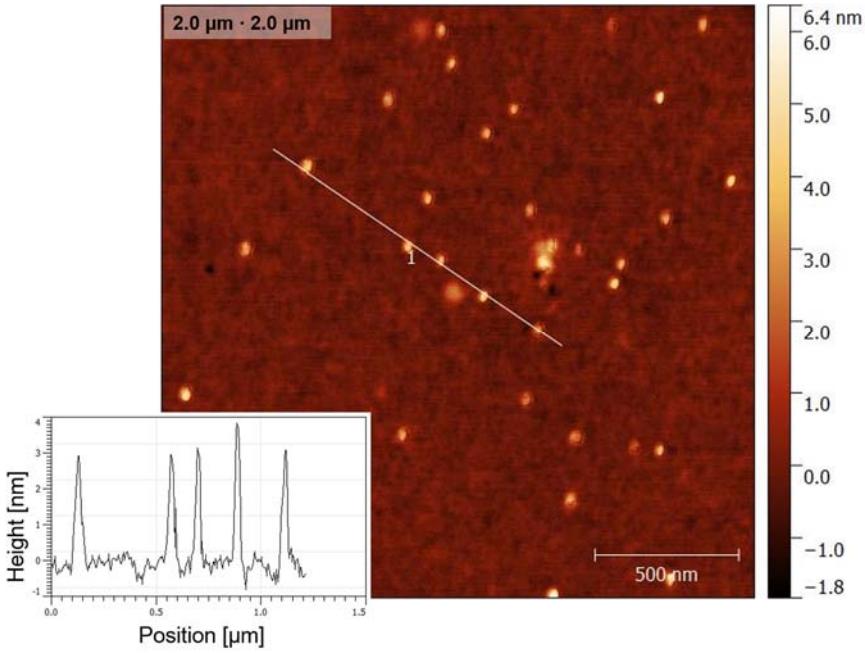

Figure 7. Intermittent contact image in air (2.0 µm by 2.0µm) of PEG_{114}-*b*-poly(*L*-Lysine)$_{134}$-*b*-PEG_{114} immobilized on mica. The corresponding profilograph can be seen next to the image. The white line indicates the line where the profile of the surface was measured.

Intermittent contact imaging (**Figure 7**) in air was done in order to determine whether the immobilization was successful and conducive to isolating

single molecules on the surface. The imaging in air was done for the sample immobilized on a freshly cleaved mica surface and obtained at a resolution of 2.0 μm by 2.0 μm. The presence of consistent, compact, white dots of widths and heights comparable to the size of the isolated molecules indicates the presence of single triblock copolymers adsorbed on the surface.

2.2 The Utilization of the Worm-like Chain Fitting as a Guide for the Selection of Force-Extension Curves

Optimally only profiles with minimal unspecific adhesion and reoccurring features were considered for analysis. The extension behaviours of a combined PEG-lysine-PEG should have characteristics pertaining to both the extension of a PEG polymer and the extension of the polypeptide. Similarly to the diblock system the force-extension profile of PEG is used as a reference in order to identify force-extension curves. When both the polypeptide and PEG are in a random coil conformation, the force-extension should exhibit a simple parabolic profile comparable with that of a random coil polymer indicating an increasing counter entropic restoring as the degrees of conformational freedom are reduced. This behaviour can be predicted with the various models approximated by statistical models of polymer mechanics. When the poly(*L*-lysine) displays the α-helical conformation, a characteristic deviation from the predicted elastic response should be apparent. When the characteristic deviations are easy to identify, such as the plateau at ≈ 30 pN observed for the PEG_{114}-*b*-poly(*L*-lysine)$_{134}$-(2-pyridyl disulphide), fitting the experimentally obtained force-extension curve with a model describing the elastic behaviour of an ideal polymer is not necessary to determine its characteristic feature. For the triblock system however, the features were difficult to identify without a fitting guide.

As mentioned previously there are various models that have been optimised to describe the elastic behaviour of PEG [6], and a generic polypeptide [18], however the simplest model to use which is applicable to both the PEG and the polypeptide segment is the WLC model introduced by Kratky and Porod [19], and interpolated for AFM by Marko and Siggia [20]. Although Oesterhelt, Rief and Gaub [6] described a modified freely-jointed chain model (FJC) to describe the extension of PEG, the behaviour of a random coil polymer coupled to a polypeptide can be better approximated by assuming that the polymer is an irregular semi-flexible string (WLC model). The WLC model has been successfully used as a fit for various protein and polypeptides [8-10, 21] in the past. The inhomogenous partially freely rotating model (iPFC) more recently introduced by Hanke et al. [18] was

developed to better model polypeptides by mimicking the peptide bonding. However, the WLC model has been shown to reproduce the results of this model, but for a 10% over estimation of the contour length [22]. Therefore the well-studied WLC model is more than a sufficient model to be used as a guide in order to determine whether the force-extension followed that of a featureless ideal polymer or if a small unique feature was apparent.

2.3 SMFS experiments of PEG_{114}-*b*-poly(*L*-Lysine)-*b*-PEG_{114} at pH 12, 10 mM NaCl

There were 4 groups of reoccurring force-extension profiles obtained for PEG_{114}-*b*-poly(*L*-Lysine)-*b*-PEG_{114} in a α-helix conformation at pH 12. A total of 17316 curves were recorded on mica and gold surfaces, and the probability of event was 2.23 % (**Table 1**). Only single peaks were analysed, and profiles with multiple peaks were considered as multiple molecule interactions. The multiple peaks were considered in the statistical count in order to obtain the event probability, but otherwise disregarded.

Table 1. Typical force-extension profiles and their percentage of occurrence observed for PEG_{114}-*b*-poly(*L*-Lysine)-*b*-PEG_{114} at pH 12. Event probability indicates the total number of observed interactions out of 17316 force-extension cycles. WLC indicates curves where the force-extension profile followed the fit obtained using the WLC model. (Curves with no evident structure beyond what has been predicted for an ideal random coil polymer).

Peak or Plateau ≤ 10 pN	Force of detachment ≤ 30 pN	Inflection	WLC	Multiple Peaks	Event Probability	Number of Recorded Curves
39 (0.22%)	80 (0.46%)	43 (0.25%)	22 (0.13%)	202 (1.17%)	2.23%	17316

The majority of the obtained profiles had a force of detachment that was below 30 pN, and could not be utilized for analysis as the molecule was not extended with enough force for characteristic features to be apparent. The rest of the obtained profiles could be separated into three groups, 1.) profiles where an inflection at 28±9 pN was apparent **(Figure 8)** 2.) profiles where a plateau or a peak could be observed at approximately 10 pN or below **(Figure 9 b.)** and 3.) profiles that could be fitted by the WLC model **(Figure 9 a.)**.

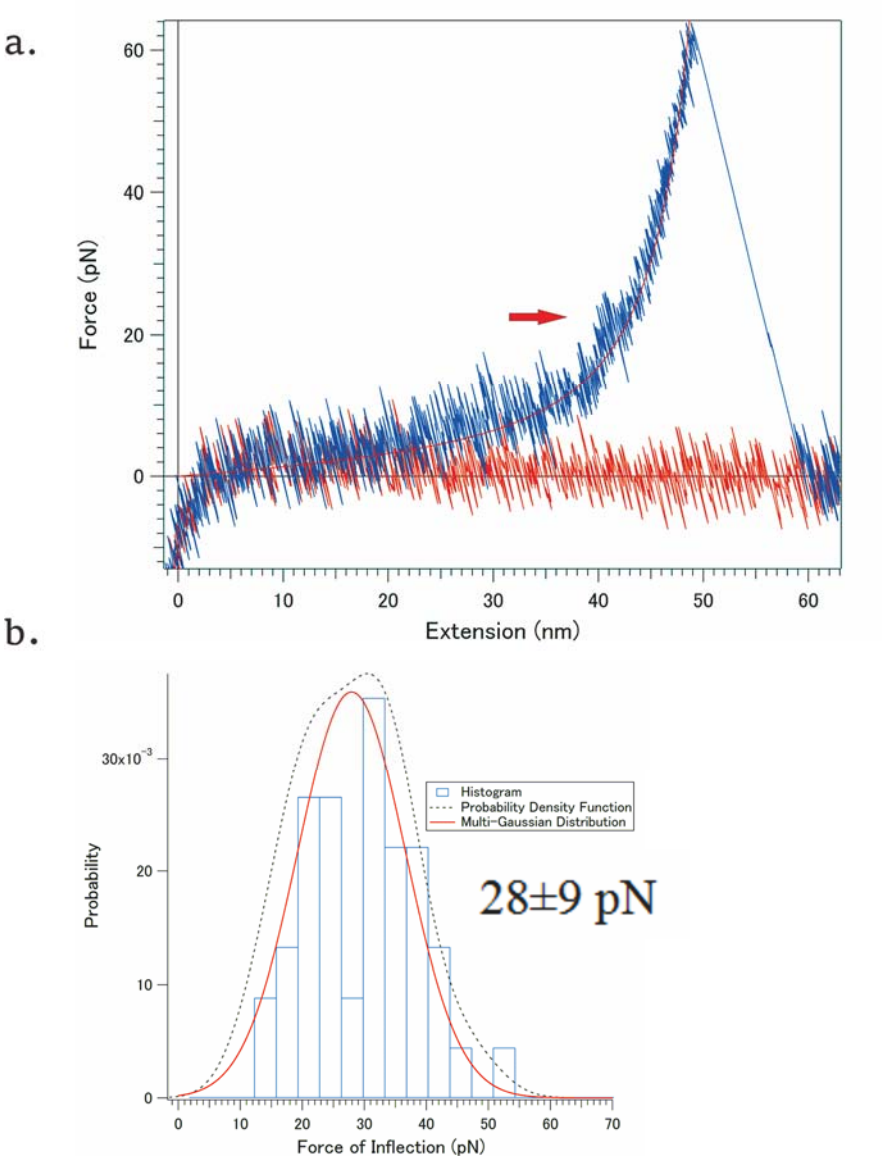

Figure 8. One of three reoccurring force-extension profiles for for PEG_{114}-*b*-poly(*L*-Lysine)-*b*-PEG_{114} in a α-helical conformation and the corresponding histogram, probability density function, and Gaussian distribution. a.) A force-extension curve showing the reoccurring inflection (red arrow). b.) Histogram, probability density function, and Gaussian distribution of the force of the inflection 28±9 pN (±s.d, n=43). The red line in **a.)** indicates a fit using the WLC model.

An inflection at 28±9 pN (**Figure 8**) could be observed for 0.25% of the total force curves. This inflection is interesting as it occurred at the same force as

the plateau observed for the diblock copolymer (27 ±4 pN and 34 ±1 pN; ±s.d, n= 86). The SMFS experiments were both conducted at 10 mM NaCl, and accordingly the results obtained using both molecules can be directly compared to determine the effect of the additional PEG segment. None of the profiles obtained for the triblock had the typical plateau shape observed for the diblock. We can tentatively predict that the inflection shows the unravelling of small helix segments, however a full complete helix could not be extended in these conditions. The smaller helix segments were stabilized by the same hydrophobic side-chain interactions that lead to a high stability of the helix for the diblock system. This offers an explanation for the appearance of an inflection for the triblock at the same force as the plateau for the diblock. Nevertheless, the conclusion must be regarded with caution as the number of force curves showing this feature was only 43. Most importantly, even if the number of obtained curves is considered statistically relevant, there is no single explanation as to why a completely folded helix was not available. The formation of a complete helix might have been inhibited due to the increased solubility of the molecule as a result of an additional PEG segment. It could also be a consequence of the molecule-surface interactions through direct adsorption of the polypeptide segment onto the surface. This is relevant because, adsorption of the molecule on the surface was typically done at neutral pH in order to ensure maximum solubility. It was only after immobilization that the molecules were exposed to higher pH conditions to induce folding into a secondary conformation.

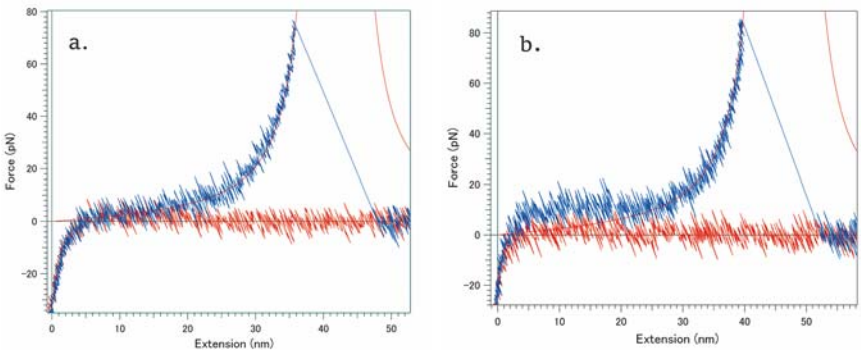

Figure 9. Two of three reoccurring force-extension profiles for PEG_{114}-*b*-poly(*L*-Lysine)-*b*-PEG_{114} in a α-helical conformation. a.) A typical force-extension profile fitted by the WLC model. b.) A typical force-extension profile with a plateau at approximately 10 pN. The red line indicates a fit using the WLC model.

For 0.13% of the curves a perfect fit using the WLC model could be obtained **(Figure 9 a.)**. A perfect fit using the WLC indicated that the force-

extension profile followed the predictions of the mechanical behaviour of an ideal random coil polymer. As no behaviour outside of what is expected from a random coil polymer was observed, we can conclude that these molecules did not adopt a helical conformation.

For 0.22 % of the force curves, a small peak or a plateau could be observed in the 10 pN range **(Figure 9 b.)**. This feature was also evident in a few force-extension profiles where an inflection was observed. The curves which displayed both features were sorted into either of the two groups depending which feature was more dominant. The origin of this low force plateau is not clear however, it is speculated that the interaction observed at low forces is the force needed to "peel" the PEG segment from the peptide segment as there is evidence also from the CD spectroscopy that the lysine and PEG segments have a tendency to interact with each other. The low force interactions may also be the force of the molecule sliding on the surface when the adsorption of the PEG segment to the surface was not sufficient for the molecule to remain immobilized during a force-extension cycle. Nonetheless the interaction at 10 pN is not attributed to the helix unravelling as this feature was not observed for the diblock and neither during SMFS experiments at pH 12 50 mM NaCl for the triblock.

From results obtained at pH 12 we can speculate that only a partially helical molecule was extended, and often the molecule was not able to fold into a α-helix at all. However these results must be regarded with caution as the number of events recorded showing both the inflection and the curves fitting the WLC are low.

2.4 SMFS experiments of PEG_{114}-*b*-poly(*L*-Lysine)-*b*-PEG_{114} at pH 7, 10 mM NaCl

When both the lysine and the PEG segments of the molecule are in a random coil conformation is it expected that the typical parabolic profile depicting the elastic behaviour of an ideal polymer would be obtained. However this was not the case, and the profiles were divided into two typical groups (**Table 2**).

Table 2. Typical force-extension profiles and their percentage of occurrence observed for PEG_{114}-*b*-poly(*L*-Lysine)-*b*-PEG_{114} at pH 7. Event probability indicates the total number of observed interactions out of 17260 force-extension cycles.

Force of detachment ≤ 30 pN	Multiple Peaks	Event Probability	Number of Recorded Curves
354 (2.05%)	436 (2.53%)	4.60%	17260

The high occurrence of multiple peaks indicates that there are many instances of multiple molecule interactions. There were also two types of multiple peak profiles, those that showed interactions occurring at higher forces ≤ 100pN, and those that occurred at lower forces (≤ 40pN). This suggests that apart from multiple molecule interactions, the molecule may also interact with itself and the surface more frequently. As mentioned previously, there is evidence from CD spectroscopy that the lysine and PEG segments interact with each other, and this can be especially relevant at pH 7 when the lysine side chains are protonated, which can form an attractive interaction to the lone pair electrons on the oxygen atoms of the PEG chain. A charged molecule is also more prone to interact with the surface.

When profiles were observed where the force of detachment was below 30 pN, they could not be utilized for analysis as the molecule was not extended with enough force for any defining features to be apparent. Compared to the experiments conducted at pH 12 there was a much higher possibility that the force of detachment was below 30 pN. Perhaps due to the lysine segment being positively charged at pH 7, it had more affinity to the PEG, hence a higher likelihood that it remained attached to the PEG rather than to adsorb strongly onto the AFM cantilever.

The results obtained at pH 7 demonstrate that the conditions are not ideal to conduct SMFS at this pH and ionic concentration. They are unfortunately not comparable to the results obtained at pH 12 as clear single molecule interactions could not be obtained despite a high number of curves recorded.

2.5 SMFS experiments of PEG_{114}-*b*-poly(*L*-Lysine)-*b*-PEG_{114} at 50mM

Single molecule force spectroscopy experiments were also conducted at 50 mM NaCl where it was hoped that some of the electrostatic interactions could be screened. When analysing the results obtained at 50 mM NaCl it was revealed

that the incidence of multiple peaks increased in comparison to experiments done at 10mM NaCl. This was later attributed to the high affinity of the Na^+ ion to the PEG molecule which forms a complex with the cation, much like a crown ether [23]. The relative intrinsic affinities for PEG with different alkali metal ions has been determined in the order of Na, K, Rb and Cs, with Na^+ having the highest affinity [24]. The less than favourable conditions made it very difficult to obtain clear force-extension profiles. Nonetheless some interesting observations were still obtained.

pH 12

Table 3. Typical force-extension profiles and their percentage of occurrence observed for PEG_{114}-*b*-poly(*L*-Lysine)-*b*-PEG_{114} at pH 12, 50 mM NaCl. Event probability indicates the total number of observed interactions out of 10976 force-extension cycles. WLC indicates curves where the force-extension profile followed the fit obtained using the WLC model. (Curves with no evident structure beyond what has been predicted for an ideal random coil polymer)

Force of detachment ≤ 30 pN	Inflection	WLC	Multiple Peaks	Event Probability	Number of Recorded Curves
102 (0.9%)	15 (0.14%)	20 (0.18%)	423 (3.85%)	5.10%	10976

At pH 12, there were multiple reoccurring groups that were evident (**Table 3**). A very large majority of the obtained force-extension profiles could not be utilized as they were not clear single molecule interactions, however a few profiles were obtained which followed the WLC fit, indicating the extension of a molecule without a secondary structure.

Even fewer profiles showed a reoccurring inflection at ≈ 18 pN (**Figure 10**). No histogram could be made for this set of data since only 15 events were observed. However considering the results obtained for the PEG_{114}-*b*-poly(*L*-lysine)$_{134}$-(2-pyridyl disulphide) diblock at 50 mM NaCl, this inflection is intriguing. An inflection at (17± 4 pN; ±s.d, n= 67) was observed for the diblock copolymer at pH 12, 50 mM NaCl attributed to the signature of a partially helical system unravelling. At an ionic concentration of 50 mM the stabilizing hydrophobic interactions between the lysine side chains are increasingly screened and as a consequence, only a partially folded helix is extended. Although the number of events obtained are far too little to make any assertion, the appearance of an inflection at the same force is still worth noting.

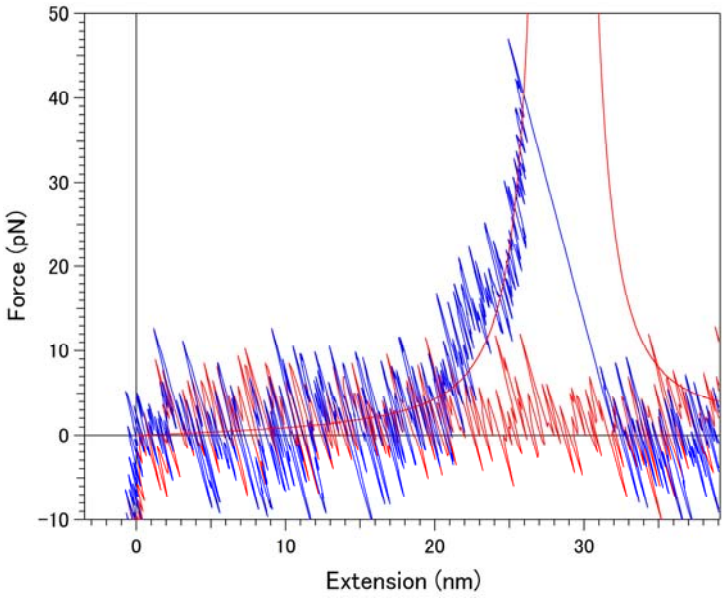

Figure 10. An example of a force-extension profile obtained with an observed inflection at approximately 18 pN (n=15) for PEG_{114}-poly(*L*-Lysine)-PEG_{114} at pH 12, 50 mM NaCl. The red line indicates a fit using the WLC model.

pH 7

Table 4 Typical force-extension profiles and their percentage of occurrence observed for PEG_{114}-*b*-poly(*L*-Lysine)-*b*-PEG_{114} at pH 7, 50 mM NaCl. Event probability indicates the total number of observed interactions out of 4691 force-extension cycles. WLC indicates curves where the force-extension profile followed the fit obtained using the WLC model. (Curves with no evident structure beyond what has been predicted for an ideal random coil polymer)

Force of detachment ≤ 30 pN	Multiple Peaks	WLC	Event Probability	Number of Recorded Curves
7 (0.15%)	240 (5.11%)	4 (0.09%)	5.30%	4691

The results from pH 7 could not be utilized to draw any conclusions as apart from 4 events no clear single molecule interactions could be observed. The incidence of multiple peaks were even higher at pH 7 than at pH 12 indicating increased non-specific interactions, when the peptide segment is charged. It is interesting to note that the instances when the force of detachment ≤ 30 pN decreased in comparison to the 10 mM NaCl condition. Perhaps this indicates the competition from the Na^+ cation decreasing the interaction between the lysine and the PEG segment, allowing the PEG tether to be in a better geometric position to adsorb onto the AFM cantilever.

Conclusion

A stimuli responsive PEG_{114}-*b*-$(PLys)_{134}$-*b*-PEG_{114} triblock was synthesized by amine coupling of PEG_{114}-*b*-poly (N^{ε}-trifluoroacetyl-*L*-lysine)$_{134}$-NH_2 with a PEG_{114}-α-methoxy-ω-NHS ester, and subsequent deprotection in basic conditions. The measured dispersity of the triblock was $Đ \frac{Mw}{Mn}$=1.14 before deprotection.

The molecule was characterized by circular dichroism spectroscopy and compared to results obtained for the diblock copolymer PEG_{114}-*b*-poly(*L*-lysine)$_{134}$-(2-pyridyl disulphide). The molecule was determined to undergo a gradual coil-helix transition with increasing pH. The transition was more gradual for the triblock due to an extra PEG segment contributing to the stabilization of the lysine helix through association. As the lysine is progressively deprotonated, the increasingly hydrophobic lysine associates with PEG which helps segregate the lysine segment from the aqueous solution. This is in line with results and explanation offered by Harada et al. [16] for PEG_{98}-poly(*L*-Lysine)$_{19}$. The stabilization of the lysine helix by interaction with the PEG segment suggests that the same problem would be apparent at the single molecule scale.

When the triblock molecule was investigated with SFMS at pH 12 in 10 mM NaCl, an inflection at (28±9 pN; ±s.d, n= 43) was observed on the force curves. The force of this inflection corresponds to the force of the plateau observed for the diblock copolymer (27± 4 pN (63%) and 34± 1 pN (37%); ±s.d, n= 86). However the presence of an inflection in lieu of a plateau demonstrates that for the triblock copolymer only a partially helical system was extended. The force of the inflection and the plateau coincided as the helical segments are stabilized by the same hydrophobic side chain interactions. Frequently, even a partial helix was not available for extension indicated by force-extension profiles that followed the theoretical fit of the WLC model. Two reasons are suggested as to why the helix did not fold completely. The formation of the helix may have been destabilized through the addition of another PEG segment increasing the solubility of the molecule. It is also probable that perhaps the adsorption of the triblock with the bare surface inhibited helix formation. This is a valid factor because the immobilization was done at neutral pH where the solubility of the molecule was the highest. Unfortunately the results obtained at pH 12 could not be compared to those obtained at pH 7. Clear single molecule interactions could not be obtained

at pH 7 due to the high incidence of profiles where the force of detachment was below 30 pN, as well as profiles that had multiple peaks. This was thought to be a consequence of the lysine segment being positively charged at neutral pH thereby forming interactions with the lone oxygen pairs on the PEG chain.

When SMFS experiments were conducted at 50 mM NaCl the incidence of multiple peaks increased. This was later attributed to PEG having a strong affinity and thus complexing with the Na^+ cations in solution. The incidence of multiple peaks were even higher at pH 7 when the peptide was charged. Under these circumstances it was difficult to obtain a statistically relevant number of clean force-extension profiles, however interesting observations could still be made. An inflection at a smaller force of approximately ≈ 18 pN was obtained for 15 curves, which corresponds to force of an inflection (17± 4 pN; ±s.d, n= 67) observed for the diblock copolymer at 50 mM NaCl. The inflection observed for the diblock was attributed to the unravelling of a partially helical system that was minimally stabilized by lysine side chain interactions.

Despite a low number of events gleaned with the triblock copolymer, it is promising that the inflections obtained at 10 mM and 50 mM NaCl each corresponded to the force of the plateau and inflection obtained at the same ionic conditions for the diblock system. The force of the inflection for the triblock decreased from 28±9 pN at 10 mM to ≈ 18 pN at 50 mM NaCl, in accordance with the increasing ionic concentration that weakens the hydrophobic interactions between the lysine side chains. The results are supportive of the prediction that the inflections indeed indicate the step-wise unravelling of helical segments predicted in theory [25, 26]. The force of the step-wise unravelling is length independent, and only depends on the stabilizing or destabilizing effect of the residues within immediate vicinity. Nonetheless, many more events must be obtained before a concrete conclusion can be given. This is especially true for events obtained at pH 7 which should function as a negative control.

Lastly, the difficulties faced using a triblock copolymer illustrate the importance of utilizing a favourable design and immobilization strategy of the molecule to facilitate the acquisition of good force-extension curves in SMFS experiments. Although many benefits were expected using an extra separation length, the utilization of a system that relies solely on adsorption for both the tip and the surface is difficult. For each successful cycle the PEG segments must be equally well adsorbed to the tip as well as to the surface. This design is not ideal if we consider that PEG interacts favourably with the lysine at neutral pH. If further experimentation is to be conducted using KCl instead of NaCl is

recommended. Although K^+ is similarly known to interact with PEG, it has a lower intrinsic affinity [24].

It should be mentioned that the experimental design utilizing the diblock copolymer as presented in the previous chapter was far less susceptible to the favourable interaction of the PEG with the charged lysine segment at neutral pH, as well as the PEG complexing with the Na^+ ions in solution. This is because firstly the diblock copolymer contained only one PEG segment that could form these disruptive interactions. The molecules were also chemically bond to the surface with a passivating layer of short PEG oligomers separating the individual molecules. This arrangement would support the molecules to be in a more upright position due to the presence of the neighbouring passivating PEG oligomers, making more likely that the PEG segment of the molecule is collapsed directly above the polypeptide segment. Therefore, this positioning limits the accessible space of the PEG tether to form disruptive interactions, making it far more likely to be in a favourable position to be caught by the AFM cantilever.

In conclusion, compared to the triblock, the diblock offers much more control of its geometric orientation, and thus during analysis there are far less experimental variables and uncertainties which must be addressed.

Materials and Methods

Material and Methods for Coupling Reaction and Characterization of PEG_{114}-*b*-$(PLys)_{134}$-*b*-PEG_{114}

The chemicals and reagents used are listed as below. Unless otherwise stated the chemicals were used as received.

Chemicals	Manufactuer	Prior processing
CaH_2	Sigma Aldrich	
Diethylether	Sigma Aldrich	
H_2O_2	Sigma Aldrich	
HCl 37%	Sigma Aldrich	
KOH 85%	Merck	
PEG_{114}-α-methoxy-ω-NHS ester	Rapp Polymere	
NaOH 97%	Alfa Aesar	
NH_4OH 28%	Prolabo	
N,N-Diisopropylethylamine (DIPEA)	Alfa Aesar	
N,N-Dimethylformamide (DMF 99.8% anhydrous)	Sigma Adrich	Dried over CaH2 (Sigma Aldrich) and cryodistilled.

Coupling of PEG_{114}-*b*-poly(N^{ε}-trifluoroacetyl-*L*-lysine)$_{134}$-NH_2 with PEG_{114}-α-methoxy-ω-NHS ester

0.30 g (0.0086 mmol) of PEG_{114}-*b*-poly(N^{ε}-trifluoroacetyl-*L*-lysine)$_{134}$-NH_2 **(4)** was dissolved in 3 ml of dry DMF and left to dissolved completely overnight. Thirty minutes prior to coupling, 0.086 g (0.017 mmol) of PEG_{114}-α-methoxy-ω-NHS ester was dissolved in 860 µL of DMF in a separate vial, and 3.06 µL (0.017 mmol) of DIPEA was added to the vial containing of PEG_{114}-*b*-poly(N^{ε}-trifluoroacetyl-*L*-lysine)$_{134}$-NH_2. The contents were left to react for 72 h at room temperature. After the coupling the excess PEG-NHS, DIPEA and solvent were separated by dialysis with 50,000 Dalton membranes Spectra/Por® and subsequent ultra-filtration using 100,000 Dalton regenerated cellulose membranes from Ultracel® Millipore.

Deprotection of PEG_{114}-*b*-poly(N^{ε}-trifluoroacetyl-*L*-lysine)$_{134}$-*b*-PEG_{114}

0.30 g (0.0075 mmol) PEG_{114}-*b*-poly(N^{ε}-trifluoroacetyl-*L*-lysine)$_{134}$-*b*-PEG_{114} was dissolved in 15.0 ml of ethanol containing 1.54 ml of 5 M KOH. The turbid mixture was left to stir for 15 minutes, then left to stir overnight in a water bath set to 35 ºC. Subsequently, the mixture was dialyzed with 35,000 Dalton membranes from Spectra/Por® for a minimum of 4 days. The final product was collected and lyophilized.

Molecular Characterization:

^{1}HNMR.

All ^{1}HNMR experiments were performed on a Bruker Avance 400MHz spectrometer using TMS as a zero-point standard. The machine was equipped with a Bruker multinuclear z-gradient direct probe head producing gradients in the z-direction with a strength of 53.5 $G \cdot cm^{-1}$. The spectra was acquired with a DI of 9 seconds and 32 scans. ^{1}HNMR samples were dissolved at 5$mg \cdot ml^{-1}$ in $(CD_3)_2SO$ and D_2O

Size-Exclusion Chromatography.

Size-exclusion chromatographs were performed using DMF LiBr 1$g \cdot L^{-1}$ at 80 degrees as the eluent, at a flow rate of 0.80 $ml \cdot min^{-1}$. A SHODEX KD-804 column was used and calibrated with PEG standards. Dilute samples of 5.0 $mg \cdot ml^{-1}$ were prepared and injected.

Circular Dichroism Spectroscopy.

The CD experiments were performed using a JASCO J-815 spectrometer equipped with a JASCO CDF-426S Peltier temperature control system. The scans were recorded between wavelengths of 180 to 260 nm and are a result of three accumulations. Block copolymer solutions were prepared at a concentration of 0.25 $mg \cdot ml^{-1}$ and 0.1 cm quartz cuvettes were used. The pH 2-12 was adjusted by the addition NaOH or HCl (0.1M and 1M). The base or acid was added by using a micropipette and the exact amount of added liquid was recorded so that the difference in dilution could be taken into consideration. All solutions were filtered with a 0.22 μm syringe filter before use.

Materials and Methods for AFM Experiments

Immobilization of the Polymer-polypeptides on to an Au-Si surface.

Au-Si Surfaces: 2 cm by 2 cm Au/Si surfaces (Sigma-Aldrich) were cleaned by using a TL1 cleaning solution (H_2O: NH_3: H_2O_2, 5:1:1, v/v/v) at 70 °C for 15 minutes. The cleaned surfaces were carefully rinsed with ultra-pure water before drying under nitrogen flow.

Mica Surfaces: Mica surfaces were freshly cleaved before functionalization.

The functionalization solution was prepared at a dilution of 0.1$mg \cdot ml^{-1}$ of PEG_{114}-*b*-$(PLys)_{134}$-*b*-PEG_{114} in 20 mM NaCl at pH 7. 50 μl of the functionalization solution was pipetted on either one of the cleaned surfaces and left for an hour.

After functionalization the surfaces were used rinsed repeatedly with ultra-pure water and used immediately for single molecule force spectroscopy experiments.

Intermittent Contact Imaging

Intermittent contact imaging was done on AC mode using PPP-NCH silicon tips (Nanosensors) with a nominal spring constant between 10-130 $N \cdot m^{-1}$. The nominal resonance frequency is between 204-497 kHz. The images were obtained in air and the processing was done using the software, Gwyddion version 2.41. The triblock copolymers were immobilized on a freshly cleaved mica surface using the same procedure as the one used for SMFS experiments. After immobilization the surface was left to dry before imaging.

Single Molecule Force Spectroscopy Experiments

SMFS was performed on a PicoPlus 5500 from Agilent Technologies with a closed loop scanner. A conventional fluid cell was used during experimentation. Force-distance curves were obtained by using gold coated silicon-nitride cantilevers (OBL series, Brucker) with a nominal spring constant at 0.06 $N \cdot m^{-1}$. The real spring constant of the cantilevers were determined by thermal noise method after every experiment.

10 mM NaCl and 50 mM NaCl solutions were prepared prior to every experiment and the pH of the solution was adjusted to either pH 7 (random coil) or pH 12 (helix) with the addition of NaOH or HCl. The pH was monitored throughout the experiment. All salt solutions, base and acids were prepared with ultra-pure water, filtered and prepared fresh prior to every experiment.

References

1. A. Ikai, A. Idiris, H. Sekiguchi, H. Arakawa and S. Nishida, *Applied Surface Science*, 2002, **188**, 506-512.
2. G. Wei, Q. Li, S. Steckbeck and L. C. Ciacchi, *Physical Chemistry Chemical Physics*, 2014, **16**, 3995-4001.
3. A.-S. Duwez and N. Willet, *Molecular manipulation with atomic force microscopy*, CRC Press, 2011.
4. T. Sulchek, R. W. Friddle and A. Noy, *Biophysical Journal*, 2006, **90**, 4686-4691.
5. A. Idiris, M. T. Alam and A. Ikai, *Protein Engineering*, 2000, **13**, 763-770.
6. F. Oesterhelt, M. Rief and H. E. Gaub, *New Journal of Physics*, 1999, **1**, 6.
7. C. Friedsam, H. E. Gaub and R. R. Netz, *Biointerphases*, 2006, **1**, MR1-MR21.
8. A. F. Oberhauser, P. E. Marszalek, H. P. Erickson and J. M. Fernandez, *Nature*, 1998, **393**, 181-185.

9. M. Rief, J. Pascual, M. Saraste and H. E. Gaub, *Journal of Molecular Biology*, 1999, **286**, 553-561.
10. M. Rief, M. Gautel, F. Oesterhelt, J. M. Fernandez and H. E. Gaub, *Science*, 1997, **276**, 1109-1112.
11. M. A. Nash and H. E. Gaub, *ACS Nano*, 2012, **6**, 10735-10742.
12. I. W. Hamley, *Biomacromolecules*, 2014, **15**, 1543-1559.
13. H.-A. Klok, H. Schlaad and S. Lecommandoux, in *Peptide Hybrid Polymers*, Springer Berlin Heidelberg, Editon edn., 2006, vol. 202, pp. 75-111.
14. K. Osada and K. Kataoka, in *Peptide Hybrid Polymers*, eds. H.-A. Klok and H. Schlaad, Springer Berlin Heidelberg, Berlin, Heidelberg, Editon edn., 2006, pp. 113-153.
15. K. Kataoka, H. Togawa, A. Harada, K. Yasugi, T. Matsumoto and S. Katayose, *Macromolecules*, 1996, **29**, 8556-8557.
16. A. Harada, S. Cammas and K. Kataoka, *Macromolecules*, 1996, **29**, 6183-6188.
17. P. Luo and R. L. Baldwin, *Biochemistry*, 1997, **36**, 8413-8421.
18. F. Hanke, A. Serr, H. J. Kreuzer and R. R. Netz, *EPL (Europhysics Letters)*, 2010, **92**, 53001.
19. O. Kratky and G. Porod, *Recueil des Travaux Chimiques des Pays-Bas*, 1949, **68**, 1106-1122.
20. J. F. Marko and E. D. Siggia, *Macromolecules*, 1995, **28**, 8759-8770.
21. F. Berkemeier, M. Bertz, S. Xiao, N. Pinotsis, M. Wilmanns, F. Gräter and M. Rief, *Proceedings of the National Academy of Sciences*, 2011, **108**, 14139-14144.
22. K. Torabi and G. C. Schatz, *Macromolecules*, 2013, **46**, 7947-7956.
23. D. Kaniansky, I. Zelensky, I. Valaskova, J. Marak and V. Zelenska, *Journal of Chromatography A*, 1990, **502**, 143-153.
24. M. J. Bogan and G. R. Agnes, *Journal of the American Society for Mass Spectrometry*, 2002, **13**, 177-186.
25. R. Rohs, C. Etchebest and R. Lavery, *Biophysical Journal*, 1999, **76**, 2760-2768.
26. B. Chakrabarti and A. J. Levine, *Physical Review E*, 2006, **74**, 031903.

Chapter 4

Preliminary Investigation of β-sheet-like Interactions formed by PEG_{114}-*b*-$(PLys)_{134}$-(2-pyridyl disulphide)

Abbreviations:

α–β Transition- α-helix to β-sheet transition

AFM- Atomic Force Microscopy

CD- Circular Dichroism

PEG_{114}-*b*-$(PLys)_{134}$-(2-dipyridyl disulphide)- Poly(ethylene glycol)$_{114}$-*b*-poly(*L*-lysine)$_{134}$-(2-pyridyl disulphide)

ROP-Ring Opening Polymerization

SMFS- Single Molecule Force Spectroscopy

Contents

Introduction

In this chapter preliminary results are introduced concerning single molecule force spectroscopy (SMFS) of the poly(ethylene glycol)$_{114}$-*b*-poly(*L*-lysine)$_{134}$-(2-pyridyl disulphide) **(PEG_{114}-*b*-$(PLys)_{134}$-(2-pyridyl disulphide)** system in the β-sheet conformation.

Poly(*L*-lysine) is considered an ideal model polypeptide to study conformational transitions between random coil, α-helix and β-sheet structures [1, 2] as it is capable of exhibiting all three secondary structures by varying pH and temperature. During the α-helix to β-sheet transition the chemical structure of lysine remains the same, allowing the direct comparison of how the conformational transition, and therefore a change in the hydrogen bonding sequence affects the mechanistic properties of the polypeptide. Protein misfolding and aggregation have been implicated as the unifying mechanism behind many neurodegenerative diseases, such as Alzheimer's disease and prion disease. The proteins and peptides that form the aggregates have no obvious correlation in size, amino acid sequence, or structure. However, the resulting aggregates are comprised of highly organized β-sheets [3, 4], and the native monomeric peptides such as prion proteins undergo a substantial loss of α-helical content during the transition [5, 6]. Thus it has been suggested that aggregation and the α–β transition that occurs antecedently is strongly influenced by sequence nonspecific hydrogen bonding interactions [5, 7]. It is hoped that a study of the α– β transition by single molecule force spectroscopy of a model polypeptide such as poly(*L*-lysine) might further our understanding of how the mechanical properties differ on an account of the conformational transition on the single molecule scale.

Although previous work has been done with SMFS on a large variety of β-sheet containing proteins [8-10], to our knowledge this is the first time the formation and extension of an isolated lysine polypeptide in the β-form was attempted at the single molecule scale.

PART I
Design and Characterization of PEG_{114}-*b*-poly(*L*-lysine)$_{134}$-(2-pyridyl disulphide) in the β-sheet Conformation for use in Single Molecule Force Spectroscopy Experiments

Briefly, the PEG_{114}-*b*-poly(*L*-lysine)$_{134}$-(2-pyridyl disulphide) system was designed and synthesized for use in single molecule force spectroscopy experiments (SMFS). The molecule was synthesized by ring-opening polymerization of *N*- Trifluoroacetyl-*L*-lysine *N*-carboxyanhydride initiated by a PEG-NH_2 initiator (M_n= 5000 $\frac{g}{mol}$). The amine end of the molecule was then coupled to a 2 pyridyl disulphide group through reaction with *N*-Succinimidyl-3(2-pyridyldithio) propionate (SPDP). The addition of the disulphide group allows the molecule to graft onto a gold surface by Au-S bonding, while the PEG tether allows the molecule to adsorb to a bare AFM cantilever in the event where the molecule is successfully captured. This design allows individual, isolated, grafted molecules to be successfully extended as demonstrated in the previous chapter. In addition a similar design of molecule has been successfully utilized by Lussis et al. to investigate rotaxane molecules [11].

In this study the same design was utilized as in the previous chapter, with the exception that the molecule will be exposed to temperatures high enough to induce a conformation transition from the α-helical to the β-sheet secondary structure prior to the experiment **(Figure 1 f.)**. (For further details on the design, please refer to the discussion on design and the synthesis of the system in **Chapter 2, pg. 70**).

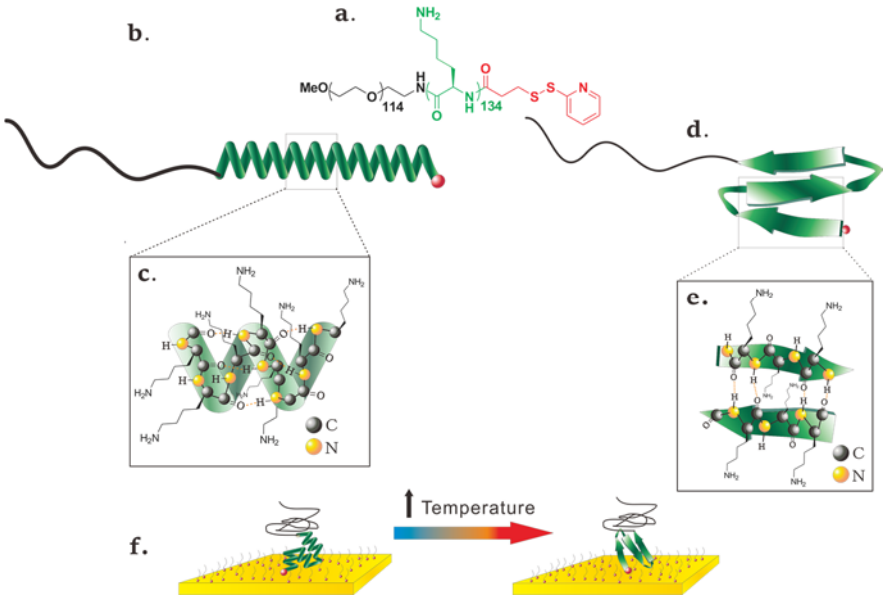

Figure 1. PEG_{114}-*b*-poly(*L*-lysine)$_{134}$-(2-pyridyl disulphide) in α-helical and an anti-parallel β-sheet conformation. a.) Chemical structure of poly(ethylene glycol)$_{114}$-*b*-poly(*L*-lysine)$_{134}$-(2-pyridyl disulphide). b.) Schematic representation of PEG_{114}-*b*-poly(*L*-lysine)$_{134}$-(2-pyridyl disulphide) in a α-helix conformation. c.) Detailed representation of side chains and H-bonding within the poly(*L*-lysine) acid α-helix. d.) Schematic representation of PEG_{114}-*b*-poly(*L*-lysine)$_{134}$-(2-pyridyl disulphide) in an antiparallel β-sheet conformation. e.) Detailed representation of side chains and H-bonding within the poly(*L*-lysine) β-sheet. f.) Schematic representation of the α–β transition that occurs after the surface functionalized with α- PEG_{114}-*b*-poly(*L*-lysine)$_{134}$-(2-pyridyl disulphide) is exposed to elevated temperatures needed to induced the transition. The molecules are surrounded by PEG_6-SH also grafted on to the surface as a passivating agent.

1.1 The Conditions Needed to Induce a α-β Transition of PEG_{114}-*b*-poly(*L*-lysine)$_{134}$-NH_2 and Investigation of its Reversibility Determined by Circular Dichroism

Previously, the pH of coil-helix transition for PEG_{114}-*b*-poly(*L*-lysine)$_{134}$-NH_2 was determined to occur rapidly between pH 9 and 10 and the estimated helix content was 70.9 % at pH 12 calculated using the expression proposed by Luo and Baldwin [12]. The β-form of poly(*L*-lysine) was indicated to be most stable at 50 °C [13-15]. Four different experiments were thus conducted to study the behaviour of PEG_{114}-*b*-poly(*L*-lysine)$_{134}$-NH_2 undergoing a α–β transition and the reversibility of such a transition.

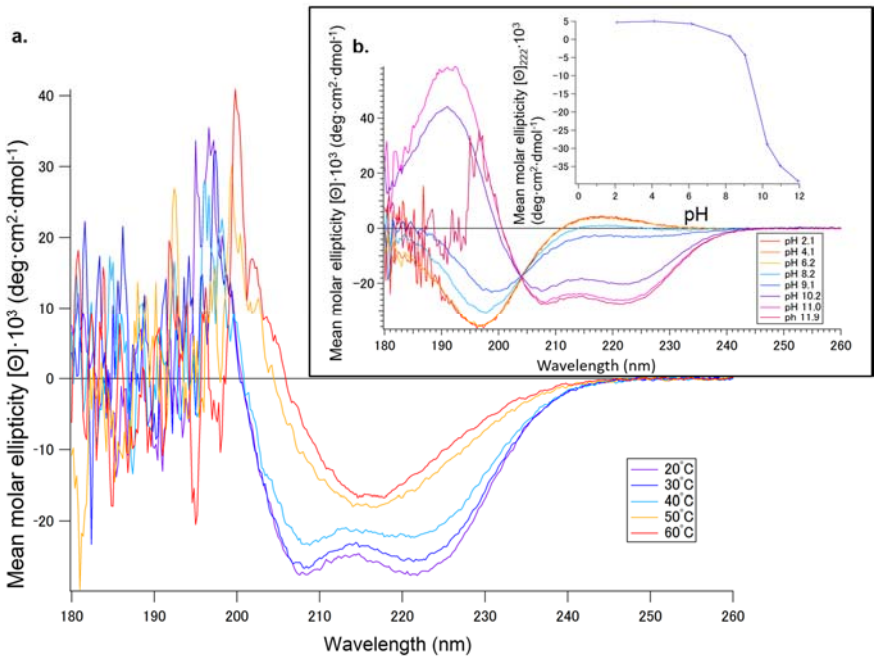

Figure 2. Circular dichroism spectra between 180 nm-260 nm of PEG_{114}-*b*-poly(*L*-lysine)$_{134}$-NH_2 at a constant pH 12 for temperatures between 20 °C to 60 °C. The inset shows the circular dichroism spectra obtained in the previous chapter, where the pH was varied incrementally from pH 2-12 when the temperature was kept constant at 20 °C . Concentration=0.25 mg/ml; cell length=0.1cm.

In the first study, the temperature was varied from 20 °C to 60 °C when the solution pH was kept constant at pH 12 to determine the minimum temperature conditions needed to induce the α−β conformational transition. From the CD spectra obtained (**Figure 2.a.**) it is evident that at pH 12 temperatures of at least 50 °C is needed to induce the transition. The addition of the PEG segment does not seem to have an effect on the pH or temperature of transition as the temperature of transition is the same as reported in literature [14]. This is contrary to the stabilizing effect that the PEG segment has on the formation of the α-helical structure as determined previously and also reported in literature [16]. The inset (**Figure 2.b**) shows the results previously obtained in Chapter 2, where the helix-coil transition behaviour of PEG_{114}-*b*-poly(*L*-lysine)$_{134}$-NH_2 was observed at 20 °C when the pH conditions were varied.

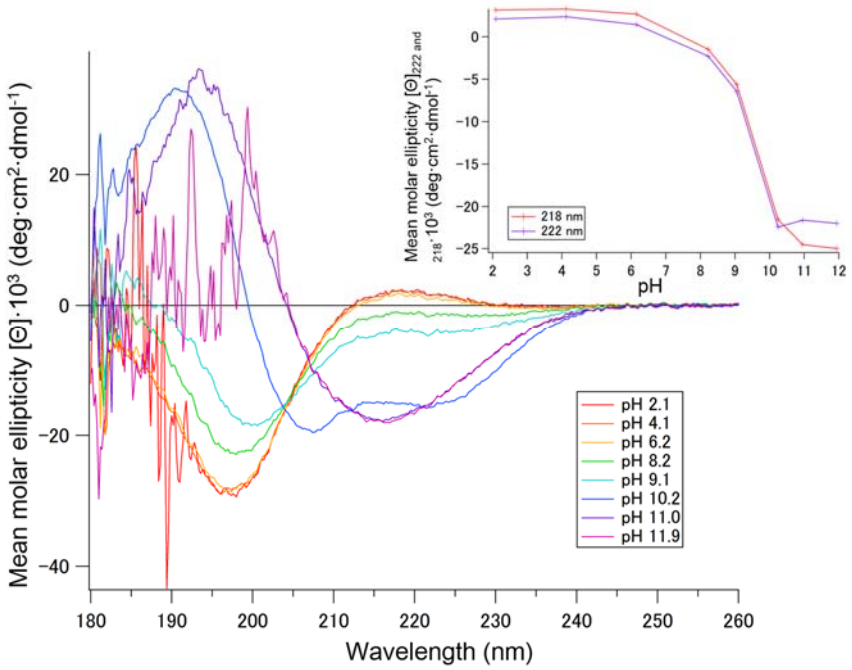

Figure 3. Circular dichroism spectra between 180 nm-260 nm of PEG_{114}-*b*-poly(*L*-lysine)$_{134}$-NH_2 in different pH conditions from pH 2-12 at 50 °C. Concentration=0.25 mg/ml; cell length=0.1cm; 50 °C. The inset compares the variation of the mean molar ellipticity $|\theta_{mean\ molar}|$ at 222 nm with the mean molar ellipticity $|\theta_{mean\ molar}|$ at 218 nm for different pH conditions.

In the second study, the pH was varied incrementally from 2 to 12, while the temperature was kept at 50 °C. This was done to determine the exact temperature and pH conditions needed to induce the α–β transition.

The CD spectra obtained at 50 °C at differing pH conditions (**Figure 3**) demonstrate that the α–β transition can only occur when both conditions, basic pH and elevated temperatures, are fulfilled. The lysine side chains must be fully deprotonated before transition can occur. At pH 9 and below, the molecule adopts a random coil conformation, indicated by a strong negative peak between 195-197 nm and a weakly positive peak at 215 nm. At pH 10 the typical characteristic trace indicative of a α-helix can be observed, suggesting that at this pH the molecule is caught at the threshold of undergoing the transition. From pH 11 onwards the appearance of the characteristic negative mean molar ellipticity at 218 nm can be observed, indicative of the anti-parallel β-sheet. The inset of (**Figure 3**) is a graph comparing the variation of the mean molar ellipticity at 222 nm corresponding to the α-helix with that of the mean molar ellipticty at 218 nm corresponding to the

β-sheet for different pH conditions. A clear shift can be perceived from pH 11 where the peak at 222 nm stagnates in value, while the signal corresponding to 218 nm becomes increasingly negative signifying the formation of the β-sheet conformation.

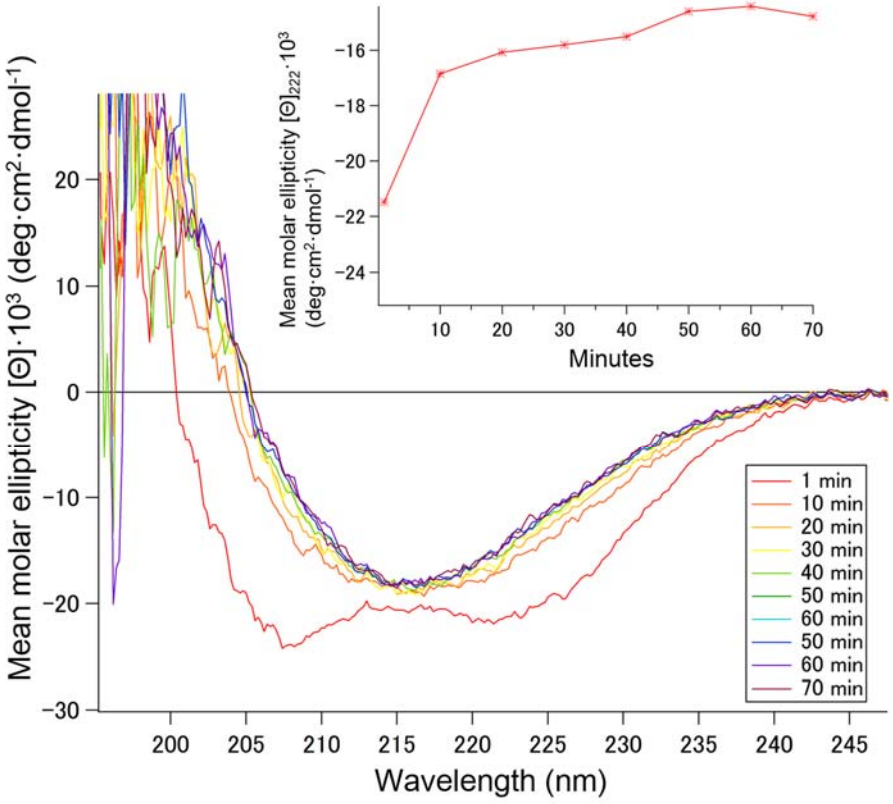

Figure 4. Circular dichroism spectra between 180 nm-260 nm of PEG_{114}-*b*-poly(*L*-lysine)$_{134}$-NH_2 at pH ≈ 12 at 50 °C from 1 min-70 min. Concentration=0.25 mg/ml; cell length=0.1cm; pH ≈ 12; 50 °C. The inset shows the evolution of the mean molar ellipticity $|\theta_{mean\ molar}|$ at 222 nm with time.

In the third study the evolution of the transition was followed at 50 °C and measurements were taken every 10 minutes to verify the amount of time needed for the transition to occur. In all the measurements the value of the negative mean molar ellipticity at 218 nm was followed which indicated the formation of the anti-parallel β–sheet structure [15]. The peak at 218 nm formed at the expense of the α-

helical structure indicated by the disappearance of the two negative peaks at 208 and 222 nm.

The spectra (**Figure 4**) demonstrates that at 50 °C the majority of the α–β transition happens within a time span of 10 minutes. Within 10 minutes of starting the measurement the characteristic double minima at 208 nm and 222 nm indicative of the α-helical conformation is lost. After this time the transition is still ongoing but to a lesser extent. The inset displays the variation of the peak at 222 nm verifying the loss of the helical conformation with time.

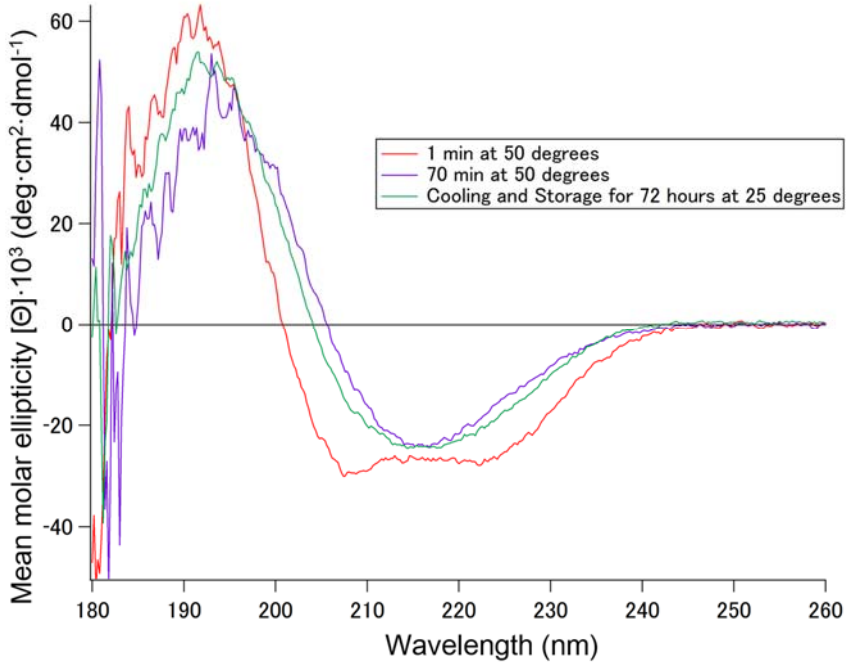

Figure 5 Circular dichroism spectra between 180 nm-260 nm of PEG_{114}-*b*-poly(*L*-lysine)$_{134}$-NH_2 at pH ≈ 12. Three different spectra are compared where measurements were taken after 1 minute at 50 °C pH 12 (red lne), after 70 min at 50 °C pH 12 (purple line) and after cooling and storage for 72 hours at 25 °C. Concentration=0.25 mg/ml; cell length=0.1cm; pH ≈ 12; 25 °C and 50 °C.

Finally in the fourth study (**Figure 5**) the reversibility of the α–β transition was investigated by comparing three different measurements taken immediately prior to the α–β transition (1 minute at 50 °C), after the transition into the anti-parallel β-sheet structure had occurred (70 min at 50 °C), and after cooling and storage for 72 hours at 25 °C to determine whether the antiparallel β-sheet structure could be retained.

After 1 minute at 50 °C the α-helical structure of the poly(*L*-lysine) segment is still evident in the double minima at 208 nm and 222 nm and the positive ellipticity at 190 nm. After 70 minutes at 50 °C the formation of the anti-parallel β-sheet is indicated by the formation of a single minima at 218 nm and the shift of the positive ellipticity to 196 nm. The spectrum of the sample after cooling and storage indicates that although some key characteristics of the anti-parallel β-sheet structure are retained, indicated by the preservation of the negative minima at 218 nm, the shift of the positive peak back to 190 nm which is indicative of a α-helical structure suggests that the structure is an intermediate between both states. The results suggest that within in the time frame of the measurements the α–β transition is not reversible, but neither could the β-sheet structure be retained. Instead the resulting structure after cooling and storage is an intermediate structure, which have characteristics pertaining to both α-helical and β-sheet structures. This is in line with also what was reported in literature where the once folded β-sheet structure was shown to not easily revert back to the α-helical conformation after cooling [13, 14].

PART II
Single Molecule Force Spectroscopy Experiments for PEG_{114}-*b*-poly(*L*-lysine)$_{134}$-(2-pyridyl disulphide) in the β-form

2.1 Heat Treatment of Functionalized Surfaces and Selection of Force-Extension Curves

The Au-Si surfaces grafted with the PEG_{114}-*b*-poly(*L*-lysine)$_{134}$-(2-pyridyl disulphide) copolymer were heated in 20 mM NaCl solution at pH 12 at 50 °C for 20 minutes to induce the α–β transition before performing SMFS experiments at room temperature. Past works on poly(*L*-lysine) mentioned below predict that the grafted molecule will be able to successfully fold into a β-sheet structure. The SMFS study was not conducted at high temperature, because at 50 °C it becomes notoriously difficult to perform experiments due to high thermal drift and noise. If a simpler method can be found to conduct the experiments at room temperature this should be attempted first.

As discussed in the previous chapter, as the length of the lysine segment is very long, hence energetically, it is more likely that the PEG_{114}-*b*-poly(*L*-lysine)$_{134}$-(2-pyridyl disulphide) is folded on the surface into a higher order structure [17]. Therefore the lysine segment still should be folded on the surface displaying energetically favourable helix-helix adhesion [18, 19] before the α–β transition. Longer helices with more turns between the helical segments have been indicated to promote greater β-sheet propensity [1]. In fact, the length of the starting α-helix is so paramount that if the lysine segment was too short, the molecule would not able to undergo a conformational transition despite elevated temperatures[1]. This effect has been attributed to the helical segments interacting favourably in an antiparallel manner resulting in water molecules to be ejected out from the inter-helical space, resulting in a more hydrophobic environment [1]. This increased hydrophobicity promotes the formation of the β structure, therefore if the lysine segment is not long enough for helix-helix adhesion to take place the α–β transition does not occur. Single molecules of poly(*L*-lysine) is predicted to also exhibit the β-structure as β-poly(*L*-lysine) has also been indicated to form by intramolecular interactions [13, 15] and not just by intermolecular interactions. The once folded β-poly(*L*-lysine) has been also shown to not easily revert back to the α-helical conformation after transition. In optical rotary dispersion and CD studies [13, 14], it was found that when β–poly(*L*-lysine) is cooled from 50 to 25 °C, the poly(*L*-lysine) did not to regain its helical conformation.

In summary by looking at the previous studies done on poly(*L*-lysine) it is hypothesized that the synthetic PEG_{114}-*b*-poly(*L*-lysine)$_{134}$-(2-pyridyl disulphide) will be able to undergo a α–β transition and does not easily revert back to the α-helix structure after cooling.

We are aware that the reported behaviour of poly(*L*-lysine) in bulk solution may differ from the behaviour of the synthesized molecule observed with SMFS. When utilizing PEG_{114}-*b*-poly(*L*-lysine)$_{134}$-(2-pyridyl disulphide) for SMFS experiments several important factors must be considered. Firstly it is important to note that the molecules are not freely swimming in solution, but immobilized on a surface. Secondly it also remains to be seen whether single chains immobilized on the surface were able to retain their β-sheet conformation after cooling. Nevertheless, the SMFS results obtained for the molecule in the β-sheet conformation could be compared with the signature force-extension profiles identified previously when the molecule is in a α-helix conformation. The range of forces observed for the rupture of a β-sheet structure was expected to be higher than the unravelling of the α-helix as they are mechanically more stable. Thus, as

a strategy for the selection of force-extension curves, curves with observed interactions at forces higher than ≈ 30 pN were sought. If the same force-extension curves were observed as those identified for the α-helix, it was assumed that the prior heat treatment method did not work, and SMFS experiments must be conducted directly at high temperatures. Needless to say, only profiles with minimal unspecific adhesion and consistent features were selected for analysis.

2.2 Preliminary SMFS Results for PEG_{114}-*b*-poly(*L*-lysine)$_{134}$-(2-pyridyl disulphide) presumably in the β-sheet conformation

After the heat treatment of the functionalized surface, single molecular force spectroscopy (SMFS) was conducted at room temperature at pH 12. An inflection at an average force of 71 pN (**Figure 6**) could be observed in 19 curves out of a total of 25 curves that had a single unfolding event. The event probability was 0.78% calculated out of a total of 2448 recorded curves. No histogram is displayed for this dataset as the number of obtained samples was too little.

The appearance of an inflection at a notably higher force than the plateau observed during previous studies when the molecule was in the α-helical conformation (**Figure 7**) (27± 4 pN (63%) and 34± 1 pN (37%); ±s.d, n= 86), suggests that after the heat treatment the lysine segment has undergone a change of structure that we attribute to a β-interaction. What is not certain is the exact structure of the β-form which this molecule adopts. As mentioned, past works [14, 20] suggest that poly(*L*-lysine) folds in to an anti-parallel β-sheet, and that the interaction is able to form intramolecularly [13, 15]. Geometrically, for a molecule bound on one end to the surface an anti-parallel interaction where the molecule folds back into itself is the most plausible. However, it is not certain if the β-sheet forms along the entirety of the available poly(*L*-lysine) segment, or if it only a select few residues take part in a beta hairpin-like interaction. In addition it is also not certain that a single molecule adopting the β-form is able to completely retain its structure after cooling. What should be noted was that for roughly half of the obtained force-extension curves, a primary inflection at ≈30 pN was observed (**Figure 8**) suggesting that the extended molecule was a mixture of both α-helical and β conformations. This is not improbable if we consider that the β-form formed by a single molecule is in all likelihood not very stable and parts of the molecule are capable of reverting back to the α-helix once cooled back to room temperature. In literature, poly(*L*-lysine) has been shown to revert back to the α-helix

conformation if the solution containing β-poly(*L*-lysine) is slowly cooled from 50 °C to 4 °C [14], therefore reversion back to the α-helical conformation has been demonstrated to be possible. Most importantly, the circular dichroism spectrum (**Figure 5**) obtained for PEG_{114}-*b*-poly(*L*-lysine)$_{134}$-(2-pyridyl disulphide) in the β-form after cooling and resting for 72 hours suggests that after cooling an intermediate structure could be formed, which has characteristics of both α-helical and β-sheet structures.

A major limitation that needs to be mentioned is that the force of detachment was for the vast majority of the cases below 50 pN for the SFMS experiments done on the α-helical system. The example in (**Figure 7**) is one of the few exceptions where the molecule could be extended up to higher forces before the molecule was lost. Therefore the comparison of the molecule in the α-helical versus the β–conformation is extremely difficult if the molecule detaches from the AFM cantilever before the range of forces corresponding to the rupture of the β-form can be reached. Nevertheless when the comparison was feasible, a prominent peak at high forces is only observed for the force-extension curves obtained for the molecule after heat treatment suggesting that the interaction observed at higher forces is a result of the molecule adopting some sort of β-conformation that was still available after cooling. The introduced method of heat treatment followed by SMFS at room temperature is therefore a compelling method to study the β-form of the poly(*L*-lysine) segment without having to perform experiments at elevated temperatures. Further acquisition of curves is required to solidify (or dispel) the conclusions drawn here and no doubt further elucidate the nature of the proposed β-interaction.

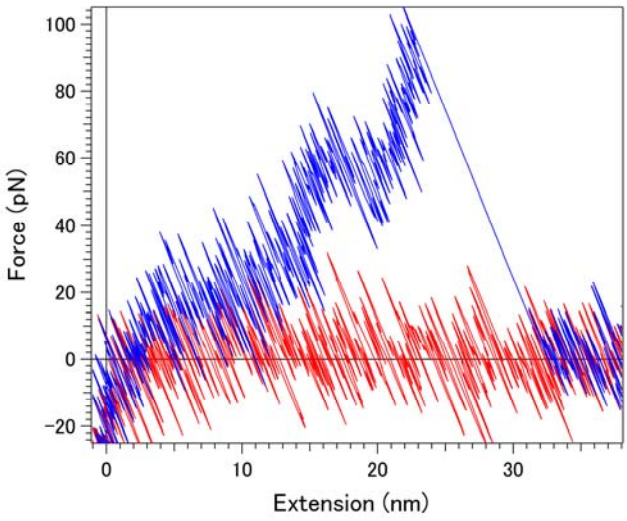

Figure 6. An example of a force-extension profile for the poly(*L*-lysine) segment presumed to be in the β-form with an observed inflection at an average of 70 pN (n=19)

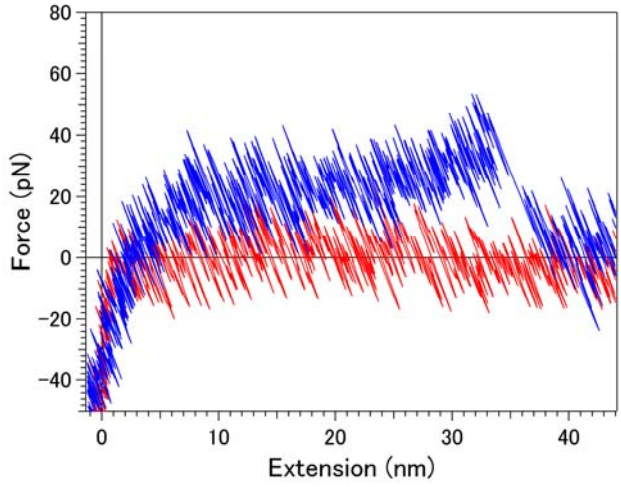

Figure 7. An example of a force-extension profile obtained for the poly(*L*-lysine) segment in the α-helical conformation obtained during a previous study with an observed reoccurring inflection at (27± 4 pN (63%) and 34± 1 pN (37%); ±s.d, n= 86).

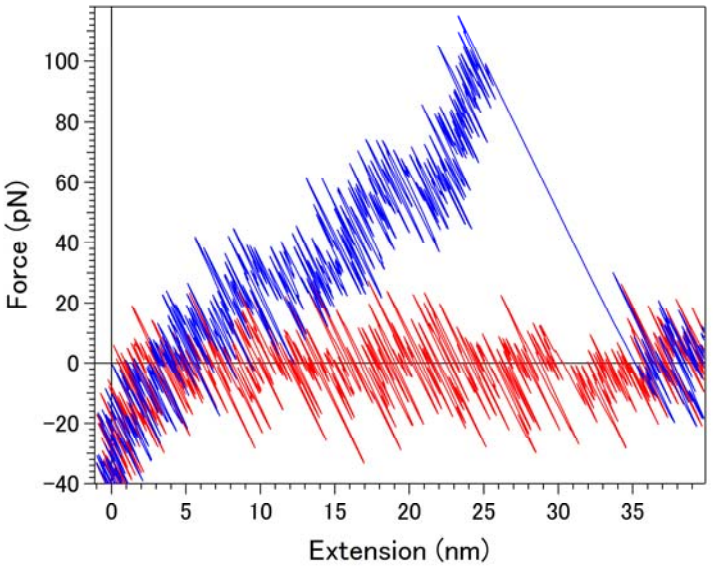

Figure 8. An example of a force-extension profile for the poly(*L*-lysine) segment presumed to be in the β-form with an observed inflection at an average of 70 pN, and a primary inflection at ≈ 30 pN suggesting a mixed α-helical and β-sheet structure.

Conclusion

In this chapter preliminary results were obtained for poly(ethylene glycol)$_{114}$-*b*-poly(*L*-lysine)$_{134}$-(2-pyridyl disulphide) **(PEG_{114}-*b*-$(PLys)_{134}$-(2-pyridyl disulphide)** presumably adopting the β-conformation. The α−β transition of the molecule was probed by circular dichroism where it was confirmed that the lysine segment of the molecule undergoes a α−β transition for pH ≥ 11, and for temperatures above 50 °C. The majority of the transition was found to take place within approximately 10 minutes. The β-form was not fully retained after cooling and resting for 72 hours. Instead it was suggested that an intermediate structure was formed, which exhibited characteristics of both α-helical and β-sheet structures.

To perform single molecule force spectroscopy (SMFS) the possibility of performing experiments at room temperature after heat treatment of the functionalized surface at pH 12 was investigated. This method was preferred because SMFS at elevated temperatures is often plagued by high thermal drift and noise. There was a notable difference when the force-extension curves obtained with this method was compared to curves obtained when the molecule was in the

α-helical conformation. An inflection at an average of 70 pN (n= 19) could be obtained for the molecules after exposing them to elevated temperatures suggesting the formation of a β-conformation. For approximately half of the obtained curves a primary inflection at ≈ 30 pN was observed perhaps indicative of a mixed α–β conformation. This is probable as the β-form adopted by a single molecule is most probably not stable, and thus parts of the molecule can revert back to the α-helical conformation once the heat source is removed. The presence of an intermediate structure exhibiting both α-helical and β-sheet structures was also suggested by a circular dichroism study (**Figure 5**).

From the limited number of curves obtained it is not certain whether the molecule adopts a β-sheet conformation involving most of the available residues or rather a beta hairpin-like interaction involving only some residues. Many more curves must be obtained before the results obtained in this preliminary study can be considered statistically relevant. Nevertheless, the introduced method of heat treatment in alkaline conditions followed by SMFS at room temperature merits further investigation. In addition for future studies the possibility of changing the temperature directly *in situ* will also be probed permitting direct comparison of the α-helical and β-conformations on the same day.

Materials and Methods

Circular Dichroism Spectroscopy.
The CD experiments were performed using a JASCO J-815 spectrometer equipped with a JASCO CDF-426S Peltier temperature control system. The scans were recorded between wavelengths of 180 to 260 nm and are a result of three accumulations. Block copolymer solutions were prepared at a concentration of 0.25 $mg \cdot ml^{-1}$ and 0.1 cm quartz cuvettes were used. The pH 2-12 was adjusted by the addition NaOH or HCl (0.1M and 1M, Sigma Aldrich). The base or acid was added by using a micropipette and the exact amount of added liquid was recorded so that the difference in dilution could be taken into consideration. All solutions were filtered with a 0.22 μm syringe filter before use.

Immobilization of the polymer-polypeptides on to an Au-Si surface.
2 cm by 2 cm Au/Si surfaces (Sigma Aldrich) were cleaned by using a TL1 cleaning solution (H_2O: NH_3: H_2O_2, 5:1:1, v/v/v) at 70 °C for 15 minutes. The cleaned surfaces were carefully rinsed with milliQ water before drying under nitrogen flow. The functionalization solution was prepared by dissolving 0.1$mg \cdot ml^{-1}$ of PEG_{114}-*b*-$PLys_{134}$-(2-pyridyl disulphide), with a short PEG_6-SH oligomer (Polypure) with a $mol \cdot mol^{-1}$ ratio of (80:20, PEG-SH: copolymer) in 100mM KH_2PO_4 (Sigma Aldrich) at pH 7.0 adjusted with NaOH or HCl (both Sigma Aldrich) respectively. After functionalization the surfaces were used rinsed repeatedly with milliQ water and used immediately for single molecule force spectroscopy experiments.

Heat Treatment of Functionalized Surface
After the surfaces were functionalized they were heated for 20 minutes in a 20 mM NaCl solution at pH 12. After the heat treatment the surfaces were immediately mounted on the AFM machine and the SMFS experiments were commenced.

Single Molecule Force Spectroscopy Experiments
SMFS was performed on a PicoPlus 5500 from Agilent Technologies with a closed loop scanner. A conventional fluid cell was used during experimentation. Force-distance curves were obtained by using gold coated silicon-nitride cantilevers

(OBL series, Brucker) with a nominal spring constant at 0.06 $N \cdot m^{-1}$. The real spring constant of the cantilevers were determined by thermal noise method after every experiment. All salt solutions, base and acids were prepared with milliQ water, filtered and prepared fresh prior to every experiment.
A solution of 20 mM NaCl at pH 12 was used during the experiment. The pH was monitored throughout the experiment.

References

1. W. Dzwolak, T. Muraki, M. Kato and Y. Taniguchi, *Biopolymers*, 2004, **73**, 463-469.
2. J. J. Grigsby, H. W. Blanch and J. M. Prausnitz, *Biophysical Chemistry*, 2002, **99**, 107-116.
3. C. Fabrizio and M. D. Christopher, *Annual Review of Biochemistry*, 2006, **75**, 333-366.
4. C. Soto, *Nat Rev Neurosci*, 2003, **4**, 49-60.
5. F. Ding, J. M. Borreguero, S. V. Buldyrey, H. E. Stanley and N. V. Dokholyan, *Proteins: Structure, Function, and Bioinformatics*, 2003, **53**, 220-228.
6. P. M. Harrison, P. Bamborough, V. Daggett, S. B. Prusiner and F. E. Cohen, *Current Opinion in Structural Biology*, 1997, **7**, 53-59.
7. F. Ding, N. V. Dokholyan, S. V. Buldyrev, H. E. Stanley and E. I. Shakhnovich, *Journal of Molecular Biology*, 2002, **324**, 851-857.
8. D. J. Brockwell, E. Paci, R. C. Zinober, G. S. Beddard, P. D. Olmsted, D. A. Smith, R. N. Perham and S. E. Radford, *Nat Struct Mol Biol*, 2003, **10**, 731-737.
9. C. He, C. Hu, X. Hu, X. Hu, A. Xiao, T. T. Perkins and H. Li, *Angewandte Chemie International Edition*, 2015, **54**, 9921-9925.
10. D. L. Guzman, A. Randall, P. Baldi and Z. Guan, *Proceedings of the National Academy of Sciences*, 2010, **107**, 1989-1994.
11. P. Lussis, T. Svaldo-Lanero, A. Bertocco, C.-A. Fustin, D. A. Leigh and A.-S. Duwez, *Nat Nano*, 2011, **6**, 553-557.
12. P. Luo and R. L. Baldwin, *Biochemistry*, 1997, **36**, 8413-8421.
13. L.-K. Li and A. Spector, *Journal of the American Chemical Society*, 1969, **91**, 220-222.
14. B. Davidson and G. D. Fasman, *Biochemistry*, 1967, **6**, 1616-1629.
15. P. K. Sarkar and P. Doty, *Proceedings of the National Academy of Sciences of the United States of America*, 1966, **55**, 981-989.
16. A. Harada, S. Cammas and K. Kataoka, *Macromolecules*, 1996, **29**, 6183-6188.
17. Z. Qin, A. Fabre and M. J. Buehler, *The European Physical Journal E*, 2013, **36**, 1-12.
18. Z. Qin, S. Cranford, T. Ackbarow and M. J. Buehler, *International Journal of Applied Mechanics*, 2009, **01**, 85-112.
19. P. Palenčár and T. Bleha, *Macromolecular Theory and Simulations*, 2010, **19**, 488-495.

20. I. H. McColl, E. W. Blanch, A. C. Gill, A. G. O. Rhie, M. A. Ritchie, L. Hecht, K. Nielsen and L. D. Barron, *Journal of the American Chemical Society*, 2003, **125**, 10019-10026.

Overall Conclusion and Perspectives

Overall Conclusion and Perspectives

In this study diblock and triblock copolymers of PEG_{114}-*b*-poly(*L*-glutamic acid)$_{85}$-(2-pyridyl disulphide), PEG_{114}-*b*-poly(*L*-lysine)$_{134}$-(2-pyridyl disulphide), and PEG_{114}-*b*-poly(*L*-lysine)$_{134}$-*b*-PEG_{114} were custom-designed, synthesized, and utilized as model artificial systems to determine the mechanical properties pertaining to secondary structures by single molecule force spectroscopy.

Two different molecular designs were investigated for the purpose of this work. One design consisted of a system with a 2-dipyridyl disulphide moiety which allowed the macromolecule to chemically bond onto a gold surface, whilst the other extremity consisted of a PEG tether. The PEG allowed the molecule to physisorb onto a bare AFM cantilever and as result the polypeptide segment in between could be caught and extended. The second design involved the addition of a second PEG spacer between the polypeptide segment and the surface in place of the 2-dipyridyl disulphide moiety, allowing the system to rely on just the direct adsorption of the triblock copolymer onto a cleaned surface.

PEG_{114}-*b*-poly(*L*-lysine)$_{134}$-(2-pyridyl disulphide) and PEG_{114}-*b*-poly(*L*-lysine)$_{134}$-*b*-PEG_{114} block copolymers were synthesized by a PEG-NH_2 initiated ring-opening polymerization of N^{ε}- trifluoroacetyl-*L*-lysine *N*-carboxyanhydride. The resulting diblock copolymer was then coupled to either *N*-succinimidyl 3-(2-pyridyldithio) propionate (SPDP) or PEG_{114}-α-methoxy-ω-NHS ester and then subsequently deprotected. The measured dispersity before deprotection was $Đ \frac{Mw}{Mn}$ =1.16 (DMF: 1g·L^{-1} LiBr) for PEG_{114}-*b*-poly(*L*-lysine)$_{134}$-(2-pyridyl disulphide), and $Đ\frac{Mw}{Mn}$=1.14 (DMF: 1g·L^{-1} LiBr) for PEG_{114}-*b*-poly(*L*-lysine)$_{134}$-*b*-PEG_{114}.

PEG_{114}-*b*-poly(*L*-lysine)$_{134}$-(2-pyridyl disulphide) was characterized by dynamic light scattering where it was found that it does not readily undergo self-assembly in response to differing pH or ionic concentrations. By utilizing circular dichroism the polymer was found to undergo a conformational transition from a random coil to a α-helix above pH 9. The diblock copolymer was found to be well suited for single molecule force spectroscopy experiments as it was able to undergo a conformational transition in response to pH while remaining well dissolved in solution. Similarly PEG_{114}-*b*-poly(*L*-lysine)$_{134}$-*b*-PEG_{114} was found to undergo a conformational transition above pH 8. The transition was found to occur more gradually and starting from a lower pH due to the additional PEG segment

interacting favourably with the lysine segment aiding the nucleation and the stabilization of the α-helix secondary structure.

The synthesis of PEG_{114}-*b*-poly(*L*-glutamic acid)$_{85}$-(2-pyridyl disulphide) was performed prior to this investigation by a different author. The reported synthesis was conducted by the ring-opening polymerization of γ-Benzyl-*L*-glutamate *N*-carboxyanhydride which was also initiated by a PEG-NH_2 initiator. The resulting diblock copolymer was coupled to *N*-succinimidyl 3-(2-pyridyldithio) propionate (SPDP) and subsequently deprotected. The measured dispersity was $Đ\frac{Mw}{Mn}$=1.18 (DMF: 1g·L^{-1} LiBr) before deprotection. Circular dichroism was also previously performed to confirm that at low pH conditions the poly(*L*-glutamic acid) segment adopts the α-helical secondary structure, and exhibits the random coil conformation at neutral to basic pH.

Single molecule force spectroscopy was conducted with these copolymers and experimental results were compared, and shown to be in good agreement with theoretical results obtained by utilizing a AGAGIR based statistical mechanical model proposed by Torabi and Schatz [1].

The helix formed by PEG_{114}-*b*-poly(*L*-Lysine)$_{134}$-(2-pyridyl disulphide) was shown to undergo a turn-by-turn unravelling indicated by a constant force plateau observed experimentally at 27 ±4 pN and 34 ±1 pN, and at 30 pN for the statistical mechanical model. A plateau length of 27 ±4 nm was observed corresponding to the theoretical difference in length (≈27 nm) between the folded and unravelled helix. According to literature [2] a long polypeptide helix such as the one in this study, would be folded on the surface into a higher-order structure separated by denatured residues in between separated helical segments. When a complete helix could not refold upon application of a small axial force, a shorter plateau length of 13 ±3 nm was observed, attributed to the unfolding of isolated, shorter helical segments. If not all the sides chains were positioned in an optimal geometric orientation to promote their helix stabilizing hydrophobic interactions, the unfolding force would be slightly lower explaining why two different populations for the plateau force was observed experimentally.

If the helical segments were less able to align due to the poor geometric positioning by the AFM cantilever, many more denatured segments would remain in the helix. In this case a tilted plateau starting at 13 ±6 pN, and ending at 36 ±9 pN was observed. The ending force of the tilted plateau and the value of the true plateau 34 ±1 pN were in good agreement evidencing the unfolding of the small remaining helical segments.

On the contrary the unfolding of the PEG-*b*-poly(*L*-glutamic acid)$_{85}$-(2-pyridyl disulphide) α-helix was identified by an inflection that could be accounted

for in both experimental, 18± 4 pN and theoretical studies 15 pN. In a few cases a plateau could also be observed at 19±2 pN, where the experimentally observed length 12±5 pN, corresponded to the theoretical difference in length (≈17 nm) between the folded and unfolded helix.

A second inflection at a higher force of 60 ±9 pN was observed for over half of the curves that displayed the first inflection, which was attributed to the formation of a metastable β-hairpin-like interaction. We suggest that the formation of this intermediate structure occurs during the unfolding of the α-helix structure as a result of the β-hairpin structure possessing a higher entropy, [3] and thus occupying an energy minima in conditions where the entropic forces dominate. The same inflection was not observed for the poly(*L*-lysine) helix due to the helix-stabilizing, hydrophobic interactions of the side chains inhibiting the formation of such an intermediate structure. The similarity in forces between the β-hairpin-like interaction observed for poly(*L*-glutamic acid) (60 ±9 pN) and the force of the inflection (≈ 70 pN) observed when poly(*L*-Lysine) was later induced to undergo a α–β transition, suggests that a similar type of interaction was involved in both cases.

The difference between the unravelling forces of the two α-helices, and the probability of unfolding a complete helix was attributed to the differing hydrophobicity of the side chains. The poly(*L*-lysine) helix was stabilized due to the greater hydrophobicity of the side chains, resulting in increased side chain interactions and higher steric hindrance that inhibited random helix-coil fluctuations. Even when a perfect plateau was not observed, the tilted plateau evidenced the stabilizing interactions even for a partially helical structure.

In a follow up experiment when the solubility of the side chains of the poly(*L*-lysine) helix was promoted by slightly increasing the salt concentration, only small inflections at 17± 4 pN was observed in lieu of the plateaus. The inflection was at a remarkably similar force to the inflections observed for the poly(*L*-glutamic acid) helix. Thus we infer that a minimum force of ≈20 pN is needed to rupture the hydrogen bonding maintaining the α-helix as this force was obtained in conditions where the side chain interactions were minimal.

The presence of plateaus or inflections at corresponding forces demonstrates that an unfolding force independent of helix length is required, which supports a turn-by-turn unravelling mechanism for the α-helix, which has been predicted theoretically [4].

For experiments utilizing PEG_{114}-*b*-poly(*L*-lysine)$_{134}$-*b*-PEG_{114}, only a low number of good force-extension curves were gleaned due to a high possibility of interaction between the polypeptide and PEG segments. Despite the

incorporation of an extra separation length, obtaining favourable interactions with a system that relies on favourable, simultaneous adsorption of the molecule on the tip and the surface was difficult. Nevertheless the inflections observed at 28±9 pN and at ≈ 18 pN, corresponded to the force of the plateaus and inflections obtained at the same two salt concentrations for the diblock copolymer. An inflection instead of a plateau was observed at the same force as only a partially helical system could be extended.

Preliminary studies were also conducted on the PEG_{114}-*b*-poly(*L*-Lysine)$_{134}$-(2-pyridyl disulphide) system presumably adopting a β-conformation after heat treatment. The α−β transition was followed by circular dichroism were the transition was found to occur for pH conditions ≥ 11, and for temperatures above 50 °C. The majority of the conformational transition was found to happen within 10 minutes of heating the molecule. After cooling and resting for 72 hours the β-form was not retained, instead it was suggested that an intermediate structure was formed which had characteristics of both α-helical and β-sheet structures.

During single molecule force experiments an inflection at a much higher force of ≈ 70 pN was obtained suggesting the formation of a β-sheet like interaction. It is however not yet certain whether the β-interaction took place along the entire length of the polypeptide or rather a β-hairpin-like structure was formed involving only a few residues.

Finally by comparing the two investigated experimental designs represented by the triblock and diblock copolymer systems it was found that the diblock copolymer containing the 2-pyridyl disulphide offered a much more controlled system for single molecule force spectroscopy experiments. This was due to one end of the molecule being secured on the surface through chemical bonding, and the absence of an additional PEG segment which could form disruptive interactions with the polypeptide segment.

The perspectives regarding the presented work are to firstly obtain more experimental data to consolidate our claim regarding the formation of the β-sheet like structure. In the future the possibility of changing the temperature directly *in situ* and conducting the single molecule experiments directly at elevated temperatures is recommended. In addition performing pulling-relaxing experiments on both secondary structures will no doubt allow us to determine the reversibility of the interactions within the timespan of the single molecule experiment. No doubt an interesting extension of this project would be if the polypeptides could be kept trapped between the tip and the surface while a transition in the secondary structure is induced, allowing the direct measurement

of the work done by the molecule during the transition. However, a new design of the experiment would probably be required where the molecule is chemically linked to the tip as well as the surface. Conducting this experiment by adsorption alone would be extremely difficult judging by the low force of the PEG tether detachment from the tip (≤ 80 pN) for a vast majority of the curves observed during this study.

It is also important to keep in mind the limitations of the current approach. Although single molecule force experiments utilizing an atomic force microscope is one of the very few techniques that allow us to probe the mechanical properties of a single molecule at real-time and *in situ*, the unfolding pathway of a molecule by extension with an atomic force microscope will inherently differ from those observed *in vivo*. Mechanical extension with a force microscope changes the energy landscape and well as the distribution and the structure of intermediates, which are not at equilibrium. Even when unfolding molecules that are mechanically implicated in *in vivo* systems, the geometry and manner at which the force is applied will be different in an artificial experimental setting.

The advantage of a single molecule experiment is that the behaviour of a single isolated molecule in a controlled setting can be observed, however the complexity of probing single molecules is that different sub-populations may be apparent and variations can exist in the unfolding behaviour as not all molecules have exactly the same structure, and even the same molecule can behave differently from time to time. To determine the average behaviour relevant to an ensemble of molecules, many experiments must be conducted in order to obtain a reoccurring and reproducible behaviour that describes the average behaviour of the molecule of interest. Accordingly, to draw any conclusion a statistically relevant number of force-extension curves must be obtained, and the determination thereof is subject to the judgement of the researcher. Secondly, although single molecule force spectroscopy is a powerful technique which allows us to probe and handle single molecules it is important to reiterate that the obtained unfolding behaviours are not perfectly comparable to the molecule in an *in vivo* setting, but merely serves to provide a most probable estimate of its real behaviour.

Lastly, extremely versatile, stimuli-responsive polymer-polypeptides were successfully utilized as model, artificial systems to observe α-helix and β-sheet secondary structures with single molecule force spectroscopy. The importance of side chain interactions in the stabilization of the α-helix structure was to our knowledge demonstrated for first time *in situ* on the single molecule level. We also suggest that the same side chain interactions that stabilize the α-

helix also inhibits the formation of an intermediate β-hairpin-like interaction when the polypeptide is mechanically deformed, which has been also predicted in the past [3].

We believe that such a bottom-up investigative strategy as demonstrated in this thesis by examining the mechanical properties of simple secondary structures will no doubt aid the understanding of more complex protein systems.

References

1. K. Torabi and G. C. Schatz, *Macromolecules*, 2013, **46**, 7947-7956.
2. Z. Qin, A. Fabre and M. J. Buehler, *The European Physical Journal E*, **36**, 1-12.
3. F. Ding, J. M. Borreguero, S. V. Buldyrey, H. E. Stanley and N. V. Dokholyan, *Proteins: Structure, Function, and Bioinformatics*, 2003, **53**, 220-228.
4. R. Rohs, C. Etchebest and R. Lavery, *Biophysical Journal*, **76**, 2760-2768.